Disease Markers

Biomarkers for Diagnosis and Prognosis of Neglected Tropical Diseases

Lead Guest Editor: Lucio Castellano
Guest Editors: Marcos Vinícius Silva and Bruno Rivas-Santiago

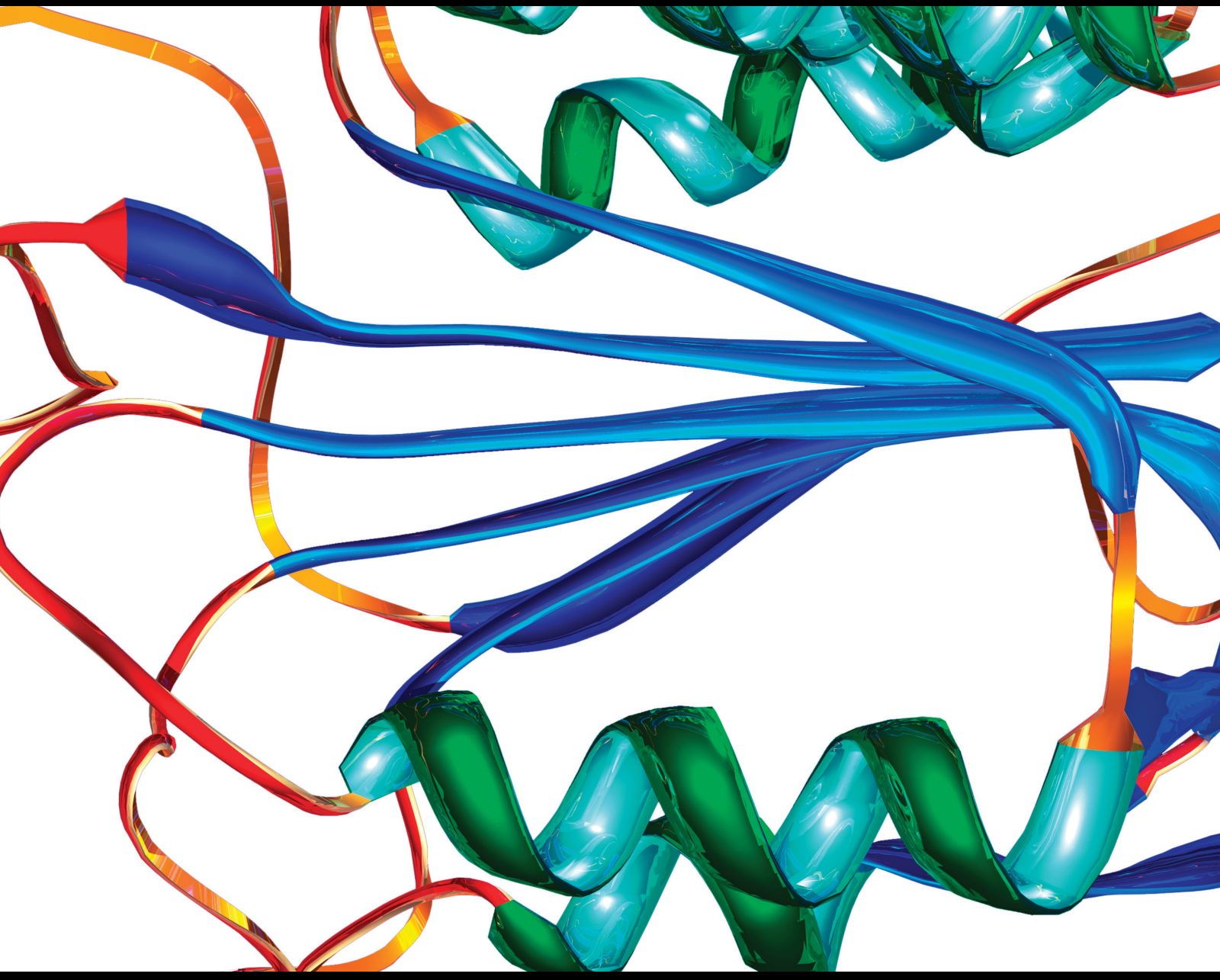

Biomarkers for Diagnosis and Prognosis of Neglected Tropical Diseases

Disease Markers

Biomarkers for Diagnosis and Prognosis of Neglected Tropical Diseases

Lead Guest Editor: Lucio Castellano
Guest Editors: Marcos Vinícius Silva and Bruno Rivas-Santiago

Contents

A *Trypanosoma cruzi* Genome Tandem Repetitive Satellite DNA Sequence as a Molecular Marker for a LAMP Assay for Diagnosing Chagas' Disease
Diego Ordóñez, Pedro Fernández-Soto, Ana M. Fernández-Martín, Beatriz Crego-Vicente, Begoña Febrer-Sendra, Juan García-Bernalt Diego, Belén Vicente, Julio López-Abán, Moncef Belhassen-García, Antonio Muro, and Manuel A. Patarroyo
Research Article (8 pages), Article ID 8074314, Volume 2020 (2020)

The Accuracy of Single MicroRNAs in Peripheral Blood to Diagnose Ovarian Cancer: An Updated Meta-Analysis
Yubao Cui, Shanchao Hong, and Xuming Zhu
Research Article (7 pages), Article ID 1075942, Volume 2020 (2020)

scFv against HSP60 of *Strongyloides* sp. and Its Application in the Evaluation of Parasite Frequency in the Elderly
Camila Botelho Miguel, Marcelo Arantes Levenhagen, Julia Maria Costa-Cruz, Luiz Ricardo Goulart, Patrícia Terra Alves, Carlos Ueira-Vieira, Patrícia Kellen Martins Oliveira Brito, Angelica Oliveira Gomes, Javier Emilio Lazo-Chica, Carlo José Freire Oliveira, and Wellington Francisco Rodrigues
Research Article (6 pages), Article ID 4086929, Volume 2020 (2020)

Diet Alters Serum Metabolomic Profiling in the Mouse Model of Chronic Chagas Cardiomyopathy
Kezia Lizardo, Janeesh Plakkal Ayyappan, Usha Ganapathi, Walderez O. Dutra, Yunping Qiu, Louis M. Weiss, and Jyothi F. Nagajyothi
Research Article (15 pages), Article ID 4956016, Volume 2019 (2019)

Cardiac Chagas Disease: MMPs, TIMPs, Galectins, and TGF-β as Tissue Remodelling Players
Arthur Wilson Florencio da Costa, Jose Rodrigues do Carmo Neto, Yarlla Loyane Lira Braga, Beatriz Aquino Silva, Amanda Borges Lamounier, Bárbara Oliveira Silva, Marlene Antônia dos Reis, Flávia Aparecida de Oliveira, Mara Rúbia Nunes Celes, and Juliana Reis Machado
Review Article (10 pages), Article ID 3632906, Volume 2019 (2019)

Hindawi
Disease Markers
Volume 2021, Article ID 6407528, 9 pages
https://doi.org/10.1155/2021/6407528

Review Article

Prognostic Role of Long Noncoding RNAs in Oral Squamous Cell Carcinoma: A Meta-Analysis

Yu Wang,[1,2] **Peng Wang**,[3] **Xin Liu**,[1] **Ziran Gao**,[1] **Xianbao Cao**,[2] **and Xilong Zhao**[1,4]

[1]*Cell Therapy Technology Transfer Medical Key Laboratory of Yunnan Province, Basic Medical Laboratory, 920th Hospital of Joint Logistics Support Force, PLA, Kunming, 650032 Yunnan Province, China*
[2]*Department of Otolaryngology, First People's Hospital of Yunnan Province, Kunming, 650032 Yunnan Province, China*
[3]*Faculty of Environmental Science and Engineering, Kunming University of Science and Technology, Kunming, 650032 Yunnan Province, China*
[4]*Qujing 69 Hospital, China RongTong Medical Healthcare Group co., Ltd, Qujing, 655000 Yunnan Province, China*

Correspondence should be addressed to Xilong Zhao; zhaoxilong@aliyun.com

Received 3 September 2019; Revised 8 October 2021; Accepted 1 December 2021; Published 26 December 2021

Academic Editor: Ayesha Obaid

Long noncoding RNAs (lncRNAs) have emerged as critical regulators of tumor progression, and lncRNA expression levels could serve as a potential molecular biomarker for the prognosis and diagnosis of some cancers. However, the prognostic value of lncRNAs in oral squamous cell carcinoma (OSCC) remains unclear. Thus, a meta-analysis was conducted to explore the potential prognostic value of lncRNAs in OSCC. We systematically searched PubMed, EBSCO, Web of Science, and Elsevier from 2005 to 2021 to identify all published studies that reported the association between lncRNAs and prognosis in OSCC. Then, we used meta-analytic methods to identify the actual effect size of lncRNAs on cancer prognosis. The hazard ratios (HRs) with 95% confidence intervals (95% CIs) were calculated to assess the strength of the association. The reliability of those results was then examined using measures of heterogeneity and testing for selective reporting biases. According to the inclusion and exclusion criteria, a total of 17 studies were eligible in our meta-analysis, involving 1384 Asian patients. The results identified a statistically significant association of high lncRNA expression with poor overall survival [adjusted pooled hazard ratio (AHR) = 1.52; 95% confidence interval (CI): [1.26–1.84], $p \leq 0.001$]. The present meta-analysis demonstrated that lncRNA expression might be used as a predictive prognostic biomarker for Asian patients with OSCC.

1. Introduction

Oral squamous cell carcinoma (OSCC) is a significant subgroup of head and neck squamous cell carcinomas [1, 2]. OSCC is characterized by invasive growth, frequent metastases, and high recurrence, and its incidence is increasing, with more than 274,000 new patients with OSCC every year worldwide [3–5]. Although considerable developments in diagnosis and combined treatments have been made in recent years, the 5-year survival rate among OSCC patients has not improved and remains less than 50% [6–8]. Therefore, it is essential to identify useful biomarkers and therapeutic targets to improve the prognosis of OSCC.

Long noncoding RNAs (lncRNAs), a class of regulatory transcripts, are synthesized by RNA polymerase II and have lengths greater than 200 nucleotides [8–10]. Recent studies have shown that dysregulated lncRNAs play essential roles in tumor cellular processes of cell proliferation, differentiation, and invasion during cancer development and progression and play essential roles in tumorigenesis and progression of ovarian [11], colorectal [11], gastrointestinal [12], and lung cancers [13]. lncRNAs are regarded as essential therapeutic targets [14, 15].

Some studies have shown that abnormal lncRNAs contribute to biological behaviors, clinical diagnosis, prognosis, and treatment options in OSCC. HOX antisense intergenic

RNA (*HOTAIR*) is a transacting lncRNA that was the first identified lncRNA [16]. *HOTAIR* is located at chromosome 12q13.13, which is a regulatory boundary in the HOXC cluster [17]. The expression level of *HOTAIR* was significantly associated with metastasis, tumor differentiation, malignant degree, and prognosis of the patients. In addition, the upregulation of *HOTAIR* expression promoted OSCC cell proliferation, invasion, metastasis, and angiogenesis by binding to *EZH2* and *H3K27me3* and ultimately E-cadherin gene silencing [18]. *H19* acts as an oncogene in OSCC by competing with miR-138 and releasing *EZH2*, thereby playing a role in cell proliferation, migration, invasion, apoptosis, and epithelial-mesenchymal transition (EMT), and high expression of *H19* was correlated with TNM stage, lymph node metastasis, and poor prognosis outcome [19]. One study demonstrated that the low expression of lncRNA AC012456.4 contributed to poor disease-free survival (DFS) and indicated that lncRNA AC012456.4 remarkably correlated with the JNK-STAT and MAPK signaling pathways in tumorigenesis and functioned as a novel target for the diagnosis, clinical treatment, and outcome of OSCC [20]. Due to varying diagnostic accuracy, limitations in sample size, different lncRNA types, and research methods, a single-center study may be inaccurate and inadequate. Based on the current research situation, the present study was aimed at clarifying the clinical feasibility of lncRNAs as potential biomarker candidates by systematically summarizing all eligible articles.

2. Materials and Methods

2.1. Search Strategy. We conducted this meta-analysis according to the Preferred Reporting Items for Systematic Reviews and Meta-Analyses (PRISMA) guidelines [21]. A systematic literature review was searched from the PubMed, EBSCO, Elsevier, Web of Science, and Elsevier databases for papers online from 2005 to 2021. The search was performed by two independent researchers (YW and XL). The following search terms were used: (oral squamous cell carcinoma or OSCC) and (lncRNA or (long noncoding RNA) or (long noncoding RNAs)) and (prognosis or prognostic or survival). In addition, the cited references in the eligible studies were also searched and reviewed.

2.2. Inclusion and Exclusion Criteria. Inclusion criteria are as follows: (1) the research design was a prospective or retrospective study, (2) the paper researched the relationship between lncRNA and the prognosis of survival in OSCC, (3) the hazard ratio and 95% CI of overall survival were reported or could be calculated from the study, (4) more than 20 cases were included, and (5) studies were published in the English language. Two researchers (YW and XL) decided the ultimate eligible studies, and disagreements were resolved by consulting a third researcher (XBC). The exclusion criteria were as follows: (1) studies without sufficient or usable data; (2) reviews, laboratory articles, letters, unpublished data, and conference abstracts; and (3) duplicate publications.

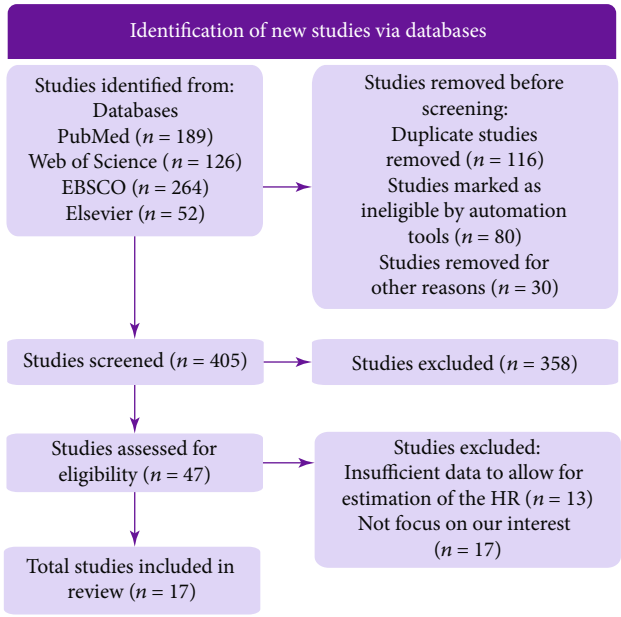

Figure 1: A flowchart of the article search.

2.3. Data Extraction and Quality Evaluation. Two investigators (YW and PW) perused the full text of the included articles and extracted relevant data independently from the eligible studies. Extracted information included the name of the first author, published year, regions, sample size, lncRNA types, HR and 95% CI, case number, outcome, HR estimation, and cutoff value [22]. The Newcastle–Ottawa quality assessment scale (NOS) was used to assess the quality of the included studies [23]. NOS scores of 1–3, 4–6, and 7–9 were designated as low, medium, and high quality, respectively. The quality evaluation was conducted by XL and PW independently, and disagreements were resolved through group discussion with a third investigator (XLZ).

2.4. Statistical Methods. $p < 0.05$ was considered statistically significant for comparing the groups with high and low expression of lncRNAs regarding survival of OSCC patients. $p \geq 0.05$ was identified as no statistically significant difference between the two groups in OSCC patients.

HRs (HRs and 95% CIs) were calculated using a reported method [24] and used to evaluate the overall survival effect. If included articles reported the HR and 95% CI or did not directly provide the HR, but they reported the O-E value (observed value minus expected value), the 95% CI or the log-rank p value, we could calculate accurate HR_S. If only the total number of cases, the number of each group, and the log-rank p value were reported, the approximate HRs could be calculated as described previously [24]. Additionally, if only valid data were provided in the form of survival curves, the data from Kaplan–Meier survival curves could be used to calculate HRs by Parmar's method [25].

Statistical heterogeneity within studies was detected by the Q statistic and I^2 statistics. If $I^2 \leq 50\%$ identified lower heterogeneity, a fixed-effect model was used. If $I^2 > 50\%$ showed higher heterogeneity, the random-effect model was used [26]. Subsequently, Egger's method was used to detect

Table 1: Necessary information about the included studies.

Study ID	lncRNA	Country	Sample	Reference	Detection method	Sample size	Outcome	Source of HR	Cutoff value	NOS
Jie Wu, 2015 [18]	HOTAIR	China	Tissues	GAPDH	qPCR	100	OS	Log rank	Median	7
Yonglong Hong, 2017 [19]	H19	China	Tissues	GAPDH	qPCR	42	OS	Sur curve	NA	6
Luyi Chai, 2018 [29]	ANRIL	China	Tissues	GAPDH	qPCR	130	OS	Sur curve	Median	6
Yan Guo, 2018 [30]	CEBPA-AS1	China	Tissues	GAPDH	qPCR	60	OS	Reported	Median	3
Gang Huang, 2018 [31]	NEAT1	China	Tissues	NEAT1/ RGS20	qPCR	30	OS	Sur curve	NA	8
Xiaohua Liu, 2018 [32]	NEAT1	China	Tissues	GAPDH	qPCR	58	OS	Sur curve	Median	7
Koyo Nishiyama, 2018 [33]	DLEU1	Japan	Tissues	ACTB (β-actin)	qPCR	252	OS	Sur curve	Median	8
Tingru Shao, 2018 [34]	AC0077271.3	China	Tissues	GAPDH	qPCR	80	OS	Reported	Median	6
Chengcao Sun, 2017 [35]	PDIA3P	China	Tissues	GAPDH	qPCR	58	OS	Sur curve	NA	3
Chengmei Yang, 2016 [36]	SOX21-AS1	China	Tissues	GAPDH	qPCR	86	OS	Reported	Median	6
Chenzheng Zhang2, 2017 [37]	FTH1P3	China	Tissues	GAPDH/ U6	qPCR	70	OS	Log rank	Mean	9
Chenzheng Zhang1, 2017 [38]	LINC00668	China	Tissues	GAPDH/ U6	qPCR	50	OS	Log rank	Mean	8
Zhongzhi Jin, 2018 [39]	MORT	China	Tissues	GAPDH	qPCR	59	OS	Reported	Median	7
Zhe Liu, 2018 [40]	HNF1A-AS1	China	Tissues	GAPDH	qPCR	62	OS	Sur curve	Median	5
Qian Lyu, 2019 [41]	MINCR	China	Tissues	GAPDH	qPCR	80	OS	Sur curve	Median	6
J, Wang, 2019 [42]	LACAT1	China	Tissues	GAPDH	qPCR	78	OS	Sur curve	Median	7
Yixin Yang, 2019 [43]	CASC9	China	Tissues	GAPDH	qPCR	84	OS	Reported	Median	9

publication bias and observed in the form of a funnel plot [27]. If publication bias was found, then the HRs were adjusted by the method of Duval and Tweedie's trim-and-fill [28].

3. Results

3.1. Literature Search and Characteristics of the Included Studies. As shown in Figure 1, 631 articles were searched in the databases of PubMed, Web of Science, EBSCO, and Elsevier. After removing duplicate studies and ineligible studies, 405 studies remained. After reading the title, abstract, and keywords and further excluding irrelevant studies ($n = 358$), 47 eligible articles were downloaded and analyzed in detail. Seventeen articles were excluded because HR could not be calculated, and 13 articles were excluded because they did not focus on our area of interest. In the end, 17 studies were included in this review [19, 20, 29–43]. The necessary information and data from the included studies are shown in Tables 1 and 2. The studies enrolled 1384 participants, with a maximum sample size of 252 and a minimum sample size of 30 patients. Eligible studies published from 2013 to 2021 reported an association between lncRNA expression level and overall survival, and all participants' ethnic backgrounds were Asian. In addition, lncRNAs and relevant targets in oral squamous cell carcinoma are shown in Table 3.

3.2. Quality Evaluation. The data were extracted from all 17 eligible studies. According to the NOS quality assessment system, 9 studies were of high quality, 6 studies were of medium quality, and 2 studies were of low quality (Table 1). The average score of all included studies was 6.53. In addition, four studies were based on multivariate analysis, and 13 studies were based on univariate analysis. HR and 95% CI of each study are shown in Table 2.

3.3. Meta-Analysis. The meta-analysis data of pooled HRs of overall survival were extracted from the 17 included studies. The results showed a pooled HR of 1.52 (95% CI, 1.26–1.84; $p < 0.001$) with statistically significant heterogeneity (Q-statistic, 75.00; $I^2 = 71.80\%$, p value < 0.001, random-effect model) (Figures 2(a) and 2(b)). Compared with the decreased lncRNA expression group, upregulated lncRNA expression was correlated with poor prognosis.

Most of the lncRNAs were investigated in a single study; only *NEAT1* was investigated in two studies. We then conducted a meta-analysis to assess the relationship between *NEAT1* expression and overall survival (OS) in OSCC patients. We noted that the heterogeneity was significant ($I^2 = 71.05\%$, $p = 0.06$). Therefore, a random-effect model was applied, and the results of the analysis showed that *NEAT1* was not significantly associated with OS (HR: 2.49, 95% CI: 0.73-8.51; $p = 0.15$) (Figure 3).

Table 2: Characteristics of the included studies.

lncRNAs	Reference	U&M analysis	Case number		OS	
			High expression	Low expression	HR (95% CI)	p value
HOTAIR	Jie Wu, 2015 [18]	U	30	70	2.64 (1.14-6.10)	0.02
H19	Yonglong Hong, 2017 [19]	U	25	17	1.10 (1.0-1.21)	0.05
ANRIL	Luyi Chai, 2018 [29]	U	57	73	1.39 (1.07-1.80)	0.01
CEBPA-AS1	Yan Guo, 2018 [30]	U	30	30	6.71 (3.61-8.73)	<0.001
NEAT1	Gang Huang, 2018 [31]	M	12	18	5.54 (1.5120.38)	0.01
NEAT1	Xiaohua Liu, 2018 [32]	U	26	32	1.52 (1.02-2.28)	0.04
DLEU1	Koyo Nishiyama, 2018 [33]	M	126	126	1.28 (1.05-1.56)	0.01
AC0077271.3	Tingru Shao, 2018 [34]	U	40	40	3.08 (0.95-10.02)	0.06
PDIA3P	Chengcao Sun, 2017 [35]	U	32	26	2.72 (1.62-6.36)	<0.001
ANRIL	Chengmei Yang, 2016 [36]	U	57	73	1.39 (1.07-1.80)	0.01
SOX21-AS1	Chenzheng Zhang2, 2017 [37]	M	57	29	5.66 (1.85-17.30)	0.002
FTH1P3	Chenzheng Zhang1, 2017 [38]	U	37	33	2.71 (1.40-5.27)	0.003
LINC00668	Zhongzhi Jin, 2018 [39]	U	15	35	2.74 (1.07-7.01)	0.03
MORT	Zhe Liu, 2018 [40]	U	31	28	1.51 (1.08-2.11)	0.02
HNF1A-AS1	Qian Lyu, 2019 [41]	U	32	30	1.75 (1.25-2.46)	<0.001
MINCR	J, Wang, 2019 [42]	U	40	40	1.64 (1.11-2.43)	0.01
LACAT1	Yixin Yang, 2019 [43]	U	34	44	2.33 (1.06-5.12)	0.04
CASC9	Jie Wu, 2015 [18]	M	53	31	2.31 (1.12-4.75)	0.02

Table 3: lncRNAs and relevant targets in oral squamous cell carcinoma.

lncRNAs	Poor prognosis	Role	Relevant targets	Function	Reference
HOTAIR	Upregulated	Oncogene	Cyclin D1, EGFR c-Myc	Proliferation/invasion/metastasis/angiogenesis	[18]
H19	Upregulated	Oncogene	miR-138, EZH2	Proliferation/invasion/apoptosis/EMT	[19]
ARNIL	Upregulated	Oncogene	miR-125a, ESRRA	Proliferation/invasion/migration	[29]
CEBPA-AS1	Upregulated	Oncogene	CEBPA, Bcl2	Proliferation/invasion/migration/apoptosis	[30]
NEAT1	Upregulated	Oncogene	miR-365, RGS20	Migration/invasion/progression	[31, 32]
DLEU1	Upregulated	Oncogene	HA-CD44	Proliferation/invasion/migration	[33]
AC007271.3	Upregulated	Oncogene	β-Catenin, CyclinD1, c-muc, Bal-2	Proliferation/invasion/migration	[34]
PDIA3P	Upregulated	Oncogene	miR-185-5p, CCND2	Proliferation.	[35]
SOX21-AS1	Upregulated	Oncogene	miR-145	Proliferation/invasion/growth	[36]
FTH1P3	Upregulated	Oncogene	miR-224-5p	Proliferation	[37]
LINC00668	Upregulated	Oncogene	miR-297/VEGFA	Progression	[38]
MORT	Upregulated	Oncogene	ROCK1	Proliferation	[39]
HNF1A-AS1	Upregulated	Oncogene	STAT3	Proliferation/migration/EMT	[40]
MINCR	Upregulated	Oncogene	Wnt/β-catenin	Proliferation/invasion	[41]
LACAT1	Upregulated	Oncogene	MicroRNA-4301	Proliferation/differentiation	[42]
CASC9	Upregulated	Oncogene	AKT/mTOR	Proliferation/apoptosis/autophagy/progression	[43]

Subsequently, we conducted subgroup analyses according to univariate and multivariate analyses, NOS score evaluation, and source of HR. The results are shown in Table 4. The combined analysis showed that upregulated lncRNA expression has significant prognostic value in OSCC: univariate analysis (AHR: 1.43, 95% CI: 1.20–1.71, $p < 0.001$), multivariate analysis (AHR: 2.50, 95% CI: 1.65–3.78, $p < 0.001$), source of HR (reported: HR: 1.85, 95% CI: 1.51-2.26, $p < 0.001$; survival curve: AHR: 1.18, 95% CI: 1.10-1.27, $p < 0.001$), and NOS score evaluation (high: 1.64, 95% CI: 1.38–1.96, $p < 0.001$; medium: 1.45, 95% CI: 1.01–2.07, $p = 0.04$; low: 3.78, 95% CI: 1.92-7.44, $p < 0.001$).

Publication bias of the included articles was evaluated by funnel plots and Begg's bias test. The shape of the funnel plot was asymmetrical, and the p value of Begg's test was 0.002 for OS of all enrolled articles, suggesting the existence

Study name	LncRNA type	Hazard ratio	Lower limit	Upper limit	Z-Value	p-Value
Chengcao Sun 2017	PDIA3P	2.718	1.162	6.358	2.306	0.021
Chengmei Yang 2016	SOX2-AS1	5.660	1.851	17.308	3.040	0.002
Chenzheng Zhang1 2017	LINC00668	2.736	1.068	7.010	2.097	0.036
Chenzheng Zhang2 2017	FTH1P3	2.714	1.397	5.271	2.948	0.003
Gang Huang 2018	NEAT1	5.540	1.506	20.382	2.576	0.010
Jie Wu 2015	HOTAIR	2.640	1.141	6.107	2.269	0.023
Koyo Nishiyama 2018	DLEU1	1.280	1.050	1.561	2.442	0.015
Luyi Chai 2018	ANRIL	1.390	1.072	1.803	2.480	0.013
Tingru Shao 2018	AC007271.3	3.083	0.940	10.112	1.858	0.063
Xiaohua Liu 2018	NEAT1	1.520	1.015	2.276	2.034	0.042
Yan Guo 2018	CEBPA-AS1	6.710	2.181	20.643	3.320	0.001
Yonglong Hong 2017	H19	1.100	1.000	1.210	1.968	0.049
Zhe Liu 2018	HNF1A-AS1	1.750	1.247	2.456	3.236	0.001
Zhongzhi Jin 2018	MORT	1.510	1.082	2.108	2.422	0.015
J,Wang 2019	LACAT1	2.330	1.060	5.122	2.105	0.035
Yixin Yang 2019	CASC9	2.310	1.123	4.752	2.275	0.023
Qian Lyu 2019	MINCR	1.640	1.106	2.432	2.461	0.014
Overall		1.841	1.510	2.243	6.046	0.001
Duval and tweedie trim-and-fill analysis					Q value	
Observed values		1.841	1.510	2.243	56.746	
Adjusted values		1.524	1.262	1.840	75.001	
(I-squared = 72%, P = 0.000)						

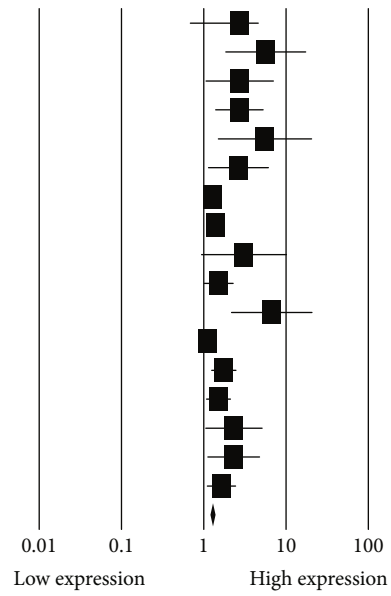

(a)

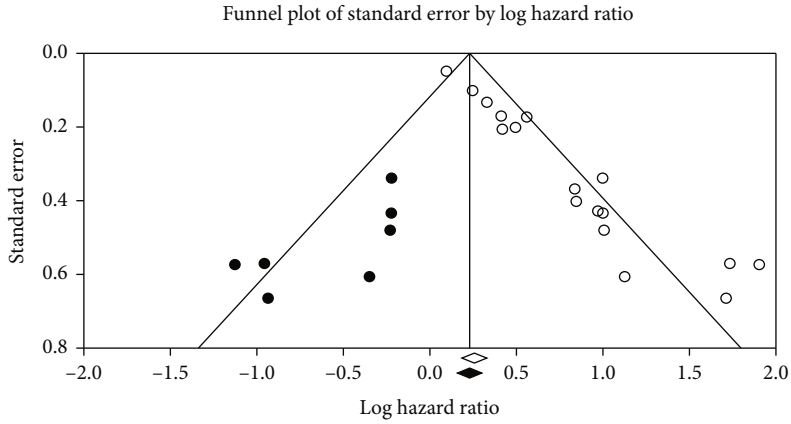

(b)

Figure 2: A meta-analysis evaluating the hazard ratio of lncRNA expression and the overall survival of OSCC. (a) The forest plot for evaluating all included studies. I^2 = 71.80% was identified as higher heterogeneity, and the random-effect model was used. Publication bias was found, and HRs were adjusted by Duval and Tweedie's trim-and-fill method. (b) The funnel plot for detecting publication bias. Observed studies were represented by white circles. Possibly missed studies, represented by black circles, were imputed by Duval and Tweedie's trim-and-fill method. The observed and theoretical combined effect sizes were represented by white and black rhombuses, respectively.

of significant publication bias in the meta-analysis. Then, we use Duval and Tweedie's trim-and-fill method to adjust the HRs. The outcome of this study was adjusted for HRs.

4. Discussion

Oral squamous cell carcinomas (OSCC) are often detected at an advanced clinical stage with metastasis, and poor prognosis of oral cancer may lead to high incidence [44]. Despite considerable advances being achieved in medical technologies for cancer diagnosis and treatment in the past decades, the 5-year survival rate for patients with OSCC remains less than 50% [45].

Accumulating evidence reveals that lncRNAs serve critical regulatory roles in diverse biological processes, including gene expression, cell invasion, migration, and tumorigenesis

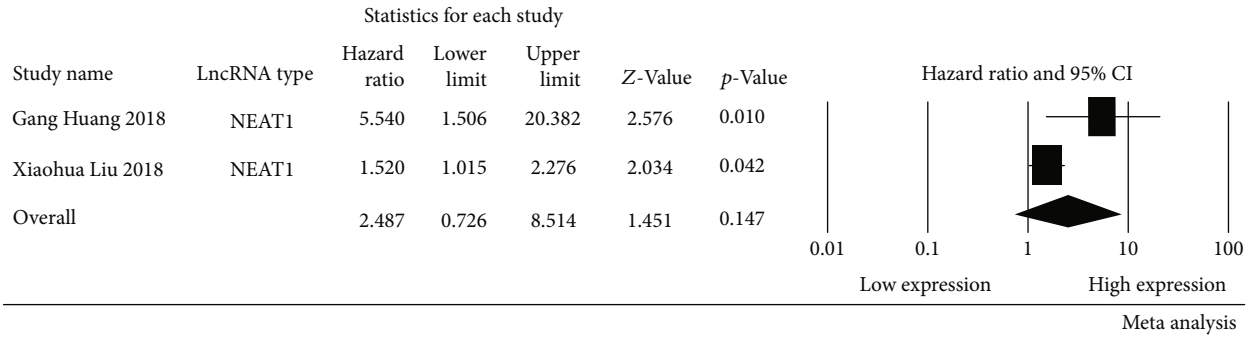

Figure 3: Forrest plots of studies evaluating hazard ratios of NEAT1 and the overall survival of OSCC patients. $I^2 = 71.05\%$ was identified as higher heterogeneity, and the random-effect model was used.

Table 4: Subgroup analyses of the prognosis of OSCC patients with lncRNA expression.

Studies (*n*)	HR (95% CI)	*p* value	Heterogeneity I^2 (%)	*p* value	*p* for Begg (2-tailed)	*p* for Egger (2-tailed)	Pub. bias	AHR[a] (95% CI)	*p* value
All studies (17)	1.84 (1.51-2.24)	<0.001	71.80	<0.01	<0.01	<0.01	Yes	1.52 (1.26-1.84)	<0.001
U&M analysis									
Univariate (13)	1.62 (1.35-1.95)	<0.001	67.48	<0.01	<0.01	<0.01	Yes	1.43 (1.20-1.71)	<0.001
Multivariate (4)	3.51 (2.16-5.71)	<0.001	9.57	0.35	0.50	0.22	Yes	2.50 (1.65-3.78)	<0.001
Source of HR									
Sur curve (9)	1.45 (1.20-1.74)	<0.001	66.98	<0.01	<0.01	<0.01	Yes	1.18 (1.10-1.27)	<0.001
Reported (8)	2.19 (1.74-2.74)	<0.001	37.28	0.12	0.04	<0.01	Yes	1.85 (1.51-2.26)	<0.001
NOS score[b]									
High (9)	1.91 (1.56-2.32)	<0.001	11.96	0.34	0.04	<0.01	Yes	1.64 (1.38-1.96)	<0.001
Medium (6)	1.92 (1.33-2.78)	<0.001	79.36	<0.01	0.05	<0.01	Yes	1.45 (1.01-2.07)	0.04
Low (2)	3.78 (1.92-7.44)	<0.001	36.72	0.21	—	—	NO	—	—

Abbreviations: HR: hazard ratio; CI: confidence interval; Pub. bias: publication bias; AHR: adjusted HR; U&M analysis: univariate & multivariate analysis. [a]AHR: if publication bias was found, the HRs were adjusted and reevaluated; if the number of combined studies was not >3, the publication bias could not be analyzed. [b]NOS score: the NOS score was used to evaluate the quality of the included studies, and NOS scores of 1–3, 4–6, and 7–9 were considered to indicate low, medium, and high quality, respectively.

[46]. Previous meta-analyses have demonstrated high expression of lncRNAs to correlate with poor prognosis in patients with various cancers, such as ovarian [11], colorectal [11], gastrointestinal [12], and lung cancers [13]. However, no meta-analyses have revealed the role of lncRNAs in OSCC prognosis.

We conducted a meta-analysis to validate the accuracy and value of the theoretical results of lncRNAs as prognostic molecular markers in patients with OSCC. A total of 17 studies, including 1384 patients, were enrolled within our meta-analysis. The expression of *PDIA3P*, *SOX21-AS1*, *LINC00668*, *FTH1P3*, *NEAT1*, *HOTAIR*, *DLEU1*, *ANPIL*, *CEBPA-AS1*, *H19*, *HNF1AAS1*, *MORT*, *LACAT1*, *CASC9*, and *MINCR* was upregulated. There are no downexpression lncRNAs in participants of this analysis. The analysis showed a reliable result for upregulated lncRNA expression to correlate with poor prognosis in OSCC (HR: 1.52, 95% CI: [1.26, 1.84]; $p < 0.001$, random effect). Also, subgroup analysis revealed that lncRNA expression correlated with prognosis, while the analysis method, source of HR, and NOS score evaluation did not significantly affect the pooled results of this meta-analysis. By our analysis, these findings suggest that lncRNA can be developed as a prognostic and therapeutic biomarker in OSCC.

Several lncRNAs with high HR in this study have also been reported in other cancers other than OSCC accidents. For example, *CEBPA-AS1* with high HRs (HR: 6.71, 95% CI: 3.61-8.73) was also reported in gastric cancer. Ke et al. found that high expression of *CEBPA-AS1* has a poor prognosis patients with gastric cancer [47]. *HOTAIR*, as one of the most crucial lncRNA, has been extensively studied, and overexpression *HOTAIR* is correlated with poor survival for breast, colon, and liver cancer patients [48]. This study also showed that patients with high expression *HOTAIR* have a poor prognosis in OSCC. While the prognostic value of *NEAT1* was assessed, and the pooled HRs were 2.49 (95% CI: 0.73–8.51, $p = 0.15$, random effect), the results showed that *NEAT1* was not statistically significantly associated with OS. Only two studies were included in this evaluation, resulting in a low power of evidence. *NEAT1* has been found to be associated with many different types of cancer prognosis. Fu et al. identified that lncRNA *NEAT1* was overexpressed in gastric cancer tissues and cell lines, and patients with high levels of *NEAT1* had more reduced survival than

those with lower levels of *NEAT1* [49]. Chen et al. found that high expression of *NEAT1* predicts poor prognosis and has a crucial regulatory role in esophageal squamous cell carcinoma [50]. Therefore, further research needs to confirm the mechanisms of *NEAT1* in the progression of OSCC.

In this study, we also collected mechanisms of lncRNAs; 9 of the included studies investigated the correlation between lncRNAs and microRNAs. It could be evidenced from these researches that the relationship between lncRNAs and microRNAs is associated with cancer incidence. The same lncRNA is associated with the occurrence and development of different cancers, but the mechanism is still unclear. In the future, research hotspots may be focused on the method of simultaneous intervention with multiple RNA by exploring the interrelationship between lncRNA and multiple types of RNA.

It should be stressed that there are several limitations in our meta-analysis. Firstly, only 17 studies were eligible in this meta-analysis, which might weaken the reliability of our results. Secondly, remarkable statistical heterogeneity ($I^2 = 71.80\%$) was observed, which may be due to the differences in cancer types, internal control, cutoff value, clinical characteristics, and sample sizes. The geographical bias may be present, as all studies were performed in Asia. As demonstrated in previous studies, people of different race/ethnicity vary in their risk of developing OCSS, and the differences in OS may link both to the genetic and the lifestyle. We hope that other countries in different regions will also conduct relevant research and reports in the future. Finally, some HRs were extracted from the survival curves, which may lead to small statistical errors.

5. Conclusion

Despite several limitations described above, the meta-analysis offers evidence that upregulated lncRNAs are significantly corrected with poor OS in Asian patients with OSCC, which demonstrated that the lncRNAs could serve as the prognostic factor for Asian patients with OSCC. However, large-scale and comprehensive studies are needed to improve the credibility of our findings and thus promote the clinical utility of lncRNAs in OSCC prognosis evaluation.

Data Availability

The data used to support the findings of this study are included within the article.

Conflicts of Interest

The authors declare that they have no conflicts of interest.

Authors' Contributions

Yu Wang and Peng Wang are equal contributors and co-first authors.

Acknowledgments

This work was supported by the Yunnan Applied Basic Research Projects (2019FB107).

References

[1] L. J. Jin, I. B. Lamster, J. S. Greenspan, N. B. Pitts, C. Scully, and S. Warnakulasuriya, "Global burden of oral diseases: emerging concepts, management and interplay with systemic health," *Oral Diseases*, vol. 22, no. 7, pp. 609–619, 2016.

[2] N. W. Johnson, P. Jayasekara, and A. A. Amarasinghe, "Squamous cell carcinoma and precursor lesions of the oral cavity: epidemiology and aetiology," *Periodontology 2000*, vol. 57, no. 1, pp. 19–37, 2011.

[3] H. Takahashi, S. Yanamoto, S. Yamada et al., "Effects of postoperative chemotherapy and radiotherapy on patients with squamous cell carcinoma of the oral cavity and multiple regional lymph node metastases," *International Journal of Oral and Maxillofacial Surgery*, vol. 43, no. 6, pp. 680–685, 2014.

[4] A. C. Chi, T. A. Day, and B. W. Neville, "Oral cavity and oropharyngeal squamous cell carcinoma–an update," *CA: A Cancer Journal for Clinicians*, vol. 65, no. 5, pp. 401–421, 2015.

[5] C. R. Leemans, B. J. Braakhuis, and R. H. Brakenhoff, "The molecular biology of head and neck cancer," *Nature Reviews. Cancer*, vol. 11, no. 1, pp. 9–22, 2011.

[6] Z. Shi and M. S. Stack, "Molecules of cell adhesion and extracellular matrix proteolysis in oral squamous cell carcinoma," *Histology and Histopathology*, vol. 25, no. 7, pp. 917–932, 2010.

[7] N. Yamamoto, K. Sato, T. Yamauchi et al., "A 5-year activity report from the oral cancer center, Tokyo Dental College," *The Bulletin of Tokyo Dental College*, vol. 54, no. 4, pp. 265–273, 2013.

[8] M. Guttman and J. L. Rinn, "Modular regulatory principles of large non-coding RNAs," *Nature*, vol. 482, no. 7385, pp. 339–346, 2012.

[9] S. Djebali, C. A. Davis, A. Merkel et al., "Landscape of transcription in human cells," *Nature*, vol. 489, no. 7414, pp. 101–108, 2012.

[10] V. A. Moran, R. J. Perera, and A. M. Khalil, "Emerging functional and mechanistic paradigms of mammalian long noncoding RNAs," *Nucleic Acids Research*, vol. 40, no. 14, pp. 6391–6400, 2012.

[11] L. Ning, Y. C. Hu, S. Wang, and J. H. Lang, "Altered long noncoding RNAs and survival outcomes in ovarian cancer: a systematic review and meta-analysis (PRISMA compliant)," *Medicine (Baltimore)*, vol. 97, no. 32, article e11481, 2018.

[12] W. Kang, Q. Zheng, J. Lei, C. Chen, and C. Yu, "Prognostic value of long noncoding RNAs in patients with gastrointestinal cancer: a systematic review and meta-analysis," *Disease Markers*, vol. 2018, Article ID 5340894, 15 pages, 2018.

[13] W. Pan, C. Wu, Z. Su et al., "Genetic polymorphisms of noncoding RNAs associated with increased head and neck cancer susceptibility: a systematic review and meta-analysis," *Oncotarget*, vol. 8, no. 37, pp. 62508–62523, 2017.

[14] Y. Sanchez and M. Huarte, "Long non-coding RNAs: challenges for diagnosis and therapies," *Nucleic Acid Therapeutics*, vol. 23, no. 1, pp. 15–20, 2013.

[15] K. Z. Thin, X. Liu, X. Feng, S. Raveendran, and J. C. Tu, "lncRNA-DANCR: a valuable cancer related long non-

coding RNA for human cancers," *Pathology, Research and Practice*, vol. 214, no. 6, pp. 801–805, 2018.

[16] Y. Wan and H. Y. Chang, "HOTAIR: flight of noncoding RNAs in cancer metastasis," *Cell Cycle*, vol. 9, no. 17, pp. 3391-3392, 2010.

[17] J. L. Rinn, M. Kertesz, J. K. Wang et al., "Functional Demarcation of Active and Silent Chromatin Domains in Human _HOX_ Loci by Noncoding RNAs," *Cell*, vol. 129, no. 7, pp. 1311–1323, 2007.

[18] Y. Wu, L. Zhang, L. Zhang et al., "Long non-coding RNA HOTAIR promotes tumor cell invasion and metastasis by recruiting EZH2 and repressing E-cadherin in oral squamous cell carcinoma," *International Journal of Oncology*, vol. 46, no. 6, pp. 2586–2594, 2015.

[19] Y. Hong, H. He, W. Sui, J. Zhang, S. Zhang, and D. Yang, "Long non-coding RNA H1 promotes cell proliferation and invasion by acting as a ceRNA of miR-138 and releasing EZH2 in oral squamous cell carcinoma," *International Journal of Oncology*, vol. 52, no. 3, pp. 901–912, 2018.

[20] X. Hu, Z. Qiu, J. Zeng, T. Xiao, Z. Ke, and H. Lyu, "A novel long non-coding RNA, AC012456.4, as a valuable and independent prognostic biomarker of survival in oral squamous cell carcinoma," *PeerJ*, vol. 6, article e5307, 2018.

[21] M. J. Page, J. E. McKenzie, P. M. Bossuyt et al., "The PRISMA 2020 statement: an updated guideline for reporting systematic reviews," *BMJ*, vol. 372, 2021.

[22] D. Moher, D. G. Altman, A. Liberati, and J. Tetzlaff, "PRISMA statement," *Epidemiology*, vol. 22, no. 1, p. 128, 2011.

[23] C. K.-L. Lo, D. Mertz, and M. Loeb, "Newcastle-Ottawa scale: comparing reviewers' to authors' assessments," *BMC Medical Research Methodology*, vol. 14, no. 1, pp. 45–45, 2014.

[24] J. F. Tierney, L. A. Stewart, D. Ghersi, S. Burdett, and M. R. Sydes, "Practical methods for incorporating summary time-to-event data into meta-analysis," *Trials*, vol. 8, no. 1, p. 16, 2007.

[25] M. K. B. Parmar, V. Torri, and L. J. S. Stewart, "Extracting summary statistics to perform meta-analyses of the published literature for survival endpoints," *Statistics in Medicine*, vol. 17, no. 24, pp. 2815–2834, 1998.

[26] J. Bowden, J. F. Tierney, A. J. Copas, and S. Burdett, "Quantifying, displaying and accounting for heterogeneity in the meta-analysis of RCTs using standard and generalised Q statistics," *BMC Medical Research Methodology*, vol. 11, no. 1, p. 41, 2011.

[27] M. Egger, G. Davey Smith, M. Schneider, and C. Minder, "Bias in meta-analysis detected by a simple, graphical test," *BMJ*, vol. 315, no. 7109, pp. 629–634, 1997.

[28] S. Duval and R. Tweedie, "Trim and fill: a simple funnel-plot-based method of testing and adjusting for publication bias in meta-analysis," *Biometrics*, vol. 56, no. 2, pp. 455–463, 2000.

[29] L. Chai, Y. Yuan, C. Chen, J. Zhou, and Y. Wu, "The role of long non-coding RNA ANRIL in the carcinogenesis of oral cancer by targeting miR-125a," *Biomedicine & Pharmacotherapy*, vol. 103, pp. 38–45, 2018.

[30] Y. Guo, Y. Ma, X. Hu, R. Song, L. Zhu, and M. Zhong, "Long non-coding RNA CEBPA-AS1 correlates with poor prognosis and promotes tumorigenesis via CEBPA/Bcl2 in oral squamous cell carcinoma," *Cancer Biology & Therapy*, vol. 19, no. 3, pp. 205–213, 2018.

[31] G. Huang, X. He, and X. L. Wei, "lncRNA NEAT1 promotes cell proliferation and invasion by regulating miR-365/RGS20 in oral squamous cell carcinoma," *Oncology Reports*, vol. 39, no. 4, pp. 1948–1956, 2018.

[32] X. Liu, W. Shang, and F. Zheng, "Long non-coding RNA NEAT1 promotes migration and invasion of oral squamous cell carcinoma cells by sponging microRNA-365," *Experimental and Therapeutic Medicine*, vol. 16, no. 3, pp. 2243–2250, 2018.

[33] K. Nishiyama, R. Maruyama, T. Niinuma et al., "Screening for long noncoding RNAs associated with oral squamous cell carcinoma reveals the potentially oncogenic actions of DLEU1," *Cell Death & Disease*, vol. 9, no. 8, p. 826, 2018.

[34] T. Shao, J. Huang, Z. Zheng, Q. Wu, T. Liu, and X. Lv, "SCCA, TSGF, and the long non-coding RNA AC007271.3 are effective biomarkers for diagnosing oral squamous cell carcinoma," *Cellular Physiology and Biochemistry*, vol. 47, no. 1, pp. 26–38, 2018.

[35] C. C. Sun, L. Zhang, G. Li et al., "The lncRNA PDIA3P interacts with miR-185-5p to modulate oral squamous cell carcinoma progression by targeting cyclin D2," *Molecular Therapy - Nucleic Acids*, vol. 9, pp. 100–110, 2017.

[36] C. M. Yang, T. H. Wang, H. C. Chen et al., "Aberrant DNA hypermethylation-silenced SOX21-AS1 gene expression and its clinical importance in oral cancer," *Clinical Epigenetics*, vol. 8, no. 1, p. 129, 2016.

[37] C. Z. Zhang, "Long non-coding RNA FTH1P3 facilitates oral squamous cell carcinoma progression by acting as a molecular sponge of miR-224-5p to modulate fizzled 5 expression," *Gene*, vol. 607, pp. 47–55, 2017.

[38] C. Z. Zhang, "Long intergenic non-coding RNA 668 regulates VEGFA signaling through inhibition of miR-297 in oral squamous cell carcinoma," *Biochemical and Biophysical Research Communications*, vol. 489, no. 4, pp. 404–412, 2017.

[39] Z. Jin, S. Jiang, S. Jian, and Z. Shang, "Long noncoding RNA MORT overexpression inhibits cancer cell proliferation in oral squamous cell carcinoma by downregulating ROCK1," *Journal of Cellular Biochemistry*, vol. 120, no. 7, pp. 11702–11707, 2019.

[40] Z. Liu, H. Li, S. Fan, H. Lin, and W. Lian, "STAT3-induced upregulation of long noncoding RNA HNF1A-AS1 promotes the progression of oral squamous cell carcinoma via activating notch signaling pathway," *Cancer Biology & Therapy*, vol. 20, no. 4, pp. 444–453, 2019.

[41] Q. Lyu, L. Jin, X. Yang, and F. Zhang, "LncRNA MINCR activates Wnt/β-catenin signals to promote cell proliferation and migration in oral squamous cell carcinoma," *Pathology, Research and Practice*, vol. 215, no. 5, pp. 924–930, 2019.

[42] J. Wang, F. Huo, X. R. Wang, and Y. Y. Xu, "lncRNA LACAT1 promotes proliferation of oral squamous cell carcinoma cells by inhibiting microRNA-4301," *European Review for Medical and Pharmacological Sciences*, vol. 23, no. 6, pp. 2427–2435, 2019.

[43] Y. Yang, D. Chen, H. Liu, and K. Yang, "Increased expression of lncRNA CASC9 promotes tumor progression by suppressing autophagy-mediated cell apoptosis via the AKT/mTOR pathway in oral squamous cell carcinoma," *Cell Death & Disease*, vol. 10, no. 2, p. 41, 2019.

[44] C. Rivera, "Essentials of oral cancer," *International Journal of Clinical and Experimental Pathology*, vol. 8, no. 9, pp. 11884–11894, 2015.

[45] A. Sharma, K. Boaz, and S. Natarajan, "Understanding patterns of invasion: a novel approach to assessment of

podoplanin expression in the prediction of lymph node metastasis in oral squamous cell carcinoma," *Histopathology*, vol. 72, no. 4, pp. 672–678, 2018.

[46] Z. Quan, D. Zheng, and H. Qing, "Regulatory roles of long non-coding RNAs in the central nervous system and associated neurodegenerative diseases," *Frontiers in Cellular Neuroscience*, vol. 11, p. 175, 2017.

[47] D. Ke, H. Li, Y. Zhang et al., "The combination of circulating long noncoding RNAs AK001058, INHBA-AS1, MIR4435-2HG, and CEBPA-AS1 fragments in plasma serve as diagnostic markers for gastric cancer," *Oncotarget*, vol. 8, no. 13, pp. 21516–21525, 2017.

[48] K. Kim, I. Jutooru, G. Chadalapaka et al., "HOTAIR is a negative prognostic factor and exhibits pro-oncogenic activity in pancreatic cancer," *Oncogene*, vol. 32, no. 13, pp. 1616–1625, 2013.

[49] J. W. Fu, Y. Kong, and X. Sun, "Long noncoding RNA NEAT1 is an unfavorable prognostic factor and regulates migration and invasion in gastric cancer," *Journal of Cancer Research and Clinical Oncology*, vol. 142, no. 7, pp. 1571–1579, 2016.

[50] X. Chen, J. Kong, Z. Ma, S. Gao, and X. Feng, "Up regulation of the long non-coding RNA NEAT1 promotes esophageal squamous cell carcinoma cell progression and correlates with poor prognosis," *American Journal of Cancer Research*, vol. 5, no. 9, pp. 2808–2815, 2015.

Hindawi
Disease Markers
Volume 2021, Article ID 9761898, 1 page
https://doi.org/10.1155/2021/9761898

Corrigendum

Corrigendum to "scFv against HSP60 of *Strongyloides sp.* and Its Application in the Evaluation of Parasite Frequency in the Elderly"

Camila Botelho Miguel,[1,2] Marcelo Arantes Levenhagen,[3] Fabiana de Almeida Araújo Santos,[3] Julia Maria Costa-Cruz,[3] Luiz Ricardo Goulart,[3] Patrícia Terra Alves,[3] Carlos Ueira-Vieira,[3] Patrícia Kellen Martins Oliveira Brito,[4] Angelica Oliveira Gomes,[2] Javier Emilio Lazo-Chica,[2] Carlo José Freire Oliveira,[2] and Wellington Francisco Rodrigues[1]

[1]*Federal University of Triângulo Mineiro (UFTM), 38061-500 Uberaba, MG, Brazil*
[2]*University Center of Mineiros-Unifimes, 75, 830-000 Mineiros, GO, Brazil*
[3]*Federal University of Uberlândia, 38400-902, Uberlandia, MG, Brazil*
[4]*University of São Paulo, 14049900, Ribeirao Preto, SP, Brazil*

Correspondence should be addressed to Wellington Francisco Rodrigues; wellington.frodrigues@hotmail.com

Received 1 June 2021; Accepted 1 June 2021; Published 14 June 2021

In the article titled "scFv against HSP60 of *Strongyloides* sp. and Its Application in the Evaluation of Parasite Frequency in the Elderly" [1], Dr. Fabiana de Almeida Araújo Santos was missing from the author list, who contributed to the data analysis, revision of the manuscript, and approval of the final version for publication. The corrected author list is shown above.

References

[1] C. B. Miguel, M. A. Levenhagen, J. M. Costa-Cruz et al., "scFv against HSP60 of Strongyloides sp. and Its Application in the Evaluation of Parasite Frequency in the Elderly," *Disease Markers*, vol. 2020, Article ID 4086929, 6 pages, 2020.

Hindawi
Disease Markers
Volume 2020, Article ID 9130719, 15 pages
https://doi.org/10.1155/2020/9130719

Research Article

In Silico Identification of New Targets for Diagnosis, Vaccine, and Drug Candidates against *Trypanosoma cruzi*

Rafael Obata Trevisan,[1] Malú Mateus Santos,[1] Chamberttan Souza Desidério,[1] Leandro Gomes Alves,[1,2] Thiago de Jesus Sousa,[2] Letícia de Castro Oliveira,[1] Arun Kumar Jaiswal,[1,2] Sandeep Tiwari,[2] Weslley Guimarães Bovi,[1] Mariana de Oliveira-Silva,[1] Juliana Cristina Costa-Madeira,[1] Lúcio Roberto Cançado Castellano,[3] Marcos Vinicius Silva,[1] Vasco Azevedo,[2] Virmondes Rodrigues Junior,[1] Carlo José Freire Oliveira,[1] and Siomar de Castro Soares[1]

[1]*Department of Microbiology, Immunology and Parasitology, Federal University of Triângulo Mineiro, Uberaba, Minas Gerais, Brazil*
[2]*Department of Genetics, Ecology and Evolution, Federal University of Minas Gerais, Belo Horizonte, Minas Gerais, Brazil*
[3]*Human Immunology Research and Education Group-GEPIH, Technical School of Health, Federal University of Paraíba, João Pessoa, Paraíba, Brazil*

Correspondence should be addressed to Carlo José Freire Oliveira; carlo.oliveira@uftm.edu.br

Received 29 November 2019; Revised 23 March 2020; Accepted 24 November 2020; Published 10 December 2020

Academic Editor: Paolo Cameli

Chagas disease is a neglected tropical disease caused by the parasite *Trypanosoma cruzi*. Despite the efforts and distinct methodologies, the search of antigens for diagnosis, vaccine, and drug targets for the disease is still needed. The present study is aimed at identifying possible antigens that could be used for diagnosis, vaccine, and drugs targets against *T. cruzi* using reverse vaccinology and molecular docking. The genomes of 28 *T. cruzi* strains available in GenBank (NCBI) were used to obtain the genomic core. Then, subtractive genomics was carried out to identify nonhomologous genes to the host in the core. A total of 2630 conserved proteins in 28 strains of *T. cruzi* were predicted using OrthoFinder and Diamond software, in which 515 showed no homology to the human host. These proteins were evaluated for their subcellular localization, from which 214 are cytoplasmic and 117 are secreted or present in the plasma membrane. To identify the antigens for diagnosis and vaccine targets, we used the VaxiJen software, and 14 nonhomologous proteins were selected showing high binding efficiency with MHC I and MHC II with potential for *in vitro* and *in vivo* tests. When these 14 nonhomologous molecules were compared against other trypanosomatids, it was found that the retrotransposon hot spot (RHS) protein is specific only for *T. cruzi* parasite suggesting that it could be used for Chagas diagnosis. Such 14 proteins were analyzed using the IEDB software to predict their epitopes in both B and T lymphocytes. Furthermore, molecular docking analysis was performed using the software MHOLline. As a result, we identified 6 possible *T. cruzi* drug targets that could interact with 4 compounds already known as antiparasitic activities. These 14 protein targets, along with 6 potential drug candidates, can be further validated in future studies, *in vivo*, regarding Chagas disease.

1. Introduction

Chagas disease is a neglected tropical disease that affects around 8 million people worldwide, caused by the protozoan *Trypanosoma cruzi* [1]. It is primarily transmitted by blood-borne vectors such as triatomines and also through oral ingestion, blood donation, and organ transplantation, especially in countries where blood donors are not screened for

T. cruzi. Clinical manifestations of the disease may vary from severe myocarditis and/or changes in the gastrointestinal system, presenting megaesophagus and/or megacolon, to an asymptomatic or undetermined form [2]. During these phases, individuals have a strong cellular and humoral immune response [3, 4]. Despite these cellular and humoral immune responses, there is no diagnostic antigen yet to characterize and identify each of these phases of the disease. Still, it is not clear which mechanisms trigger the transition from asymptomatic to symptomatic but what is known are the factors involved in the etiopathogenesis that are related to the parasite strains, parasite load, infection phase, and the host immune response [5].

The development of an anti-*T. cruzi* vaccine has proven to be a challenging task due to difficulties of finding antigens or formulations with effective protection and also because of the risk of developing autoimmunity, which is considered by many to be a potential cause of disease progression and/or pathogenesis [6]. In this regard, a wide variety of vaccine formulations have been tested over the past decade, thus providing strong evidence that *T. cruzi* can be controlled by vaccines in experimental models. However, these studies have shown that vaccine formulation and vaccine antigens are still not satisfactory; thus, further studies are essential to obtain a vaccine that is truly effective for the entire population [6, 7].

The vaccines developed using conventional approaches and already tested in experimental models are based on inactivated or attenuated pathogens or isolated parasite antigens. Although successful in several cases, these vaccines were not enough for their approval or multicenter trials in humans [8–10]. Regarding the vaccines based on previously selected antigens, there are still few studies investigating such antigen properties, being necessary to explore their origin and diversity, as well the most important epitopes and immune response activated against each one [6, 7]. The application of computational methods to analyze the immunological process, known as immunoinformatics, is revolutionizing vaccine development. In this regard, reverse vaccinology is approachable to identify vaccine candidates in the postgenomic era with reduced cost and time. It is a genome-based screening of epitopes for B and T cells from predicted proteins that can elicit an immune response. First, conserved proteins among all strains of any species of interest are predicted using immunoinformatics approaches such as pangenomics aimed at finding common vaccine targets against all pathogen strains. Since vaccines may eventually induce an autoimmune response, it is important to analyze conserved predicted proteins against host proteins through a subtractive genomics approach. The subcellular localization prediction is also needed since the membrane and secreted proteins are the first to contact the host. Then, MHC I and II bindings are predicted, looking forward to possible diagnosis and vaccine targets. All stages are aimed at filtering targets until they reach what is most likely to generate an effective immune response [11].

The available drug used for Chagas disease treatment presents various side effects and variable cure rates at different stages of the disease. Moreover, these drugs were developed in the 1970s when there are only a few studies focused on this area. Considering this, molecular docking analysis is a useful tool that describes the interaction between small molecules (compound/ligand) with active sites, receptor residues (protein) of interest [12]. This approach is considered successful when it can identify the nearest ligand with the receptor, discovering the geometrical shape of the ligand within a boundary of specific obstructions and their connections [12]. It had become an important computational technique, playing an essential role in drug discovery against various pathogens.

Thus, this present study is aimed at identifying potential diagnostic and vaccine candidates and pharmacological targets for *T. cruzi*/Chagas disease using subtractive genomics, reverse vaccinology, and molecular docking tools.

2. Material and Methods

2.1. Data Collection, Gene Prediction, and Orthology Analyses. The complete genome sequences of 28 *T. cruzi* strains were obtained from the GenBank database, available on the National Center for Biotechnology Information (NCBI). Then, the GeneMark group software was used for gene prediction, homogenizing the predictions in order to avoid unexpected results and possible misinterpretations.

The orthology of the predicted proteins was determined using OrthoFinder through standard mode parameters in the Diamond tool (v0.9.22.123) all-versus-all. OrthoFinder is a fast, accurate, and comprehensive analysis tool used in comparative genomics. This software finds orthologists and orthogroups, determining phylogenetic trees, and also provides comprehensive statistics for comparative genomics analysis [13].

2.2. Identification of Intraspecies Conserved Proteins Nonhomologous to the Host. Vaccine and drug targets must avoid autoimmune responses, and diagnostic targets must be molecules specific for only one microorganism. For this, subtractive genomics was carried out to identify, in the core, nonhomologous proteins to the host. We used BLASTp from the core genome against human proteins, which are found in databases provided by NCBI; proteins from the core genome that were homologous to human proteins were excluded.

2.3. Protein Subcellular Localization. The proteins were evaluated for their subcellular localization using PSORT [14] and von Heijne signal sequence recognition [15]. PSORT predicts the presence of signal peptide by the McGeoch method [14], which is considered an N-terminally charged region and a central hydrophobic region. A score is calculated from 3 values: length of the hydrophobic region, the peak value of that region, and the net charge in the N-terminally charged region. Thus, a large positive discriminant score indicates a high possibility of having a signal sequence, whether cleaved or not. After PSORT, a second method is used: von Heijne signal sequence recognition [15]. This is a weight matrix method and incorporates information around the cleavage site, meaning it can detect signal sequences or not. A large positive output means more chances of being a cleavable signal sequence [16]. Data generated by PSORT classify proteins

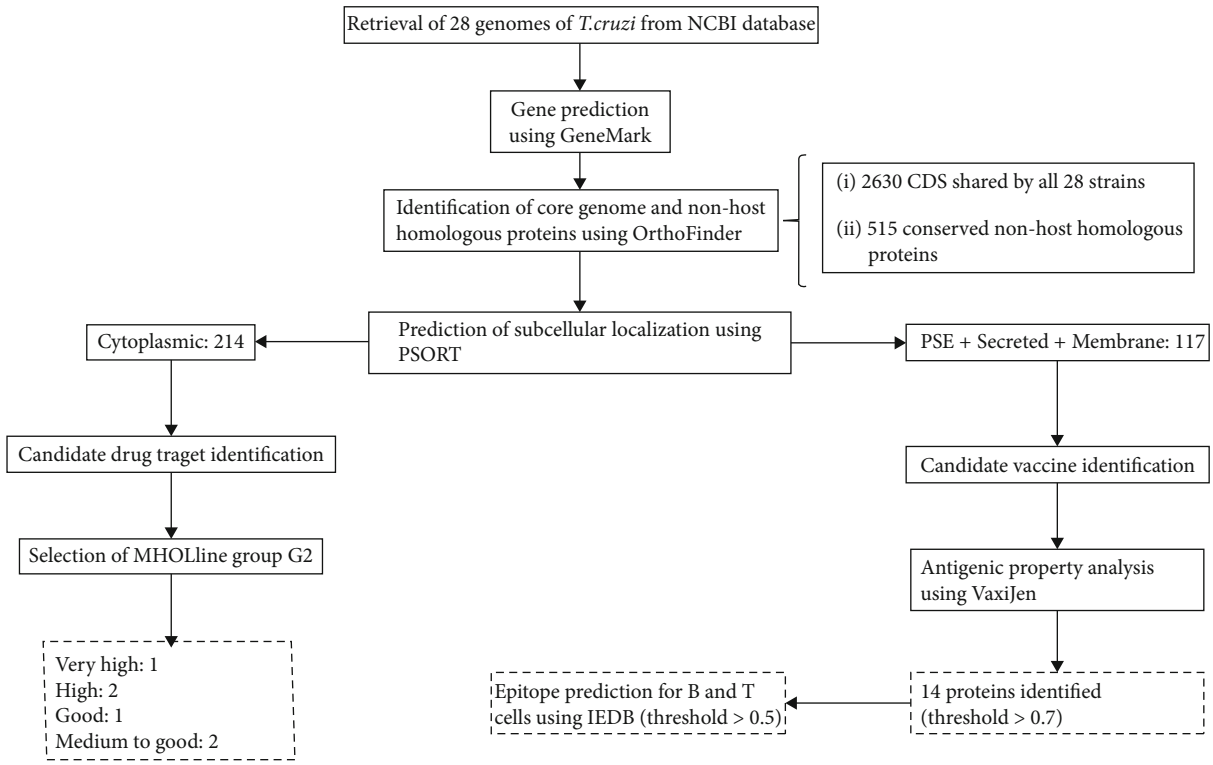

Figure 1: Workflow with the methods and the total number of proteins identified in each step.

as cytoplasmic, secreted (those that present signal to the endoplasmic reticulum and secretory system vesicles), nuclear, or membrane proteins. We submitted to MHOLline the multifasta files containing all amino acid sequences, regardless of their subcellular location [17]. This online tool uses various dependencies such as HMMTOP, BLAST, BATS, MODELLER, and PROCHECK to predict the three-dimensional modeling of target proteins. Only very high, high, good, and medium to good quality sequences were used from MHOLline classified groups G2. G2 structures are those that have high levels of identity and were chosen for the docking molecular process [17].

2.4. Identification of Targets for Vaccines. The proteins predicted as secreted and present in the plasma membrane of the parasite *T. cruzi* were submitted to VaxiJen to evaluate antigenicity and immunogenicity [18]. This tool is based on the transformation of cross-auto-covariance (ACC) of protein sequences into uniform vectors of major amino acid properties [18]. Thus, ACC transformations remove the influence of sequence length. Antigenicity and immunogenicity are not simple linear properties, and the ACC physicochemical properties process adequately reflects the discrimination between antigen and nonantigen [18]. All proteins that indicated antigenicity above the cutoff (>0.7) were considered possible vaccine targets. The molecules identified were also evaluated for their similarities to proteins of other trypanosomatids to prospect targets that could be used as diagnostic tools.

2.5. Identification of Targets for Diagnosis. The proteins predicted as secreted and present in the plasma membrane of the parasite *T. cruzi* were also submitted to BLASTp (protein-protein blast), NCBI, to evaluate similarities to other organisms, including other trypanosomatids. This is important because the molecule could induce a great immune response and be particular to only one parasite such as the case of *T. cruzi*. All proteins that indicated antigenicity above the cutoff (>0.7) were considered possible for a diagnostic target but only one was specific for *T. cruzi*.

2.6. Epitope Prediction. The Immune Epitope Database and Analysis Resource (IEDB) contains a diverse catalog of information on immunogenic epitopes and immune response cells, using this information to predict and analyze epitope candidates, i.e., molecular targets of the adaptive immune response [19]. T cell epitope prediction for MHC I and II was performed through the tool PredictionMethod: IEDB recommended version 2.19, available at https://www.iedb.org/. For the epitope prediction for MHC I, the option human MHC was selected and all HLA allele references were used, and for MHC II (http://tools.iedb.org/mchii/), the following alleles were analyzed: HLA-DRB1∗03:01, HLA-DBR1∗07:01, HLA-DRB1∗15:01, HLA-DRB3∗01:01, HLA-DRB3∗02:02, HLA-DRB4∗01:01, and HLA-DRB5∗01:01. B cell epitopes were predicted using the tool found at http://tools.iedb.org/main/bcell/: linear prediction of protein sequence epitopes. Some methods are used to predict linear B cell epitopes, based on antigen sequence characteristics

Table 1: General information about the 28 *T. cruzi* strains used in this work.

DTU	Strain	Protein number[1]	Size	GC (%)	Assembly
I	G	12544	25, 2	47, 4	GCA_003719455.1
I	Dm28c	29158	27, 3	50, 6	GCA_000496795.1
I	Colombiana	18033	30, 9	50, 8	GCA_003594625.1
I	B7	19174	34, 2	50, 9	GCA_000300495.1
I	Sylvio X10/1	22851	38, 6	51, 2	GCA_000188675.2
I	JR cl. 4	23024	41, 5	51, 2	GCA_000331405.1
I	Dm28c	15105	51	51, 6	GCA_002219105.2
I	Dm28c	30416	53, 3	51, 6	GCA_003177105.1
II	S44a	8043	17, 2	45	GCA_003594705.1
II	S154a	9007	19, 3	—	GCA_003594715.1
II	Ycl6	12514	25, 8	46, 6	GCA_003594465.1
II	Ycl2	12647	25, 9	46, 6	GCA_003594485.1
II	Ycl4	12734	26, 1	46, 6	GCA_003594405.1
II	S92a	12924	27, 1	46, 4	GCA_003594445.1
II	S162a	12953	27, 3	45, 3	GCA_003594605.1
II	S15	13140	27, 5	46, 2	GCA_003594585.1
II	S23b	13073	28, 1	45, 2	GCA_003594425.1
II	S11	13264	28, 5	45, 1	GCA_003594385.1
II	Y	21829	30	50, 6	GCA_003594645.1
II	Esmeraldo cl. 3	19931	38, 1	50, 6	GCA_000327425.1
II	Y	21829	39	—	GCA_002749425.1
III	231	19054	35, 4	48, 6	GCA_900252365.1
V	Arequipa	12912	19, 1	—	GCA_003594685.1
V	Bug2148	31880	55, 2	51, 3	GCA_002749415.1
VI	CL	28855	65	39, 8	GCA_003719155.1
VI	Tula cl2	44849	83, 5	51, 1	GCA_000365225.1
VI	TCC	51888	87, 1	51, 7	GCA_003177095.1
VI	CL Brener	51521	89, 9	51, 7	GCA_000209065.1

[1]GeneMarkPrediction.

using amino acid scales and HMMs (*hidden Markov model*); the sequence of interest was analyzed by the BepiPred 2.0 linear epitope prediction.

2.7. Identification of Drug Targets. Compounds described in the literature with antiparasitic activity, whether natural, isolated from medicinal plants, or secondary metabolites, were selected and a library of ligands was created. The structures of 67 compounds were downloaded from PubChem (https://pubchem.ncbi.nlm.nih.gov/) [20] in .sdf format and converted to .PDB using the Open Babel tool (v-2.4.1) [21]. PDB format was used to assign Gasteiger atomic partial loads and convert all binders to PDBQT format using the prepare_ligand4.py script on the terminal.

The 3D structure information and drainage analysis play an important role in pathogen target prioritization and authentication [22]. The three-dimensional structure of the final drug targets identified by the MHOLline workflow (http://www.mholline.lncc.br/) was submitted to the DoGSiteScorer druggability analysis [23]. DoGSiteScorer is an automated online tool that calculates the drug's ability to interact with protein wells. For each identified cavity, the tool provides the cavity residues and a capacity score ranging from 0 to 1 [23]. Additionally, three-dimensional drug target protein structures were identified and converted to the required PDBQT format using ADT (Auto Dock Tool), MGL Tool (Version 1.5.4) [24]. For each target, a grid box in the center of the active site (comprising residues obtained from DoGSiteScorer) was created for docking analysis.

Table 2: Subcellular localization of *T. cruzi* proteins by PSORT.

Localization	Number of proteins
Cytoplasmic	214
Nuclear	183
Endoplasmic reticulum	78
Plasma membrane	36
Vesicle secretory system	3
Vacuolar	1

Table 3: Potential vaccine candidates against *T. cruzi*.

Product-protein	Protein access	Subcellular location	VaxiJen (threshold > 0.7)	*E* value
MASP *T. cruzi* Dm28c	AYLP01000395	Plasma membrane	0.9138	0.0
MASP *T. cruzi* Dm28c	AYLP01000301	Plasma membrane	0.8387	0.0
MASP *T. cruzi* Dm28c	AYLP01000226	Plasma membrane	0.8157	0.0
Hypothetical protein *T. cruzi* CL Brener	XP_815161	Endoplasmic reticulum	0.7957	$5E-119$
Hypothetical protein TcG_12168	MKKV01000794	Vesicle secretory system	0.7869	$4E-19$
Surface protease GP63	MKQG01002643	Endoplasmic reticulum	0.7859	$2E-16$
Hypothetical protein TCSYLVIO_002493	ADWP02012584	Plasma membrane	0.7623	$3E-153$
MASP *T. cruzi*	MBSY01000665	Endoplasmic reticulum	0.7565	$5E-67$
Hypothetical protein BCY84_22404	MBSY01000777	Endoplasmic reticulum	0.7431	0.0
Hypothetical protein C4B63_41g197	PRFA01000041	Plasma membrane	0.7429	0.0
MASP *T. cruzi*	MBSY01000212	Endoplasmic reticulum	0.7410	$3E-94$
Putative retrotransposon hot spot protein	PRFA01000105	Endoplasmic reticulum	0.7402	$5E-40$
MASP *T. cruzi* Dm28c	AYLP01000565	Plasma membrane	0.7194	0.0
Hypothetical protein TCSYLVIO_000872	ADWP02002940	Plasma membrane	0.7037	0.0

2.8. Molecular Docking and Virtual Screening. The ligands and proteins/receptors were submitted to the AutoDock Vina software for molecular docking analyses, using the vina_screen_local.sh script [25]. Furthermore, the best-ranked molecules were identified by the script in python top-molecule.py. The three-dimensional positions of the docking molecules were analyzed by Chimera [26], and PoseView was used for two-dimensional representations [27].

3. Results

The workflow of our approach, methods, and the total proteins found in each step is shown in Figure 1. We compared 28 genomes of *T. cruzi* strains (Table 1). The coding DNA sequences (CDSs) shared by all strains, known as core genome, correspond to 2630 CDSs. Among these CDSs, considering the human genome as the host genome, we found 515 conserved proteins not homologous to the host.

The subcellular localization of the proteins was predicted, in which secreted proteins (present in the endoplasmic reticulum), membrane proteins, and proteins belonging to the vesicle secretory system were selected since they are probably the most antigenic proteins and can be readily recognized by the immune system [28]. From those 515 conserved proteins not homologous to the host, 117 are secreted, membrane protein component, or proteins belonging to the vesicle secretory system (Table 2). Subsequently, these 117 proteins were submitted to VaxiJen to find proteins with a probability of MHC I and MHC II binding greater than 0.7. We found 14 proteins that are likely to be presented as antigens, from which 6 are mucin-associated surface proteins (MASPs), 6 are hypothetical proteins from different parasite strains, 1 is GP63 surface protease, and the latter was identified as putative retrotransposon hot spot protein (Table 3).

The epitopes from 14 proteins identified by the VaxiJen software were predicted using the IEDB-based algorithms for both B cells and T cells (MHC I and MHC II). B cell epitope analysis was performed, and according to the previous cellular localization prediction, 100, 50, and 2 epitopes were found for those proteins present in the plasma membrane, endoplasmic reticulum, and vesicle secretory system, respectively. Graphs A, B, and C in Figure 2 demonstrate the epitopes' localization. A standard cut line greater than 0.5 was used, where the above cut epitopes are represented in yellow. The average, maximum, and minimum values are described in the legend of each graph.

HLA genes are highly polymorphic and differ among populations in both frequency and presence or absence of alleles. Thus, we used a software that classifies the epitopes according to the probability of MHC binding, in which those closer to 0 have a higher probability of binding to MHC, i.e., a greater chance of being recognized as an epitope. Due to the great diversity of alleles, the 30 best proteins classified for MHC I were selected, from which 20 are present in the plasma membrane, 9 in the endoplasmic reticulum, and only 1 in the vesicle secretory system (Table 4). For MHC II, the best 30 were also selected, being 25 present in the plasma membrane and 5 in the endoplasmic reticulum (Table 5).

Currently, phytotherapics and natural plant products are frequently used in health services in both developed and developing countries and play important roles in recent drug development. They are known as a combination of chemicals that are synthesized by plants, having a moderate impact due to very low absorption by oral administration [29, 30]. The compounds selected by our group are described as medicinal plants or natural products with antiprotozoal activity against *T. cruzi*. For each target protein, all ligand compounds were used for docking analysis with drug residues in the cavity identified by the DoGSiteScorer [23] (Table 6). The best binding affinity score-based compounds generated by AutoDock Vina were analyzed for better position detection (Table 7). As a result, the predicted protein-ligand interactions for the best ligand compounds with each target that showed a significant interaction with most drug pouch

Figure 2: Possible epitopes that bind to B lymphocytes. (a) Epitopes present on proteins found in the endoplasmic reticulum. (b) Epitopes present on plasma membrane proteins. (c) Epitopes present in proteins of the vesicle secretory system. All amino acid sequences that exceed the cutoff line, standardized at >0.5, are considered possible yellow-labeled epitopes

residues, lower binding affinity scores, and number of hydrogen bonds are described in Table 7; moreover, we represented 3D and 2D target protein docking analysis (Figures 3–5).

4. Discussion

The vast repertoire of MASP sequences in the *T. cruzi* genome and the fact that they can be secreted by the parasite contribute to the ability of this protozoan to infect various host cell types and/or to participate in mechanisms of its immune evasion. MASP protein has been shown to induce the process of endocytosis in Vero cells, a process by which the parasite's trypomastigote forms actively invade host cells. Additionally, MASP peptides can elicit different antibody responses to both IgG (Immunoglobulin G) and IgM (Immunoglobulin M) and the level of antibodies to a peptide may vary after sequential passage in mice. Moreover, it has been shown that changes in the repertoire of antigenic MASP peptides may contribute to the evasion of the host immune response during the acute phase of the disease [31].

The proteomic and immunoinformatics techniques showed that several members of the MASP family, expressed

Table 4: Prediction of the MHC I binding.

Allele	Protein access	Size (start-end)	Peptide	Rank
HLA-A∗11:01	PRFA01000041	914-922	SAMDSMILK	0.06
HLA-A∗11:01	ADWP02002940	82-90	TTYYFAVYK	0.06
HLA-A∗33:01	ADWP02012584	146-154	DLLLYRWFR	0.06
HLA-A∗11:01	MBSY01000777	67-76	AVYDPNYLPK	0.06
HLA-B∗44:03	ADWP02002940	93-101	GEYLLIISW	0.06
HLA-A∗02:06	PRFA01000041	760-768	FVWDYFTTL	0.06
HLA-A∗02:01	MBSY01000777	219-228	FLLLFMPMFV	0.07
HLA-A∗68:01	PRFA01000041	1142-1151	SVISVITQYR	0.07
HLA-B∗53:01	MBSY01000212	705-714	LPLLLLLGLW	0.07
HLA-B∗57:01	MBSY01000665	273-282	RSTRCGFYCW	0.09
HLA-B∗15:01	ADWP02002940	113-121	FMFPDTVAF	0.1
HLA-B∗07:02	MBSY01000212	94-102	LPAKNAGAM	0.1
HLA-B∗07:02	ADWP02002940	159-167	SPRFLWIAV	0.1
HLA-B∗35:01	PRFA01000041	663-671	FPLPSSVAF	0.1
HLA-A∗68:02	PRFA01000041	726-734	MTSFFAEQV	0.1
HLA-A∗32:01	MBSY01000777	146-154	ITMFLFYAL	0.1
HLA-B∗58:01	MKKV01000794	64-72	MAAGMVILW	0.1
HLA-A∗30:01	PRFA01000041	502-510	KSRNPPLFA	0.1
HLA-A∗68:01	ADWP02002940	82-90	TTYYFAVYK	0.11
HLA-B∗44:02	PRFA01000041	487-495	AENMFMSLF	0.11
HLA-B∗44:02	ADWP02002940	93-101	GEYLLIISW	0.11
HLA-A∗26:01	PRFA01000041	1142-1150	SVISVITQY	0.11
HLA-A∗23:01	ADWP02012584	149-158	LYRWFRWYHF	0.11
HLA-A∗23:01	PRFA01000041	1112-1121	LYIAVAILSF	0.11
HLA-A∗23:01	ADWP02002940	77-86	LFMIATTYYF	0.11
HLA-B∗44:03	MBSY01000777	201-210	RESVQILWWF	0.11
HLA-B∗44:03	PRFA01000041	686-695	REFIIALKGY	0.11
HLA-A∗68:02	ADWP02002940	266-275	TTSFGVVFAV	0.11
HLA-A∗33:01	PRFA01000105	48-56	WMSLLLWLR	0.11
HLA-A∗68:01	MBSY01000665	78-86	EVAYVAAQR	0.11

in the trypomastigote form, present various MHC I and II epitopes, becoming valuable targets for vaccine development. It has been revealed that a synthetic 20-mer peptide (MASPpep) containing potential overlapping of B cells and T CD4 and T CD8 cell epitopes can induce immunity mediated by these two cell types against *T. cruzi* infection in mice. These data demonstrated that a MASPpep synthetic peptide-based vaccine can effectively control *T. cruzi* infection, prolonging survival and possibly reducing disease progression by inducing optimal immune stimulation, i.e., involving humoral and cellular responses [32]. The central region of MASP is highly variable, contributing to a vast repertoire of peptides that can interact with several receptors of different host cell types. Therefore, it is interesting to investigate whether MASP induces the immune system, especially during the acute phase of infection, when there are many circulating trypomastigotes in the human host organism [33].

Proteases are present in different protozoan parasites and appear to be important to several aspects of parasite-host interactions, regardless of their participation in pathogen nutrition [34]. Metalloproteases have been described in several parasites, but only those present in *Leishmania* spp. were completely characterized [35]. On its external surface of the plasma membrane, *Leishmania spp*. express an important 63 kDa glycosylphosphatidylinositol- (GPI-) anchored glycoprotein called gp63 or leishmanolysin, which represents more than 1% of the total cellular protein content [36, 37]. Gp63 plays several roles in parasite-host interactions and is an important virulence factor [38]. In *T. cruzi*, different metalloprotease activities have been described [39]; some of them expressed only during the metacyclogenesis phase [40, 41]. Four gp63 homologous genes have already been identified in *T. cruzi*; some of which are predominantly expressed at the mRNA level in the amastigote phase [42].

Immunocomplexes (ICs) are direct and real-time products of humoral immune responses. Among the various parasitic antigens incorporated in ICs, gp63 is relatively well known for its function [43]. Antipeptide antibodies against the C-terminal epitope, present in a subset of gp63 proteins, are recognized at all stages of the parasite and subsequently

Table 5: Prediction of the MHC II binding.

Allele	Protein access	Size (start-end)	Peptide	Rank
HLA-DRB5∗01:01	PRFA01000041	487-501	AENMFMSLFSGAKHE	0.01
HLA-DRB5∗01:01	PRFA01000041	488-502	ENMFMSLFSGAKHEK	0.01
HLA-DRB5∗01:01	PRFA01000041	489-503	NMFMSLFSGAKHEKS	0.01
HLA-DRB3∗01:01	ADWP02002940	72-86	VLTCSLFMIATTYYF	0.01
HLA-DRB3∗01:01	ADWP02002940	73-87	LTCSLFMIATTYYFA	0.01
HLA-DRB3∗01:01	ADWP02002940	74-88	TCSLFMIATTYYFAV	0.01
HLA-DRB3∗01:01	ADWP02002940	75-89	CSLFMIATTYYFAVY	0.01
HLA-DRB3∗01:01	ADWP02002940	76-90	SLFMIATTYYFAVYK	0.01
HLA-DRB3∗01:01	ADWP02002940	77-91	LFMIATTYYFAVYKQ	0.01
HLA-DRB3∗01:01	ADWP02002940	78-92	FMIATTYYFAVYKQC	0.01
HLA-DRB3∗01:01	MBSY01000777	139-153	SCAGFLFITMFLFYA	0.02
HLA-DRB3∗01:01	MBSY01000777	140-154	CAGFLFITMFLFYAL	0.02
HLA-DRB3∗01:01	MBSY01000777	141-155	AGFLFITMFLFYALS	0.02
HLA-DRB3∗01:01	MBSY01000777	217-231	PPFLLLFMPMFVAAM	0.02
HLA-DRB3∗01:01	PRFA01000041	1518-1532	ELEGSMIDLDAEVSI	0.02
HLA-DRB3∗01:01	PRFA01000041	1519-1533	LEGSMIDLDAEVSIP	0.02
HLA-DRB3∗01:01	PRFA01000041	1520-1534	EGSMIDLDAEVSIPQ	0.02
HLA-DRB3∗01:01	PRFA01000041	1521-1535	GSMIDLDAEVSIPQQ	0.02
HLA-DRB3∗01:01	PRFA01000041	1522-1536	SMIDLDAEVSIPQQK	0.02
HLA-DRB5∗01:01	PRFA01000041	486-500	HAENMFMSLFSGAKH	0.02
HLA-DRB5∗01:01	PRFA01000041	490-504	MFMSLFSGAKHEKSR	0.02
HLA-DRB5∗01:01	PRFA01000041	491-505	FMSLFSGAKHEKSRN	0.02
HLA-DRB1∗07:01	MBSY01000212	299-313	DCWVKEYVTASATMI	0.03
HLA-DRB3∗01:01	PRFA01000041	600-614	STALHAIPWDQRAFI	0.03
HLA-DRB3∗01:01	PRFA01000041	601-615	TALHAIPWDQRAFIP	0.03
HLA-DRB3∗01:01	PRFA01000041	602-616	ALHAIPWDQRAFIPI	0.03
HLA-DRB3∗01:01	PRFA01000041	603-617	LHAIPWDQRAFIPIS	0.03
HLA-DRB3∗01:01	PRFA01000041	604-618	HAIPWDQRAFIPISG	0.03
HLA-DRB3∗01:01	PRFA01000041	1108-1122	RRLILYIAVAILSFL	0.03
HLA-DRB1∗15:01	ADWP02002940	272-286	VFAVMLFGSIFVTLL	0.03

inhibit host cell trypomastigote infection [34]. *In vitro* studies also demonstrate that the presence of anti-gp63 serum has a significant inhibitory effect on *T. cruzi* infection [44].

Retrotransposon hot spot (RHS) proteins are encoded by a multigenic family present in *T. cruzi* and *Trypanosoma brucei*, but are not found in the *Leishmania* spp. genome [45]. A recent proteomic analysis was able to identify around 39 HRH isoforms that were expressed in the *T. cruzi* circulating trypomastigote form [46]. In ELISA tests, only the RHS recombinant has shown a strong serum response in patients with different clinical manifestations of Chagas disease [47]. Studies demonstrate through proteomics that *T. brucei* expresses the RSH protein [48]. However, several RHS protein sequence alignments showed that *T. cruzi* and *T. brucei* share less than 33% identity. No cross-reactivity between *T. cruzi* RHS protein in serum from patients with African sleeping sickness or leishmaniasis has been observed, thus indicating that HRH can be used as an antigen to increase the specificity of the diagnosis of Chagas disease [47]. More importantly, this protein could be tested to build a diagnostic test that could determine the clinical forms of the disease, a test that is not yet available.

Understanding antigen recognition at the molecular level opens the way to design new epitopic vaccines [49]. The identification of epitopes for both B and T cells is required to develop such vaccines since the antigenic determinants are immunodominant and capable of inducing a specific immune response [50]. Tools capable of predicting epitopes can serve as filters, i.e., they rule out regions that are probably not epitopes of additional experimental analysis [51]. This leads to the nomination of new candidates for more assertive and probably more efficient vaccines [49]. Therefore, by using reverse vaccinology, our work found possible vaccine targets that, after purification, will give rise to a prophylactic vaccine where the predicted antigens will be purified and tested *in vitro* and *in vivo* together with adjuvants, in order to generate greater efficiency.

The PDB ID: 3K81 model (*T. brucei* editosome central interaction protein in the single-domain antibody complex) crystalline structure showed identity ≥ 75% with the T M18

Table 6: Identification of the druggability cavities obtained by DoGSiteScorer.

Protein	Volume (angstrom^3)	Surface area (angstrom^2)	Drug score	Residues
RNA editing complex protein M18	1494.7	2197.05	0.81	VAL28, GLY29, VAL30, VAL31, HIS32, ASP33, ILE34, GLN35, THR45, GLN46, PHE47, THR48, THR50, THR51, THR52, LYS67, HIS69, ILE72, CYS74, PHE79, VAL83, LYS84, GLN85, LYS86, VAL87, LYS88, GLU89, GLY90, ASN91, VAL92, VAL93, VAL95, ASN9, VAL120, GLN126, VAL127, VAL129, HIS131, GLY132, ASP133, ARG134, ARG135, ASN136, THR137, PRO138, VAL139, SER140, VAL141, ASN142, PRO143, THR144, ALA145, GLU146
Hypothetical protein TCDM_03925	1131.67	1451.37	0.81	GLU235, ARG238, GLY239, GLU240, LEU241, ARG242, GLY245, CYS246, VAL247, ALA248, HIS300, THR337, VAL338, ASP339, PRO340, THR341, ALA342, VAL343, GLU394, LEU395, GLY396, SER397, ARG398, LEU399, GLY444, SER446, PRO503, MET504, GLN505, ARG506, LEU579, GLY582, LYS583, LEU585, LYS586, LEU587, LEU588, TYR589, SER590, PRO591, GLU596, PRO597, ARG598, ASN599, VAL600, PHE602, TYR603, SER604, GLU605, ALA607, ALA608, ILE610, GLU611, ALA639, ARG640, ARG641, PHE642, ALA659
Inosine-guanine nucleoside hydrolases	794.5	907.63	0.81	ASP11, GLY13, GLY14, ASP15, ASP16, ASN40, VAL41, THR77, VAL78, GLN79, TRP80, GLY81, GLY82, PHE83, GLY84, ARG85, ASP86, GLY87, LEU131, GLY132, PRO133, MET162, ASN171, SER172, GLU177, PHE178, ASN179, TRP205, TRP215, PHE247, LEU250, THR254, ASP273, THR275, CYS276, VAL277, ILE278, PRO279, ASP280
Mitochondrial RNA-binding protein 1	858.62	1230.81	0.82	ILE34, HIS35, ASP36, ARG38, PRO41, ALA42, LEU43, GLY44, THR45, MET46, THR47, GLN60, TYR61, PRO62, GLN63, LEU64, GLY65, ASP79, ASP81, ARG82, ILE84, ILE131, HIS132, ARG133, VAL134, ALA135, SER136, LYS138, GLU140, ASP141, TRP142, SER143, VAL144, ASN145, PHE146, ASP147, LYS148, PHE150
Calpain-like cysteine peptidase	213.06	409.93	0.27	SER6, SER7, THR8, SER9, GLU32, ILE34, GLY35, SER38, GLU42, THR43, GLY44, GLU45
Trans-sialidase	431.81	805.62	0.72	THR22, SER99, GLY100, GLY101, ALA102, GLY103, VAL104, PHE113, PRO114, TYR151, PRO152, ARG153, VAL154, THR155, LEU162, MET163, SER164, VAL165, ASP166, ARG172, VAL173, LEU190, TRP194, LYS206

Table 7: Molecular docking studies of all 6 drug target proteins.

Compound name	Compound PubChem ID	AutoDock Vina binding affinity	No. of H-bond/interacted residues
RNA editing complex protein M18			
Diospirin	CID308140	-7.5	2/GLU89, SER140
Hypothetical protein TCDM_03925			
(1R)-1,6,6-Trimethyl-1,2,7,8-tetrahydronaphtho[1,2-g][1]benzofuran-9,10,11-trione	CID9995530	-7.9	2/ARG641
Inosine-guanine nucleoside hydrolases			
Emodin	CID3220	-9.6	5/ASP15, TRP60, ASN40
Mitochondrial RNA-binding protein 1			
(1R)-1,6,6-Trimethyl-1,2,7,8-tetrahydronaphtho[1,2-g][1]benzofuran-9,10,11-trione	CID9995530	-9.1	4/THR45, GLN60
Calpain-like cysteine peptidase			
Usambarensine	CID5281413	-7.3	1/GLU42
Trans-sialidase			
Usambarensine	CID5281413	-9.4	1/THR155

protein RNA editing complex target-protein I. M18 protein RNA editing complex plays an important role in the RNA editing process in the mechanism of trypanosomatids to insert and exclude posttranscriptional uridylates at multiple sites in most mitochondrial pre-mRNAs for the production of mature mRNAs [52]. RNA editing is composed of a

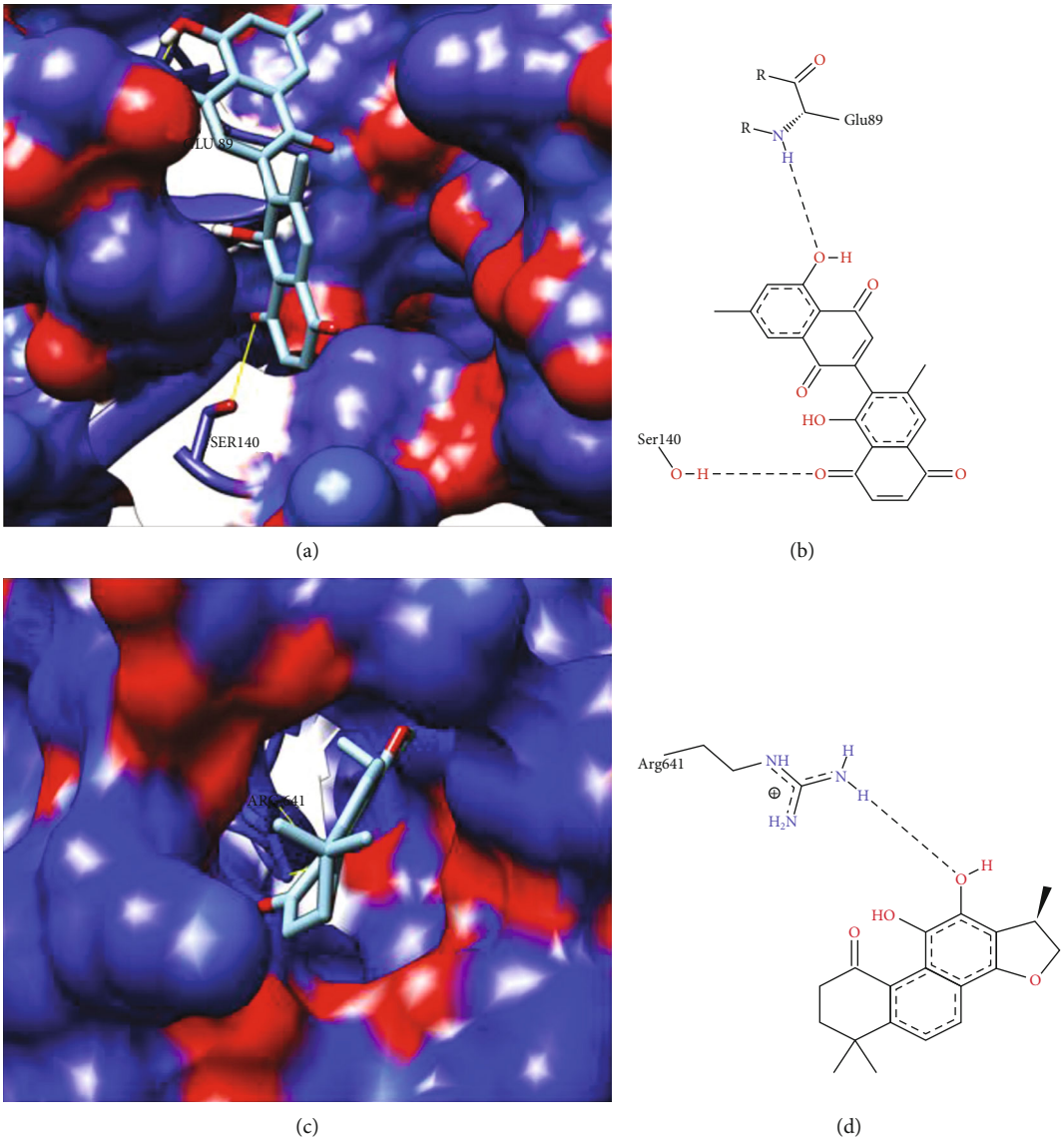

Figure 3: 3D and 2D representation of target protein anchor analysis M18 protein RNA editing complex and hypothetical protein TCDM_03925. (a) 3D surface representation of M18 protein RNA editing complex protein with compound Diospirin. (b) 2D surface representation of M18 protein RNA editing complex protein with Diospirin compound. (c) 3D surface representation of hypothetical protein TCDM_03925 with compound (1R)-1,6,6-trimethyl-1,2,7,8-tetrahydronaphtho[1,2-g][1]benzofuran-9,10,11-trione. (d) 2D representation of the hypothetical protein TCDM_03925 with compound (1R)-1,6,6-trimethyl-1,2,8,8-tetrahydronaphto[1,2-g][1]benzofuran-9,10,11-trione.

cascade of reactions that usually begins from 3′ to 5′ in a transcript, resulting in a population of relatively edited as well as preedited and fully edited molecules for each protozoan. Mitochondrial cryptogeny was previously described participating in the development of efficient and specific chemotherapeutic targets against trypanosomatid pathogens [53, 54]. Molecular docking analysis for this protein with prepared ligand library druggability site residues showed that the Diospirin compound interacted with the active residues of GLU89 and SER140 (Table 7). Figures 3(a) and 3(b) show the three-dimensional and two-dimensional interaction, respectively, with the compound Diospirin.

The hypothetical protein TCDM_03925 showed homology to model PDB ID: 4YJ1 (*T. brucei* MRB1590-ADP crystal structure bound to poly-U RNA) with identity ≥ 50% and ≤75%. Residue ARG641 interacted with (1R)-1,6,6-trimethyl-1,2,7,8-tetrahydronaphtho[1,2-g][1]benzofuran-9,10,11-trione. The three-dimensional and two-dimensional representation with the compound (1R)-1,6,6-trimethyl-1,2,7,8-tetrahydronaphtho[1,2-g][1]benzofuran-9,10,11-trione is represented in Figures 3(c) and 3(d), respectively.

Inosine-guanine nucleoside hydrolases have homology to model ID PDB: 3FZ0 (inosine-guanosine nucleoside hydrolase- (IG-NH-) *Trypanosoma brucei*) with identity ≥ 50% and ≤75%. The nucleoside hydrolase (NH) class is common in all kingdoms except mammals, in which their absence in the host has been highly recommended as potential targets for the antitrypanosomal drug [55]. Studies have also mentioned that NH inhibitors exhibit selective inhibition of isoenzyme for IAG-NH and IG-NH due to variation in the

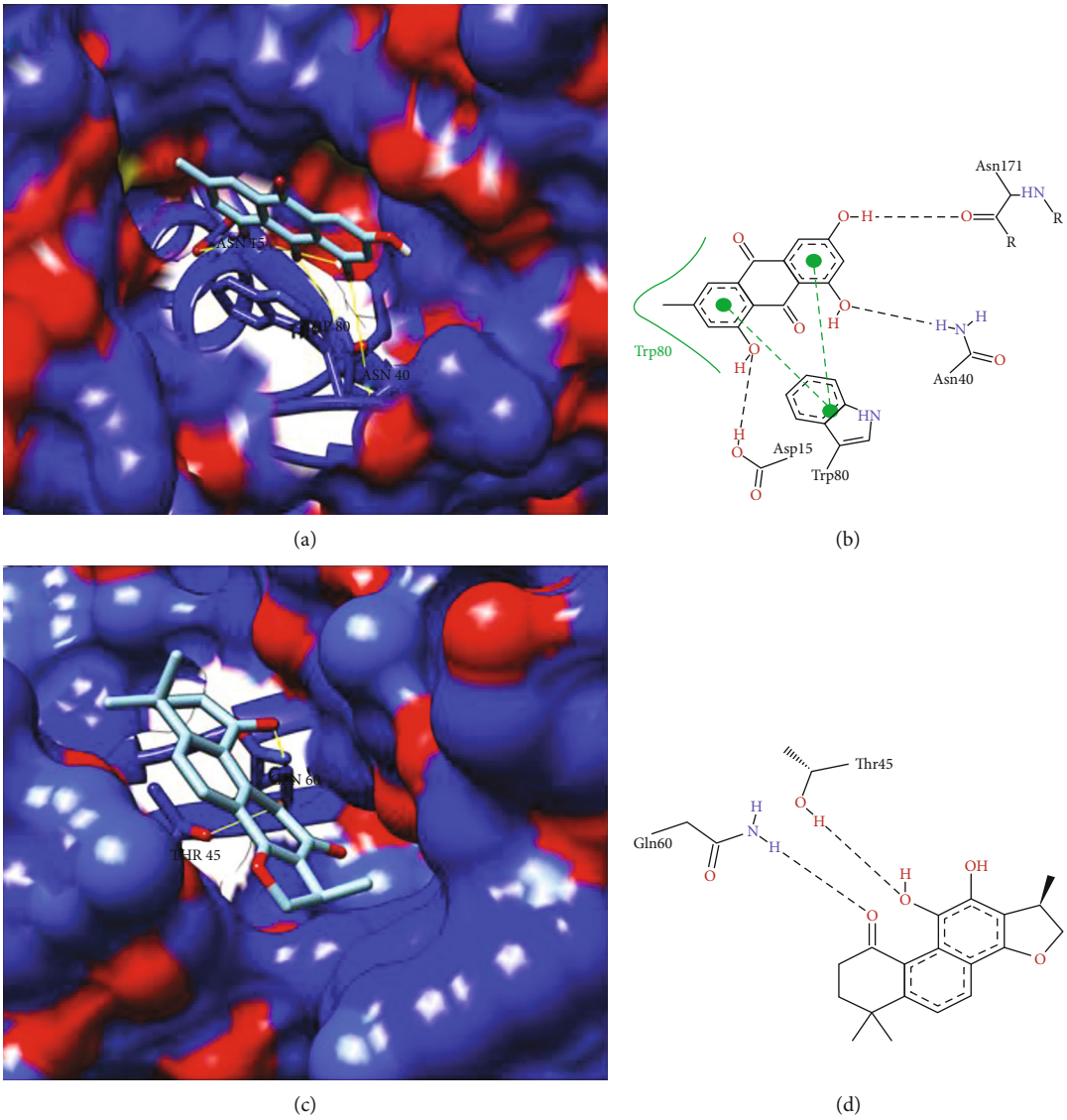

Figure 4: 3D and 2D representation of target protein docking analysis inosine-guanine nucleoside hydrolases and mitochondrial RNA-binding protein 1. (a) 3D surface representation of inosine-guanine nucleoside hydrolases with Emodin compound. (b) 2D representation of protein inosine-guanine nucleoside hydrolases with Emodin compound. (c) 3D surface representation of protein mitochondrial RNA-binding protein 1 with (1R)-1,6,6-trimethyl-1,2,7,8-tetrahydronaphtho[1,2-g][1]benzofuran-9,10,11-trione. (d) 2D representation of RNA-binding protein mitochondrial 1 with compound (1R)-1,6,6-trimethyl-1,2,7,8-tetrahydronaphtho[1,2-g][1]benzofuran-9,10,11-trione.

active site characteristics, and inhibition of only one NH is not sufficient to impair the purine salvage pathway in parasites [56, 57]. Comparing the DoGSiteScorer active site identification analysis (Table 6) and our molecular docking analysis for this protein, we found that the Emodin compound showed high interaction with ASP15, TRP60, and ASN40 (Table 7) residues with good scores linked to our active site identification analysis. Figures 4(a) and 4(b) show the three-dimensional and two-dimensional interaction, respectively, with the compound Diospirin.

Mitochondrial RNA-binding protein 1 showed homology to model ID PDB: 2GIA (*T. brucei* MRP1/MRP2 crystal structures) with identity ≥ 50%. RNA-binding proteins are essential and play an important role in posttranscriptional gene regulation, coordinating the processing, storage, and control of cellular RNAs, which ultimately influences the expression of each gene in the cell [58]. Trypanosomatids have been considered for the identification of new biological mechanisms, such as RNA trans-splicing, mitochondrial RNA editing, and antigenic variation [59]. RBPs cannot be tested as drug targets because of their lack of enzymatic activity. In this sense, it is speculated that the enzymes (kinases, phosphatases, SUMO E3 ligases, and methyltransferases) responsible for these posttranslational modifications could be good candidates for new drugs [59]. Residues of the mitochondrial RNA-binding protein 1 active site, based on a DoGSiteScorer comparison active site identification analysis (Table 6) and our molecular docking analysis, found that compound (1R)-1,6,6-trimethyl-1,2,7,8-tetrahydronaphtho[1,2-g][1]benzofuran-9,10,11-trione showed a high interaction

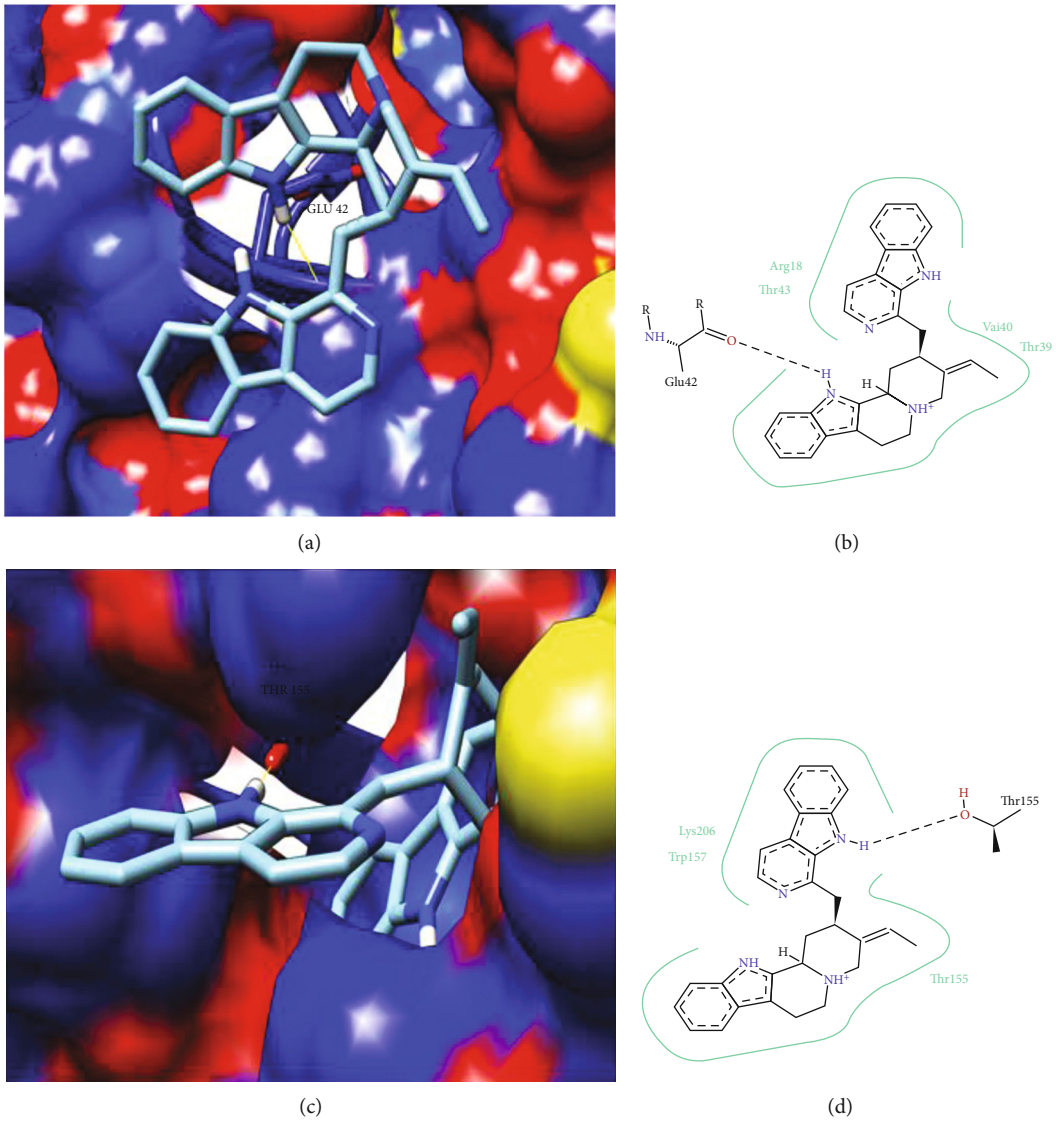

Figure 5: 3D and 2D representation of docking analysis of the target protein calpain-like cysteine peptidase and trans-sialidase. (a) 3D surface representation of calpain-like cysteine peptidase protein with compound Usambarensine. (b) 2D representation of calpain-like cysteine peptidase protein with compound Usambarensine. (c) 3D surface representation of trans-sialidase with compound Usambarensine. (d) 2D trans-sialidase representation with the Usambarensine compound.

with relapses THR45 and GLN60. Figures 4(c) and 4(d) show the 3D and 2D representation, respectively, with compound (1R)-1,6,6-trimethyl-1,2,7,8-tetrahydronaphtho[1,2-g][1]benzofuran-9,10,11-trione.

Calpain-like cysteine peptidase showed homology to PDB model ID: 2FE0 (SMP-1 small myristoylated protein from *Leishmania major*) with identity ≥ 25% and <35%. Calpains are calcium-dependent heterodimeric cysteine peptidases that have been widely studied in mammals and exist in two major isoforms, μ-calpain (calpain 1) and m-calpain (calpain 2), which require micromolar concentrations and millimolar Ca2+, respectively, for its activation. These proteins are composed of a large subunit (divided into four subunits) of approximately 80 kDa and a small subunit of 28 kDa [60]. Proteases are enzymes that break the peptide bonds and are essential for numerous biological activities: peptide digestion, activation of other enzymes, immune system modulation, cell cycle participation, differentiation, and autophagy [61]. Given that the calpain protein family plays an important role in a distinct range of human disease and biological processes, it has a crucial therapeutic potential, and much has been done to develop or identify selective calpain inhibitors [62]. These proteins in trypanosomatids can turn them candidates for drug targets. In our molecular docking analysis for this protein, we found that the Usambarensine compound showed a high interaction and binding energy with the GLU42 residue (Table 6). Figures 5(a) and 5(b) show the three-dimensional and two-dimensional representation, respectively, with the compound Usambarensine.

Trans-sialidase (TS) had homology to the PDB model ID: 1WCS (*Trypanosoma rangeli* sialidase mutant exhibiting trans-sialidase activity) with identity ≥ 25% and <35%. *T.*

cruzi trans-sialidase plays a key role in immunopathological events. The trans-sialidase enzyme catalyzes the displacement of glycoconjugate sialic acid molecules from the host to receptor molecules on the parasite surface. The activity of TS causes several biological effects that lead to the subversion of the host immune system, favoring both parasite survival and the establishment of chronic infection (Nardy et al., 2016). Trans-sialidase protein has been reported as a drug target against Chagas disease (Miller III; Roitberg, 2013). In our molecular docking analysis for this protein, we found that the Usambarensine compound showed notable interaction and binding energy with the THR155 residue (Table 6). Figures 5(c) and 5(d) show the three-dimensional and two-dimensional interaction, respectively, with the Usambarensine compound.

Trypanosomatids, *T. brucei* spp., *T. cruzi*, and *Leishmania spp*. cause disease in humans and animals being potentially fatal. Unfortunately, there are no effective vaccines against these parasites, and current drug treatments are highly toxic, have a low tolerance, and require long patient compliance [59]. While current drug treatments may be effective during the acute stage of infection, newer, safer, and more effective treatments against these neglected diseases are needed. Due to the toxicity and efficacy of available antiprotozoal drugs and the emergence of drug resistance, new trypanosomatid target discovery and new bioactive compounds are of utmost importance. Here, we performed subtractive genomics for drug target identification and molecular docking analysis with 6 identified drug targets. Interestingly, some of the identified targets are already reported as drug targets for Chagas disease. We prepared the binder library from a robust literature search and performed ligand-based docking. In our anchor analysis, we identified compounds such as Diospirin, Emodin, and Usambarensine showing high binding affinity with the number of targets identified.

The compound Diospirin is a plant product with a significant inhibitory effect on *Leishmania donovani* promastigote growth. This compound inhibits the catalytic activity of parasitic DNA topoisomerase I [63]. Emodin is a natural trihydroxyanthraquinone and is obtained from the roots and bark of numerous plants (particularly rhubarb and hawthorn), being an active ingredient in several Chinese herbs. It has a role as a tyrosine kinase inhibitor, an antineoplastic agent, a laxative, and a plant metabolite [64]. Usambarensine is a plant product isolated from the roots of *Strychnos usambarensis* in Central Africa. This compound exhibits strong antimalarial and cytotoxic effect activities. Its toxicity to B16 melanoma cells has been described [65].

5. Conclusions

Due to the absence of diagnostic tests that can determine a clinical form of the disease, it is necessary to develop a vaccine for the prevention and new drugs for the treatment of Chagas disease. Here, we apply the reverse vaccinology approach and identify 14 vaccine candidate proteins; these can also be used as a target for the diagnosis of clinical forms of the disease since it is specific for the *T. cruzi* parasite. We have also identified potential targets for already available drugs and natural products through molecular docking. We emphasize that both approaches are important but require a lot of time which can be further validated through *in vitro* and *in vivo* experiments.

Data Availability

All data generated or analyzed during this study are included in this published article. Additional information about the data is available from the corresponding author on reasonable request.

Conflicts of Interest

The authors declare that they have no conflict of interests.

Acknowledgments

This work was supported by the Fundação de Amparo à Pesquisa do Estado de Minas Gerais (FAPEMIG): Grant Number APQ-01323-15, Coordenação de Aperfeiçoamento de Pessoal de Nível Superior (CAPES): Finance Code 001, and Conselho Nacional de Desenvolvimento Científico e Tecnológico (CNPq): Grant # 134636/2015-5 (INCT-EM) and 465678/2014-9 (INCT-EM).

References

[1] WHO, "Chagas disease (American trypanosomiasis)," 2017, https://www.who.int/en/news-room/fact-sheets/detail/chagas-disease-(american-trypanosomiasis).

[2] A. R. Bogliolo, L. Lauria-Pires, and W. C. Gibson, "Polymorphisms in *Trypanosoma cruzi*: evidence of genetic recombination," *Acta Tropica*, vol. 61, no. 1, pp. 31–40, 1996.

[3] M. C. Albareda, S. A. Laucella, M. G. Alvarez et al., "*Trypanosoma cruzi* modulates the profile of memory $CD8^+$ T cells in chronic Chagas' disease patients," *International Immunology*, vol. 18, no. 3, pp. 465–471, 2006.

[4] W. O. Dutra, O. A. Martins-filho, J. R. Cançado et al., "Chagasic patients lack CD28 expression on many of their circulating T lymphocytes," *Scandinavian Journal of Immunology*, vol. 43, pp. 88–93, 1996.

[5] S. B. Boscardin, A. C. T. Torrecilhas, R. Manarin et al., "Chagas' disease: an update on immune mechanisms and therapeutic strategies," *Journal of Cellular and Molecular Medicine*, vol. 14, pp. 1373–1384, 2010.

[6] E. Dumonteil, "Vaccine development against *Trypanosoma cruzi* and *Leishmania* species in the post-genomic era," *Infection, Genetics and Evolution*, vol. 9, no. 6, pp. 1075–1082, 2009.

[7] C. Teh-poot and E. Dumonteil, "Mining Trypanosoma cruzi Genome Sequences for Antigen Discovery and Vaccine Development," in *T. cruzi Infection: Methods and Protocols*, vol. 1955, pp. 23–34, Springer New York, 2019.

[8] M. A. Basombrio, M. A. Segura, L. Gomez, and M. C. Mora, "Field trial of vaccination against American trypanosomiasis (Chagas' disease) in dogs," *The American Journal of Tropical Medicine and Hygiene*, vol. 49, no. 1, pp. 143–151, 1993.

[9] M. A. Basombrio, L. Gomez, A. M. Padilla, M. Ciaccio, T. Nozaki, and G. A. M. Cross, "Targeted deletion of the GP72 gene decreases the infectivity of *Trypanosoma cruzi* for

mice and insect vectors," *The Journal of Parasitology*, vol. 88, no. 3, 2002.

[10] C. P. Brandan and M. Á. Basombrío, "Genetically attenuated *Trypanosoma cruzi* parasites as a potential vaccination tool," *Bioengineered*, vol. 3, no. 4, pp. 242–246, 2012.

[11] S. C. Soares, E. Trost, R. T. J. Ramos et al., "Genome sequence of *Corynebacterium pseudotuberculosis* biovar *equi* strain 258 and prediction of antigenic targets to improve biotechnological vaccine production," *Journal of Biotechnology*, vol. 167, no. 2, pp. 135–141, 2013.

[12] B. Jackie, S. Sagar, H. Alamgir et al., "in silico Molecular Docking and ADME/T Analysis of Some Selected Isolated Compounds of Phyllanthus emblica against Type 2 Diabetics," *American Journal of Ethnomedicine*, vol. 5, 2018.

[13] D. M. EmmsSteven Kelly, "OrthoFinder: solving fundamental biases in whole genome comparisons dramatically improves orthogroup inference accuracy," *Genome Biology*, vol. 16, no. 1, 2015.

[14] M. G. DJ, "On the predictive recognition of signal peptide sequences," *Virus Research*, vol. 3, no. 3, pp. 271–286, 1985.

[15] G. von Heijne, "A new method for predicting signal sequence cleavage sites," *Nucleic Acids Research*, vol. 14, no. 11, pp. 4683–4690, 1986.

[16] "Nakai KPSORT Users' Manual," 2004, https://psort.hgc.jp/helpwww2.html.

[17] P. V. S. Z. Capriles, A. C. R. Guimarães, T. D. Otto, A. B. Miranda, L. E. Dardenne, and W. M. Degrave, "Structural modelling and comparative analysis of homologous, analogous and specific proteins from *Trypanosoma cruzi* versus *Homo sapiens*: putative drug targets for Chagas' disease treatment," *BMC Genomics*, vol. 11, no. 1, 2010.

[18] I. A. Doytchinova and D. R. Flower, "Bioinformatic approach for identifying parasite and fungal candidate subunit vaccines," *The Open Vaccine Journal*, vol. 1, no. 1, pp. 22–26, 2008.

[19] R. Vita, J. A. Overton, J. A. Greenbaum et al., "The immune epitope database (IEDB) 3.0," *Nucleic Acids Research*, vol. 43, no. D1, pp. D405–D412, 2015.

[20] S. Kim, J. Chen, T. Cheng et al., "PubChem 2019 update: improved access to chemical data," *Nucleic Acids Research*, vol. 47, no. D1, pp. D1102–D1109, 2019.

[21] N. M. O'Boyle, M. Banck, C. A. James, C. Morley, and T. Vandermeersch, "Open Babel: an open chemical toolbox," *Journal of Cheminformatics*, vol. 3, no. 10, 2011.

[22] S. B. Jamal, S. S. Hassan, S. Tiwari et al., "An integrative *in-silico* approach for therapeutic target identification in the human pathogen *Corynebacterium diphtheriae*," *PLoS One*, vol. 12, no. 10, p. e0186401, 2017.

[23] A. Volkamer, D. Kuhn, F. Rippmann, and M. Rarey, "Dogsitescorer: a web server for automatic binding site prediction, analysis and druggability assessment," *Bioinformatics*, vol. 28, no. 15, pp. 2074-2075, 2012.

[24] G. M. Morris, R. Huey, W. Lindstrom et al., "AutoDock4 and AutoDockTools4: Automated docking with selective receptor flexibility," *Journal of Computational Chemistry*, vol. 30, no. 16, pp. 2785–2791, 2009.

[25] T. Oleg and A. J. Olson, "AutoDock Vina: improving the speed and accuracy of docking with a new scoring function, efficient optimization, and multithreading," *Journal of Computational Chemistry*, vol. 31, pp. 455–461, 2010.

[26] E. F. Pettersen, T. D. Goddard, C. C. Huang et al., "UCSF Chimera?A visualization system for exploratory research and analysis," *Journal of Computational Chemistry*, vol. 25, pp. 1605–1612, 2004.

[27] K. Stierand, P. C. Maaß, and M. Rarey, "Molecular complexes at a glance: automated generation of two-dimensional complex diagrams," *Bioinformatics*, vol. 22, no. 14, pp. 1710–1716, 2006.

[28] M. Mora, D. Veggi, L. Santini, M. Pizza, and R. Rappuoli, "Reverse vaccinology," *Drug Discovery Today*, vol. 8, no. 10, pp. 459–464, 2003.

[29] A. Kumar Srivastava, "Significance of medicinal plants in human life," in *Synthesis of Medicinal Agents from Plants*, pp. 1–24, Elsevier, 2018.

[30] C. Veeresham, "Natural products derived from plants as a source of drugs," *Journal of Advanced Pharmaceutical Technology and Research*, vol. 3, no. 4, pp. 200-201, 2012.

[31] S. L. dos Santos, L. M. Freitas, F. P. Lobo et al., "The MASP family of *Trypanosoma cruzi*: changes in gene expression and antigenic profile during the acute phase of experimental infection," *PLoS Neglected Tropical Diseases*, vol. 6, no. 8, article e1779, 2012.

[32] C. Serna, J. A. Lara, S. P. Rodrigues, A. F. Marques, I. C. Almeida, and R. A. Maldonado, "A synthetic peptide from *Trypanosoma cruzi* mucin-like associated surface protein as candidate for a vaccine against Chagas disease," *Vaccine*, vol. 32, no. 28, pp. 3525–3532, 2014.

[33] D. C. Bartholomeu, G. C. Cerqueira, A. C. A. Leao et al., "Genomic organization and expression profile of the mucin-associated surface protein (masp) family of the human pathogen *Trypanosoma cruzi*," *Nucleic Acids Research*, vol. 37, no. 10, pp. 3407–3417, 2009.

[34] I. C. Cuevas, J. J. Cazzulo, and D. O. Sánchez, "gp63 homologues in *Trypanosoma cruzi*: surface antigens with metalloprotease activity and a possible role in host cell infection," *Infection and Immunity*, vol. 71, no. 10, pp. 5739–5749, 2003.

[35] J. Bouvier, P. Schneider, and R. Etges, "Leishmanolysin: Surface metalloproteinase of Leishmania," in *Proteolytic Enzymes: Aspartic and Metallo Peptidases*, pp. 614–633, Elsevier, 1995.

[36] R. Etges, J. Bouvier, and C. Bordier, "The major surface protein of *Leishmania* promastigotes is anchored in the membrane by a myristic acid-labeled phospholipid," *The EMBO Journal*, vol. 5, no. 3, pp. 597–601, 1986.

[37] J. Bouvier, R. J. Etges, and C. Bordier, "Identification and purification of membrane and soluble forms of the major surface protein of *Leishmania* promastigotes," *The Journal of Biological Chemistry*, vol. 260, pp. 15504–15509, 1985.

[38] P. B. Joshi, B. L. Kelly, S. Kamhawi, D. L. Sacks, and W. R. McMaster, "Targeted gene deletion in *Leishmania major* identifies leishmanolysin (GP63) as a virulence factor," *Molecular and Biochemical Parasitology*, vol. 120, no. 1, pp. 33–40, 2002.

[39] S. Greig and F. Ashall, "Electrophoretic detection of *Trypanosoma cruzi* peptides," *Mol Biochem Parasitol*, vol. 39, no. 1, pp. 31–37, 1990.

[40] M. C. Bonaldo, L. N. d'Escoffier, J. M. Salles, and S. Goldenberg, "Characterization and expression of proteases during *Trypanosoma cruzi* metacyclogenesis," *Experimental Parasitology*, vol. 73, no. 1, pp. 44–51, 1991.

[41] C. M. Lowndes, M. C. Bonaldo, N. Thomaz, and S. Goldenberg, "Heterogeneity of metalloprotease expression *inTrypanosoma cruzi*," *Parasitology*, vol. 112, no. 4, pp. 393–399, 1996.

[42] P. M. Grandgenett, B. C. Coughlin, L. V. Kirchhoff, and J. E. Donelson, "Differential expression of GP63 genes in *Trypanosoma cruzi*," *Molecular and Biochemical Parasitology*, vol. 110, no. 2, pp. 409–415, 2000.

[43] K. Ohyama, N. T. Huy, H. Yoshimi et al., "Proteomic profile of circulating immune complexes in chronic Chagas disease," *Parasite Immunol*, vol. 38, no. 10, pp. 609–617, 2016.

[44] M. M. Kulkarni, C. L. Olson, D. M. Engman, and B. S. McGwire, "*Trypanosoma cruzi* GP63 proteins undergo stage-specific differential posttranslational modification and are important for host cell infection," *Infection and Immunity*, vol. 77, no. 5, pp. 2193–2200, 2009.

[45] F. Bringaud, N. Biteau, S. E. Melville et al., "A new, expressed multigene family containing a hot spot for insertion of retroelements is associated with polymorphic subtelomeric regions of *Trypanosoma brucei*," *Eukaryotic Cell*, vol. 1, no. 1, pp. 137–151, 2002.

[46] G. V. F. Brunoro, M. A. Caminha, A. T. S. Ferreira et al., "Reevaluating the *Trypanosoma cruzi* proteomic map: the shotgun description of bloodstream trypomastigotes," *Journal of Proteomics*, vol. 115, pp. 58–65, 2015.

[47] N. L. Bautista-López, M. Ndao, V. Camargo et al., "Characterization and diagnostic application of *Trypanosoma cruzi* trypomastigote excreted-secreted antigens shed in extracellular vesicles released from infected mammalian cells," *Journal of Clinical Microbiology*, vol. 55, no. 3, pp. 744–758, 2017.

[48] A. Geiger, C. Hirtz, T. Bécue et al., "Exocytosis and protein secretion in *Trypanosoma*," *BMC Microbiology*, vol. 10, no. 1, 2010.

[49] S. Raza, K. Siddique, M. Rabbani et al., "*In silico* analysis of four structural proteins of aphthovirus serotypes revealed significant B and T cell epitopes," *Microbial Pathogenesis*, vol. 128, pp. 254–262, 2019.

[50] S. Dermime, D. E. Gilham, D. M. Shaw et al., "Vaccine and antibody-directed T cell tumour immunotherapy," *Biochimica et Biophysica Acta (BBA) - Reviews on Cancer*, vol. 1704, no. 1, pp. 11–35, 2004.

[51] M. C. Jespersen, B. Peters, M. Nielsen, and P. Marcatili, "BepiPred-2.0: improving sequence-based B-cell epitope prediction using conformational epitopes," *Nucleic Acids Research*, vol. 45, no. W1, pp. W24–W29, 2017.

[52] A. K. Panigrahi, A. Schnaufer, N. Carmean et al., "Four related proteins of the *Trypanosoma brucei* RNA editing complex," *Molecular and Cellular Biology*, vol. 21, no. 20, pp. 6833–6840, 2001.

[53] E. S. Gerasimov, A. A. Gasparyan, I. Kaurov et al., "Trypanosomatid mitochondrial RNA editing: dramatically complex transcript repertoires revealed with a dedicated mapping tool," *Nucleic Acids Research*, vol. 46, no. 2, pp. 765–781, 2018.

[54] R. Salavati, H. Moshiri, S. Kala, and N. H. Shateri, "Inhibitors of RNA editing as potential chemotherapeutics against trypanosomatid pathogens," *International Journal for Parasitology: Drugs and Drug Resistance*, vol. 2, pp. 36–46, 2012.

[55] F. Giannese, M. Berg, P. van der Veken et al., "Structures of purine nucleosidase fromTrypanosoma bruceibound to isozyme-specific trypanocidals and a novel metalorganic inhibitor," *Acta Crystallographica Section D: Biological Crystallography*, vol. 69, no. 8, pp. 1553–1566, 2013.

[56] M. Berg, L. Kohl, P. Van der Veken et al., "Evaluation of nucleoside hydrolase inhibitors for treatment of african trypanosomiasis," *Antimicrobial Agents and Chemotherapy*, vol. 54, no. 5, pp. 1900–1908, 2010.

[57] H. CHH, A. Fatima, and A. Gaurav, "In Silico Investigation of Flavonoids as Potential Trypanosomal Nucleoside Hydrolase Inhibitors," *Advances in Bioinformatics*, vol. 1, Article ID 826047, 10 pages, 2015.

[58] H. Antonicka, F. Sasarman, T. Nishimura, V. Paupe, and E. A. Shoubridge, "The Mitochondrial RNA-Binding Protein GRSF1 Localizes to RNA Granules and Is Required for Post-transcriptional Mitochondrial Gene Expression," *Cell Metabolism*, vol. 17, no. 3, pp. 386–398, 2013.

[59] M. A. Romaniuk, "Regulation of RNA binding proteins in trypanosomatid protozoan parasites," *World Journal of Biological Chemistry*, vol. 7, no. 1, pp. 146–157, 2016.

[60] M. Branquinha, F. Marinho, L. Sangenito et al., "Calpains: potential targets for alternative chemotherapeutic intervention against human pathogenic trypanosomatids," *Current Medicinal Chemistry*, vol. 20, no. 25, pp. 3174–3185, 2013.

[61] J. L. Siqueira-Neto, A. Debnath, L.-I. McCall et al., "Cysteine proteases in protozoan parasites," *PLOS Neglected Tropical Diseases*, vol. 12, no. 8, article e0006512, 2018.

[62] M. E. Saez, R. Ramirez-Lorca, F. J. Moron, and A. Ruiz, "The therapeutic potential of the calpain family: new aspects," *Drug Discovery Today*, vol. 11, no. 19-20, pp. 917–923, 2006.

[63] S. Ray, B. Hazra, B. Mittra, A. Das, and H. K. Majumder, "Diospyrin, a bisnaphthoquinone: a novel inhibitor of type I DNA topoisomerase of *Leishmania donovani*," *Molecular Pharmacology*, vol. 54, no. 6, pp. 994–999, 1998.

[64] X. Dong, J. Fu, X. Yin et al., "Emodin: a review of its pharmacology, toxicity and pharmacokinetics," *Phytotherapy Research*, vol. 30, no. 8, pp. 1207–1218, 2016.

[65] L. Dassonneville, N. Wattez, C. Mahieu et al., "The plant alkaloid usambarensine intercalates into DNA and induces apoptosis in human HL60 leukemia cells," *Anticancer research*, vol. 19, no. 6B, pp. 5245–5250, 1999.

Hindawi
Disease Markers
Volume 2020, Article ID 4716793, 10 pages
https://doi.org/10.1155/2020/4716793

Research Article

Lack of Efficacy of Combined Carbohydrate Antigen Markers for Lung Cancer Diagnosis

Zhineng Wen,[1] Ying Huang,[1] Zhougui Ling,[1] Jifei Chen,[2] Xiaomou Wei,[2] Rui Su,[1] Zhenming Tang,[1] Zhongwei Wen,[1] Youping Deng,[3] and Zhuojun Hu[1]

[1]*Department of Pulmonary and Critical Care Medicine, The Fourth Affiliated Hospital of Guangxi Medical University, No. 1, Liushi Road, Liuzhou 545000, China*
[2]*Clinical Laboratory, The Fourth Affiliated Hospital of Guangxi Medical University, No. 1, Liushi Road, Liuzhou 545000, China*
[3]*Department of Quantitative Health Sciences, University of Hawaii John A. Burns School of Medicine, Honolulu, HI 96813, USA*

Correspondence should be addressed to Zhougui Ling; lzg228@163.com and Zhuojun Hu; huzhuojun1964@163.com

Received 25 December 2019; Revised 11 October 2020; Accepted 26 November 2020; Published 10 December 2020

Academic Editor: Marcos Vinícius Silva

Background. Lung cancer (LC) is top-ranked in cancer incidence and is the leading cause of cancer death globally. Combining serum biomarkers can improve the accuracy of LC diagnosis. The identification of the best potential combination of traditional tumor markers is essential for LC diagnosis. *Patients and Methods*. Blood samples were collected from 132 LC cases and 118 benign lung disease (BLD) controls. The expression levels of ten serum tumor markers (CYFR21, CEA, NSE, SCC, CA15-3, CA 19-9, CA 125, CA50, CA242, and CA724) were assayed, and that the expression in the levels of tumor markers were evaluated, isolated, and combined in different patients. The performance of the biomarkers was analyzed by receiver operating characteristic (ROC) analyses, and the difference between combinations of biomarkers was compared by Chi-square (χ^2) tests. *Results*. As single markers, CYFR21 and CEA showed good diagnostic efficacy for nonsmall cell lung cancer (NSCLC) patients, while NSE and CEA were the most sensitive in the diagnosis of small cell lung cancer (SCLC). The area under the curve (AUC) value was 0.854 for the panel of four biomarkers (CYFR21, CEA, NSE, and SCC), 0.875 for the panel of six biomarkers (CYFR21, CEA, NSE, SCC, CA125, and CA15-3), and 0.884 for the panel of ten markers (CYFR21, CEA, NSE, SCC, CA125, CA15-3, CA19-9, CA50, CA242, and CA724). With a higher sensitivity and negative predictive value (NPV), the diagnostic accuracy of the three panels was better than that of any single biomarker, but there were no statistically significant differences among them (all P values > 0.05). However, the panel of six carbohydrate antigen (CA) biomarkers (CA125, CA15-3, CA19-9, CA50, CA242, and CA724) showed a lower diagnostic value (AUC: 0.776, sensitivity: 59.8%, specificity: 73.0%, and NPV: 60.4%) than the three panels (P value < 0.05). The performance was similar even when analyzed individually by LC subtypes. *Conclusion*. The biomarkers isolated are elevated for different types of lung cancer, and the panel of CYFR21, CEA, NSE, and SCC seems to be a promising serum biomarker for the diagnosis of lung cancer, while the combination with carbohydrate antigen markers does not improve the diagnostic efficacy.

1. Introduction

In the United States, lung cancer (LC) has the second-highest incidence rate of new cases and the highest cancer-related death rate in both men and women [1] (Siegel, Miller et al. 2019). Globally, low- and middle-income countries now estimate more than 50% of mortality every year [2] (Torre, Siegel et al. 2016). There are three main histological subtypes: squamous cell carcinomas (SCC), adenocarcinomas (AdC), and small cell carcinoma [3] (Lortet-Tieulent, Soerjomataram et al. 2014) [4, 5] (Adjei 2019, Feng, Zong et al. 2019). Early identification and surgical resection are regarded as the mainstay to reduce the mortality of lung cancer patients [6] (Satoh, Hoshi et al. 2007). Currently, the initial diagnostic approaches for lung cancer include clinical presentations, chest X-ray, computed tomography (CT) scans, blood biomarkers, and biopsy. Since many of the symptoms of lung cancer are common but nonspecific, in primary care

practice, it is very difficult to identify lung cancer patients from patients with other benign lung diseases (BLDs) [7] (Weller, Peake et al. 2019). Histopathological examination is the gold standard for the diagnosis of LC, and there are numerous invasive ways to obtain pathological tissue, such as bronchoscopy and biopsy guided by CT scan. However, these invasive approaches are painful, inconvenient, and expensive. Therefore, chest CT and tumor biomarker tests preceding biopsy are essential.

Blood biomarkers are minimally invasive, simple, and relatively inexpensive and have no potential radiological hazards as that of CT examinations. Thus, they could serve as a convenient, complementary method for both the diagnosis and assessment of the possible pathological types of LC [8, 9] (Isaksson, Jonsson et al. 2017, Chen, Huang et al. 2018). Although novel promising biomarkers have been discovered and developed, such as autoantibodies, microRNAs (especially small noncoding RNAs (ncRNAs)), circulating tumor DNA, DNA methylation, complement fragments, blood protein profiling, and RNA airway or nasal signatures, the objective of these new biomarkers is mainly for use in early-stage LC screening [10, 11] (Dou, Zhu et al. 2018, Seijo, Peled et al. 2019). Currently, traditional tumor-associated antigen (TAA) biomarkers, such as cytokeratin 19 fragment antigen 21-1 (CYFRA21-1), neuron-specific enolase (NSE), carcinoembryonic antigen (CEA), squamous cell carcinoma antigen (SCC), carbohydrate antigen (CA) 125, CA15-3, CA19-9, and CA72-4, remain widely used as reference diagnoses for lung cancer [9, 10] (Isaksson, Jonsson et al. 2017, Seijo, Peled et al. 2019). Single markers have limited sensitivity and specificity, and combinations of tumor markers (TMs) can improve the diagnostic accuracy [12–15] (Yoon, Kwon et al. 2016, Li, Zhang et al. 2017, Liu, Teng et al. 2017, Fang, Zhu et al. 2018), but few studies have compared different panels of TAAs, and some of these biomarkers may be increased in patients with BLD. Therefore, the aim of this study was to identify the best potential combinations of these traditional tumor markers in distinguishing lung cancer patients from BLD controls.

2. Materials and Methods

2.1. Patients. This was a retrospective study approved by the Ethics Committee of the Fourth Affiliated Hospital of Guangxi Medical University (number KY2019208). We systematically reviewed all patients who had been hospitalized at the Department of Pulmonary and Critical Care Medicine of the hospital between January 2017 and May 2019. Written informed consent was provided by each participant. The patients' clinicopathological information, including age, sex, smoking history, and lung cancer histology, was obtained from electronic medical records. A "never smoker" was defined as a person who had smoked less than 100 cigarettes during his/her lifetime. LC was defined based on CT scans and verified by histopathology according to the World Health Organization Classification of Tumors [16] (Travis, Brambilla et al. 2015). The diagnosis of BLD was established by clinical data and CT scans. Complete and detailed case information was available for all cases.

2.2. Tumor Marker Measurement. Fasting blood samples were collected the morning after patient admission before any therapeutics were administered. Sera were separated after blood collection, and the tests were completed immediately to avoid attenuation. The serum concentrations of TAAs were quantitated by an electrochemiluminescence immunoassay at the Clinical Laboratory of the Fourth Affiliated Hospital of Guangxi Medical University. All assays were performed according to the instrument and reagent specifications.

According to the manufacturers, the cutoff values were as follows: CYFR21 < 3.3 ng/mL, CEA < 3.4 ng/mL, NSE < 16.3 ng/mL, SCC < 2.5 ng/mL, CA125 < 36 U/mL, CA153 < 25 U/mL, CA199 < 27 U/mL, CA50 < 25 U/mL, CA242 < 10 U/mL, and CA724 < 6 U/mL. The laboratory technicians were blinded to the patients' identity, but the results were unblinded and analyzed by our investigators.

2.3. Statistical Analysis. The data are described as means with standard deviations (SDs) for the continuous variables and frequencies with percentages for the categorical variables. The differences in the serum levels between LC patients and BLD controls were compared using a two-sample Mann–Whitney U test. The sensitivity, specificity, negative predictive value (NPV), and positive predictive value (PPV) were calculated to evaluate the performance of combination panels and the different biomarkers. The area under the curve (AUC) and standard error (SE) for the respective receiver operating characteristic (ROC) curves were calculated. An AUC greater than 0.9 implied excellent diagnostic efficacy, whereas an AUC between 0.7 and 0.9 implied good diagnostic efficacy, and an AUC between 0.5 and 0.7 implied poor diagnostic efficacy. Finally, an AUC of no more than 0.5 implied the lack of a diagnostic value for the marker [17] (Yang, Zhang et al. 2018). The ROC curves were constructed by calculating the sensitivity/specificity of the test for a succession of deviations from the original cut-offs, with the same deviation for each antigen in the panel. Chi-square (χ^2) tests were used to compare a significant difference between two panels of biomarkers. All analyses were conducted using SPSS 20.0 (SPSS Inc., Chicago, IL, USA), MedCalc 18.2, and GraphPad Prism 5.0 software (GraphPad Software Inc., San Diego, CA, USA). A 2-sided P value < 0.05 was considered statistically significant.

3. Results

3.1. Patients' Characteristics. A total of 132 patients with pathologically confirmed lung cancer (including 102 with non-small cell lung cancer (NSCLC) and 30 with small cell lung cancer (SCLC)), and 118 patients with benign lung diseases were included in the study. There were more LC patients in the late stage (III-IV) (87.9%) than in the early stage (I-II) (12.1%), and the LC subtypes included adenocarcinoma (55.2%), squamous-cell carcinoma (22.0%), SCLC (22.0%), and large cell lung carcinoma (0.8%). The etiologic diagnoses of the BLD group included bronchitis, community-acquired pneumonia (CAP), chronic obstructive pulmonary disease (COPD), cough variant asthma (CVA), obstructive sleep apnea syndrome (OSAS), bronchiectasis, parapneumonic effusion,

Table 1: Clinical characteristics of the LC patients and BLD controls.

Parameters	LC (n = 132)	BLD (n = 118)	P value
Age (year)			
Range	40-82	35-87	
Mean (SD)	61.4 (9.9)	57.9 (10.6)	0.164
Gender			
Male	106	84	0.092
Female	26	34	0.092
Smoking, n (%)			
Ever/current	89 (67.4)	72 (61.0)	0.291
Never	43 (32.6)	46 (39.0)	0.291
Cancer stage, n (%)		Diseases (n)	
I	6 (4.5)	Bronchitis (26)	
II	10 (7.6)	CAP (55)	
III	47 (35.6)	COPD (8)	
IV	69 (52.3)	Bronchiectasis (12)	
Cancer subtype, n (%)		Pulmonary tuberculosis (6)	
Adenocarcinoma	73 (55.2)	Parapneumonic effusion (4)	
Squamous-cell carcinoma	29 (22.0)	OSAS (4)	
Large cell lung carcinoma	1 (0.8)	CVA (3)	
SCLC	29 (22.0)		

SD: standard deviation; LC: lung cancer; SCLC: small cell lung cancer; BLD: benign lung diseases; CAP: community-acquired pneumonia; COPD: chronic obstructive pulmonary disease; CVA: cough variable asthma; OSAHS: obstructive sleep apnea syndrome.

and pulmonary tuberculosis. Age, sex, and history of smoking did not differ significantly between the groups ($P > 0.05$). Table 1 summarizes the patients' characteristics.

3.2. The Significance of Single Markers for LC Screening. To determine the reactivity of a single marker, ten TAAs (CYFR21, CEA, NSE, SCC, CA15-3, CA 19-9, CA 125, CA50, CA242, and CA724) were measured from 132 LC patients and 118 BLD controls. The results showed that the serum concentrations of six biomarkers were significantly higher in LC patients than in BLD controls: CYFR21 ($P = 0.008$), CEA ($P = 0.004$), NSE ($P = 0.0041$), CA125 ($P < 0.0001$), CA15-3 ($P < 0.0001$), and CA19-9 ($P = 0.0203$). The serum concentrations of the remaining four TAAs were similar in the LC patients to those in the BLD controls: SCC ($P = 0.117$), CA50 ($P = 0.151$), CA242 ($P = 0.863$), and CA724 ($P = 0.097$) (Figure 1). Among the ten serum biomarkers, CYFR21 displayed the highest AUC (0.806, 95% CI: 0.743-0.859) with a sensitivity of 73.5%, followed by CEA (AUC = 0.797, 95% CI: 0.741–0.845; sensitivity: 65.4%) and CA15-3 (AUC = 0.703, 95% CI: 0.642–0.759; sensitivity: 37.1%). The other markers demonstrated poor diagnostic efficacy for lung cancer screening, with low AUC values (<0.7) and similarly low sensitivities. The ROC curve and screening value of each marker for identifying lung cancer patients and BLD patients can be found in Figure 2(a) and Table 2.

3.3. The Value of the Combined Detection of Markers for the Detection of Lung Cancer. To assess the diagnostic value of the combination of TAAs in distinguishing LC from BLD, we evaluated different combinations of TAA markers. We combined biomarkers into four different panels: panel 1 containing four biomarkers: CYFR21, CEA, NSE, and SCC; panel 2 containing six biomarkers: CYFR21, CEA, NSE, SCC, CA125, and CA15-3; panel 3 containing only the six CA markers: CA125, CA15-3, CA19-9, CA50, CA242, and CA724; and panel 4 containing all ten biomarkers: CYFR21, CEA, NSE, SCC, CA125, CA15-3, CA19-9, CA50, CA242, and CA724. The AUC, sensitivity, specificity, PPV, and NPV for the tumor marker combinations were as follows: panel 1 (0.854, 89.4%, 61.9%, 72.4%, and 83.9%), panel 2 (0.875, 95.5%, 57.6%, 71.6%, and 91.9%), panel 3 (0.776, 59.8%, 73.0%, 72.5%, and 60.4%), and panel 4 (0.884, 95.5%, 52.5%, 69.2%, and 91.2%) (Figure 2(b), Table 2). Except for panel 3, which contained six CA biomarkers, the performance of three panels of biomarkers was better than that of any single marker (Table 2). However, panel 3 has good diagnostic efficacy and is shown to be less than two individual biomarkers (CYFR21 and CEA) and superior to the rest of the unique biomarkers (8 biomarkers).

3.4. The Best Marker Combinations for Lung Cancer Screening. To further investigate the value of the four combinations of TAA markers and to identify the best potential panel of biomarkers for LC diagnosis, we performed pairwise comparisons. Without obvious differences in AUC values, the diagnostic value of panel 1 was not inferior to that of panel 2 (all P values > 0.05); there was also no significant difference between panels 1 and 2 compared with panel 4 (all P values > 0.05) (Table 3). However, panel 3, consisting

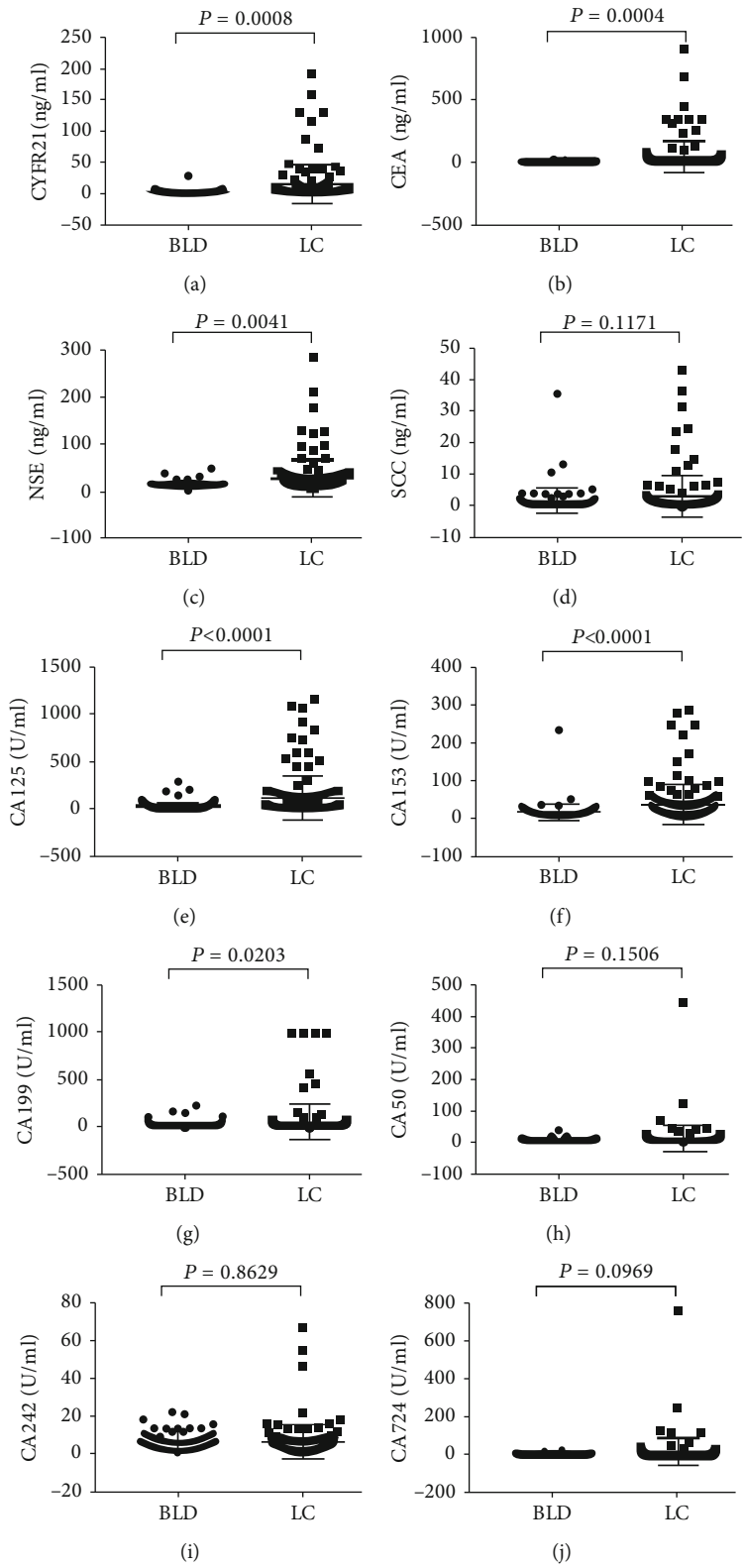

Figure 1: Concentrations of each biomarker between lung cancer (LC) cases and benign lung diseases (BLD) controls. The bold horizontal lines in the box plots are medians, and the lower and upper limits of the boxes are 25th and 75th percentiles of values, respectively. The *P* values were obtained from Mann–Whitney *U* test.

of only CA biomarkers, showed a lower diagnostic accuracy than any of the other three panels; its AUC, sensitivity, and NPV were significantly lower than those of the three panels. Interestingly, adding two of the CA biomarkers (CA125 and CA15-3) to panel 1 to create panel 2 did not improve the diagnostic efficacy.

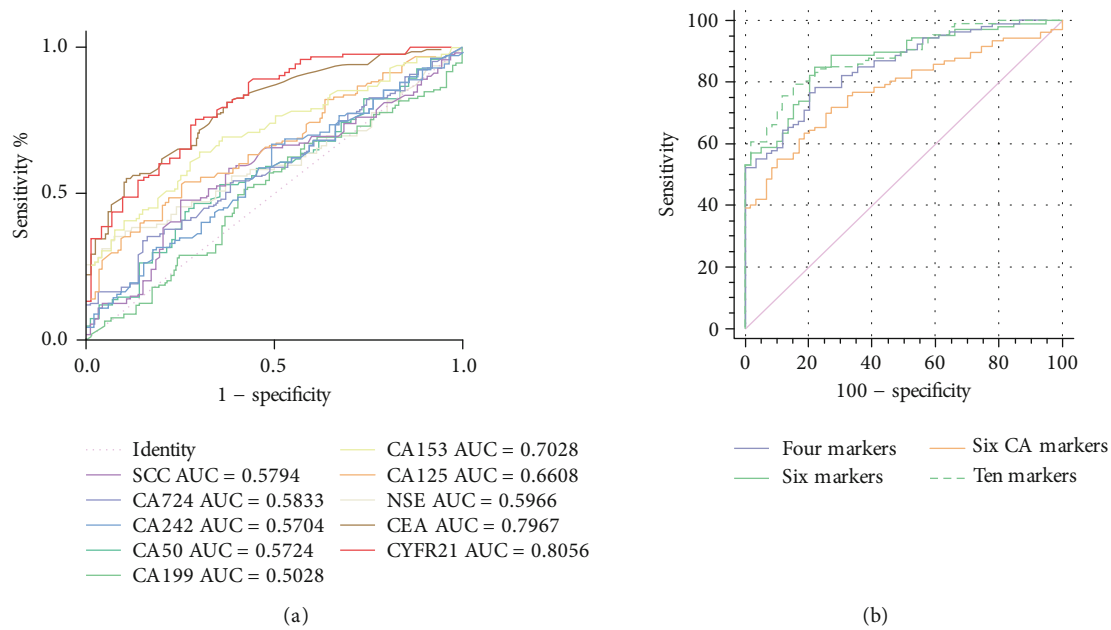

Figure 2: ROC curves to assess the value of single marker and combined markers in lung cancer patients versus benign lung disease controls. (a) ROC of single marker; (b) ROC of combined markers.

Table 2: Performances of biomarkers in lung cancer diagnosis.

Biomarkers	Sensitivity	Specificity	PPV	NPV	AUC (95% CI)
CYFR21	0.735	0.732	0.824	0.619	0.806 (0.743-0.859)
CEA	0.654	0.827	0.817	0.669	0.797 (0.741-0.845)
NSE	0.444	0.757	0.757	0.444	0.597 (0.525-0.665)
SCC	0.192	0.848	0.862	0.426	0.579 (0.511-0.645)
CA125	0.400	0.879	0.833	0.493	0.661 (0.598-0.720)
CA15-3	0.371	0.951	0.920	0.500	0.703 (0.642-0.759)
CA199	0.190	0.915	0.786	0.478	0.503 (0.439-0.567)
CA50	0.063	0.988	0.889	0.411	0.572 (0.494-0.651)
CA242	0.095	0.871	0.522	0.394	0.570 (0.492-0.649)
CA724	0.157	0.941	0.800	0.428	0.583 (0.507-0.660)
The panel 1	0.894	0.619	0.724	0.839	0.854 (0.791-0.904)
The panel 2	0.955	0.576	0.716	0.919	0.875 (0.815-0.921)
The panel 3	0.598	0.730	0.725	0.604	0.776 (0.705-0.837)
The panel 4	0.955	0.525	0.692	0.912	0.884 (0.825-0.928)

PPV: positive predictive value; NPV: negative predictive value; Pane l = CYFR21, CEA, NSE, and SCC; panel 2 = CYFR21, CEA, NSE, SCC, CA125, and CA15-3; panel 3 = CA125, CA15-3, CA19-9, CA50, CA242, and CA724; panel 4 = CYFR21, CEA, NSE, SCC, CA125, CA15-3, CA19-9, CA50, CA242, and CA724.

3.5. Diagnostic Efficacy of the Biomarkers for Lung Cancer Subtypes. To evaluate the diagnostic value of the biomarkers for different subtypes of LC, we performed further histological classification of the patients with lung cancer. For the performance of single markers, CEA (AUC: 0.812; sensitivity: 63.9%) was the most related to lung adenocarcinoma (Figure 3(a), Table 4); CYFR21 (AUC: 0.847; sensitivity: 84.6%) and CEA (AUC: 0.804; sensitivity: 70.0%) were the best suited for squamous-cell carcinoma (Figure 3(b), Table 5); and NSE (AUC: 0.819; sensitivity: 69.0%) and CEA (AUC: 0.808; sensitivity: 60.7%) were the most related to SCLC (Figure 3(c), Table 6). For the performance of the combined markers, without obvious differences in AUC and sensitivity values, there was no significant difference among panels 1, 2, and 4, and all of them showed a higher diagnostic accuracy than panel 3 (Figure 4, Tables 3–5).

4. Discussion

Tumor biomarkers are mainly used for potential diagnosis and for monitoring the efficacy of therapy in lung cancer patients. In this study, we evaluated the detection value of single or combined serum biomarkers for individuals with potential LC. Our results confirmed that CYFRA21-1 and

Table 3: Compare the four panels of biomarkers in lung cancer diagnosis.

Panels	Sensitivity (*P* value)	Specificity (*P* value)	PPV (*P* value)	NPV (*P* value)	AUC (*P* value)
Panel 1 vs. panel 2	0.063	0.507	0.870	0.126	0.194 ($z = 1.300$)
Panel 1 vs. panel 3	<0.0001	0.073	0.988	<0.0001	0.039 ($z = 2.06$)
Panel 1 vs. panel 4	0.063	0.148	0.519	0.180	0.10 ($z = 1.66$)
Panel 2 vs. panel 3	<0.001	0.015	0.871	<0.0001	<0.0001 ($z = 3.44$)
Panel 2 vs. panel 4	1.000	0.432	0.625	0.878	0.387 ($z = 0.86$)
Panel 3 vs. panel 4	<0.001	0.001	0.557	<0.0001	<0.0001 ($z = 4.25$)

Panel = CYFR21, CEA, NSE, and SCC; panel 2 = CYFR21, CEA, NSE, SCC, CA125, and CA15-3; panel 3 = CA125, CA15-3, CA19-9, CA50, CA242, and CA724; panel 4 = CYFR21, CEA, NSE, SCC, CA125, CA15-3, CA19-9, CA50, CA242, and CA724.

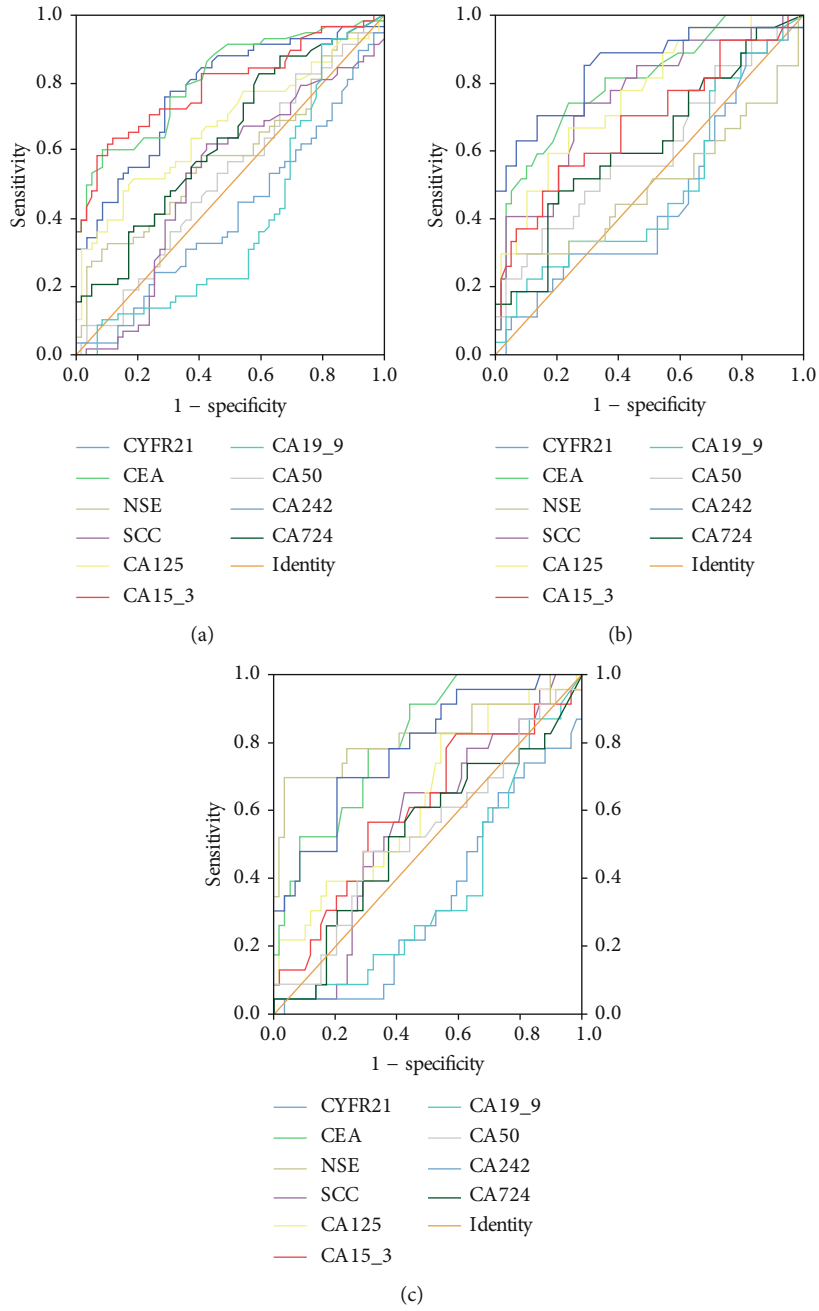

Figure 3: ROC curves to assess the value of single marker in lung cancer subtypes. (a) Adenocarcinoma; (b) squamous-cell carcinoma; (c) small cell lung cancer.

Table 4: Performances of biomarkers in lung adenocarcinoma diagnosis.

Biomarkers	Sensitivity	Specificity	PPV	NPV	AUC (95% CI)
CYFR21	0.766	0.732	0.721	0.776	0.777 (0.693-0.862)
CEA	0.639	0.827	0.667	0.787	0.812 (0.734-0.890)
NSE	0.409	0.757	0.600	0.589	0.589 (0.485-0.694)
SCC	0.123	0.848	0.643	0.549	0.523 (0.415-0.630)
CA125	0.414	0.879	0.744	0.640	0.674 (0.575-0.773)
CA15-3	0.471	0.951	0.892	0.678	0.793 (0.710-0.876)
CA199	0.121	0.915	0.727	0.356	0.399 (0.293-0.505)
CA50	0.042	0.988	0.750	0.547	0.525 (0.420-0.630)
CA242	0.129	0.871	0.450	0.548	0.416 (0.312-0.519)
CA724	0.192	0.941	0.700	0.627	0.640 (0.541-0.740)
The panel 1	0.849	0.619	0.579	0.869	0.864 (0.787-0.922)
The panel 2	0.867	0.576	0.561	0.883	0.897 (0.826-0.946)
The panel 3	0.644	0.730	0.595	0.768	0.794 (0.708-0.864)
The panel 4	0.945	0.525	0.552	0.939	0.904 (0.834-0.951)

Table 5: Diagnostic efficacy of biomarkers with squamous-cell carcinoma.

Biomarkers	Sensitivity	Specificity	PPV	NPV	AUC (95% CI)
CYFR21	0.846	0.732	0.537	0.929	0.847 (0.749-0.945)
CEA	0.700	0.827	0.500	0.914	0.804 (0.702-0.905)
NSE	0.321	0.757	0.333	0.747	0.501 (0.350-0.651)
SCC	0.517	0.848	0.517	0.848	0.758 (0.646-0.870)
CA125	0.464	0.879	0.565	0.830	0.767 (0.661-0.874)
CA15-3	0.321	0.951	0.692	0.804	0.687 (0.559-0.816)
CA199	0.310	0.915	0.750	0.615	0.493 (0.357-0.630)
CA50	0.138	0.988	0.800	0.766	0.599 (0.463-0.735)
CA242	0.172	0.871	0.313	0.755	0.456 (0.322-0.590)
CA724	0.172	0.941	0.455	0.800	0.622 (0.490-0.753)
The panel 1	0.966	0.619	0.364	0.986	0.903 (0.819-0.957)
The panel 2	0.966	0.576	0.359	0.986	0.923 (0.843-0.970)
The panel 3	0.724	0.730	0.396	0.915	0.782 (0.678-0.864)
The panel 4	0.966	0.525	0.333	0.984	0.939 (0.865-0.980)

CEA were the most sensitive as a single marker in the diagnosis of NSCLC, while NSE was the best suited, followed by CEA, for the diagnosis of SCLC, which is in accordance with previous reports [14, 18, 19] (Molina, Agusti et al. 1994, Vinolas, Molina et al. 1998, Liu, Teng et al. 2017). We also found that other individual biomarkers yielded low efficacy for diagnosing LC, especially some CA markers. Even in combination, the CA markers maintained poor diagnostic efficacy with low AUC, sensitivity, and NPV. In contrast, some combinations of multiple markers were shown to improve the diagnostic accuracy over their individual component biomarkers. Our data demonstrated that improved diagnostic accuracy can be achieved with panels combining biomarkers. In particular, panel 1, consisting of 4 TAAs (CYFR21, CEA, NSE, and SCC), panel 2, consisting of 6 TAAs (CYFR21, CEA, NSE, SCC, CA125, and CA15-3), and panel 4, consisting of 10 TAAs (CYFR21, CEA, NSE, SCC, CA125, CA15-3, CA19-9, CA50, CA242, and CA724), showed improved diagnostic efficacy in different types of lung cancer patients. Even when analyzed separately by LC subtypes, their performance was similar. The lack of a difference between their AUCs could be accounted for by assuming that the addition of more markers could not improve the detection rate of LC. However, we did not evaluate the efficacy of combined markers specifically in early-stage patients because of the small number of these patients in this study.

It is well known that different lung cancers have the same antigens, and a single type of cancer will elevate different biomarkers. The value of the detection of single markers for identifying patients with lung cancer is low; therefore, many others have identified combinations of TAA biomarkers that are useful for detecting LC. Most recently, Qu et al. [20] (Qu, Zhang et al. 2019) showed that the combination of thioredoxin (Trx), CYFRA21-1, and SCC biomarkers can improve both specificity and sensitivity to diagnose lung cancer patients from healthy subjects. Jiang et al. [21] (Jiang, Wang

Table 6: Diagnostic efficacy of biomarkers with SCLC.

Biomarkers	Sensitivity	Specificity	PPV	NPV	AUC (95% CI)
CYFR21	0.586	0.732	0.472	0.813	0.783 (0.672-0.894)
CEA	0.607	0.827	0.459	0.897	0.808 (0.711-0.905)
NSE	0.690	0.757	0.526	0.862	0.819 (0.696-0.943)
SCC	0.074	0.848	0.125	0.757	0.557 (0.425-0.690)
CA125	0.269	0.879	0.412	0.793	0.633 (0.498-0.768)
CA15-3	0.160	0.951	0.500	0.788	0.607 (0.466-0.748)
CA199	0.214	0.915	0.667	0.593	0.367 (0.238-0.497)
CA50	0.071	0.988	0.667	0.759	0.531 (0.387-0.674)
CA242	0.077	0.871	0.154	0.755	0.340 (0.213-0.467)
CA724	0.038	0.941	0.143	0.793	0.529 (0.385-0.673)
The panel 1	0.931	0.619	0.355	0.972	0.884 (0.794-0.945)
The panel 2	0.931	0.576	0.659	0.882	0.908 (0.822-0.961)
The panel 3	0.483	0.730	0.304	0.851	0.720 (0.609-0.814)
The panel 4	0.931	0.525	0.325	0.969	0.928 (0.848-0.973)

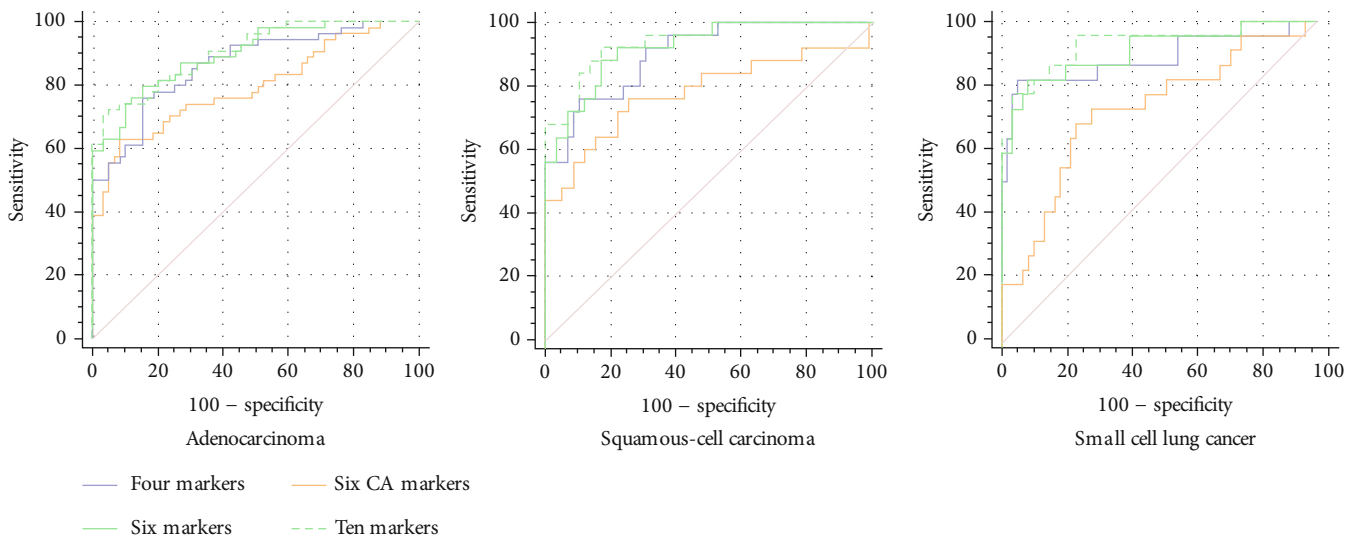

Figure 4: ROC curves to assess the value of combined markers in lung cancer subtypes.

et al. 2018) investigated a combination of CEA, CYFRA21, NSE, and thymidine kinase 1 (TK1) for lung cancer diagnosis; the results showed that the diagnostic value of TK1 combined with CEA, CYFRA21-1, and NSE was significantly higher than that of each biomarker alone. In addition, TK1 combined with CEA, CYFRA21-1, or NSE could improve the diagnosis of squamous cell carcinoma, adenocarcinoma, or small cell lung cancer, respectively. Mazzone et al. [22] (Mazzone, Wang et al. 2018) also validated a panel of biomarkers, including hepatocyte growth factor (HGF), CEA, CYFRA21-1, CA125, and New York esophageal cancer-1 antibody (NY-ESO-1), together with clinical variables (including age, sex, COPD status, and smoking history). They reported an increase in AUC from 0.81 to 0.86 for the biomarkers combined with the clinical variables, with a specificity of 88% and sensitivity of 67%. Yoon et al. [15] (Yoon, Kwon et al. 2016) discovered a combination of six biomarkers (HE4, CEA, RANTES, ApoA2, TTR, and sVCAM-1) with a sensitivity of 93.33% and specificity of 92.00% in the diagnosis of lung cancer. Liu et al. [14] (Liu, Teng et al. 2017) found that the combination of six tumor markers (CEA, CYFRA21-1, SCC, NSE, ProGRP, and CA125) could discriminate the histological types of lung cancer between SCLC and NSCLC. Korkmaz et al. [23] (Korkmaz, Koksal et al. 2018) suggested a panel of three serum tumor biomarkers, CYFRA21-1, HE4, and progastrin-releasing peptide (ProGRP) that might contribute to discriminating lung cancer from BLD. They reported an increase in the diagnostic value (AUC = 0.899) for CYFRA21-1 combined with HE4 for discriminating LC from BLD, while ProGRP alone had the highest diagnostic value (AUC = 0.875) for discriminating SCLC from NSCLC. Fang et al. [13] (Fang, Zhu et al. 2018) found that a panel of PRL, CEA, and CYFRA21 biomarkers was more effective than the individual biomarkers alone, with

a relatively high sensitivity and specificity for the diagnosis of NSCLC. Consistent with these observations, we found that some panels of combined TAA biomarkers yielded a better, more optimal diagnostic efficacy for cancer patients than the individual biomarkers alone. We found that the panel consisting of 4 TAAs (CYFR21, CEA, NSE, and SCC) showed good diagnostic efficacy for lung cancer screening in BLD, with an AUC of 0.854 and a sensitivity of 89.4%. The diagnostic value of the four-TAA combination was not inferior to that of the panel of 6 TAAs (CYFR21, CEA, NSE, SCC, CA125, and CA15-3) or 10 TAAs (CYFR21, CEA, NSE, SCC, CA125, CA15-3, CA19-9, CA50, CA242, and CA724) because there were no statistically significant differences among them (all P values > 0.05). Even when analyzed individually by LC subtypes, the performance of these combinations was also similar. This means that the addition of more markers did not improve the detection rate of LC patients.

However, not all combinations of biomarkers improve diagnostic efficacy. Mauro et al. [24] (Mauro, Passerini et al. 2019) found that using two markers (ProGRP and NSE) did not increase the accuracy over either marker individually for small cell lung cancer diagnosis. Yang et al. [17] (Yang, Zhang et al. 2018) also showed that a two-marker combination is more suitable than a multimarker combination for the serological screening of tumors. In the present study, we found that a panel of six CA biomarkers (CA125+ CA15-3+ CA19-9+ CA50+ CA242+ CA724) did not yield better diagnostic efficacy for lung cancer patient screening, whether overall or for LC subtypes. The diagnostic accuracy of the combination including CA markers was not only inferior to that of the other three panels but was also not superior to some of the single biomarkers, such as CYFRA21 or CEA. It is probable that the reason is linked to the similar serum concentrations of three of the six CA markers (CA50+ CA242+ CA724) between LC patients and BLD controls, and others demonstrate poor diagnostic efficacy for lung cancer screening. The serum CA levels not only increase in lung cancer and other types of cancers but also in nonneoplasm diseases and healthy individuals [25–29] (Glasgow, Pacheco-Rodriguez et al. 2018, Dou, Sun et al. 2019, Shan, Tian et al. 2019, Zeng, Li et al. 2019, Zhang, Zhang et al. 2019). However, even adding CA125 and CA15-3 into the panel with 4 markers (CEA + CY211 + NSE + SCC) could not improve the diagnostic efficacy of LC and BLD identification. These results indicate that a single biomarker or a panel that includes CA biomarkers is not a good choice for this purpose.

In conclusion, CYFR21 and CEA were elevated in patients with LC and could potentially be used as effective single serum biomarkers for the diagnosis of NSCLC, while NSE and CEA were the most sensitive for the diagnosis of SCLC. As a less expensive test to distinguish between LC and BLD in general practice clinics, the combination of four serum biomarkers (CYFR21, CEA, NSE, and SCC) seems more promising for the diagnosis of lung cancer and should be used in common practice. However, combinations including CA biomarkers may not be appropriate for diagnosing lung cancer. Our research also has some limitations. Due to the lack of samples, the efficacy of combined markers specifically in early-stage patients needs to be improved. We will collect more samples of early-stage patients to verify our findings.

Data Availability

The data used to support the findings of this study are available from the corresponding author upon request.

Conflicts of Interest

The authors declare that they have no conflicts of interest.

Authors' Contributions

ZL conceived and designed the experiments. ZW and YH performed the experiments. JC and XW analyzed the data. ZT and RS contributed reagents/materials/analysis tools. ZL and YD contributed to the writing of the manuscript. Final approval of the version is to be submitted by ZH. Zhineng Wen and Ying Huang contributed equally to this work.

Acknowledgments

We are grateful to Laura Tipton for her excellent assistance. This work was supported in part by funding from the Key Research and Development Program of Guangxi Zhuang Autonomous Region (No. AB16380152), in part from the Key Research and Development Program of Liuzhou (2018BJ10509), and in part from'139' Incubation Program for high-level medical talents in Guangxi.

References

[1] R. L. Siegel, K. D. Miller, and A. Jemal, "Cancer statistics, 2019," *CA: a cancer journal for clinicians*, vol. 69, no. 1, pp. 7–34, 2018.

[2] L. A. Torre, R. L. Siegel, and A. Jemal, "Lung cancer statistics," in *Lung cancer and personalized medicine*, pp. 1–19, Springer, 2016.

[3] J. Lortet-Tieulent, I. Soerjomataram, J. Ferlay, M. Rutherford, E. Weiderpass, and F. Bray, "International trends in lung cancer incidence by histological subtype: Adenocarcinoma stabilizing in men but still increasing in women," *Lung Cancer*, vol. 84, no. 1, pp. 13–22, 2014.

[4] A. A. Adjei, "Lung cancer worldwide," *Journal of Thoracic Oncology*, vol. 14, no. 6, p. 956, 2019.

[5] R. M. Feng, Y. N. Zong, S. M. Cao, and R. H. Xu, "Current cancer situation in China: good or bad news from the 2018 global cancer statistics?," *Cancer Community*, vol. 39, no. 1, p. 22, 2019.

[6] Y. Satoh, R. Hoshi, Y. Ishikawa, T. Horai, S. Okumura, and K. Nakagawa, "Recurrence patterns in patients with early stage non-small cell lung cancers undergoing positive pleural lavage cytology," *The Annals of Thoracic Surgery*, vol. 83, no. 1, pp. 197–202, 2007.

[7] D. P. Weller, M. D. Peake, and J. K. Field, "Presentation of lung cancer in primary care," *NPJ Primary Care Respiratory Medicine*, vol. 29, no. 1, p. 21, 2019.

[8] Z. Q. Chen, L. S. Huang, and B. Zhu, "Assessment of seven clinical tumor markers in diagnosis of non-small-cell lung cancer," *Disease Markers*, vol. 2018, 7 pages, 2018.

[9] S. Isaksson, P. Jönsson, N. Monsef et al., "CA 19-9 and CA 125 as potential predictors of disease recurrence in resectable lung

adenocarcinoma," *PLoS One*, vol. 12, no. 10, article e0186284, 2017.

[10] L. M. Seijo, N. Peled, D. Ajona et al., "Biomarkers in lung cancer screening: achievements, promises, and challenges," *Journal of Thoracic Oncology*, vol. 14, no. 3, pp. 343–357, 2019.

[11] Y. Dou, Y. Zhu, J. Ai et al., "Plasma small ncRNA pair panels as novel biomarkers for early-stage lung adenocarcinoma screening," *BMC Genomics*, vol. 19, no. 1, p. 545, 2018.

[12] X. Li, Q. Zhang, X. Jin, and L. Cao, "Combining serum miRNAs, CEA, and CYFRA21-1 with imaging and clinical features to distinguish benign and malignant pulmonary nodules: a pilot study," *World Journal of Surgical Oncology*, vol. 15, no. 1, p. 107, 2017.

[13] R. Fang, Y. Zhu, V. S. Khadka, F. Zhang, B. Jiang, and Y. Deng, "The evaluation of serum biomarkers for non-small cell lung cancer (NSCLC) diagnosis," *Frontiers in Physiology*, vol. 9, p. 1710, 2018.

[14] L. Liu, J. Teng, L. Zhang et al., "The combination of the tumor markers suggests the histological diagnosis of lung cancer," *BioMed Research International*, vol. 2017, 9 pages, 2017.

[15] H. I. Yoon, O. R. Kwon, K. N. Kang et al., "Diagnostic value of combining tumor and inflammatory markers in lung cancer," *Journal of Cancer Prevention*, vol. 21, no. 3, pp. 187–193, 2016.

[16] W. D. Travis, E. Brambilla, A. G. Nicholson et al., "The 2015 World Health Organization classification of lung tumors: impact of genetic, clinical and radiologic advances since the 2004 classification," *Journal of Thoracic Oncology*, vol. 10, no. 9, pp. 1243–1260, 2015.

[17] Q. Yang, P. Zhang, R. Wu, K. Lu, and H. Zhou, "Identifying the best marker combination in CEA, CA125, CY211, NSE, and SCC for lung cancer screening by combining ROC curve and logistic regression analyses: is it feasible?," *Disease Markers*, vol. 2018, 12 pages, 2018.

[18] N. Viñolas, R. Molina, M. C. Galán et al., "Tumor markers in response monitoring and prognosis of non-small cell lung cancer: preliminary report," *Anticancer Research*, vol. 18, no. 1B, pp. 631–634, 1998.

[19] R. Molina, C. Agusti, X. Filella et al., "Study of a new tumor marker, CYFRA 21-1, in malignant and nonmalignant diseases," *Tumour Biology*, vol. 15, no. 6, pp. 318–325, 1994.

[20] T. Qu, J. Zhang, N. Xu et al., "Diagnostic value analysis of combined detection of Trx, CYFRA21-1 and SCCA in lung cancer," *Oncology Letters*, vol. 17, no. 5, pp. 4293–4298, 2019.

[21] Z. F. Jiang, M. Wang, and J. L. Xu, "Thymidine kinase 1 combined with CEA, CYFRA21-1 and NSE improved its diagnostic value for lung cancer," *Life Sciences*, vol. 194, pp. 1–6, 2018.

[22] P. J. Mazzone, X. F. Wang, X. Han et al., "Evaluation of a serum lung cancer biomarker panel," *Biomarker Insights*, vol. 13, p. 117727191775160, 2018.

[23] E. T. Korkmaz, D. Koksal, F. Aksu et al., "Triple test with tumor markers CYFRA 21.1, HE4, and ProGRP might contribute to diagnosis and subtyping of lung cancer," *Clinical Biochemistry*, vol. 58, pp. 15–19, 2018.

[24] C. Mauro, R. Passerini, L. Spaggiari et al., "New and old biomarkers in the differential diagnosis of lung cancer: progastrin-releasing peptide in comparison with neuron-specific enolase, carcinoembryonic antigen, and CYFRA 21-1," *The International Journal of Biological Markers*, vol. 34, no. 2, pp. 163–167, 2019.

[25] M. Shan, Q. Tian, and L. Zhang, "Serum CA50 levels in patients with cancers and other diseases," *Progress in Molecular Biology and Translational Science*, vol. 162, pp. 187–198, 2019.

[26] H. Dou, G. Sun, and L. Zhang, "CA242 as a biomarker for pancreatic cancer and other diseases," *Progress in Molecular Biology and Translational Science*, vol. 162, pp. 229–239, 2019.

[27] Y. Zhang, M. Zhang, X. Bai, C. Li, and L. Zhang, "Increased serum CA724 levels in patients suffering gout vs cancers," *Progress in Molecular Biology and Translational Science*, vol. 162, pp. 177–186, 2019.

[28] P. Zeng, H. Li, Y. Chen, H. Pei, and L. Zhang, "Serum CA199 levels are significantly increased in patients suffering from liver, lung, and other diseases," *Progress in Molecular Biology and Translational Science*, vol. 162, pp. 253–264, 2019.

[29] C. G. Glasgow, G. Pacheco-Rodriguez, W. K. Steagall et al., "CA-125 in disease progression and treatment of lymphangioleiomyomatosis," *Chest*, vol. 153, no. 2, pp. 339–348, 2018.

Hindawi
Disease Markers
Volume 2020, Article ID 8042705, 11 pages
https://doi.org/10.1155/2020/8042705

Research Article

Molecular Markers for Detecting *Schistosoma* Species by Loop-Mediated Isothermal Amplification

Pedro Fernández-Soto,[1] Catalina Avendaño,[2] Anna Sala-Vizcaíno,[1] Beatriz Crego-Vicente,[1] Begoña Febrer-Sendra,[1] Juan García-Bernalt Diego,[1] Ana Oleaga,[3] Julio López-Abán,[1] Belén Vicente,[1] Manuel A. Patarroyo,[4,5] and Antonio Muro[1]

[1]*Infectious and Tropical Diseases Research Group (e-INTRO), Biomedical Research Institute of Salamanca, Research Centre for Tropical Diseases at the University of Salamanca (IBSAL-CIETUS), Faculty of Pharmacy, University of Salamanca, 37007 Salamanca, Spain*
[2]*Animal Science Faculty, Universidad de Ciencias Aplicadas y Ambientales (U.D.C.A), 111166 Bogotá, Colombia*
[3]*Parasitología Animal, Instituto de Recursos Naturales y Agrobiología de Salamanca (IRNASA, CSIC), Cordel de Merinas, 40-52, 37008 Salamanca, Spain*
[4]*Fundación Instituto de Inmunología de Colombia (FIDIC), 111321, Bogotá, Colombia*
[5]*School of Medicine and Health Sciences, Universidad del Rosario, 112111 Bogotá, Colombia*

Correspondence should be addressed to Manuel A. Patarroyo; mapatarr.fidic@gmail.com and Antonio Muro; ama@usal.es

Received 23 October 2019; Revised 20 June 2020; Accepted 1 July 2020; Published 24 July 2020

Academic Editor: Lucio Castellano

Schistosomiasis is considered a neglected parasitic disease. Around 280,000 people die from it annually, and more than 779 million people are at risk of getting infected. The schistosome species which infect human beings are *Schistosoma mansoni*, *Schistosoma haematobium*, *Schistosoma intercalatum*, *Schistosoma japonicum*, *Schistosoma guineensis*, and *Schistosoma mekongi*. This disease is also of veterinary significance; the most important species being *Schistosoma bovis* since it causes the disease in around 160 million livestock in Africa and Asia. This work was aimed at designing and developing a genus-specific loop-mediated isothermal amplification (LAMP) method for detecting the most important schistosome species affecting humans and for the species-specific detection of *S. bovis*. Bioinformatics tools were used for primer design, and the LAMP method was standardised for detecting the ITS-1 region from *S. intercalatum*, *S. haematobium*, *S. mansoni*, *S. japonicum*, and *S. bovis* DNA (generic test) and the NADH 1 gene for specifically detecting *S. bovis* (at different DNA concentrations). Detection limits achieved were 1 pg DNA for *S. mansoni*, 0.1 pg for *S. haematobium*, 1 pg for *S. intercalatum*, and 10 pg for *S. bovis*. No amplification for *S. japonicum* DNA was obtained. The LAMP designed for the amplification of *S. bovis* NADH-1 worked specifically for this species, and no other DNA from other schistosome species included in the study was amplified. Two highly sensitive LAMP methods for detecting different *Schistosoma* species important for human and veterinary health were standardised. These methods could be very useful for the diagnosis and surveillance of schistosome infections.

1. Introduction

Schistosomiasis is a parasitic disease caused by several species of trematode worms of the genus *Schistosoma*. It is one of the 20 tropical diseases on the World Health Organization's (WHO) list of Neglected Tropical Diseases (NTDs) [1]. The disease affects at least 240 million people worldwide and more than 779 million are at risk of contracting it [2]. The infection is endemic in 78 countries, mainly in tropical and subtropical areas, although it predominates in Sub-Saharan Africa where more than 80% of the cases occur, leading to around 280,000 deaths annually. The Global Burden of Disease study attributed 1.43 million disability-adjusted life years (DALYs) to it in 2017 [2–5].

Of the 23 *Schistosoma* species described to date, *S. mansoni*, *S. haematobium*, and *S. japonicum* are the main human species [6, 7]. Nevertheless, schistosomes also represent a health problem for animals, including ruminants, rodents, and primates. The species causing animal schistosomiasis are mainly *Schistosoma bovis*, *S. japonicum*, *S. mekongi*, *S. mattheei*, *S. curassoni*, *S. margrebowiei*, *S. leiperi*, *S. indicum*, and *S. spindale*. *S. bovis* is one of the most important ones parasitizing cattle and causing significant economic losses, affecting around 160 million animals in Africa and Asia [8, 9].

Schistosomes have a complex life cycle requiring an aquatic snail as intermediate host and a vertebrate as definitive host [10]. Schistosomiasis is acquired by direct contact with fresh water contaminated by parasite larvae (called cercariae), which have been emitted into an aquatic environment by the aquatic snails, actively penetrating the skin of a susceptible host [11]. Paired couples of adult schistosome worms live in a definitive host's mesenteric or perivascular veins where they reproduce and lay their eggs. The eggs are released into the environment through urine (*S. haematobium*) or faeces (the rest of the species) or can be retained in host tissues where they induce an inflammatory response [7].

Both *S. mansoni* and *S. haematobium* are found in Africa and the Middle East, whereas *S. mansoni* is the only species found in South America. *S. japonicum* occurs in Asia, especially in the Philippines and China; *S. mekongi* in the Mekong river basin, and *S. guineensis* and *S. intercalatum* in West and Central Africa [7]. *S. bovis* can be found throughout the African continent, south-western Asia (Israel, Iran, Iraq, Syria, and Turkey), Mediterranean islands (Corsica, Sardinia, and Sicily), and the Iberian peninsula [12].

Schistosomiasis can be treated if an accurate diagnosis is made and a prompt treatment with praziquantel (PZQ) is administered. Using appropriate and sensitive diagnostic techniques is thus essential for identifying infected individuals [13]. Parasitological diagnosis is specific, cheap, and simply performed. However, in laboratories with limited resources, it is not very sensitive, especially when infection intensity is low, as occurs in areas with low prevalence and/or in individuals having been recently infected or having low parasite load. Furthermore, this can only be done after egg production and elimination has begun, approximately two months after infection [11]. Immunodiagnostic tests have been shown to have high sensitivity in cases where parasitological techniques have provided false negative results [13]. However, they have problems related to obtaining antigens and false positive results since it is difficult to differentiate between active and/or past infections or reinfections and there can also be problems regarding specificity with other helminths or even between different species from the genus *Schistosoma*. Furthermore, such tests are not useful during the disease's acute phase, since antibodies targeting the parasite would not yet have appeared [11, 13]. On the other hand, immunodiagnostic tests based on detecting the circulating cathodic antigen (CCA) or circulating anodic antigen (CAA) in either urine or blood have the advantage of not requiring a trained personnel for their interpretation or specialised equipment, being more sensitive and specific than egg detection in faeces by microscopy, although they could give false positive results. It is worth highlighting that such techniques detect adult forms and not eggs, so xenomonitoring combining either CAA or CCA with molecular biology techniques is thus recommended for verification and maintaining elimination [14].

Molecular diagnosis is particularly useful regarding infections with low parasitaemia [15, 16]. PCR and its variants have been of great use, and some authors have proposed such techniques as the gold standard for diagnosing schistosomiasis [17]. However, they are expensive and require a specialised personnel and equipment, meaning that they are not useful for diagnosis in field conditions and their use is limited to just a few reference laboratories [18].

Several molecular techniques based on isothermal methods exist, such us nucleic acid sequence-based amplification (NASBA, also known as transcription-mediated amplification, TMA), signal-mediated amplification of ribonucleic acid (RNA) technology (SMART), helicase-dependent amplification (HDA), recombinase polymerase amplification (RPA), rolling circle amplification (RCA), multiple displacement amplification (MDA), loop-mediated isothermal amplification (LAMP), and strand displacement amplification (SDA); such techniques might provide an alternative tool regarding other more complex molecular methods [19]. The development and application of new methods meeting the characteristics for the ideal diagnosis of schistosomiasis should include high sensitivity and specificity, ease of use and interpretation, being able to use different sample types, rapidity, low cost, and being able to be applied in disease-endemic areas having scarce economic resources [20]. This work describes designing and developing a LAMP method for detecting species-specific *S. bovis* and a genus-specific LAMP method for detecting the most important schistosome species affecting humans.

2. Materials and Methods

2.1. Selecting Targets for LAMP Amplification of Schistosoma bovis and Genus Schistosoma. When this study started, the *S. bovis* genome had not been yet completely sequenced and there was limited sequence information in databases. Thus, a thorough search in the GenBank database (https://www.ncbi.nlm.nih.gov/genbank/) was carried out to locate all possible available DNA sequences. An alignment of the sequences found was carried out using ClustalW to obtain a consensus sequence. When the comparison did not allow generating a consensus sequence, different sequence groups were made up based on their greater identity. Subsequently, the BLAST program (Basic Local Alignment Search Tool; https://blast.ncbi.nlm.nih.gov/Blast.cgi) was used to assess the identity of *S. bovis* sequences obtained to other species. Then, to refine the search and obtain greater accuracy in the results, the sequences were compared in two other schistosome-specific databases: SchistoDB (Schistosoma Genomic Resources; http://schistodb.net/schisto/), which contains the genome of *S. mansoni*, *S. haematobium*, and *S. japonicum*, and the Wellcome Trust Sanger Institute database (http://www.sanger.ac.uk/), which houses continuously updated genome sequencing results of 50 helminths,

including several *Schistosoma* species (50 Helminth Genomes Project; http://www.sanger.ac.uk/science/collaboration/50hgp). Once all *S. bovis* sequences were compared and analysed, the most suitable one was selected for designing specific primers for the LAMP.

Useful sequences for designing the specific primers for developing a LAMP method for amplifying the genus *Schistosoma* were selected following similar steps as those described above for *S. bovis*.

2.2. Designing LAMP Primers. LAMP primer sets complementary to the selected specific nucleotide sequences were designed using both the online PrimerExplorer V5 software (Eiken Chemical Co., Ltd., Japan; https://primerexplorer.jp/e/) and the LAMP Designer software (OptiGene Ltd., UK; http://www.optigene.co.uk/lamp-designer/) since the two programs use different design parameters. HPLC grade primers were used (Thermo Fisher Scientific Inc., Madrid, Spain). Lyophilised primers were resuspended in ultrapure water to a final 100 pmol/μL concentration and stored at -20°C until use.

2.3. Obtaining and Preparing Schistosoma Species DNA. S. bovis adult worms were obtained from hamsters experimentally infected in the laboratory of Animal Parasitology, Institute of Natural Resources and Agrobiology of Salamanca (IRNASA-CSIC), Spain. *S. bovis* genomic DNA (gDNA) was extracted from worms kept frozen using the NucleoSpin Tissue Kit (Macherey-Nagel, GmbH&Co., Germany) following the manufacturers' instructions.

S. mansoni DNA (Brazilian strain) was extracted from frozen adult male and female worms available in our laboratory. This strain has been maintained by serial passages in mice routinely infected in the Laboratory of Parasitic and Molecular Immunology, CIETUS, University of Salamanca. Genomic DNA from adult male and female *S. haematobium* (Egyptian Strain; NR-31682) and genomic DNA from adult male and female *S. japonicum* (Chinese Strain; NR-36066) were obtained from the Schistosomiasis Resource Centers for distribution by BEI Resources, NIAID, NIH (https://www.beiresources.org/Collection/51/Schistosome-Resource-Centers.aspx). *S. intercalatum* DNA was provided by Doctor José Manuel da Costa from the Center for Parasite Biology and Immunology, National Institute of Health Doutor Ricardo Jorge, Porto, Portugal. This DNA comes from a donation from Centers for Disease Control and Prevention, Atlanta, USA. All gDNAs were measured three times by spectrophotometry using a Nanodrop ND-100 spectrophotometer (Nanodrop Technologies) to obtain an average concentration and then diluted with ultrapure water to a final 5 ng/μL concentration. Subsequently, serial 10-fold dilutions from schistosomes' DNA were prepared with ultrapure water ranging from 1×10^{-1} to 1×10^{-9} and stored at -20°C until use. DNAs thus prepared were used as positive controls in all LAMP and PCR reactions as well as for assessing sensitivity and specificity of both assays.

2.4. PCR with F3 and B3 External Primers. A touchdown PCR (TD-PCR) using designated F3 and B3 external primers was initially tested to verify that the correct target sequence selected *in silico* was amplified. The PCR assay was conducted in a 25 μL reaction mixture containing 2.5 μL of 10x buffer, 1.5 μL of 25 mM $MgCl_2$, 2.5 μL of 2.5 mM dNTPs, 0.5 μL of 100 pM F3 and B3, 2 U *Taq*-polymerase, and 2 μL (10 ng) of DNA template. Initial denaturation was conducted at 94°C for 1 min, followed by a touchdown program for 15 cycles with successive annealing temperature decrements of 1.0°C every 2 cycles. For these 2 cycles, the reaction was denatured at 94°C for 20 s followed by annealing at 65°C–60°C for 20 s and extension at 72°C for 30 s. The following 15 amplification cycles were similar, except that the annealing temperature was 59°C. The final extension was performed at 72°C for 10 min. The same reaction mixture was used in all PCR reactions (except for the primers), and the amplification conditions varied according to different annealing temperatures of the primers used.

DNA samples (2 μL; 0.5 ng/μL) from the *Schistosoma* species included were used to evaluate specificity; negative (ultrapure water instead of DNA) and positive (DNA from each species) controls were included in each PCR assay.

2.5. LAMP Assay. The LAMP primer sets designed were evaluated by using a reaction mixture containing 40 pmol each of FIP and BIP primers, 5 pmol each of F3 and B3 primers, 1.4 mM each of dNTP (Intron), 1x Isothermal Amplification Buffer-20 mM Tris-HCl (pH 8.8), 50 mM KCl, 10 mM $(NH_4)_2SO_4$, 2 mM $MgSO_4$, 0.1% Tween20 (New England Biolabs, UK)-betaine (1 M) (Sigma, USA), supplementary $MgSO_4$ (4 mM) (New England Biolabs, UK), and 8 U of *Bst* polymerase 2.0 WarmStart (New England Biolabs, UK) with 2 μL (1 ng) of template DNA. LAMP reactions were performed in 0.2 mL tubes that were incubated in a dry bath heat block at 63°C-65°C for 60 min and then heated at 80°C for 5-10 min to stop the reaction.

Schistosome DNA samples mentioned above were used to evaluate the specificity of the LAMP assay; the lower detection limit of the LAMP assay was established by using 10-fold serial dilutions prepared as previously described. Positive controls (DNA from all species tested) and negative controls (ultrapure water instead of DNA) were included in all LAMP reactions.

2.6. Detection of Amplification Products. PCR amplification products were monitored using 1.5% agarose gel electrophoresis stained with ethidium bromide and visualised under UV light.

LAMP reaction results were visually inspected by colorimetric change by adding 2 μL (1 : 10, 10,000x) SYBR Green I fluorescent dye (Invitrogen, Carlsbad, California, USA) to the reaction tubes. Green fluorescence was observed in positive reactions whilst it remained original orange in negative reactions; additionally, the products (3-5 μL) were monitored by 1.5% agarose gel electrophoresis and visualised under UV light. All electrophoresed PCR and LAMP agarose gels were photographed using an ultraviolet gel documentation system (UVItec, UK).

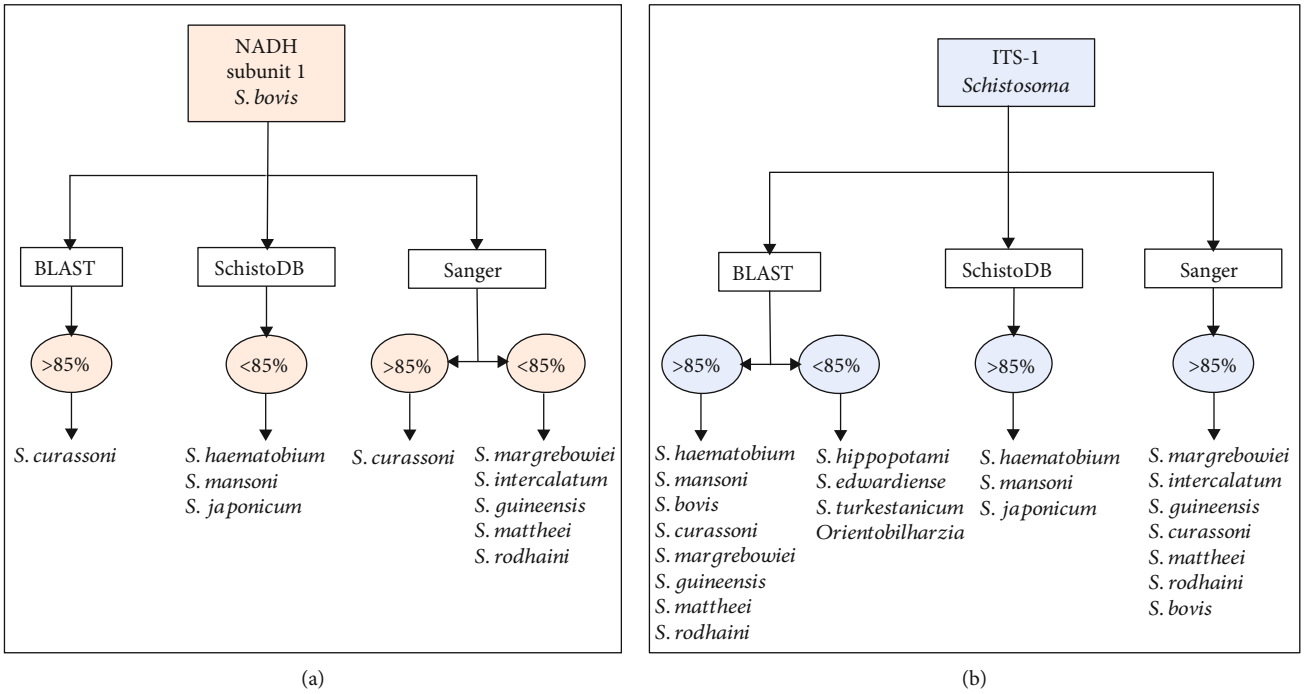

Figure 1: Degree of sequence similarity detected amongst the selected sequences for designing the LAMP primers and schistosome sequences queried in each database. (a) *S. bovis* mitochondrial NADH subunit 1 sequence. (b) ITS-1 sequence from several *Schistosoma* species.

3. Results

3.1. Selecting Targets for LAMP Amplification of Schistosoma bovis and Genus Schistosoma. Sequence similarity analysis of the selected sequences downloaded from the GenBank, SchistoDB, and Sanger databases allowed selecting several potentially useful sequences to design primers for the specific detection by LAMP of *S. bovis* and for the simultaneous detection of several schistosome species (genus *Schistosoma*) (Tables S1, S2). After comparison, a 678 bp sequence derived from mitochondrial NADH subunit 1 (NADH-1) (GenBank access number HM594942) and a 457 bp sequence from the internal transcribed spacer 1 (ITS-1) (GenBank access number GU257398) were selected for detecting *S. bovis* and *Schistosoma* spp., respectively (Figure 1).

3.2. Designing and Synthesising Primers for LAMP Amplification. Specific LAMP primers were designed using two programs: LAMP Designer and PrimerExplorer V5. Different primer sets were generated depending on the particular characteristics and parameters evaluated by each software. A set of 6 primers (including 2 loop primers) were thus selected to amplify the *S. bovis* NADH-1 sequence as designed by the LAMP Designer software, whilst a set of 5 primers (including 1 loop primer) to amplify *Schistosoma* species ITS-1 sequence, as designed in the PrimerExplorer software (Table 1).

3.3. TD-PCR with F3 and B3 External Primers. After testing several different reaction temperatures and cycles, amplification conditions for TD-PCR were finally established for *S. bovis* NADH-1 (range 58-53°C; 53°C × 15 cycles) and *Schistosoma* spp. ITS-1 fragment (range 61-57°C; 57°C × 30 cycles). An approximately 420 bp PCR product was obtained for *S. bovis* NADH-1 sequence (400 bp predicted *in silico*) (Figure 2). This sequence was only amplified when using *S. bovis* DNA, but no amplicons were obtained with DNA samples from other schistosome species tested.

On the other hand, a PCR product between 220 and 225 bp was obtained for *Schistosoma* spp. ITS-1 sequence (216 bp predicted *in silico*) (Figure 3). This PCR product was successfully amplified when DNA samples from the schistosome species included in the study were analysed. However, amplicons obtained for *S. mansoni*, *S. haematobium*, and *S. bovis* showed a greater signal intensity than those obtained for *S. japonicum* and *S. intercalatum*.

3.4. LAMP for Amplifying S. bovis NADH-1 and Genus Schistosoma ITS-1 Target Sequences. As shown in Figure 4, only LAMP products were obtained when *S. bovis* DNA was used as template to amplify NADH-1 sequence. No false positive amplification was observed when using DNA from other schistosomes (Figure 4(a)), thus indicating the high specificity of the designed LAMP primers. Regarding sensitivity, the results indicated that the detection limit of LAMP for *S. bovis* NADH-1 amplification was 0.01 ng (10 pg) (Figure 4(b)).

LAMP results when using the specific primers to amplify ITS-1 sequence for several schistosome species DNA are shown in Figure 5. Amplification products were observed when using DNA from *S. mansoni*, *S. haematobium*, *S. intercalatum*, and *S. bovis*, but not from *S. japonicum*. Colour change was clearly visualised in positive results, and also, a

Table 1: Primer sets selected in this work for amplifying the *S. bovis* NADH subunit 1 and the ITS-1 region from the genus *Schistosoma*.

(a) LAMP primers for the *S. bovis* sequence (LAMP Designer)

NADH subunit 1 Primer	5′ pos	3′ pos	Length (bp)	Tm (°C)	GC ratio (%)	Sequence
SbF3	219	236	18	56.8	38.9	TTCATTGTTAGGTTGCGT
SbB3	642	619	24	57	33.3	TCTATATTCTACTCTAATCCCTCT
SbFIP			48			TCAGTATCATCTCAAACATCACACTAGTAGTATGTTCTGTCTTA AGTT
SbBIP			45			TTTGTAGTACCTCTGGTTTACATCATTCACTCTCAGACTCTACAT
SbF2	327	349	23	56.8	30.4	AGTAGTATGTTCTGTCTTAAGTT
SbF1c	424	448	25	62.1	36	TCAGTATCATCTCAAACATCACACT
SbB2	593	612	20	57	40	TTCACTCTCAGACTCTACAT
SbB1c	520	544	25	61.8	36	TTTGTAGTACCTCTGGTTTACATCA
SbLF	364	388	25	61.9	36	ACTTAGACCATGAACATCAACCTAT
SbLB	560	584	25	61.9	40	TACTAAGTGAGAGTAATCGAACACC

(b) LAMP primers for the genus *Schistosoma* sequence (Primer Explorer V5)

ITS-1 Primer	5′ pos	3′ pos	Length (bp)	Tm (°C)	GC ratio (%)	Sequence
SF3	2	19	18	59.7	61	TTGACCGGGGTACCTAGC
SB3	200	218	19	59.5	53	CGTGAATGGCAAGCCAAAC
SFIP			39			ATCGCCCTTGGCAGATCAGGCTGTCGTATGCCCTGATGG
SBIP			40			ATATGCATGCAAATCCGCCCCGCGGATCGCTTCAACAGTGTA
SF2	20	38	19	59.2	58	CTGTCGTATGCCCTGATGG
SF1c	61	80	20	64.2	60	ATCGCCCTTGGCAGATCAGG
SB2	180	199	20	59.5	50	CGGATCGCTTCAACAGTGTA
SB1c	135	156	20	65.9	55	ATATGCATGCAAATCCGCCCCG
SLF	39	60	22	60.4	45	CAGATCAGGCAACCCGAAAG

For *S. bovis* (Sb) and genus *Schistosoma* (S): F3=forward outer primer; B3=backward outer primer; FIP=forward inner primer (comprising F1c and F2 sequences); BIP=backward inner primer (comprising B1c and B2 sequences); LF=loop forward primer; LB=loop backward primer.

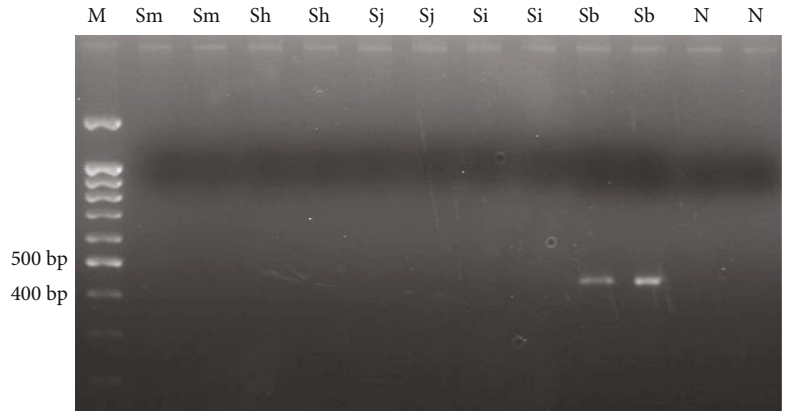

Figure 2: TD-PCR F3-B3 for amplifying *S. bovis* NADH-1. A 58-53°C temperature range and 53°C × 15 cycles were used. Sm: *S. mansoni* DNA; Sh: *S. haematobium* DNA; Sj: *S. japonicum* DNA; Si: *S. intercalatum* DNA; Sb: *S. bovis* DNA; N: negative control (ultrapure water, no DNA). M: molecular weight marker (100 bp PLUS BLUE DNA ladder).

typical ladder-like band pattern was observed on agarose gel electrophoresis.

When evaluating the sensitivity of the established LAMP assays for ITS-1 sequence, the detection limit in *Schistosoma* spp. genomic DNA amplification was different depending on the species used as template (Figure 6). Thus, a detection limit of 0.001 ng (1 pg) was obtained for *S. mansoni* and *S. intercalatum* (Figures 6(a) and 6(c)), 0.0001 ng (0.1 pg) for

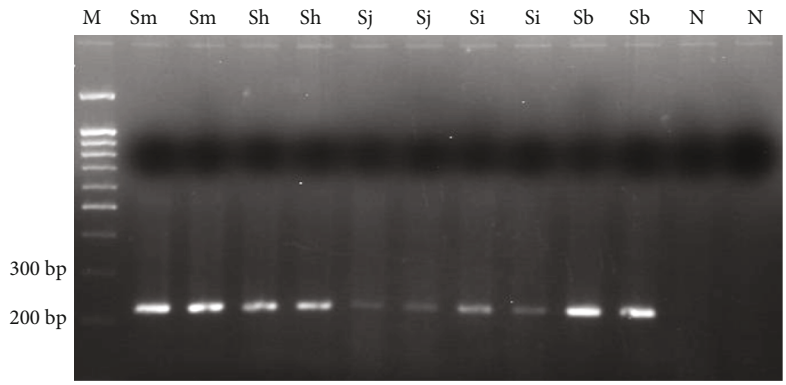

Figure 3: TD-PCR F3-B3 for amplifying genus *Schistosoma* ITS-1. A 61-57°C temperature range, and 57°C × 30 cycles were used. Sm: *S. mansoni* DNA; Sh: *S. haematobium* DNA; Sj: *S. japonicum* DNA; Si: *S. intercalatum* DNA; Sb: *S. bovis* DNA; N: negative control (ultrapure water, no DNA). M: molecular weight marker (100 bp PLUS BLUE DNA ladder).

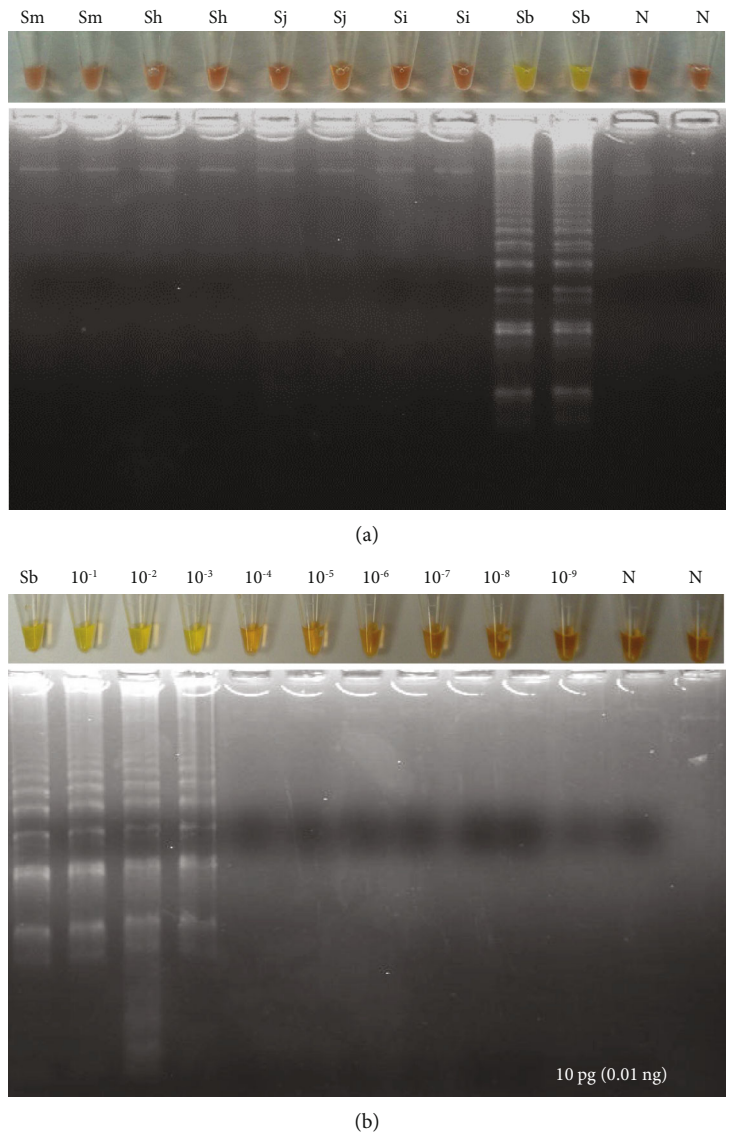

Figure 4: LAMP assay for amplifying *S. bovis* NADH-1. (a). Specificity assessment. Only NADH-1 was amplified using *S. bovis* DNA. Sm: *S. mansoni* DNA; Sh: *S. haematobium* DNA; Sj: *S. japonicum* DNA; Si: *S. intercalatum* DNA; Sb: *S. bovis* DNA; N: negative controls (ultrapure water, no DNA). (b). Sensitivity assessment. Sb: *S. bovis genomic* DNA (10 ng/μL); lanes 10^{-1}-10^{-9}, 10-fold serially dilutions.

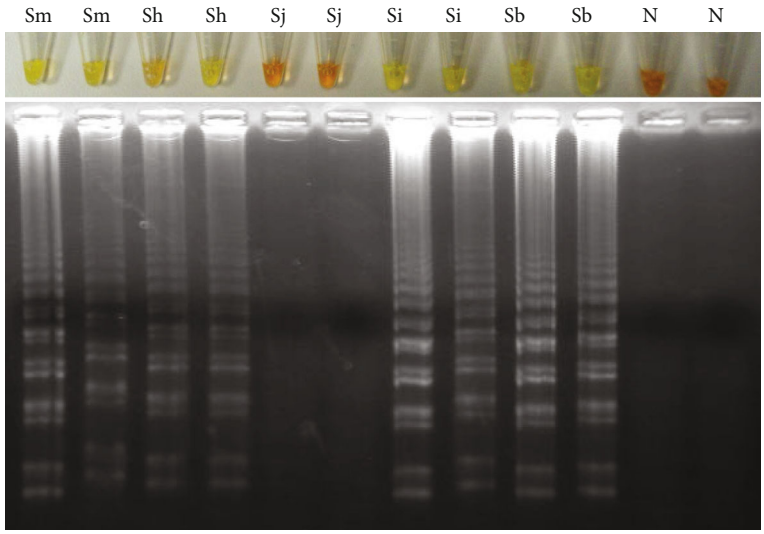

Figure 5: LAMP for amplifying the genus *Schistosoma* ITS-1 sequence. Lanes Sm, Sh, Sj, Si, and Sb mean *S. mansoni*, *S. haematobium*, *S. japonicum*, *S. intercalatum*, and *S. bovis* DNAs, respectively; Lanes N: negative controls (ultrapure water, no DNA).

S. haematobium (Figure 6(b)), and 0.01 ng (10 pg) for *S. bovis* (Figure 6(d)).

4. Discussion

Schistosomiasis is a neglected tropical disease widespread in 74 tropical and subtropical countries. The most important schistosome species regarding human schistosomiasis are *S. japonicum* in the Republic of China, the Philippines, and Indonesia; *S. haematobium* in Africa and in some countries of the Arabian peninsula (it has also recently emerged on the French island of Corsica); and *S. mansoni* in Africa, the Arabian peninsula, and Latin America. Meanwhile, *S. guineensis* and *S. intercalatum* (both endemic in Central and West Africa) and *S. mekongi* (restricted to a short stretch of the Mekong River in southern Lao People's Democratic Republic and eastern Cambodia) are of local regional importance [21]. The disease can also cause chronic, debilitating infection in animals, and it has been estimated that more than 165 million cattle are infected worldwide causing high levels of morbidity amongst susceptible animals (cattle, goats, sheep, horses, camelids, and pigs) and causing considerable production losses due to liver damage, reduced reproductive performance/yields, increased susceptibility to other infectious agents, and death [9]. There is no data on the current prevalence of *S. bovis* (animal schistosomiasis), but in the past, it had a wide distribution and prevalence in many Mediterranean, African, and Asian countries [22].

Hybridisations between schistosomes have already been identified between different human-specific schistosome species, different animal-specific schistosome species, and between human-specific and animal-specific schistosome species. The hybrid forms between human-specific and animal-specific schistosome species are particularly startling because they raise the possibility of the spread of hybrids, particularly zoonotic hybrids, that could prove problematic in terms of maintaining transmission if the can replace existing species and parasite strains, extend intermediate and definitive host ranges, or present and increase infectivity and virulence [23].

In addition, the hybrid status of the parasite may impair the parasitological, serological, and molecular diagnostic.

This work provides new LAMP assays for the specific detection of *S. bovis* and, additionally, for the simultaneous detection of a number of other human-infecting *Schistosoma* species.

The LAMP method designed for the simultaneous detection of different species of the *Schistosoma* genus achieved DNA amplification of four of the five species including *S. mansoni*, *S. haematobium*, *S. intercalatum*, and *S. bovis*; all of which are found in Africa. The *S. japonicum* DNA could not be amplified, possibly due to the few—although determinant—differences that its sequence presents with respect to DNA sequences from other African schistosomes, which share higher levels of identity [24, 25]. However, when performing the TD-PCR with the external primers F3 and B3 to check the *in silico* size of the selected ITS-1 sequence, it was possible to amplify the DNA of all species analysed, including *S. japonicum*. This could be explained by the additional primers required for the amplification in the LAMP technique, so internal primers might have not annealed in the *S. japonicum* DNA sequence. Moreover, it is important to highlight that due to the different origin of African and Asian schistosomes, it is very difficult to design primers for the amplification of common sequences amongst all species taking into account geographical variation [26, 27]. On the other hand, the ITS-1 sequence type selected for primer design was that obtained from *S. haematobium* and, for that reason, a higher degree of identity is expected for all African species, whilst Asian species share less identity.

Regarding the sensitivity of the developed LAMP methods, the detection limit of the LAMP for the *S. bovis* NADH-1 amplification was 10 pg of genomic DNA. On the other hand, the detection limit achieved with the LAMP for the amplification of the ITS-1 region of the *Schistosoma* genus was found to be 1 pg, 0.1 pg, 1 pg, and 10 pg for

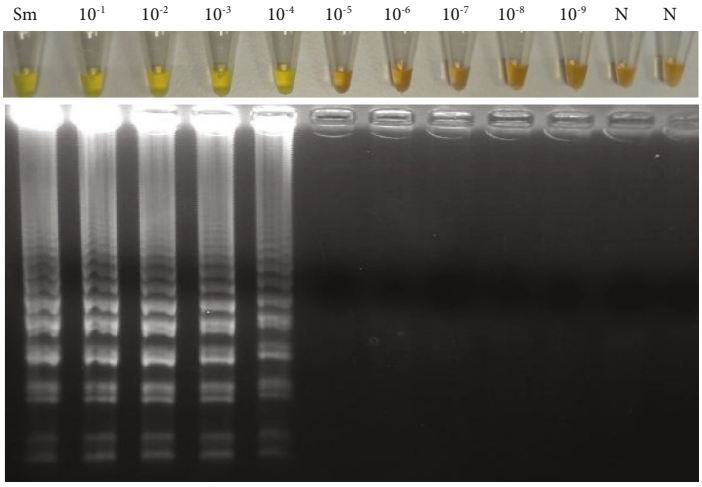

(a)

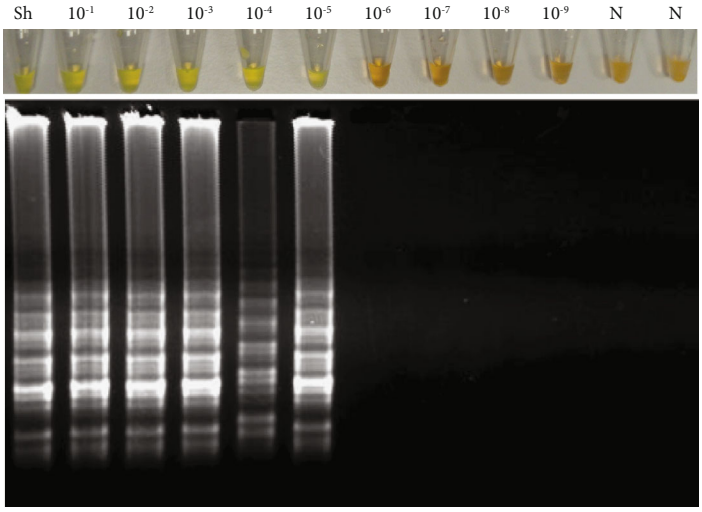

(b)

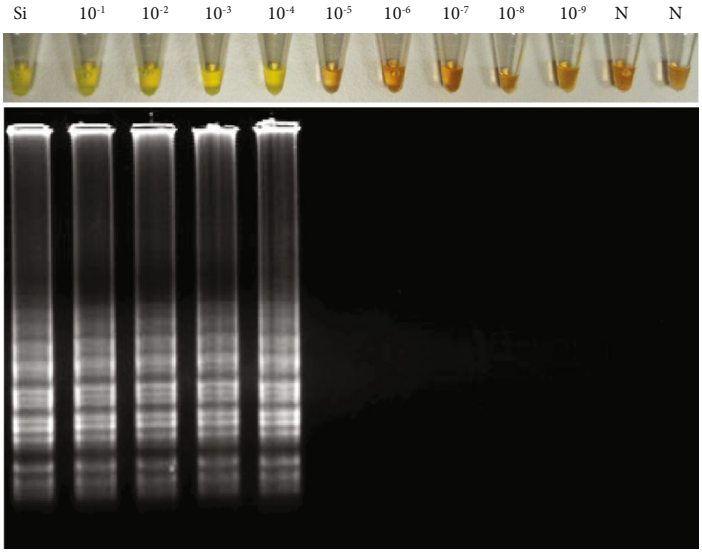

(c)

Figure 6: Continued.

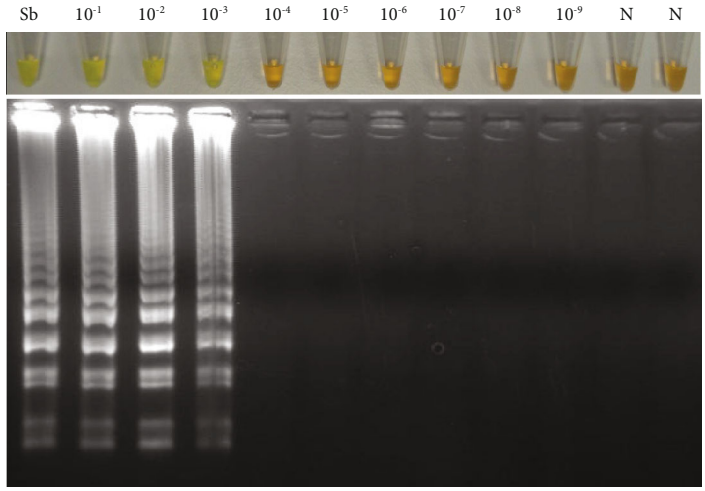

(d)

Figure 6: Sensitivity assessment of LAMP for amplifying *Schistosoma* ITS-1 sequence using DNA from different schistosome species. (a) Detection limit for *S. mansoni* (1 pg). (b) Detection limit for *S. haematobium* (0.1 pg). (c) Detection limit for *S. intercalatum* (1 pg). (d) Detection limit for *S. bovis* (10 pg). Lanes Sm, Sh, Si, and Sb mean *S. mansoni*, *S. haematobium*, *S. intercalatum*, *and S. bovis* DNAs, respectively. Lanes 10^{-1}-10^{-9}: 10-fold serial dilutions of DNA. Lanes N: negative controls (no DNA template).

S. mansoni, *S. haematobium*, *S. intercalatum*, and *S. bovis*, respectively. These differences in the sensitivity obtained for the different species may be due to the small differences between the nucleotide sequences that may end up influencing primer annealing and, therefore, LAMP performance. It makes sense that *S. haematobium* is the species displaying the highest detection limit (0.1 pg), since its own sequence was used as a reference when designing the generic LAMP.

In terms of specificity, the LAMP designed for *S. bovis* NADH-1 amplification worked specifically for this species and no DNA from other schistosome species included in the study was amplified. On the other hand, the *Schistosoma* genus ITS-1 region LAMP amplified the DNA of all species tested except for *S. japonicum.* A LAMP method for the specific detection of *S. bovis* and another for the simultaneous detection of different schistosome species that can produce human schistosomiasis have thus been developed. It should be noted that comparisons of genetic distances from pairs of congeners for both mitochondrial DNA and ITS sequences have demonstrated that mitochondrial DNA sequences of platyhelminths (including schistosomes) accumulate nucleotide substitutions at a much higher rate than ITS [28]. Moreover, until now, most of the *S. haematobium-S. bovis* hybrids reported demonstrate the existence of a mitochondrial DNA (i.e., cox 1 and microsatellite DNA) introgressive hybridisation of *S. haematobium* by *S. bovis* [29]. Thus, our developed LAMP assay based on NADH-1 for *S. bovis* detection would be very useful for detecting *S. haematobium-S. bovis* hybrids, as most hybrids have a mitochondrial *S. bovis* signature and a *S. haematobium* ITS signature.

5. Conclusions

Two highly sensitive LAMP methods for detecting different *Schistosoma* species important for human and veterinary health were standardised. It is worth highlighting that LAMP assays are easier to turn into point-of-care tests since no specialised lab equipment is required. Considering that human cases due to *S. intercalatum* are currently increasing and hybridisation events between *S. bovis* and *S. haematobium* have been reported in Senegal and France [22], LAMP methods here developed could be very useful for the diagnosis and surveillance of schistosome infections.

Data Availability

The data used to support the findings of this study are included within the article.

Conflicts of Interest

The authors declare that there is no conflict of interest regarding the publication of this paper.

Authors' Contributions

Pedro Fernández-Soto and Catalina Avendaño contributed equally to this work.

Acknowledgments

We would like to thank BEI Resources (http://www.beiresources.org), NIAID, NIH, for kindly providing schistosomes' DNA samples. We would also like to thank Jason Garry for translating this manuscript. This work was funded by the Institute of Health Carlos III, ISCIII, Spain (http://www.isciii.es), grants: RICET RD16/0027/0018 (AMA), PI19/01727 (PFS), PI-0001-2019 Junta de Andalucía (AMA, PFS), European Union cofinancing by FEDER (Fondo Europeo de Desarrollo Regional) "Una manera de hacer Europa" and by the Plan TCUE 2018–2020 European Union

cofinancing by FEDER and the Junta de Castilla y León. We also acknowledge support by Predoctoral Fellowship Program of University of Salamanca and cofinancing by Santander Bank, Predoctoral Fellowship Program of Junta de Castilla y León and Technical support staff for research support, National Youth Guarantee System, cofinancing with the European Social Fund, Youth Employment Initiative, BDNS: 376072. We would like to thank the Universidad del Rosario for assuming open access charges.

Supplementary Materials

Table 1: gene sequences located and analysed for *S. bovis*. Table 2: degree of ITS-1 and ITS-2 sequence identity regarding schistosome species in the different databases. *(Supplementary Materials)*

References

[1] WHO, "Neglected tropical diseases," WHO, 2018, August 2019, https://www.who.int/neglected_diseases/diseases/en/.

[2] M. L. Nelwan, "Schistosomiasis : life cycle, diagnosis, and control," *Current Therapeutic Research*, vol. 91, pp. 5–9, 2019.

[3] WHO, "Schistosomiasis," WHO, 2019, August 2019, https://www.who.int/schistosomiasis/en/.

[4] GBD 2017 DALYs and HALE Collaborators, "Global, regional, and national disability-adjusted life-years (DALYs) for 359 diseases and injuries and healthy life expectancy (HALE) for 195 countries and territories, 1990-2017: a systematic analysis for the Global Burden of Disease Study 2017," *The Lancet*, vol. 392, no. 10159, pp. 1859–1922, 2018.

[5] J. García-Bernalt Diego, P. Fernández-Soto, B. Crego-Vicente et al., "Progress in loop-mediated isothermal amplification assay for detection of *Schistosoma mansoni* DNA: towards a ready-to-use test," *Scientific Reports*, vol. 9, no. 1, p. 14744, 2019.

[6] B. L. Webster, V. Southgate, and D. Littlewood, "A revision of the interrelationships of *Schistosoma* including the recently described *Schistosoma guineensis*," *International Journal for Parasitology*, vol. 36, no. 8, pp. 947–955, 2006.

[7] D. G. Colley, A. L. Bustinduy, W. E. Secor, and C. H. King, "Human schistosomiasis," *The Lancet*, vol. 383, no. 9936, pp. 2253–2264, 2014.

[8] T. Engdaw and A. Abuhay, "Overview on *Schistosoma* infection with reference to its economic importance," *European Journal of Applied Sciences*, vol. 7, pp. 268–273, 2015.

[9] H. You, P. Cai, B. Tebeje, Y. Li, and D. McManus, "Schistosome vaccines for domestic animals," *Tropical Medicine and Infectious Disease*, vol. 3, no. 2, p. 68, 2018.

[10] L. A. Tchuem Tchuenté, D. Rollinson, J. R. Stothard, and D. Molyneux, "Moving from control to elimination of schistosomiasis in sub-Saharan Africa: time to change and adapt strategies," *Infectious Diseases of Poverty*, vol. 6, no. 1, p. 42, 2017.

[11] A. Muro, L. Pérez del Villar, V. Velasco, and J. L. Pérez-Arellano, "Infecciones por trematodos," *Medicine - Programa de Formación Médica Continuada Acreditado*, vol. 10, no. 55, pp. 3717–3728, 2010.

[12] H. Moné, G. Mouahid, and S. Morand, "The distribution of *Schistosoma bovis* Sonsino, 1876 in relation to intermediate host mollusc-parasite relationships," *Advances in Parasitology*, vol. 44, pp. 99–138, 1999.

[13] K. G. A. D. Weerakoon, G. N. Gobert, P. Cai, and D. P. McManus, "Advances in the diagnosis of human schistosomiasis," *Clinical Microbiology Reviews*, vol. 28, no. 4, pp. 939–967, 2015.

[14] D. G. Colley, T. S. Andros, and C. H. Campbell Jr., "Schistosomiasis is more prevalent than previously thought: what does it mean for public health goals, policies, strategies, guidelines and intervention programs?," *Infectious Diseases of Poverty*, vol. 6, no. 1, p. 63, 2017.

[15] L. A. Pontes, E. Dias-Neto, N. Katz, A. Rabello, and M. C. Oliveira, "Comparison of a polymerase chain reaction and the Kato-Katz technique for diagnosing infection with *Schistosoma mansoni*," *The American Journal of Tropical Medicine and Hygiene*, vol. 68, no. 6, pp. 652–656, 2003.

[16] C. A. Gordon, L. P. Acosta, D. J. Gray et al., "High prevalence of *Schistosoma japonicum* infection in Carabao from Samar Province, the Philippines: implications for transmission and control," *PLoS Neglected Tropical Diseases*, vol. 6, no. 9, article e1778, 2012.

[17] L. Meurs, E. Brienen, M. Mbow et al., "Is PCR the next reference standard for the diagnosis of *Schistosoma* in stool? A comparison with microscopy in Senegal and Kenya," *PLoS Neglected Tropical Diseases*, vol. 9, no. 7, article e0003959, 2015.

[18] T. Notomi, Y. Mori, N. Tomita, and H. Kanda, "Loop-mediated isothermal amplification (LAMP): principle, features, and future prospects," *Journal of Microbiology*, vol. 53, no. 1, pp. 1–5, 2015.

[19] J. Li, J. Macdonald, and F. Von Stetten, "Review: a comprehensive summary of a decade development of the recombinase polymerase amplification," *Analyst*, vol. 144, no. 1, pp. 31–67, 2019.

[20] Z. K. Njiru, "Loop-mediated isothermal amplification technology: towards point of care diagnostics," *PLoS Neglected Tropical Diseases*, vol. 6, no. 6, article e1572, 2012.

[21] D. P. McManus, R. Bergquist, P. Cai, S. Ranasinghe, B. M. Tebeje, and H. You, "Schistosomiasis—from immunopathology to vaccines," *Seminars in Immunopathology*, vol. 42, no. 3, pp. 355–371, 2020.

[22] E. de la Torre-Escudero, R. Pérez-Sánchez, R. Manzano-Román, and A. Oleaga, "*Schistosoma bovis*-host interplay: proteomics for knowing and acting," *Molecular and Biochemical Parasitology*, vol. 215, pp. 30–39, 2017.

[23] E. Leger and J. P. Webster, "Hybridizations within the genus *Schistosoma*: implications for evolution, epidemiology and control," *Parasitology*, vol. 144, no. 1, pp. 65–80, 2017.

[24] N. D. Young, A. R. Jex, B. Li et al., "Whole-genome sequence of *Schistosoma haematobium*," *Nature Genetics*, vol. 44, no. 2, pp. 221–225, 2012.

[25] M. Mitreva, "The genome of a blood fluke associated with human cancer," *Nature Genetics*, vol. 44, no. 2, pp. 116–118, 2012.

[26] B. L. Webster and V. R. Southgate, "Mating interactions of *Schistosoma haematobium* and *S. intercalatum* with their hybrid offspring," *Parasitology*, vol. 126, no. 4, pp. 327–338, 2003.

[27] S. P. Lawton, H. Hirai, J. E. Ironside, D. A. Johnston, and D. Rollinson, "Genomes and geography: genomic insights into

the evolution and phylogeography of the genus *Schistosoma*," *Parasites & Vectors*, vol. 4, no. 1, p. 131, 2011.

[28] R. Vilas, C. D. Criscione, and M. S. Blouin, "A comparison between mitochondrial DNA and the ribosomal internal transcribed regions in prospecting for cryptic species of platyhelminth parasites," *Parasitology*, vol. 131, no. 6, pp. 839–846, 2005.

[29] E. K. Angora, J. F. Allienne, O. Rey et al., "High prevalence of *Schistosoma haematobium* × *Schistosoma bovis* hybrids in schoolchildren in Côte d'Ivoire," *Parasitology*, vol. 147, no. 3, pp. 287–294, 2020.

Hindawi
Disease Markers
Volume 2020, Article ID 3904947, 9 pages
https://doi.org/10.1155/2020/3904947

Research Article

FASN Protein Overexpression Indicates Poor Biochemical Recurrence-Free Survival in Prostate Cancer

Zhi Cao,[1] Yalong Xu,[1] Fei Guo,[1] Xi Chen,[1] Jin Ji,[1] Huan Xu,[1] Jingyi He,[1] Yongwei Yu,[2] Yinghao Sun,[1] Xin Lu,[1] and Fubo Wang[1]

[1]*Department of Urology, Changhai Hospital, Navy Medical University, Shanghai, China*
[2]*Department of Pathology, Changhai Hospital, Navy Medical University, Shanghai, China*

Correspondence should be addressed to Xin Lu; luxin_smmu@163.com and Fubo Wang; wangbofengye@163.com

Received 9 September 2019; Revised 12 May 2020; Accepted 5 June 2020; Published 19 June 2020

Academic Editor: Lucio Castellano

Backgrounds. Fatty acid synthase (FASN) has been regarded as a prognostic marker in prostate cancer (PCa). In this study, we evaluated FASN expression at both mRNA and protein levels and assessed the association between FASN expression and prognosis in male Han Chinese with PCa treated with radical prostatectomy (RP). *Methods*. Expression profile and prognostic value of FASN were analyzed in tissue microarray (TMA) and data retrieved from databases including TCGA public database, GEO database, and our sequencing data with whole clinicopathological characteristics. *Results*. FASN expression was associated with clinical parameters and biochemical recurrence of prostate cancer. The relative expression of FASN mRNA was higher in the tumor tissue in all public databases and our sequencing data ($p < 0.001$). A similar result was seen in tissue microarray (TMA) ($p < 0.001$). Analysis of our sequencing data indicated that FASN's relative expression was associated with tumor stage ($p = 0.048$), and FASN expression was positively associated with the Gleason score ($p = 0.004$) and seminal vesicle invasion ($p = 0.011$) in TMA. We found that high FASN expression was an independent predictor of shorter BCR-free survival with univariate and multivariate survival analysis ($p < 0.05$), rendering FASN an optimal prognostic biomarker in male Han Chinese with prostate cancer. *Conclusions*. Our study demonstrated that FASN was overexpressed at mRNA and protein levels in PCa. We found that patients with high FASN expression had a shorter BCR-free survival, showing its value as a prognostic biomarker in male Han Chinese with PCa.

1. Introduction

Prostate cancer (PCa) ranks 2nd in male tumor morbidity and 5th in mortality worldwide [1]. According to the latest report, the annual growth rate of PCa morbidity and mortality in China is as high as 7.2% and 5.5%, respectively, making it the fastest-growing tumor in China [2]. Early PCa was confined to the capsule; radical prostatectomy (RP) or radiotherapy is often recommended [3]. However, although most patients respond to the treatments initially, a large portion of them will progress to recurrence and/or metastasis. The percentage of PCa patients who undergo radical prostatectomy experiencing biochemical recurrence (BCR) is approximately 25% [4, 5]. Therefore, timely and accurate estimation of BCR risk for patients with poor prognosis, especially for those who need adjuvant treatment, is of utmost importance to improve outcomes. The present clinical prognostic parameters, such as prostate-specific antigen (PSA), Gleason score (GS), and clinical or pathological tumor stage, with limitations in the differentiation of the biological heterogeneity of tumors, are unable to accurately estimate the risk of aggressive prostatic tumors. Therefore, the identification of a novel sensitive and specific biomarker to monitor the prognosis of PCa is urgently needed.

As we know, a significant hallmark of PCa is abnormal lipid metabolism, as first observed by Medes and colleagues in 1953 [6]; actually, a lipogenic phenotype is a distinctive feature of PCa cells. Fatty acids (FAs) are the essential constituents for energy metabolism, which is consistent with exogenous FAs (from diet) and endogenous FAs (synthesized *in vivo*). Adequate energy to support uncensored growth and proliferation of cancer cells relies on the utilization of FAs by

their β-oxidation to generate ATP, while exogenous FA uptake from the diet alone cannot meet the energy demands. Accordingly, FAs generated through de novo FA synthesis play a pivotal role in cancer tissue with a 270 kDa key enzyme named Fatty acid synthase (FASN), which is involved in the process of transformation of acetyl-CoA and malonyl-CoA to FAs that are minimally expressed in many normal tissues except liver and adipose tissue [7], as well as tumor tissue. In fact, FASN is often overexpressed in both the early (prostatic intraepithelial neoplasia) and late (metastasis) stages of PCa, suggesting that it is involved in the process of the initial phases of prostate tumorigenesis, maintenance, and biological aggressiveness [8–10]. It is considered that FASN is a *bona fide* oncogene based on its high expression in prostate cancer and its effect in protecting cancer cells from apoptosis [11]. Several studies have shown that the inhibition of FASN expression induces apoptosis in multiple types of tumors, including PCa. De Schrijver et al. reported that silencing FASN with siRNA significantly inhibited LNCaP cell growth and ultimately led to apoptosis [12]. Kridel et al. also demonstrated that the novel FASN inhibitor Orlistat significantly inhibited proliferation, migration, and invasion of PC-3 tumor cells and induced cell apoptosis in mouse xenograft models [13], which has also been demonstrated both *in vivo* and *in vitro* lately by Migita et al. [14]. Moreover, increased expression of FASN is significantly related to poor prognosis, which means it may be used as a prognostic biomarker for PCa [15, 16]. It has also been reported that the expression of FASN can predict the Gleason score and pathological stage [16, 17]. However, all these studies were mainly done in the western population. No literature has reported its role in male Han Chinese. Thus, in the present study, we explored the expression profile of FASN and its prognostic value by database retrieval and immunohistochemistry in male Han Chinese.

2. Method and Materials

2.1. Gene Expression Analysis. We obtained TCGA prostate cancer gene expression data from the University of California Santa Cruz (UCSC) Cancer Genomics Browser, which contained 495 prostate cancer cases and 52 paracancerous controls with whole clinicopathological characteristics. The sequencing data of our research center involved 65 prostate cancer cases with their cancerous and matched paracancerous normal tissue. In addition, an independent GEO database (GSE46602, GSE6752) was also downloaded to extract information on the mRNA expression of FASN for further analysis.

2.2. Patients Cohort for the Construction of the Tissue Microarray (TMA). A total of 188 patients who had undergone radical prostatectomy at the Department of Urology, Changhai Hospital, from October 2002 to December 2008 were eligible for this study. Their archived tissues from the Department of Pathology were used to construct TMA. None of these patients were treated preoperatively with hormonal or radiation therapy. Patients' medical records were accessible for the clinical and pathological information. Two pathologists observed the prostatectomy specimens and evaluated them according to the College of American Pathologists [16] without knowing patients' clinical outcomes or follow-up data. All 188 cases' pathological stages were classified according to the 2002 staging criteria of the American Joint Committee on Cancer (AJCC). This protocol was approved by our institutional medical ethics review committee.

2.3. Follow-Up. All patients' serum PSA levels were evaluated every 3 months in the first year, every 6 months from the second year to the fifth year, and annually thereafter. Their follow-up data were accessible by consulting the hospital medical records and calling to patients or their family members. We defined BCR as the sustained elevation of the serum total PSA level above 0.2 ng/ml for at least twice. Overall biochemical recurrence-free survival was defined as the time from the date of surgery to the date of BCR (first detection of PSA level above 0.2 ng/ml).

2.4. TMA Construction. As we described previously, TMA was constructed with formalin-fixed paraffin-embedded tissue blocks from prostate cancer patients who underwent radical prostatectomy [18]. The slides were selected by two pathologists originally with cancerous tissue and matched paracancerous normal tissue without inflammatory zones that colored with different dyes. Then, the TMA was cut into 3 mm sections and stained with hematoxylin–eosin to ensure that the cores adequately represented the diagnostic areas.

2.5. Immunohistochemistry and Evaluation of Immunostaining. The expression of FASN was detected by immunohistochemistry (IHC) using a commercial FASN antibody (dilution 1 : 200; Abcam, Cambridge, UK). The IHC assay was conducted according to the manufacturer's instructions with all the staining reagents. The evaluation of IHC staining was performed by two independent pathologists without knowing the patients' clinical information using a modified histological score method based on both the percentage of positively stained cells and the intensity of staining. Under 40× visual field magnification, the intensity score (I) of staining was classified into four grades (ranks 0 to 3), while the extent score (E) of stained cells was classified into five grades (ranks 0 to 4). The IE score was constructed as follows: intensity score (I) × extent score (E), with a maximum score of 12. If the interobserver variability exceeded 15%, the sample sides would be rescored to reach a consensus for each patient's slide. We arbitrarily defined IE score (0-5) as low expression and IE score (6-12) as high expression.

2.6. Statistical Analysis. SPSS software version 21.0 (IBM Corp., Armonk, NY, USA) was utilized for the statistical analysis. FASN expression (high expression vs. low expression) between different PSA levels, Gleason score, and pathological grading was evaluated by the Kruskal–Wallis H-test. Associations between FASN expression and histological subtypes and clinical variables (surgical margin, seminal vesicle invasion, and the pathological lymph node category) were analyzed using the Mann–Whitney U-test for categorical variables. The association between FASN expression levels and risk of BCR following RP was analyzed by the

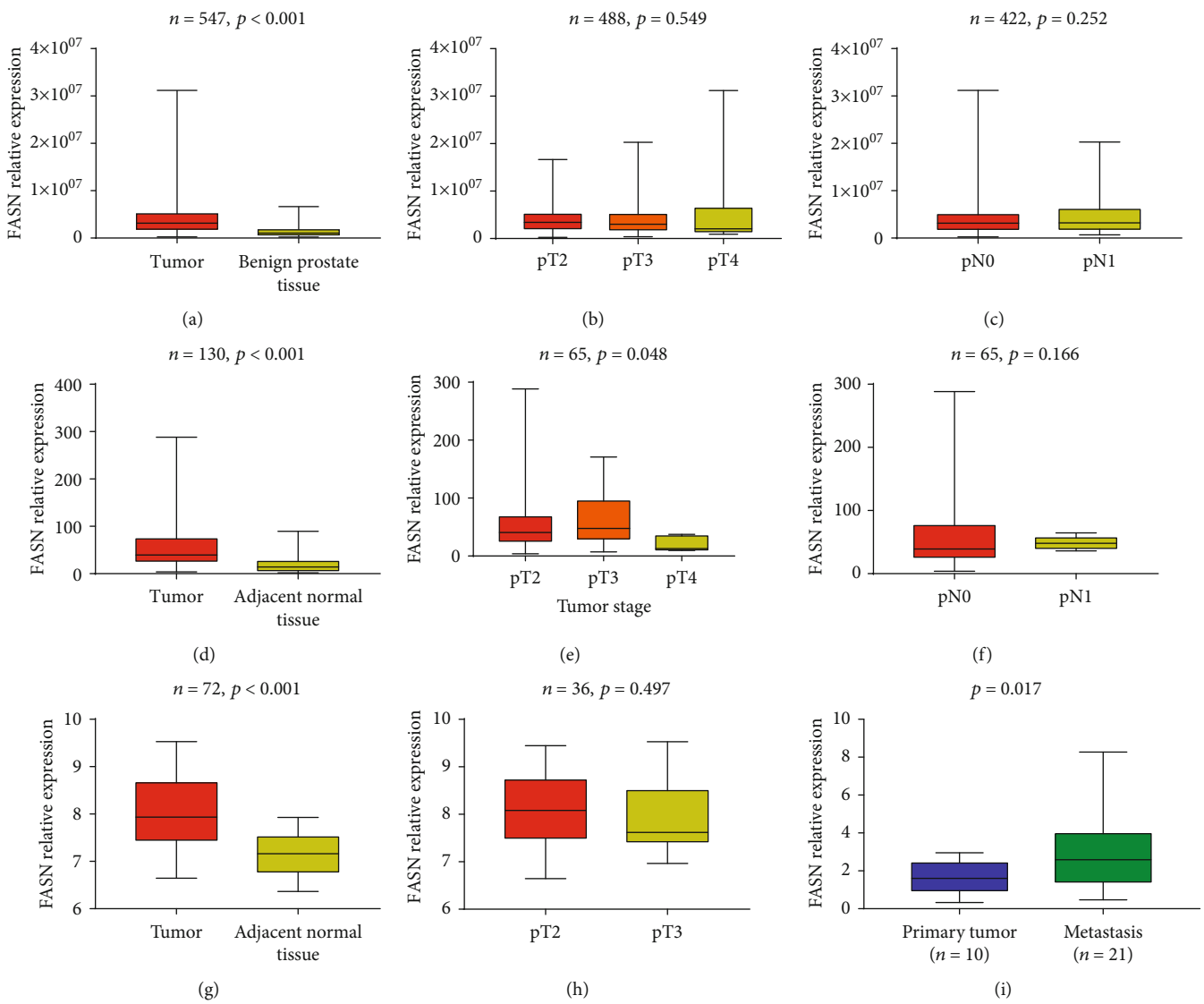

Figure 1: mRNA expression of FASN in TCGA public database (a–c), our sequencing data (d–f), GSE46602 (g, h), and GSE6752 (i). FASN expressions comparison between tumor and benign prostate tissue (a, d, g). FASN relative expression pattern among lymph node categories (c, f) and tumor stages (b, e, h). Comparison of FASN expression in primary prostate tumor tissue and metastasis (i) (note: T2: tumor stage 2; T3: tumor stage 3; T4: tumor stage 4; pN0: pathology lymph nodes 0; pN1: pathology lymph nodes 1).

Kaplan-Meier estimator and log-rank tests. Moreover, all the independent factors (age, PSA level, Gleason score, TNM categories, and FASN expression level) were further tested using Cox's proportional hazard regression for multivariate comparison as the outcome. Differences were considered statistically significant with $p < 0.05$.

3. Results

3.1. FASN mRNA Expression in the Database. The heatmaps of differential genes including FASN in different databases could be seen in Supplementary Figure 1, as well as LogFC forms of the differential genes (Supplementary Table 1, Supplementary Table 2, and Supplementary Table 3). In the TCGA database, we found that the relative expression of FASN mRNA was significantly higher in tumor tissue compared to benign tissue ($p < 0.001$, Figure 1(a)). However, FASN relative expression was not associated with tumor stage ($p = 0.549$, Figure 1(b)) or pathological lymph node status ($p = 0.252$, Figure 1(c)). A similar result was observed in our sequencing data and GSE46602: FASN mRNA expression in tumor tissue was relatively high ($p < 0.001$, Figure 1(d); $p < 0.001$ Figure 1(g)), but FASN relative expression was not associated with tumor stage in GSE46602 ($p = 0.497$, Figure 1(h)), while in our sequencing data PCa in pT3 showed higher expression of FASN ($p = 0.048$, Figure 1(e)). Furthermore, our results indicated that PCa with metastasis expressed higher FASN ($p < 0.017$, Figure 1(i)).

3.2. Patients Description in TMA. The clinical and pathological characteristics, which enrolled 188 patients with a mean age of 61.03 ± 6.84 years in the study, are summarized in Table 1.

Table 1: The clinical and pathological characteristics of patients.

Variable	n	Percentage (%)
Age (year)		
<50	4	2.1
50-60	23	12.2
60-70	82	43.6
≥70	76	40.4
NA	3	1.6
Preoperative PSA level (ng/ml)		
<4	2	1.1
4-10	37	19.7
10-20	69	36.7
>20	79	42.0
NA	1	0.5
Gleason score		
≤3 + 3	9	4.8
3 + 4	60	31.9
4 + 3	34	18.7
≥4 + 4	79	43.4
NA	6	3.2
pT category		
pT2a–2b	34	18.1
pT2c	79	42.0
pT3a-b	71	37.8
pT4	4	2.1
pN category		
pN0	121	64.4
pN+	32	17
NA	35	18.6
Surgical margin		
Negative	106	56.4
Positive	82	43.6
Capsular invasion		
Yes	68	36.2
No	120	63.8
Seminal vesicle invasion		
Yes	42	22.3
No	146	77.7
Nerve invasion		
Yes	80	42.6
No	108	57.4

3.3. FASN Expression in TMA. In our study, FASN was expressed wildly in both the prostatic epithelial cells and paracancerous normal tissue. We used the IE score to measure the expression of FASN protein. Representative FASN IE score patterns are shown in Figure 2. For further analysis, we defined a cut-off value of IE score of 5 after calculating the average IE score, of which ≥6 was regarded as high expression. The relationship of FASN expression and clinicopathological parameters was calculated in Table 2. The staining of FASN in tumor tissue was significantly stronger than in paracancerous normal tissue ($p < 0.001$, Figure 3(a)). There was no difference in FASN expression among different preoperative PSA levels ($p = 0.618$, Figure 3(b)), pathological tumor stages ($p = 0.569$), pathological lymph node categories ($p = 0.294$), or surgical margin status ($p = 0.187$). FASN expression was positively associated with Gleason score ($p = 0.004$, Figure 3(c)) and seminal vesicle invasion ($p = 0.011$, Figure 3(d)).

3.4. Association between FASN Expression and BCR. The follow-up data were extracted from the GEO database (GSE46602), in which 22 of 36 patients experienced BCR after an average postoperative follow-up duration of 23.9 ± 22.2 months. It seems that low expression of FASN had an association with longer BCR-free survival, while the log-rank test indicated that there were no significant differences ($p = 0.33$, Figure 4(a)). The same result was found in the TCGA database, with a nonsignificant association between FASN expression and BCR ($p = 0.32$, Figure 4(a)). On the other hand, 188 patients' follow-up information was available in TMA, which included 114 patients who experienced BCR with a postoperative follow-up duration of 13.7 ± 18.1 months. In these patients, the log-rank test indicated that patients with higher FASN expression had shorter BCR-free survival ($p = 0.01$, Figure 4(c)). In the univariate Cox proportional hazards regression analyses, FASN expression was associated with BCR after radical prostatectomy ($p = 0.011$). After adjusting for some clinicopathological parameters, multivariate Cox analysis revealed that FASN expression ($p = 0.004$), preoperative PSA level ($p = 0.002$), Gleason score ($p < 0.001$), and pathological lymph node category ($p < 0.001$) were all associated with recurrence (Table 3).

4. Discussion

Cancer cell metabolism is quite distinctive in that DNA and protein synthesis are increased due to overconsumption of energy [19, 20]. Another hallmark is increased de novo FA synthesis related to the glycolytic pathway, which promotes cell growth, survival, and drug resistance. Moreover, continuous synthesis of de novo FAs is required to provide lipids as the raw material for membrane production and energy metabolism in highly proliferating cancer cells [21]. Many malignant carcinomas, including PCa, behave in the same lipid metabolism patterns involving the pivotal enzyme FASN. A more important fact is that further study demonstrated that accumulated cholesteryl ester is associated with prostate cancer aggressiveness [22]. Pelton et al. also reported that the evaluated level of circulating cholesterol was positively linked to the development of prostate cancer [23]. Actually, an analysis included 22 separate studies from the Oncomine public database revealed that FASN mRNA expression, as well as other lipid metabolic enzyme genes, is increased in PCa [24], which is consistent with the results of our study. Of these, both databases and immunohistochemistry results showed high FASN mRNA expression in prostate cancerous tissue compared to paracancerous normal tissue.

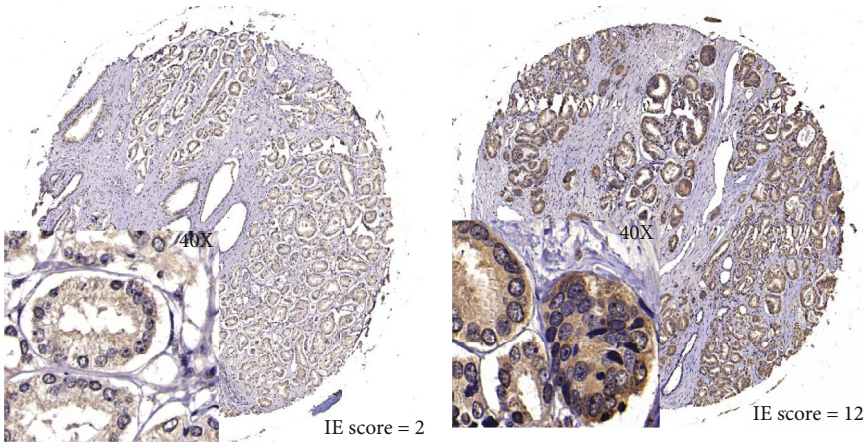

(a) (b)

Figure 2: FASN expression pattern was analyzed by the IE score in prostate cancer tissues (40 times zoom in square).

Table 2: FASN expression status in TMA.

Variable	No. of successfully analysed samples	FASN immunohistochemistry result		
		Low	High	*p*
Tissue type	188			<0.001
Prostate cancer	188	57	131	
Paracancerous tissue	188	118	70	
Preoperative PSA level (ng/ml)	187			0.618
<4	2	0	2	
4-10	37	9	28	
10-20	69	23	46	
≥20	79	24	55	
Gleason score	182			0.004
≤3 + 3	9	7	2	
3 + 4	60	21	39	
4 + 3	34	12	22	
≥4 + 4	79	17	62	
pT category	188			0.569
pT2a–2b	34	12	22	
pT2c	79	25	54	
pT3a-b	71	18	53	
pT4	4	2	2	
pN category	153			0.294
pN0	121	38	83	
pN+	32	7	25	
Seminal vesicle invasion	188			0.011
Yes	42	6	36	
No	146	51	95	
Surgical margin	188			0.187
Negative	106	28	78	
Positive	82	29	53	

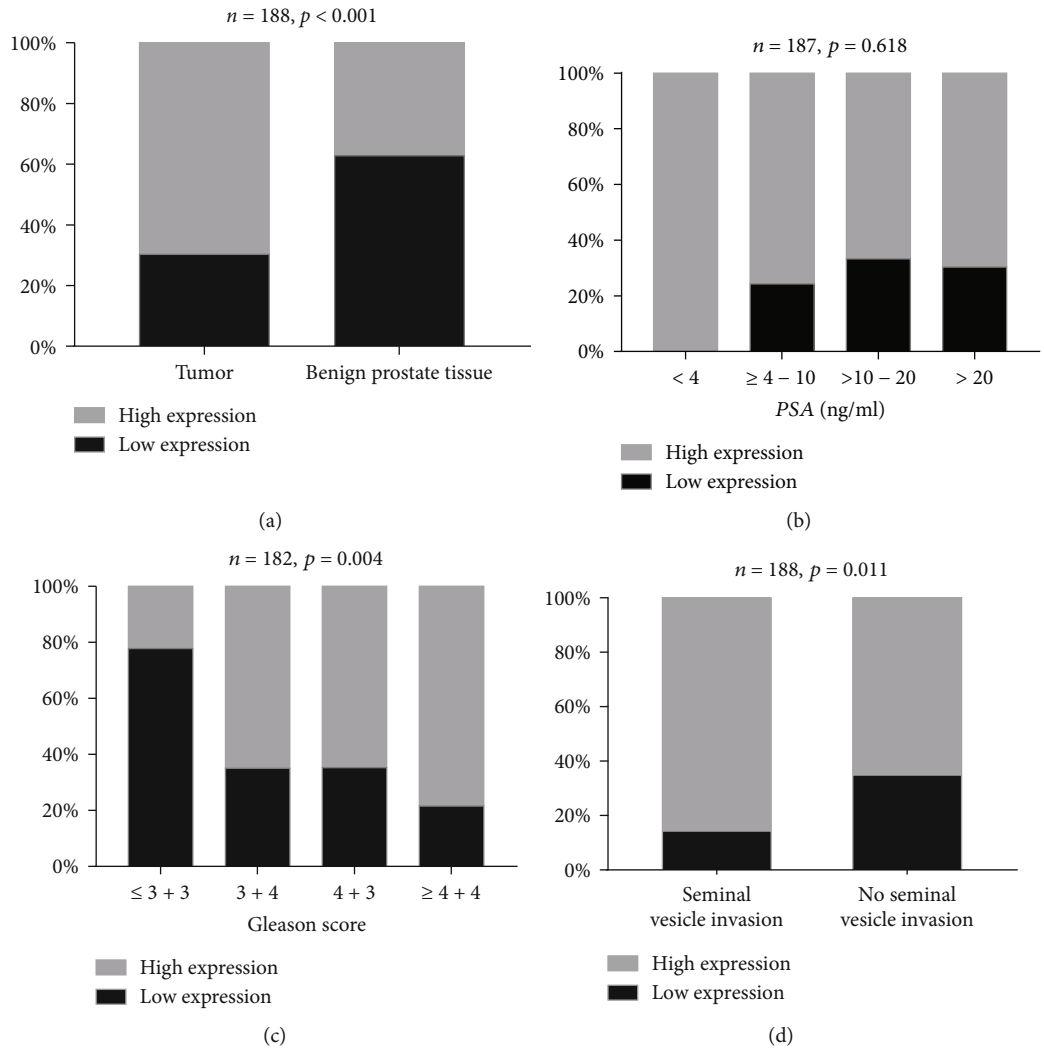

Figure 3: FASN expression in TMA by IHC. Comparison between tumor tissue and benign tissue (a). The relationship between FASN expression and preoperation PSA (b), Gleason score (c), and seminal vesicle invasion (d).

It has been demonstrated that FASN acts as an oncogene involved in the intrinsic pathway of apoptosis. Migita et al. reported an inverse relationship between FASN expression and the apoptotic rate in human PCa samples and transgenic mice expressing FASN showed an increased rate of proliferation and decreased rate of castration-induced apoptosis in the prostate [14]. De Schrijver et al. showed that attenuated cancer cell growth and induced apoptosis were positively associated with the downregulation of FASN expression mediated by siRNA [12]. Ample evidence has revealed that FASN may act as a biomarker in promoting tumor progression, including cell proliferation, cell adhesion, migration, and invasion, as well as pseudopodia formation, which plays a critical role in PCa proliferation and metastasis [25, 26]. Moreover, androgen, which has been proven to be related to PCa progression, regulates FASN expression and its activity in human prostate cancer cell lines by activating the expression of ubiquitin-specific protease-2a (USP2a), which stabilizes FASN expression to prolong PCa cell survival [27]. In contrast, increased FASN expression promoted PCa cells to resist apoptosis as the tumor progressed to androgen independence, which rendered the gene a metabolic oncogene [28, 29]. However, the heterogeneity of FASN expression among individuals has been observed in many studies. Genomic amplification of FASN has been reported in approximately one-fourth of patients with PCa [9]. Rossi et al. evaluated FASN expression levels in 64 patients with primary PCa by immunohistochemistry and showed that FASN expression is weakly in more than half of patients, while strongly in 8% and moderately in 30% [10]. Similarly, Migita et al. reported that gene expression varied among individuals [14]. Because the overexpression of FASN in PCa is significantly heterogeneous, it is supposed that FASN is a prognostic biomarker [15].

It has been reported that FASN upregulation participated in the progression of PCa, which is the initial event in PCa development and increased substantially from prostatic intraepithelial neoplasia to low grade, to high grade, and to androgen-independent bone metastases [10]. Our TMA data also indicated that FASN expression was positively related to the Gleason score ($p = 0.004$), which is consistent with a previous study [30]. The mechanism was proposed as the

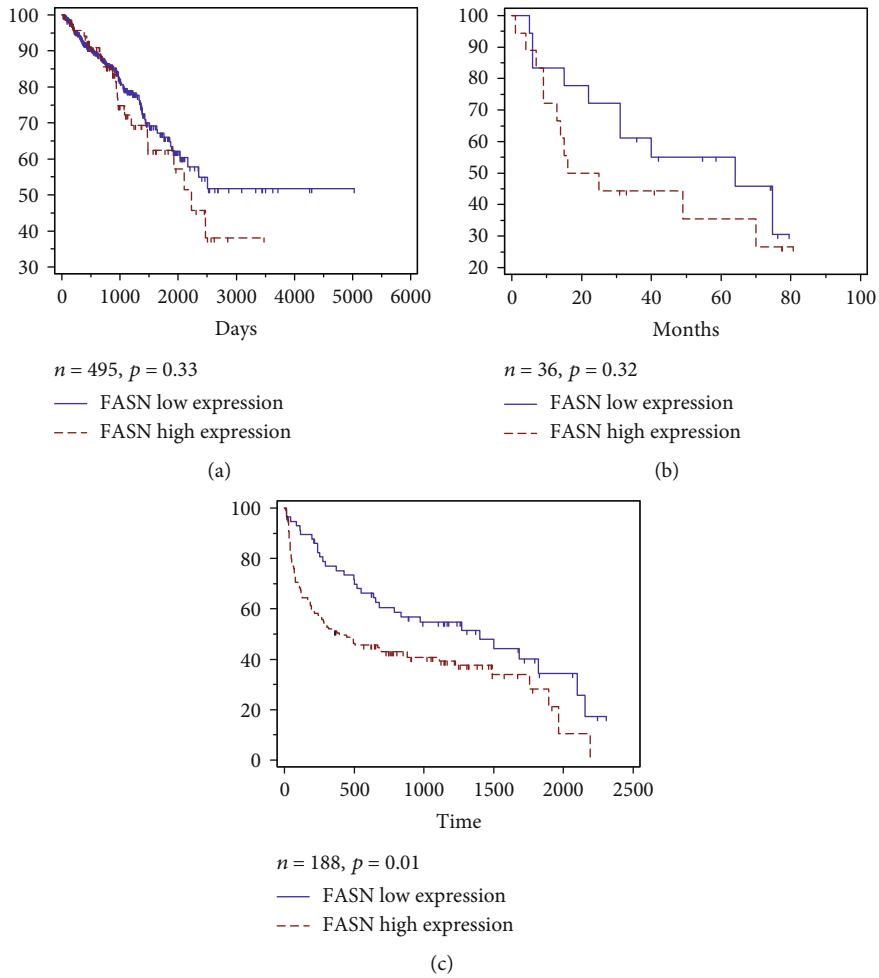

Figure 4: The relationship between FASN expression and patient prognosis. (a) Kaplan–Meier analysis of BCR-free survival in patients' data retrieved from TCGA ($n = 495$, $p = 0.33$), (b) Correlation between FASN expression and BCR-free survival in GEO dataset ($n = 36$, $p = 0.32$). (c) Disease-free survival in TMA patients ($n = 188$, $p = 0.01$). The log-rank test shows that PCa patients with high FASN expression have shorter disease-free survival time.

Table 3: Univariate and multivariate analyses of survival of FASN expression.

	Univariate analysis		Multivariate analysis	
	HR (95% CI)	p value	HR (95% CI)	p value
FASN (high/low)	1.717 (1.132-2.604)	0.011	2.005 (1.248-3.221)	0.004*
PSA level (>10/≤10)	3.060 (1.675-5.589)	<0.001	2.903 (1.486-5.669)	0.002*
Gleason score (≥8/<8)	3.122 (2.125-4.587)	<0.001	2.375 (1.493-3.778)	<0.001*
pT category (T3+T4/T2)	2.951 (2.023-4.305)	<0.001	1.503 (0.912-2.477)	0.110
pN category (pN1/pN0)	4.083 (2.573-6.477)	<0.001	3.024 (1.846-4.953)	<0.001*
Age (>70/≤70)	0.792 (0.531-1.181)	0.253		

result of activation and nuclear localization of Akt and cytoplasmic stabilization of β-catenin, subsequently affecting membranal function and antiapoptotic proteins [14, 31].

In addition, we analyzed the prognostic value of FASN in predicting BCR in patients who undergo RP using public database and immunohistochemistry. The results of BCR-free survival time of the TCGA and GEO databases indicated a correlation between high FASN expression and shorter disease-free survival, albeit statistically nonsignificant. In contrast, the analyses of our TMA data subsequently illustrated that low expression of FASN was associated with longer BCR-free survival, as reported by Shurbaji et al. [15] in 1996, which demonstrated FASN's potential prognostic role in PCa progression. We proposed that there may be no ethical difference in FASN expression in PCa, as our data indicated a similar pattern in Han Chinese patients as the

foreign population (TCGA and GEO databases). Thus, we believe that FASN may act as a prognostic biomarker. In the univariate logistic analysis, significant effects of the pT category to predict BCR were observed, while not observed in the multivariate analysis, which could be explained as the difference contributing to the included factors. In addition, FASN expression was found significantly both in univariate analysis and multivariate analysis, high FASN expression was identified as a significant factor to predict poor BCR and PCa progression. In spite of the differences in samples and ethnicity of the three datasets, we could still draw a conclusion of the oncogenic effect of FASN in PCa.

Our study still has several limitations. First, it was limited in sample size as a single-center study. Second, our study focused only on RNA and protein levels, more studies are needed to explore its potential mechanisms. Furthermore, our follow-up time was relatively short compared with other cohorts.

5. Conclusion

Our study demonstrated that FASN was overexpressed at mRNA and protein levels in PCa. We found that patients with high FASN expression had a shorter BCR-free survival, showing its value as a prognostic biomarker in male Han Chinese with PCa.

Data Availability

Answer: No. Comment: The data used to support the findings of this study are available from the corresponding author upon request.

Conflicts of Interest

The authors declare no competing financial interests.

Authors' Contributions

Zhi Cao, Yalong Xu and Fei Guo contributed equally to this work.

Acknowledgments

This study was supported by the National Natural Science Foundation of China (81430058, Yinghao Sun), the Precision Medicine Program of Second Military Medical University (2017JZ35, Fubo Wang), and the Clinical Research Project of Shanghai Municipal Commission of Health and Family Planning (20184Y0130, Fubo Wang).

Supplementary Materials

Supplementary Figure 1: the heatmap of the differential genes in TCGA (A), GSE46602 (B), and GSE6752 (C). Supplementary Table 1: the LogFC form of the differential genes in TCGA. Supplementary Table 2: the LogFC form of the differential genes in GSE46602. Supplementary Table 3: the LogFC form of the differential genes in GSE6752. *(Supplementary Materials)*

References

[1] R. L. Siegel, K. D. Miller, and A. Jemal, "Cancer statistics, 2019," *CA: A Cancer Journal for Clinicians*, vol. 69, no. 1, pp. 7–34, 2018.

[2] W. Chen, R. Zheng, P. D. Baade et al., "Cancer statistics in China, 2015," *CA: A Cancer Journal for Clinicians*, vol. 66, no. 2, pp. 115–132, 2016.

[3] N. Mottet, J. Bellmunt, M. Bolla et al., "EAU-ESTRO-SIOG guidelines on prostate cancer. Part 1: screening, diagnosis, and local treatment with curative intent," *European Urology*, vol. 71, no. 4, pp. 618–629, 2017.

[4] A. J. Stephenson, P. T. Scardino, J. A. Eastham et al., "Preoperative nomogram predicting the 10-year probability of prostate cancer recurrence after radical prostatectomy," *JNCI: Journal of the National Cancer Institute*, vol. 98, no. 10, pp. 715–717, 2006.

[5] M. Han, A. W. Partin, C. R. Pound, J. I. Epstein, and P. C. Walsh, "Long-term biochemical disease-free and cancer-specific survival following anatomic radical retropubic prostatectomy: the 15-year johns hopkins experience," *The Urologic Clinics of North America*, vol. 28, no. 3, pp. 555–565, 2001.

[6] G. Medes, A. Thomas, and S. Weinhouse, "Metabolism of neoplastic tissue. IV. A study of lipid synthesis in neoplastic tissue slices in vitro," *Cancer Research*, vol. 13, no. 1, pp. 27–29, 1953.

[7] T. Kusakabe, M. Maeda, N. Hoshi et al., "Fatty acid synthase is expressed mainly in adult hormone-sensitive cells or cells with high lipid metabolism and in proliferating fetal Cells1," *Journal of Histochemistry & Cytochemistry*, vol. 48, no. 5, pp. 613–622, 2016.

[8] S. Ashida, H. Nakagawa, T. Katagiri et al., "Molecular features of the transition from prostatic intraepithelial neoplasia (PIN) to prostate cancer: genome-wide gene-expression profiles of prostate cancers and PINs," *Cancer Research*, vol. 64, no. 17, pp. 5963–5972, 2004.

[9] U. S. Shah, R. Dhir, S. Gollin et al., "Fatty acid synthase gene overexpression and copy number gain in prostate adenocarcinoma," *Human Pathology*, vol. 37, no. 4, pp. 401–409, 2006.

[10] S. Rossi, E. Graner, P. Febbo et al., "Fatty acid synthase expression defines distinct molecular signatures in prostate cancer," *Molecular Cancer Research*, vol. 1, no. 10, pp. 707–715, 2003.

[11] F. P. Kuhajda, "Fatty acid synthase and cancer: new application of an old pathway," *Cancer Research*, vol. 66, no. 12, pp. 5977–5980, 2006.

[12] E. De Schrijver, K. Brusselmans, W. Heyns, G. Verhoeven, and J. V. Swinnen, "RNA interference-mediated silencing of the fatty acid synthase gene attenuates growth and induces morphological changes and apoptosis of LNCaP prostate cancer cells," *Cancer Research*, vol. 63, no. 13, pp. 3799–3804, 2003.

[13] S. J. Kridel, F. Axelrod, N. Rozenkrantz, and J. W. Smith, "Orlistat is a novel inhibitor of fatty acid synthase with antitumor activity," *Cancer Research*, vol. 64, no. 6, pp. 2070–2075, 2004.

[14] T. Migita, S. Ruiz, A. Fornari et al., "Fatty acid synthase: a metabolic enzyme and candidate oncogene in prostate cancer," *JNCI: Journal of the National Cancer Institute*, vol. 101, no. 7, pp. 519–532, 2009.

[15] M. S. Shurbaji, J. H. Kalbfleisch, and T. S. Thurmond, "Immunohistochemical detection of a fatty acid synthase (OA-519) as a predictor of progression of prostate cancer," *Human Pathology*, vol. 27, no. 9, pp. 917–921, 1996.

[16] J. I. Epstein, M. Carmichael, and A. W. Partin, "OA-519 (fatty acid synthase) as an independent predictor of pathologic state in adenocarcinoma of the prostate," *Urology*, vol. 45, no. 1, pp. 81–86, 1995.

[17] S. Bandyopadhyay, S. K. Pai, M. Watabe et al., "FAS expression inversely correlates with PTEN level in prostate cancer and a PI 3-kinase inhibitor synergizes with FAS siRNA to induce apoptosis," *Oncogene*, vol. 24, no. 34, pp. 5389–5395, 2005.

[18] G. Kristiansen, F. R. Fritzsche, K. Wassermann et al., "GOLPH2 protein expression as a novel tissue biomarker for prostate cancer: implications for tissue-based diagnostics," *British Journal of Cancer*, vol. 99, no. 6, pp. 939–948, 2008.

[19] M. J. Clemens, "Targets and mechanisms for the regulation of translation in malignant transformation," *Oncogene*, vol. 23, no. 18, pp. 3180–3188, 2004.

[20] D. Voeller, L. Rahman, and M. Zajac-Kaye, "Elevated levels of thymidylate synthase linked to neoplastic transformation of mammalian cells," *Cell Cycle*, vol. 3, no. 8, pp. 1003–1005, 2014.

[21] F. P. Kuhajda, "Fatty-acid synthase and human cancer: new perspectives on its role in tumor biology," *Nutrition*, vol. 16, no. 3, pp. 202–208, 2000.

[22] S. Yue, J. Li, S. Y. Lee et al., "Cholesteryl ester accumulation induced by PTEN loss and PI3K/AKT activation underlies human prostate cancer aggressiveness," *Cell Metabolism*, vol. 19, no. 3, pp. 393–406, 2014.

[23] K. Pelton, M. R. Freeman, and K. R. Solomon, "Cholesterol and prostate cancer," *Current Opinion in Pharmacology*, vol. 12, no. 6, pp. 751–759, 2012.

[24] D. R. Rhodes, J. Yu, K. Shanker et al., "*ONCOMINE*: A Cancer Microarray Database and Integrated Data-Mining Platform," *Neoplasia*, vol. 6, no. 1, pp. 1–6, 2004.

[25] Y. Yoshii, T. Furukawa, N. Oyama et al., "Fatty acid synthase is a key target in multiple essential tumor functions of prostate cancer: uptake of radiolabeled acetate as a predictor of the targeted therapy outcome," *PLoS One*, vol. 8, no. 5, article e64570, 2013.

[26] Y. Wang, J. A. Kelber, H. S. T. Cao et al., "Pseudopodium-enriched atypical kinase 1 regulates the cytoskeleton and cancer progression [corrected]," *Proceedings of the National Academy of Sciences*, vol. 107, no. 24, pp. 10920–10925, 2010.

[27] J. V. Swinnen, M. Esquenet, K. Goossens, W. Heyns, and G. Verhoeven, "Androgens stimulate fatty acid synthase in the human prostate cancer cell line LNCaP," *Cancer Research*, vol. 57, no. 6, pp. 1086–1090, 1997.

[28] J. A. Menendez, J. P. Decker, and R. Lupu, "In support of fatty acid synthase (FAS) as a metabolic oncogene: extracellular acidosis acts in an epigenetic fashion activating FAS gene expression in cancer cells," *Journal of Cellular Biochemistry*, vol. 94, no. 1, pp. 1–4, 2005.

[29] A. Baron, T. Migita, D. Tang, and M. Loda, "Fatty acid synthase: a metabolic oncogene in prostate cancer?," *Journal of Cellular Biochemistry*, vol. 91, no. 1, pp. 47–53, 2004.

[30] N. Dalmau, J. Jaumot, R. Tauler, and C. Bedia, "Epithelial-to-mesenchymal transition involves triacylglycerol accumulation in DU145 prostate cancer cells," *Molecular BioSystems*, vol. 11, no. 12, pp. 3397–3406, 2015.

[31] T. Van de Sande, T. Roskams, E. Lerut et al., "High-level expression of fatty acid synthase in human prostate cancer tissues is linked to activation and nuclear localization of Akt/PKB," *The Journal of Pathology*, vol. 206, no. 2, pp. 214–219, 2005.

Hindawi
Disease Markers
Volume 2020, Article ID 5265198, 10 pages
https://doi.org/10.1155/2020/5265198

Research Article

Strong-LAMP Assay Based on a *Strongyloides* spp.-Derived Partial Sequence in the 18S rRNA as Potential Biomarker for Strongyloidiasis Diagnosis in Human Urine Samples

Pedro Fernández-Soto,[1] Carmen T. Celis-Giraldo,[2] Coralina Collar-Fernández,[1] Óscar Gorgojo,[1] Milena Camargo,[3,4] José Muñoz,[5] Joaquín Salas-Coronas,[6] Manuel A. Patarroyo,[3,7] and Antonio Muro[1]

[1]*Infectious and Tropical Diseases Research Group (e-INTRO), Biomedical Research Institute of Salamanca-Research Centre for Tropical Diseases at the University of Salamanca (IBSAL-CIETUS), Faculty of Pharmacy, University of Salamanca, Salamanca 37007, Spain*
[2]*Animal Science Faculty, Universidad de Ciencias Aplicadas y Ambientales (U.D.C.A), Bogotá 111166, Colombia*
[3]*Molecular Biology and Immunology Department, Fundación Instituto de Inmunología de Colombia (FIDIC), Bogotá 111321, Colombia*
[4]*PhD Programme in Biomedical and Biological Sciences, School of Medicine and Health Sciences, Universidad del Rosario, Bogotá 112111, Colombia*
[5]*ISGlobal, Barcelona Ctr. Int. Health Res. (CRESIB), Hospital Clínic-Universitat de Barcelona, Barcelona 08036, Spain*
[6]*Unidad de Medicina Tropical, Hospital de Poniente, El Ejido 04700, Almería, Spain*
[7]*Basic Sciences Department, School of Medicine and Health Sciences, Universidad del Rosario, Bogotá 112111, Colombia*

Correspondence should be addressed to Manuel A. Patarroyo; mapatarr.fidic@gmail.com and Antonio Muro; ama@usal.es

Received 28 August 2019; Accepted 24 April 2020; Published 31 May 2020

Academic Editor: Lucio Castellano

Human strongyloidiasis a soil-transmitted infection caused by *Strongyloides stercoralis* is one of the most neglected amongst the so-called Neglected Tropical Diseases (NTDs). *S. stercoralis* is a nematode, which is distributed worldwide; it has been estimated that it could affect millions of people, mainly in tropical and subtropical endemic regions. The difficulties of diagnosis lead to infection rates being underreported. Asymptomatic patients have chronic infections that can lead to severe hyperinfection syndrome or disseminated strongyloidiasis in immunocompromised patients. Strongyloidiasis can easily be misdiagnosed because conventional faecal-based techniques lack of sensitivity for the morphological identification of infective larvae in faeces. None of the currently used molecular methods have used urine samples as an alternative to faecal samples for diagnosing strongyloidiasis. This study was thus aimed at comparing, for the first time, the use of a new loop-mediated isothermal amplification (LAMP) molecular assay (*Strong*-LAMP) to traditional methods on patients' urine samples. Twenty-four urine samples were taken from patients included in a study involving two Spanish hospitals for strongyloidiasis screening using parasitological and serological tests. *Strongyloides* larvae were found in 11 patients' faecal samples, thereby ascertaining that they had the disease. Other patients had high antibody titres but no larvae were found in their faeces. All urine samples were analysed by PCR and *Strong*-LAMP assay. No amplification occurred when using PCR. *Strong*-LAMP led to detecting *S. stercoralis* DNA in urine samples from patients having previously confirmed strongyloidiasis by parasitological tests and/or a suspicion of being infected by serological ones. The *Strong*-LAMP assay is a useful molecular tool for research regarding strongyloidiasis in human urine samples. After further validation, the *Strong*-LAMP assay could also be used for complementary and effective diagnosis of strongyloidiasis in a clinical setting.

1. Introduction

Strongyloidiasis is an infection caused by the parasitic nematodes from the genus *Strongyloides*: *S. stercoralis* and to a lesser extent *Strongyloides fuelleborni.* Originally known as "anguilulosis" or "Cochinchina diarrhoea", the World Health Organisation (WHO) now considers it a neglected tropical disease (NTD) [1, 2]. *S. stercoralis* has a cosmopolitan distribution in tropical and subtropical regions [3]. It can also be found in temperate areas, such as the Mediterranean region, southern USA, and Japan. Regarding *S. fuelleborni*, although primarily affecting nonhuman primates, human cases have also been described in Africa and Southeast Asia, mainly in Papua New Guinea [4, 5].

Strongyloidiasis worldwide has currently been calculated as ranging from 30-100 million infected people, mainly in low-income countries and those having poor sanitary conditions [6, 7]. Such variation regarding its estimation is largely due to its asymptomatic clinical picture, the tremendous difficulties regarding its diagnosis, and the affected people's lack of access to a health system. The disease's prevalence is considered to be greatly underestimated [8]. *S. stercoralis* is an autochthonous parasite in Spain all along its Mediterranean coastline, particularly in La Safor region within the province of Valencia, Spain, where it reaches 12.4% in high-risk groups related to agricultural work [6, 9]; cases have also been reported on the banks of the Ebro river [10]. Most European cases have been concerned with parasitosis imported by immigrants from strongyloidiasis-endemic areas, to a lesser extent, cases of travellers visiting such areas [11, 12] .

Strongyloidiasis clinical manifestations depend on parasite development and invasion stage, its self-infection capability, and a patient's immunological state. This may appear as an acute infection and chronic infection and produce a hyperinfection syndrome and/or a disseminated infection. Acute strongyloidiasis is not common and usually appears in travellers returning from a highly-endemic area suffering from pruritic dermatitis (due to the larvae penetrating the skin), pneumonitis accompanied by cough and expectoration (when the larvae enter the lungs), and fever. The parasites produce gastrointestinal pain accompanied by diarrhoea, nausea, and, occasionally, vomiting when they reach the intestines. Chronic (or low intensity) strongyloidiasis is usually asymptomatic, although it can have slight to moderate symptomatology, accompanied by gastrointestinal, pulmonary and cutaneous manifestations, and eosinophilia (in 75% of patients) [13].

It can produce the hyperinfection syndrome in immunosuppressed individuals when the larvae migrate, accompanied by more severe intestinal and pulmonary manifestations, fever, weakness, and a greater amount of larvae in faeces and sputum. Immunosuppressive treatments involving corticosteroids, solid or haematopoietic organ transplants, cancer, and HTLV-1 infection are considered the most important associated risk factors [4], along with malnutrition and associated infections in areas having high endemicity [14]. Anti-TNF therapies (stand alone or in combination with glucocorticoids) have favoured the development of clinical pictures and hyperinfections as they affect Th2 cells' immune response [15, 16].

The larvae can cross the blood-brain barrier, producing encephalitis and up to 87% mortality rates. The treatment usually used for strongyloidiasis is no longer effective at this point [17]; screening individuals suspected of having strongyloidiasis before immunosuppressive treatment is thus essential [4]. Ivermectin has been seen to be the most therapeutically effective drug used in control strategy; it continues being the drug of first choice regarding other options such as albendazole, thiabendazole, or mebendazole which are less effective and less safe [6, 16, 18, 19].

However, diagnosis is undoubtedly the main problem regarding strongyloidiasis due to little knowledge being available concerning the disease, its effects in nonendemic areas, current diagnostic techniques having little sensitivity and specificity, the parasitological methods requiring specialised personnel, and centres and no gold standard for diagnosis. This means that the case definition and the possible validation of new diagnostic methods are enormously hampered [20].

Current parasitological and immunological *S. stercoralis* diagnostic methods are thus being complemented by molecular methods [17, 21, 22]. Different approaches to the molecular detection of *S. stercoralis* in faecal samples have been developed from the description of the *Strongyloides* spp. 18S ribosomal subunit sequence, using polymerase chain reaction (PCR), both simple and nested techniques, and real time-PCR (RT-PCR) [8, 23]. Another recent molecular alternative method for diagnosing strongyloidiasis in patients' faecal samples [24] is the loop-mediated isothermal amplification (LAMP) of nucleic acids which has numerous advantages over other more complex molecular diagnosis techniques [25, 26].

LAMP is currently considered a technique having great potential for use in field conditions, mainly in endemic areas, as a future, highly effective, point-of-care testing method [27]. Fernández-Soto and colleagues [28] have developed a new LAMP method called *Strong*-LAMP for the molecular detection of *Strongyloides* spp. in urine and faecal samples in a murine model. It has also been used for analysing stool samples from patients previously diagnosed by parasitological and molecular (RT-PCR) methods, thereby making it a highly efficient diagnosis technique [28]. In this work, the *Strong*-LAMP is used for the first time in human urine samples from patients attending at two hospitals in Spain and compared with parasitological and serological methods.

2. Materials and Methods

2.1. Obtaining the Samples. The urine samples used in this study were obtained from patients (mostly immigrants) attending the Tropical Medicine Unit in Hospital Clínic de Barcelona (Barcelona, Spain) and Hospital de Poniente (El Ejido Almería, Spain) as part of a strongyloidiasis diagnosis screening study. The inclusion criteria were being a patient having simultaneous blood, faeces, and urine samples; having a positive parasitological and/or serological diagnosis for Strongyloides who had been recruited for a

Table 1: Nucleotide sequences from a set of primers selected from the 329 bp sequence (GenBank Acc. num.: AJ417026.1) for LAMP amplification of *Strongyloides* spp. DNA [28].

Primer	Length (bp)	Sequence (5′-3′)
F3	21	ACACGCTTTTTATACCACATT
B3	18	GTGGAGCCGTTTATCAGG
FIP	49	ACCAGATACACATACGGTATGTTTTGGATTTGATGAAACCATTTTTTCG
BIP	43	ATCAACTTTCGATGGTAGGGTATTGCCTATCCGGAGTCGAACC

multicentre study for strongyloidiasis diagnosis; a convenience sampling was thus performed, considering the abovementioned criteria. Each individual's clinical picture was recorded. All the patients included in the study were first analysed by *S. stercoralis* serology using a Microwell ELISA kit (IVD Research, Inc., Carlsbad, CA) (https://ivdresearch.com/elisa/strongyloides-serum-antibody-detection-microwell-elisa/) and coproparasitological analysis performed on only one sample (Ritchie technique and agar-plate culture for patients attending the Hospital de Poniente and just agar-plate culture for the Hospital Clínic de Barcelona patients) for detecting *S. stercoralis*. Samples whose optical density (OD) values were ≥1 in the IVD-ELISA test were considered positive (according to the manufacturers' specifications). The study involved 24 urine samples: 16 from Hospital Clínic (Barcelona) and 8 from Hospital de Poniente (Almería). All samples were sent to CIETUS in 10 mL tubes and stored frozen until use.

2.2. Ethical Considerations. Both hospitals' Ethics Committees approved the study; the urine samples were obtained after the patients had signed informed consent forms regarding their analysis.

2.3. Obtaining and Preparing the DNA Samples

2.3.1. Obtaining and Preparing Strongyloides venezuelensis DNA. DNA from *S. venezuelensis* infective filiform larvae (L3) was used as amplification positive control for PCR and LAMP reactions; their biological cycle is routinely maintained in experimentally-infected Wistar rats in the CIETUS, Universidad de Salamanca. A NucleoSpin Tissue kit (Machery-Nagel) was used for extracting DNA from the larvae, following the manufacturers' instructions. The DNA concentration was measured on a NanoDrop spectrophotometer (ND-1000) and adjusted to the final 5 ng/μL concentration. This DNA (2 μL) was then used as positive control for all subsequent PCR and LAMP reactions.

2.3.2. Obtaining and Preparing DNA from Patients' Urine. This involved taking 2 mL aliquots of patients' urine from the unfrozen vials; the rest remained frozen at -20°C. The vials to be analysed were spun at 4,000 rpm for 15 min to obtain sediment for extracting the DNA using the i-genomic Urine DNA Extraction Mini Kit (Intron Biotechnology), following the manufacturers' instructions. A NanoDrop spectrophotometer (ND-1000) was used for measuring the DNA concentration from each urine sample (100 μL elution volume); they were then labelled and stored until use at -20°C in two vials (50 μL in each).

2.4. Amplification Target and Specific Primers for LAMP Amplifying Strongyloides spp. DNA. The *Strong*-LAMP method previously validated and developed at CIETUS was used for *Strongyloides* spp. DNA amplification [17]. Briefly, the selected amplification target was a *Strongyloides venezuelensis* partial 18S rRNA gene (GenBank Accession number: AJ417026.1) 329 base pair (bp) sequence; Primer Explorer V.4 software (https://primerexplorer.jp/e/) was used for designing a set of four primers (F3, B3, FIP, and BIP) on this sequence (Table 1 shows the selected primer sequences). A Fisher Scientific synthesis kit was used, and purified products were suspended in ultrapure water at 100 pmol/μL final concentration.

2.5. Molecular Analysis of Patients' Urine Samples

2.5.1. PCR Analysis of F3 and B3 External Primers. The urine samples were analysed by PCR using F3 and B3 external primers from the set of 4 primers for the LAMP assay; correct PCR functioning had already been verified with *S. venezuelensis* DNA. A touchdown PCR (TD-PCR) was carried out consisting of decreasing the annealing temperature by one degree per each amplification cycle for guaranteeing a suitable range of annealing temperatures for correct target sequence amplification [29]; briefly, TD-PCR was performed as follows: 94°C for 60 seconds and a touchdown program involving 18 cycles; Table 2 shows the reaction mixture and amplification conditions used in the TD-PCR. A 96-well thermal cycler (Gradient Mastercycler, Eppendorf) was used for all PCR reactions.

2.5.2. LAMP Analysis of Patients' Urine Samples. All the urine samples were analysed by the *Strong*-LAMP previously described by Fernández-Soto et al. [28]. Table 3 describes the reaction mixture used. All reactions were incubated for 60 min at 63°C in a heating block (K Dry-Bath) plus 10 min at 80°C for deactivating the enzyme and stopping the reaction; 2 μL DNA from each urine sample were used for amplification; *S. venezuelensis* DNA (2 μL) and ultrapure water instead of DNA (2 μL) were used as positive and negative controls, respectively.

2.5.3. Detecting the Amplification Products

(1) PCR. PCR amplification products were detected on 1.5% agarose gels (100 mL 0.5X TBE, 1.5 g agarose), stained with ethidium bromide at 60 V for 20 min and then at 90-100 V for one hour. The gels were visualised and photographed using an ultraviolet imaging system (UVITEC Gel Documentation System, Cambridge, UK).

Table 2: Reaction mixture (a) and amplification conditions used in TD-PCR using F3 and B3 external primers (b). *Taq* polymerase, buffer, $MgCl_2$, and dNTPs were supplied by Intron.

(a)

Components	Volume (μL)
H_2O	17.1
10x buffer	2.5
MgCl2 (25 mM)	1.5
dNTPs (2.5 mM)	0.5
F3 (pmol)	0.5
B3 (pmol)	0.5
Taq polymerase (2 U)	0.4
Template DNA	2
Total	25

(b)

Temperature (°C)	Time (sec)	Cycle
94	60	X 1
94	20	
57-52	20	X 2
72	30	
94	60	
51	20	X 15
72	30	
72	60	X 1

Table 3: Reaction mixture used in *Strong*-LAMP assays. *Bst* polymerase, buffer, and $MgSO_4$ were supplied by New England Biolabs, betaine by SIGMA, and the dNTPs by Intron.

Component	Volume (μL)
H_2O	7.7
Betaine (1 M)	5
$MgSO_4$	1.5
dNTPs (2.5 mM)	3.5
10x buffer	2.5
FIP (40 pmol/μL)	0.4
BIP (40 pmol/μL)	0.4
F3 (5 pmol/μL)	0.5
B3 (5 pmol/μL)	0.5
Bst polymerase 2.0	1
DNA	2
Total	25

(2) Strong-LAMP. LAMP amplification products were visually detected by observing white turbidity at the bottom of the reaction tube and by colorimetric change on adding 2 μL SYBR Green I fluorescent dye (Invitrogen) (1 : 10; 10,000X) to each reaction tube. Green indicated a positive result and orange a negative one (i.e., maintaining the dye's original colour). Colorimetric results were verified by 1.5% agarose electrophoresis for observing the characteristic pattern of bands which appears in positive LAMP results. The gels were then photographed and the images saved in digital format for editing.

2.6. Statistical Analysis. Stata MP 14.0 statistical software was used for analysing the data. A descriptive analysis was made; quantitative variables are shown as Medians or Means with their corresponding dispersion measures (Interquartile range-IQR or Standard Deviation-SD); 5% significance confidence intervals were calculated for each test. Agreement between serological and coproparasitological screening tests with *Strong*-LAMP results in this study was quantified and analysed using the kappa coefficient (κ), interpreted as: <0.00 poor, $0 \leq \kappa \leq 0.2$ slight, $0.21 \leq \kappa \leq 0.40$ fair, $0.41 \leq \kappa \leq 0.60$ moderate, $0.61 \leq \kappa \leq 0.80$ substantial, and >0.80 almost perfect [30].

3. Results

3.1. Serological and Parasitological Data. The study results showed that 54% of the samples came from Latin-American patients (mainly from Bolivia (9/24) and the remainder from Africa (specifically Gambia (4/24) and Guinea-Bissau (2/24)). The patients' epidemiological data stated that 62.5% (15/24) were male, most being aged from 30 to 60 years old (75%), with a mean = 41.1 (SD = 12.6). Regarding their clinical pictures, 50% (12/24) of the target population had symptoms such as abdominal pain, diarrhoea, urticaria, and pruritus. Eosinophilia was observed in 45.8% (11/24) of the population, with a median = 870 (IQR = 680 – 1900), accompanied by high IgE levels in 52.15% of them (12/23), with a median = 1320.5 (IQR = 542 – 2438) (Table 4). Strongyloidiasis diagnosis test revealed that 87.5% of the study population had ≥1 titres for IVD-ELISA with a median = 2.22 (IQR = 1.71 – 4.52). However, 37.5% (0.19-0.614 95% CI) of the population was positive by coproparasitological analysis by agar culture plate method (individual results in Supplementary material Tables 1 and 2. Once diagnosed, 95.8% (23/24) of the individuals were treated with ivermectin; all but one patient were followed-up.

3.2. Human Urine Samples Analysed by TD-PCR F3-B3 Assay. Figure 1 shows the TD-PCR amplification results; there was no amplification in any of the samples analysed.

3.3. Strong-LAMP Analysis of Patients' Urine Samples. It was found that 50% of the individuals (0.25-0.67 95% CI) were positive according to test parameters. Figure 2 shows *Strong*-LAMP results from analysing the patients' urine samples from the Hospital Clínic de Barcelona and Figure 3 from the Hospital de Poniente; results from other tests are also shown.

3.4. Agreement between Screening Analysis and Strong-LAMP. Strong-LAMP results were compared to the IVD test results and then to the coproparasitological analysis results. The numbers in the figure represent the total of samples proving positive in each test analysed. The scale on the lower axis indicates the percentage in relation to the total of

Table 4: Descriptive statistics regarding the population's epidemiological characteristic, clinical status (a), and haematological results (b).

(a)

Epidemiological characteristic	Total (n (%))
Origin	
Bolivia	9 (37.5)
Gambia	4 (16.6)
Ecuador	2 (8.3)
Guinea Bissau	2 (8.3)
Spain	2 (8.3)
Other[1]	5 (20.83)
Gender	
Female	9 (37.5)
Male	15 (62.5)
Age (years)	
<30	4 (16.6)
30-60	18 (75)
>60	2 (8.3)
Clinical status	
Asymptomatic	12 (50)
Symptomatic	12 (50)

(b)

Laboratory test	n	Median	IQR
Haematological result			
Eosinophils	23	400	(100-870)
IgE	22	358	(72-1653)

[1]Only one person by country (Colombia, Cuba, Mali, Nigeria, and Portugal).
[2]Optical density (OD) according to the maker's specifications.

positive individuals (Figure 4); 37.5% agreement was observed and poor correlation according to κ value for IVD and *Strong*-LAMP analysis ($\kappa = -0.25$; $p = 0.968$). Such data differed from that observed regarding coprology and *Strong*-LAMP results where agreement was 79.17%. The κ value gave moderate correlation ($\kappa = 0.5833$; $p = 0.0016$), according to the classification described above.

4. Discussion

One of the main problems regarding strongyloidiasis continues being the lack of a true gold standard for diagnosing the disease. Even though parasitological methods continue being considered "clinical or certainty diagnosis" (i.e., they enable visualising the larvae in faecal samples), they involve great disadvantages, mainly regarding their sensitivity [6, 21].

Serological methods also have problems regarding sensitivity (especially during the disease's acute phase) and specificity due to often producing crossed reactions concerning a diagnosis of other nematodes. PCR-based molecular methods and variants (e.g., RT-PCR) have been advanced during recent years as the most suitable ones for diagnosing strongyloidiasis, even though requiring complex infrastructure and specialised equipment and personnel which are not available in routine practice and are expensive and very difficult to perform in field conditions in strongyloidiasis-endemic areas [17, 31].

The lack of a suitable and standardised diagnosis method has led to underestimating the disease's real prevalence. Although migrants were screened in this study, it was interesting that most individuals came from Latin America, mainly from Bolivia. Studies have been inconsistent when reporting the disease's prevalence in Latin America; values have been higher than 20% in Argentina, Ecuador, Venezuela, Perú, and Brazil [32] whilst a study by Gétaz [33] in Bolivia estimated prevalence at 20.0%. Eosinophilia being found in 45.8% (11/24) of the target population accompanied by increased IgE production in 9 patients is parameters which have been reported in strongyloidiasis cases [34]. However, individuals suffering eosinophilia cannot always be identified as this depends on the parasite's cycle and concomitant infections [35]. Regarding IgE levels, normal levels have been reported in individuals infected by *Strongyloides stercoralis* who also proved positive for human T-cell lymphotropic virus type 1 (HTLV-1) [36].

Difficulties regarding diagnosis are especially important regarding immunocompromised people or immunosuppression candidates (e.g., in transplants) who could develop hyperinfection leading to a fatal outcome for the patient [4]. A study by Luvira et al. [37], involving patients who were immunocompromised due to different causes, analysed factors such as age, gender, and level of immunocompromise and reported that they were not associated with strongyloidiasis; prevalence ranged from 5%-7% and coproparasitological analysis in agar was the most sensitive technique in this study [37]. New sensitive, specific, technically easy, and economically affordable diagnosis methods must thus be developed; they must also become incorporated into routine clinical practice as a screening method for strongyloidiasis in patients who are candidates for immunosuppressive treatment.

However, most molecular diagnosis methods for detecting *S. stercoralis* have been based on using faecal or soil samples in the search for larvae. Faecal samples involve problems associated with collecting (serial, at least 3 samples), processing (usually requiring them to be concentrated), and storing them. Urine analysis is an alternative for making a diagnosis [20, 28, 38, 39]. A new molecular diagnosis method such as LAMP for use on urine samples thus provides an interesting approach, combining this technique's advantages over other molecular methods (i.e., PCR) and the advantages of analysing urine samples. Previous studies have evaluated the parasite's presence in urine; a study by Lodh et al. [40] detected *S. stercoralis*-derived DNA by molecular methods, Formenti et al. [41] evaluated parasite diagnosis by conventional and molecular methods such as q-PCR analysing urine samples and faecal material; they found that qPCR urine analysis sensitivity was just 17% compared to faecal material analysis having 63% sensitivity [41].

In a previous work, *Strong*-LAMP adaption of the LAMP method for detecting *Strongyloides venezuelensis* has proved

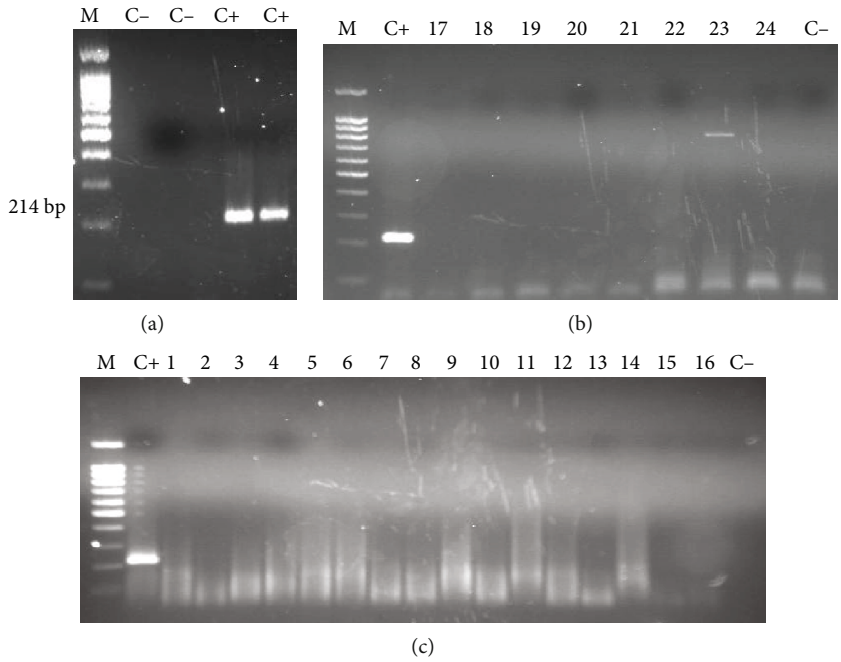

Figure 1: TD-PCR analysis of patients' urine samples. (a) PCR for verifying F3 and B3 primer functioning for amplifying the 214 bp fragment. (b) Samples from the Hospital de Poniente (El Ejido, Almería). (c) Samples from the Hospital Clínic de Barcelona. M: molecular weight marker (DNA Ladder 100 bp PLUS BLUE); C+: *Strongyloides venezuelensis* DNA (positive control); C–: ultrapure water, no DNA (negative control).

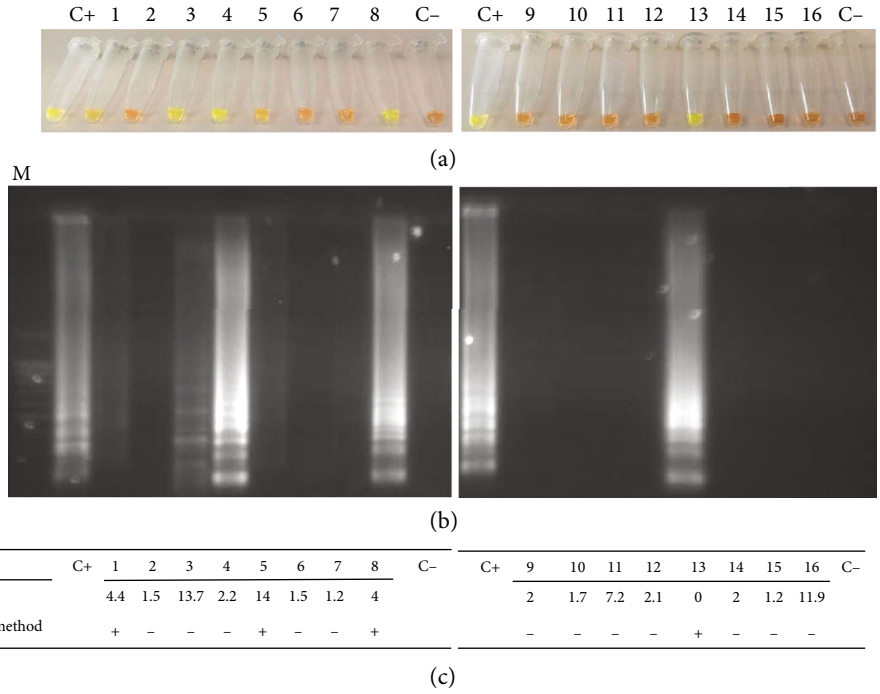

Technique/sample	C+	1	2	3	4	5	6	7	8	C–	C+	9	10	11	12	13	14	15	16	C–
Serology (IVD)		4.4	1.5	13.7	2.2	14	1.5	1.2	4			2	1.7	7.2	2.1	0	2	1.2	11.9	
Agar culture plate method		+	–	–	–	+	–	–	+			–	–	–	–	+	–	–	–	

(c)

Figure 2: *Strong*-LAMP analysis of urine samples from patients attending Hospital Clínic de Barcelona (Barcelona). (a) Colorimetric results from adding SYBR Green I. (b) Agarose gel electrophoresis results. (c) Serological (IVD index, OD values) and agar plate culture results. M: molecular weight marker (DNA Ladder 100 bp PLUS BLUE); C+: *Strongyloides venezuelensis* DNA (positive control); C-: ultrapure water, no DNA (negative control).

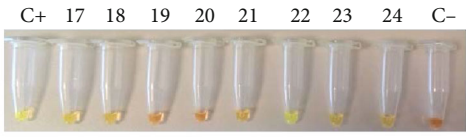

(a)

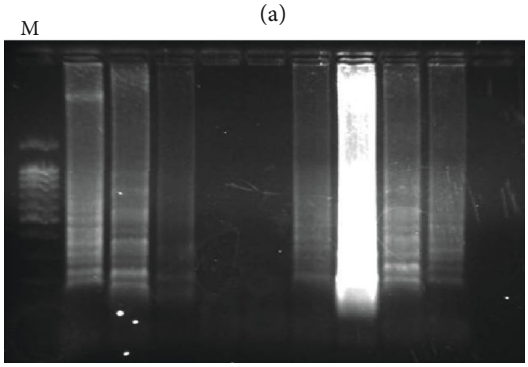

(b)

Technique/sample	C+	17	18	19	20	21	22	23	24	C–
Serology (IVD)		4.52	4.10	1.39	1.97	0.48	3.22	8.31	0.39	
Ritchie technique		+	+	–	–	+	+	–	+	
Agar culture plate method		+	+	+	–	–	+	+	–	

(c)

Figure 3: *Strong*-LAMP analysis of urine samples from patients attending Hospital de Poniente (El Ejido, Almería). (a) Colorimetric results by adding SYBR Green I. (b) Agarose gel electrophoresis results. (c) Serological (IVD index, OD values), Ritchie technique and agar plate culture results. M: molecular weight marker (DNA Ladder 100 bp PLUS BLUE); C+: *Strongyloides venezuelensis* DNA (positive control); C-: ultrapure water, no DNA (negative control).

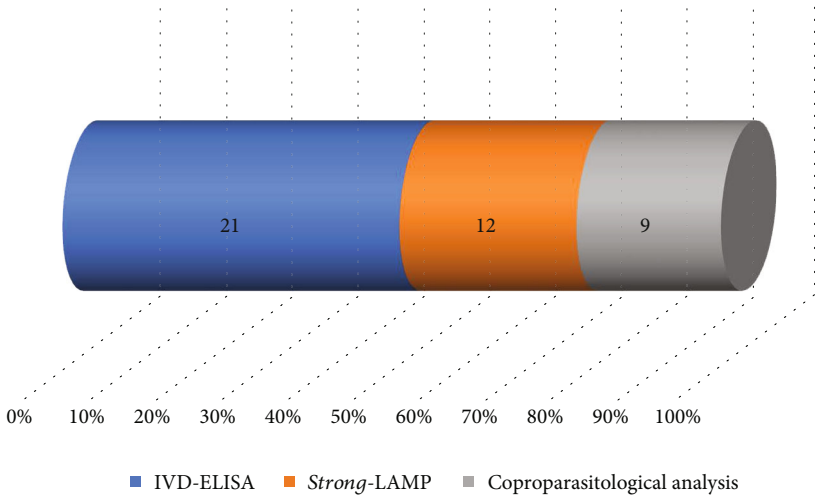

95% C.I	(06.67-0.97)	(0.25-0.67)	(0.19-0.61)
Agreement (%)	37.5[a]	79.17[b]	
Kappa	–0.25	0.5833	

a) Agreement between IVD-ELISA and *Strong*-LAMP
b) Agreement between *Strong*–LAMP and coproparasitological analysis

Figure 4: Agreement between *Strong*-LAMP, IVD detection techniques, and coproparasitological analysis in the studied samples with strongyloidiasis.

effective regarding faecal and urine samples in an experimental infection model involving rodents and also regarding faecal samples from patients having a confirmed *S. stercoralis* infection [28]. The present work has evaluated, for the first time, the *Strong*-LAMP method as a molecular method for detecting *S. stercoralis* in patients' urine samples.

PCR was initially used with F3 and B3 external primers (even though none of the samples became amplified) for verifying whether PCR could be used as a molecular method for analysing urine samples. Single PCR has been used in other studies providing good results for detecting *S. stercoralis* DNA in faecal samples and has been prosed as a complementary molecular method to larval concentration in faecal samples before DNA extraction [42]. PCR F3-B3 (with 0.01 ng *Strongyloides* spp. DNA detection limit) has been effective in detecting *S. venezuelensis* in faecal samples in an experimental infection model [28].

However, positive amplification results have not been obtained when using PCR F3-B3 on patients' urine samples, meaning that it cannot be proposed as a complementary molecular method for a definitive diagnosis of strongyloidiasis. Nevertheless, using the *Strong*-LAMP method with samples has led to positive visible amplification results concerning colorimetric change and resolving reaction products on agarose gels.

Eleven of the 24 urine samples analysed had parasitologically positive results for *S. stercoralis* by at least one of the coproparasitological diagnosis methods (i.e., Ritchie technique and/or agar plate culture), and 45.83% of the samples were positive by *Strong*-LAMP. Furthermore, 16% of the samples turned a less pronounced green (indicating amplification) than the rest of the positive samples, and a pattern of bands was obtained which was dimmer on agarose gel. The high protein concentration in these samples could have limited amplification; the 260/280 ratio for absorbance regarding DNA extracted from the samples (often less than 1, most being around 0.5) was well below the expected value for pure nucleic acids (between 1.8 and 2.0; ≥1.8 for DNA), thereby limiting analytical purposes. Such high protein concentration would have been the main cause of inhibiting PCR analysing the samples.

Strong-LAMP amplification of two urine samples (I.D: 3 and 4) was obtained in patients having negative faecal sample results by agar plate culture. Given poor sensitivity for coproparasitological technique when analysing a single sample of a patient's faeces, both samples could have proved positive if a serial analysis had been performed (at least three samples from the same patient, taken on alternating days) for visualising *S. stercoralis* larvae [21].

Regarding serological analysis results, most samples had a serological IVD index greater than 1 OD, considered the cut-off limit for considering a result positive by this technique [43]. For example, the sample 3 had a very high IVD index (13.7 OD), indicating anti-*S. stercoralis* antibodies. It is worth noting that sample 13 which was positive by both agar plate culture and *Strong*-LAMP had an IVD serological index considered negative (0.005 OD). It has been noted that false negatives sometimes appear when using the IVD serological test [43]. Only one individual who was HIV positive (stage A2) proved positive in all tests carried out in this study. The tests are more efficient for detecting the parasite in such individuals since they may have a hyperinfection syndrome, as observed in a case report by Grossi et al. [44] describing a HIV-positive male having peripheral T-cell lymphoma who developed hyperinfection syndrome and was successfully treated with subcutaneous ivermectin [44]. A study in Brazil by Marchi-Blatt and Aparecida-Cantos [45] compared *Strongyloides stercoralis* diagnosis techniques on HIV positive and negative patients; it found that HIV positive patients had higher *S. stercoralis* infection frequency (odds ratio = 5.687) [45]. A study regarding urine analysis in Ethiopia by Hailegebriel et al. [46] demonstrated that agreement between coproparasitological analysis and *Strong*-LAMP for urine samples in this study was 78%; it should thus be worthwhile evaluating the test's efficiency in a broader population.

Despite the fact that PCR using external primers F3-B3 and the *Strong*-LAMP method has been shown to have the same limit for detecting *Strongyloides* spp. DNA (0.01 ng) [28], the results obtained from analysing the urine samples were consistent with the LAMP method having greater tolerance as described by other authors concerning possible inhibitors in biological samples analysed regarding PCR [47].

Although more studies are needed which would involve increasing the amount of urine samples to be analysed, the present work's results suggest that the *Strong*-LAMP method and those obtained in faeces [28] have demonstrated that the technique could be used as a complementary molecular tool when diagnosing strongyloidiasis. It could be used as a routine molecular method as it has certain advantages over PCR, i.e., it is cheaper as samples are amplified at constant temperature (59-66°C) making equipment such as water baths and thermal blocks sufficient, it can detect small concentrations of DNA in samples and is highly specific making it a simple technique to use [48–50].

5. Conclusions

The *Strong*-LAMP molecular diagnosis method was used for the first time for detecting *Strongyloides* spp. DNA in patients' urine samples. The *Strong*-LAMP method proved effective in detecting *S. stercoralis* DNA in the urine samples of patients with confirmed strongyloidiasis and/or the serological suspicion of infection by the parasite. The *Strong*-LAMP method could be used on urine samples as a complementary method for detecting *S. stercoralis* infection.

Data Availability

All data used to support the findings of this study are included in the manuscript and figures.

Disclosure

The funders had no role in study design, data collection and analysis, decision to publish, or preparation of the manuscript.

Conflicts of Interest

The authors declare that there is no conflict of interest regarding the publication of this paper.

Authors' Contributions

Pedro Fernández-Soto and Carmen T. Celis-Giraldo equally contributed equally to this work.

Acknowledgments

We would like to thank Jason Garry for translating the manuscript. This study was supported by the Institute of Health Carlos III, ISCIII, Spain (http://www.isciii.es), grants: RICET RD16/0027/0018, DTS16/00207, PI16/01784, and the European Union cofinancing by FEDER (Fondo Europeo de Desarrollo Regional) "Una manera de hacer Europa". The Universidad del Rosario, Bogotá (Colombia), covered the open access charges.

Supplementary Materials

Table 1. Individual patients results from the Hospital Clínic de Barcelona, Barcelona, Spain. Table 2. Individual patients results from Hospital de Poniente, El Ejido, Almería, Spain. *(Supplementary Materials)*

References

[1] A. Olsen, L. van Lieshout, H. Marti et al., "Strongyloidiasis-the most neglected of the neglected tropical diseases?," *Transactions of the Royal Society of Tropical Medicine and Hygiene*, vol. 103, no. 10, pp. 967–972, 2009.

[2] R. Toledo, C. Munoz-Antoli, and J. G. Esteban, "Strongyloidiasis with emphasis on human infections and its different clinical forms," *Advances in Parasitology*, vol. 88, pp. 165–241, 2015.

[3] G. A. Schad, L. M. Aikens, and G. Smith, "*Strongyloides stercoralis*: is there a canonical migratory route through the host?," *The Journal of Parasitology*, vol. 75, no. 5, pp. 740–749, 1989.

[4] F. Schär, U. Trostdorf, F. Giardina et al., "*Strongyloides stercoralis*: global distribution and risk factors," *PLoS Neglected Tropical Diseases*, vol. 7, no. 7, article e2288, 2013.

[5] T. Thanchomnang, P. M. Intapan, O. Sanpool et al., "First molecular identification of *Strongyloides fuelleborni* in long-tailed macaques in Thailand and Lao People's Democratic Republic reveals considerable genetic diversity," *Journal of Helminthology*, vol. 93, no. 5, pp. 608–615, 2019.

[6] S. Puthiyakunnon, S. Boddu, Y. Li et al., "Strongyloidiasis–an insight into its global prevalence and management," *PLoS Neglected Tropical Diseases*, vol. 8, no. 8, article e3018, 2014.

[7] A. Tuyizere, A. Ndayambaje, T. D. Walker et al., "Prevalence of *Strongyloides stercoralis* infection and other soil-transmitted helminths by cross-sectional survey in a rural community in Gisagara District, Southern Province, Rwanda," *Transactions of the Royal Society of Tropical Medicine and Hygiene*, vol. 112, no. 3, pp. 97–102, 2018.

[8] M. Dorris and M. Blaxter, "The small subunit ribosomal RNA sequence of Strongyloides stercoralis," *International Journal for Parasitology*, vol. 30, no. 8, pp. 939–941, 2000.

[9] R. I. Adell and V. D. Márquez, "Estrongiloidiasis: epidemiología, manifestaciones clínicas y diagnóstico. Experiencia en una zona endémica: la comarca de La Safor (Valencia)," *Enfermedades Infecciosas y Microbiología Clínica*, vol. 25, pp. 38–44, 2007.

[10] P. R. Sánchez, A. P. Guzman, S. M. Guillen et al., "Endemic strongyloidiasis on the Spanish Mediterranean coast," *QJM: An International Journal of Medicine*, vol. 94, no. 7, pp. 357–363, 2001.

[11] G. Ramirez-Olivencia, M. Á. C. Espinosa, A. B. Martín et al., "Imported strongyloidiasis in Spain," *International Journal of Infectious Diseases*, vol. 18, pp. 32–37, 2014.

[12] W. Winnicki, M. Eder, P. Mazal, F. J. Mayer, G. Sengolge, and L. Wagner, "Prevalence of _Strongyloides stercoralis_ infection and hyperinfection syndrome among renal allograft recipients in Central Europe," *Scientific Reports*, vol. 8, no. 1, article 15406, 2018.

[13] T. B. Nutman, "Human infection with *Strongyloides stercoralis* and other related Strongyloides species," *Parasitology*, vol. 144, no. 3, pp. 263–273, 2017.

[14] D. C. Pichard, J. R. Hensley, E. Williams, A. B. Apolo, A. D. Klion, and J. J. DiGiovanna, "Rapid development of migratory, linear, and serpiginous lesions in association with immunosuppression," *Journal of the American Academy of Dermatology*, vol. 70, no. 6, pp. 1130–1134, 2014.

[15] T. Ali, S. Kaitha, S. Mahmood, A. Ftesi, J. Stone, and M. S. Bronze, "Clinical use of anti-TNF therapy and increased risk of infections," *Drug, Healthcare and Patient Safety*, vol. 5, pp. 79–99, 2013.

[16] M. F. Khaliq, R. E. Ihle, and J. Perry, "Immunosuppression with antitumour necrosis factor therapy leading to Strongyloides hyperinfection syndrome," *Case Reports in Infectious Diseases*, vol. 2018, Article ID 6341680, 4 pages, 2018.

[17] D. Buonfrate, F. Formenti, F. Perandin, and Z. Bisoffi, "Novel approaches to the diagnosis of *Strongyloides stercoralis* infection," *Clinical Microbiology and Infection*, vol. 21, no. 6, pp. 543–552, 2015.

[18] Y. Suputtamongkol, N. Premasathian, K. Bhumimuang et al., "Efficacy and safety of single and double doses of ivermectin versus 7-day high dose albendazole for chronic strongyloidiasis," *PLoS Neglected Tropical Diseases*, vol. 5, no. 5, article e1044, 2011.

[19] C. Henriquez-Camacho, E. Gotuzzo, J. Echevarria et al., "Ivermectin versus albendazole or thiabendazole for *Strongyloides stercoralis* infection," *Cochrane Database of Systematic Reviews*, article CD007745, 2016.

[20] A. Requena-Mendez, P. Chiodini, Z. Bisoffi, D. Buonfrate, E. Gotuzzo, and J. Munoz, "The laboratory diagnosis and follow up of strongyloidiasis: a systematic review," *PLoS Neglected Tropical Diseases*, vol. 7, no. 1, article e2002, 2013.

[21] M. Montes, C. Sawhney, and N. Barros, "*Strongyloides stercoralis*: there but not seen," *Current Opinion in Infectious Diseases*, vol. 23, no. 5, pp. 500–504, 2010.

[22] F. M. Paula, F. M. Malta, P. D. Marques et al., "Molecular diagnosis of Strongyloides stercoralis among transplant candidates," *Transplant Infectious Disease*, vol. 20, no. 4, article e12909, 2018.

[23] A. Perera, J. P. Maia, F. Jorge, and D. J. Harris, "Molecular screening of nematodes in lacertid lizards from the Iberian Peninsula and Balearic Islands using 18S rRNA sequences," *Journal of Helminthology*, vol. 87, no. 2, pp. 189–194, 2013.

[24] M. R. Watts, G. James, Y. Sultana et al., "A loop-mediated isothermal amplification (LAMP) assay for *Strongyloides stercoralis* in stool that uses a visual detection method with SYTO-82 fluorescent dye," *The American Journal of Tropical Medicine and Hygiene*, vol. 90, no. 2, pp. 306–311, 2014.

[25] M. Parida, S. Sannarangaiah, P. K. Dash, P. V. Rao, and K. Morita, "Loop mediated isothermal amplification (LAMP): a new generation of innovative gene amplification technique; perspectives in clinical diagnosis of infectious diseases," *Reviews in Medical Virology*, vol. 18, no. 6, pp. 407–421, 2008.

[26] K. Dhama, K. Karthik, S. Chakraborty et al., "Loop-mediated isothermal amplification of DNA (LAMP): a new diagnostic tool lights the world of diagnosis of animal and human pathogens: a review," *Pakistan Journal of Biological Sciences*, vol. 17, no. 2, pp. 151–166, 2014.

[27] Z. K. Njiru, "Loop-mediated isothermal amplification technology: towards point of care diagnostics," *PLoS Neglected Tropical Diseases*, vol. 6, no. 6, article e1572, 2012.

[28] P. Fernández-Soto, A. Sánchez-Hernández, J. Gandasegui et al., "Strong-LAMP: A LAMP Assay for *Strongyloides spp*. detection in stool and urine samples. Towards the diagnosis of human Strongyloidiasis starting from a rodent model," *PLOS Neglected Tropical Diseases*, vol. 10, no. 7, article e0004836, 2016.

[29] P. Fernandez-Soto, V. Velasco Tirado, C. Carranza Rodriguez, J. L. Perez-Arellano, and A. Muro, "Long-term frozen storage of urine samples: a trouble to get PCR results in Schistosoma spp. DNA detection?," *PLoS One*, vol. 8, no. 4, article e61703, 2013.

[30] A. Petrie and C. Sabin, "Assessing agreement," in *Medical Statistics at a Glance*, A. Petrie and C. Sabin, Eds., pp. 118–121, Wiley, UK, 3rd edition, 2009.

[31] M. A. Levenhagen and J. M. Costa-Cruz, "Update on immunologic and molecular diagnosis of human strongyloidiasis," *Acta Tropica*, vol. 135, pp. 33–43, 2014.

[32] D. Buonfrate, M. A. Mena, A. Angheben et al., "Prevalence of strongyloidiasis in Latin America: a systematic review of the literature," *Epidemiology and Infection*, vol. 143, no. 3, pp. 452–460, 2015.

[33] L. Gétaz, R. Castro, P. Zamora et al., "Epidemiology of *Strongyloides stercoralis* infection in Bolivian patients at high risk of complications," *PLoS Neglected Tropical Diseases*, vol. 13, no. 1, article e0007028, 2019.

[34] A. Mir, D. Benahmed, R. Igual et al., "Eosinophil-selective mediators in human strongyloidiasis," *Parasite Immunology*, vol. 28, no. 8, pp. 397–400, 2006.

[35] C. Carranza-Rodriguez, M. Escamilla-Gonzalez, I. Fuentes-Corripio, M. J. Perteguer-Prieto, T. Garate-Ormaechea, and J. L. Perez-Arellano, "Helminthosis and eosinophilia in Spain (1990-2015)," *Enfermedades Infecciosas y Microbiología Clínica*, vol. 36, no. 2, pp. 120–136, 2018.

[36] M. Higashiarakawa, T. Hirata, T. Tanaka et al., "Normal serum IgE levels and eosinophil counts exhibited during *Strongyloides stercoralis* infection," *Parasitology International*, vol. 66, no. 1, pp. 807–812, 2017.

[37] V. Luvira, K. Trakulhun, M. Mungthin et al., "Comparative diagnosis of Strongyloidiasis in immunocompromised patients," *The American Journal of Tropical Medicine and Hygiene*, vol. 95, no. 2, pp. 401–404, 2016.

[38] S. Abdel-Rahman and A. Metwally, "Obstacles in the diagnosis of Strongyloides stercoralis," *Parasitologists United Journal*, vol. 7, no. 1, pp. 5–12, 2014.

[39] A. Requena-Mendez, D. Buonfrate, Z. Bisoffi, and J. M. Gutiérrez, "Advances in the diagnosis of human Strongyloidiasis," *Current Tropical Medicine Reports*, vol. 1, no. 4, pp. 207–215, 2014.

[40] N. Lodh, R. Caro, S. Sofer, A. Scott, A. Krolewiecki, and C. Shiff, "Diagnosis of *Strongyloides stercoralis*: detection of parasite-derived DNA in urine," *Acta Tropica*, vol. 163, pp. 9–13, 2016.

[41] F. Formenti, G. la Marca, F. Perandin et al., "A diagnostic study comparing conventional and real-time PCR for *Strongyloides stercoralis* on urine and on faecal samples," *Acta Tropica*, vol. 190, pp. 284–287, 2019.

[42] H. Moghaddassani, H. Mirhendi, M. Hosseini, M. Rokni, G. Mowlavi, and E. Kia, "Molecular diagnosis of *Strongyloides stercoralis* infection by PCR detection of specific DNA in human stool samples," *Iranian Journal of Parasitology*, vol. 6, no. 2, pp. 23–30, 2011.

[43] B. Bon, S. Houze, H. Talabani et al., "Evaluation of a rapid enzyme-linked immunosorbent assay for diagnosis of strongyloidiasis," *Journal of Clinical Microbiology*, vol. 48, no. 5, pp. 1716–1719, 2010.

[44] P. A. Grossi, D. Lombardi, A. Petrolo et al., "*Strongyloides stercoralis* hyperinfection in an HIV-infected patient successfully treated with subcutaneous ivermectin," *Tropical Medicine and Infectious Disease*, vol. 3, no. 2, p. 46, 2018.

[45] J. Marchi Blatt and G. Aparecida Cantos, "Evaluation of techniques for the diagnosis of *Strongyloides stercoralis* in human immunodeficiency virus (HIV) positive and HIV negative individuals in the city of Itajaí, Brazil," *The Brazilian Journal of Infectious Diseases*, vol. 7, no. 6, pp. 402–408, 2003.

[46] T. Hailegebriel, B. Petros, and T. Endeshaw, "Evaluation of parasitological methods for the detection of *Strongyloides stercoralis* among individuals in selected health institutions In Addis Ababa, Ethiopia," *Ethiopian Journal of Health Sciences*, vol. 27, no. 5, pp. 515–522, 2017.

[47] M. H. Deng, L. Y. Zhong, O. Kamolnetr, Y. Limpanont, and Z. Y. Lv, "Detection of helminths by loop-mediated isothermal amplification assay: a review of updated technology and future outlook," *Infectious Diseases of Poverty*, vol. 8, no. 1, p. 20, 2019.

[48] P. R. Sahoo, K. Sethy, S. Mohapatra, and D. Panda, "Loop mediated isothermal amplification: an innovative gene amplification technique for animal diseases," *Veterinary World*, vol. 9, no. 5, pp. 465–469, 2016.

[49] S. Khurana and S. Sethi, "Laboratory diagnosis of soil transmitted helminthiasis," *Tropical Parasitology*, vol. 7, no. 2, pp. 86–91, 2017.

[50] M. Keikha, "LAMP method as one of the best candidates for replacing with PCR method," *Malaysian Journal of Medical Sciences*, vol. 25, no. 1, pp. 121–123, 2018.

Hindawi
Disease Markers
Volume 2020, Article ID 8074314, 8 pages
https://doi.org/10.1155/2020/8074314

Research Article

A *Trypanosoma cruzi* Genome Tandem Repetitive Satellite DNA Sequence as a Molecular Marker for a LAMP Assay for Diagnosing Chagas' Disease

Diego Ordóñez,[1] Pedro Fernández-Soto,[2] Ana M. Fernández-Martín,[2] Beatriz Crego-Vicente,[2] Begoña Febrer-Sendra,[2] Juan García-Bernalt Diego,[2] Belén Vicente,[2] Julio López-Abán,[2] Moncef Belhassen-García,[2] Antonio Muro,[2] and Manuel A. Patarroyo[3,4]

[1]*Animal Science Faculty, Universidad de Ciencias Aplicadas y Ambientales (U.D.C.A), 111166 Bogotá, Colombia*
[2]*Infectious and Tropical Diseases Research Group (e-INTRO), Biomedical Research Institute of Salamanca, Research Centre for Tropical Diseases at the University of Salamanca (IBSAL-CIETUS), Faculty of Pharmacy, University of Salamanca, 37007 Salamanca, Spain*
[3]*School of Medicine and Health Sciences, Universidad del Rosario, 112111 Bogotá, Colombia*
[4]*Fundación Instituto de Inmunología de Colombia (FIDIC), 111321 Bogotá, Colombia*

Correspondence should be addressed to Antonio Muro; ama@usal.es and Manuel A. Patarroyo; mapatarr.fidic@gmail.com

Received 5 December 2019; Accepted 17 January 2020; Published 24 February 2020

Guest Editor: Marcos Vinícius da Silva

Chagas' disease is a neglected tropical disease caused by *Trypanosoma cruzi* which is endemic throughout Latin America and is spread by worldwide migration. Diagnosis is currently limited to serological and molecular techniques having variations regarding their sensitivity and specificity. This work was aimed at developing a new sensitive, applicable, and cost-effective molecular diagnosis technique for loop-mediated isothermal amplification-based detection of *T. cruzi* (Tc-LAMP). The results led to determining a highly homologous satellite repeat region (231 bp) among parasite strains as a molecular marker for diagnosing the disease. Tc-LAMP was performed correctly for detecting parasite DNA (5 fg for the CL Brener strain and 50 fg for the DM28, TcVI, and TcI strains). Assay results proved negative for DNA from 16 helminth species and 7 protozoa, including *Leishmania* spp. Tc-LAMP based on the highly repeated *T. cruzi* satellite region is thus proposed as an important alternative for diagnosing *T. cruzi* infection, overcoming other methods' limitations such as their analytic capability, speed, and requiring specialized equipment or highly trained personnel. Tc-LAMP could be easily adapted for point-of-care testing in areas having limited resources.

1. Introduction

American trypanosomiasis, or Chagas' disease, is a zoonotic disease, usually consisting of chronic parasitic infection caused by the kinetoplastid protozoan *Trypanosoma cruzi*. The World Health Organization (WHO) recognizes Chagas' disease as one of the 20 neglected tropical diseases (NTD) [1] and one of the 13 most NTD worldwide [2]. Chagas' disease was considered a strictly rural disease for many decades; however, socioeconomic changes, rural exodus, deforestation, and urbanization have transformed the disease's epidemiological profile, making it an increasingly urban phenomenon and a major public health problem [3]. The disease can currently be found in 21 Latin American countries, and it has been estimated that at least 8 million people are infected worldwide. Migration has increased the disease's incidence, and it has been spread to other continents [2, 4].

Chagas' disease diagnosis depends on the phase in which a patient is found to be. Parasitemia is high during the acute phase and the congenital form, as well as in reactivations

caused by immunosuppression during the chronic phase. The parasite can be detected by microscopy in peripheral blood by thin or thick smear with Giemsa staining [5]. Sensitivity can be increased by concentration techniques such as microhematocrite concentration or Strout (double centrifugation) methods [6]. Techniques like hemoculture or xenodiagnosis have already been abandoned [7]. The parasite can sometimes be detected in cerebrospinal liquid [8]. Direct parasitological methods usually prove negative in 30%-60% of patients during the disease's chronic phase (having minimum parasitemia). Diagnosis is thus serological during this phase, based on detecting anti-*T. cruzi* IgG antibodies.

Conventional serological techniques (indirect immunofluorescence (IFI), indirect hemagglutination (IHA), and multienzyme assays (ELISA)) use the complete parasite or antigen mixtures as an antigen. However, less conventional serological assays use purified and/or recombinant antigens and synthetic peptides. Such techniques are more sensitive than direct observation methods but involve problems regarding poor specificity associated with antigen differences between recombinant proteins from different parasite lineages [9]. As no available serological test has 100% sensitivity and specificity, the WHO defines the diagnosis of the disease during its chronic phase by positivity in two serological tests carried out using different methods. A third test must be performed in case of discrepancy between the forgoing two results to confirm or discard infection [8]. Discrepancies are often due to crossed reactions with other trypanosomatids, including *Leishmania* spp.

Detecting *T. cruzi* DNA in peripheral blood by polymerase chain reaction (PCR) has become increasingly more used during the last few years, and the Special Program for Research and Training in Tropical Diseases (TDR-WHO) supported a comparative international study of PCR for detecting *T. cruzi* [10]. Kinetoplastid DNA, satellite DNA repeated sequences, and ribosomal RNA genes are the most used amplification targets [11]. PCR has proven useful during acute-phase or chronic-phase reactivations due to its greater sensitivity compared to microscopy methods [12].

PCR use during the chronic phase is debatable because it gives a positive result in 40%-70% of patients who have previously been diagnosed by conventional serological methods, depending on the degree of parasitemia, sample volume, DNA purification, PCR target region, the study population's characteristics, and the great genetic variability between the parasite's discrete typing units (DTUs). Furthermore, a negative result does not exclude infection [13].

PCR has also been used for following up treatment efficacy so that a positive result at the end of treatment would indicate therapeutic failure [14]. Real-time (quantitative) PCR (qPCR) has been developed enabling parasite DNA detection and quantification from clinical samples, although having very variable levels regarding analytical reliability, specificity, and sensitivity [15–18] thereby hampering its standardization for use in routine clinical matters. Such methods are impracticable in endemic areas lacking resources since they are techniques requiring sophisticated equipment and qualified personnel and are expensive, making them unfeasible for use in field conditions in endemic areas having scarce resources.

Other sensitive and specific molecular techniques, which are simpler, faster, and cheaper than PCR and its variants, must thus be used in diagnosing Chagas' disease, such as nucleic acid isothermal amplification, i.e., loop-mediated isothermal amplification (LAMP). Such technique has recently been revealed as an alternative having great potential for diagnosis in endemic areas [19–22]. Progress has been described in recent years regarding new LAMP methodologies for Chagas' disease diagnosis [19]. However, such laboratory tools are still being developed and larger amounts of reagents and materials are needed which could increase the value of diagnosis in communities living in endemic areas, mainly in the third world. This work has thus been aimed at developing a new sensitive, applicable, and cost-effective LAMP assay for the molecular detection of *T. cruzi*.

2. Methods

2.1. DNA from T. cruzi and Other Parasites. A DNeasy Blood & Tissue Kit (Qiagen, Hiden, Germany) was used for DNA extraction according to the manufacturer's instructions. The *T. cruzi* genomic DNA (gDNA) used in this study was obtained from CL Brener and Dm28 in vitro parasite strain culture maintained at the University of Granada's Biochemistry and Molecular Parasitology Department, Spain. A NanoDrop spectrophotometer (ND-1000) was used for measuring DNA from both strains which was subsequently diluted with ultrapure distilled water to final 0.5 ng/μL concentration. Serial 10-fold dilutions (1×10^{-1} to 1×10^{-9} ng/μL) from both *T. cruzi* DNA strains were then prepared and stored at -20°C until use. The prepared DNA was used as a positive control in all LAMP reactions for evaluating the molecular assays' analytical sensitivity and specificity.

Twenty-three DNA samples taken from several other parasites available in our laboratory were also evaluated for determining LAMP assay specificity, including trematodes (*Schistosoma mansoni*, *S. haematobium*, *Fasciola hepatica*, *Amphimerus* sp., *Dicrocoelium dendriticum*, and *Echinostoma caproni*), cestodes (*Hymenolepis diminuta*, *Echinococcus granulosus*, *Taenia saginata*, and *T. solium*), nematodes (*Anisakis simplex*, *Brugia pahangi*, *Loa*, *Mansonella perstans*, *Strongyloides venezuelensis*, and *Ascaris suum*), and protozoa (*Giardia intestinalis*, *Cryptosporidium parvum*, *Entamoeba histolytica*, *Plasmodium malariae*, *P. vivax*, *Leishmania infantum*, and *L. donovani*). All DNA sample concentrations were measured with a NanoDrop spectrophotometer (ND-1000) and then diluted with ultrapure water to a final 0.5 ng/μL concentration and kept at -20°C until use.

2.2. Designing LAMP Primers. The GenBank database (http://www.ncbi.nlm.nih.gov/) was searched for identifying possible sequences which could have been proven useful for detecting *T. cruzi* DNA. Once the sequences for starting the analysis had been located, they were saved in FASTA text-based format for handling and edition using BioEdit Sequence Alignment Editor v7.2.5 [23]. It was then ascertained whether the sequences were also available in the

Table 1: Main molecular targets for *Trypanosoma cruzi* DNA or RNA detection using PCR or RT-PCR. GenBank database accession numbers, the amplification method used (PCR for DNA or RT-PCR for RNA), base pair length, and references are indicated.

Molecular target	Accession number	PCR/RT-PCR	Base pairs	Reference
Nuclear satellite DNA	AY520036	PCR	195	[24]
Putative flagellar calcium-binding protein	Z54193	PCR	692	[25]
E13 repeated element	M74536	PCR	220	[26]
Kinetoplast minicircle variable region	AJ748042	PCR	330	[27]
24S ribosomal RNA alpha-subunit	L14468	RT-PCR	100	[28]
Ribosomal intergenic spacer	M63895	PCR	1174	[29]
Transposon-like E22 repeated element	X95485	PCR	863	[30]
Subtelomeric conserved junction	AF100651	PCR	822	[31]

Table 2: Similarity degree among TriTrypDB sequences.

Target	Identity	*E* value	Strain	Notes*
Nuclear satellite DNA	100%	$3e-96$	CL Brener/Tulahuen c12	Most abundant repetitive sequence in *T. cruzi* genome (up to 9%)
Putative flagellar calcium-binding protein	99%	0.0	CL Brener/JRc14/Tulahuen c12/Dm28c/Marinkellei	Sequence present in a single copy. Low sensitivity
E13 repeated element	97%	0.0	Tulahuen c12/CL Brener/Dm28c/Esmeraldo	Abundant repetitive sequence in *T. cruzi* genome (up to 7%)
Variable region of kinetoplast minicircles	100%	$6e-172$	CL Brener/Tulahuen c12/JRc14/Esmeraldo	Variable region with low specificity for LAMP primer design
24S ribosomal RNA alpha-subunit	97%	$2e-44$	JRc14/SylvioX10/Dm28c/ Tulahuen c12/Marinkellei/ CL Brener/Esmeraldo	Small size for LAMP design and very conserved in trypanosomatids
Ribosomal intergenic spacer	95%	$2e-107$	JRc14/SylvioX10/Dm28c/ Tulahuen c12/ Esmeraldo/Brener	Scarcely used for *T. cruzi* detection
Transposon-like E22 repeated element	98%	0.0	CL Brener/Tulahuen c12/Esmeraldo/Dm28c	Scarcely used for *T. cruzi* detection
Subtelomeric conserved junction	96%	0.0	Tulahuen c12/JRc14/ CL Brener/Esmeraldo/Dm28c	Scarcely used for *T. cruzi* detection

*Consult the bibliography shown in Table 1 for more details about sequences.

TriTrypDB database (http://tritrypdb.org/tritrypdb/) which stores the complete *T. cruzi* genome. The sequences were then compared using the basic local alignment search tool (BLAST; https://blast.ncbi.nlm.nih.gov/Blast.cgi) for ascertaining the degree of homology and/or difference from the other specific trypanosomatid sequences available in the database. The resulting sequence was used for designing specific primers for *T. cruzi* amplification using LAMP Designer software (http://www.premierbiosoft.com/isothermal/lamp.html). Thermo Fisher Scientific synthesized the selected primers.

2.3. LAMP Assay for T. cruzi. LAMP reaction mixtures (25.2 μL) each contained 40 pmol FIP and BIP primers, 5 pmol F3 and B3 primers, 5 pmol LB and LF primers, 2.5 mM dNTPs (Intron), 0.8 mM $MgSO_4$ (New England Biolabs, UK), 1 M betaine (Sigma, USA), 1x isothermal amplification buffer-20 mM Tris-HCl (pH 8.8), and 8 U Bst polymerase 2.0 WarmStart (New England Biolabs, UK) with 2 μL (1 ng) of template DNA.

LAMP reactions were performed in 0.5 mL microcentrifuge tubes incubated in a heating block (K Dry Bath) at 63°C-65°C for 30 min, 45 min, and 60 min to optimize the reaction; the temperature was then increased to 80°C for 5-10 min to deactivate the enzyme and stop the reaction. DNA contamination was prevented by using sterile tools at all times, each analysis step is performed in separate work areas, and reaction tube manipulation is minimized. Template DNA was replaced by ultrapure water as a negative control in each LAMP reaction. *T. cruzi* gDNA (10-fold serial dilutions as mentioned above) was also amplified for determining the LAMP assay's lower detection limit. LAMP assay specificity for only amplifying *T. cruzi* DNA was tested against 23 DNA samples from other parasites.

2.4. Detecting LAMP-T. cruzi Products. The LAMP amplification results were visualized by adding 2 μL of 1 : 10 diluted SYBR Green I fluorescent dye (Invitrogen, Carlsbad, California, USA) to the reaction tubes. Green fluorescence was

Table 3: Sequences and characteristics of the primers used.

Primer	Len	Tm	3′dG	GC rate (%)	Sequence (5′ to 3′)
F3	18	60.8	-1	50	AACTATCCGCTGCTTGGA
B3	18	60.2	-0.4	50	AAGAGCTCGCGAAATTCC
FIP (F1c-F2)	41				CCCACCATTCACAATCGGAAACCACTCGGCTGATCGTTTT
BIP (B1c-B2)	41				AGTCAGAGGCACTCTCTGTCAACCAAGCAGCGGATAGTTC
F2	19	60.3	-0.7	50	CACTCGGCTGATCGTTTT
F1c	20	65.1	0.1	55.6	CCCACCATTCACAATCGGAAAC
B2	18	65.1	-0.9	50	CCAAGCAGCGGATAGTTC
B1c	22	72.5	-0.9	50	AGTCAGAGGCACTCTCTGTCAA
LF	19	60.1	0.1	50	TTGGACCACAACGTGTGAT
LB	20	64.4	-0.4	50	TTCACACACTGGACACCAAA

observed in positive LAMP reactions whilst keeping its original orange in negative reactions. LAMP products (3-5 μL) were also monitored by electrophoresis in 1.5-2% agarose gel electrophoresis to corroborate colorimetric results. The gels were visualized under UV light and photographed using an ultraviolet Gel Documentation System (Uvitec, UK).

3. Results

3.1. Searching for and Selecting Molecular Targets for Designing LAMP Primers. Table 1 summarizes eight molecular targets found in literature and database analysis that have been traditionally used in PCR studies for *T. cruzi* DNA or RNA amplification.

The TriTrypDB database (http://tritrypdb.org) was used for a BLASTN local search and alignment analysis [32] to verify these target sequences in the *T. cruzi* genome; different degrees of homology were obtained when comparing them to different parasite strains (Table 2).

The satellite nuclear DNA 195 bp sequence [24] was selected as a target for LAMP primer design following in silico analysis of the selected sequences and studying their main characteristics using TriTrypDB. This small 195 bp sequence was included in a larger 938 bp one (Tcruzi_30851; TriTrypDB), identical for many strains and highly repeated (up to 9%) in the *T. cruzi* genome. Furthermore, PCR amplification of parasite DNA analytical sensitivity and specificity has been proven in a number of studies. This small 195 bp sequence was manually extended to 231 bp to guarantee producing LAMP primers regarding the minimum size supported by LAMP Designer software. A single set of six primers (F3, B3, FIP, BIP, LF, and LB) was produced. Table 3 shows the characteristics of the primers and nucleotide sequences.

3.2. Setting Up the LAMP Assay for T. cruzi: Tc-LAMP. The best amplification results and test reproducibility for CL Brener and Dm28 strains were obtained when the reaction mixtures were incubated at 65°C for 60 min. Color changes were clearly observed when adding SYBR Green I to the post-amplification tubes, as was a ladder-like pattern in agarose gel electrophoresis (Figure 1).

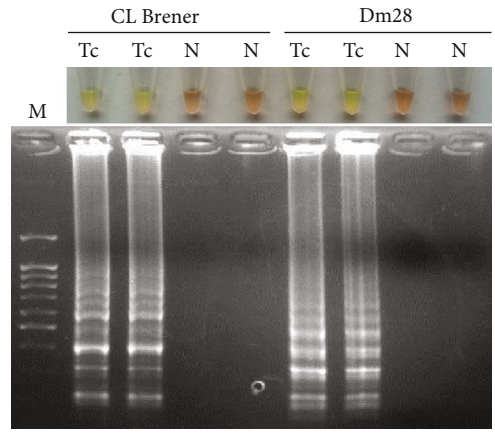

Figure 1: LAMP detection of *Trypanosoma cruzi* CL Brener and Dm28 strain DNA. Lanes Tc: *T. cruzi* DNA (0.5 ng/μL) from CL Brener and Dm28 strains; lanes N: negative controls (ultrapure water, no DNA). M: molecular weight marker (100 bp Plus Blue DNA Ladder).

The CL Brener strain DNA amplification detection limit was 5 fg when evaluating Tc-LAMP reaction's analytical sensitivity, whereas the Dm28 strain detection limit was 50 fg (Figure 2).

Tc-LAMP assay specificity was also tested using heterogeneous DNA samples as controls. Positive amplification was only observed using *T. cruzi* DNA (CL Brener or Dm28). DNA samples from other specimens tested were not amplified, thereby indicating that cross-reactions had not occurred. Colorimetric assay positive and negative results were clearly visualized and no ladders for bands were observed on agarose gels (Figure 3).

4. Discussion

Chagas' disease is an endemic protozoosis on the American continent, affecting its poorest communities, and has become a public health problem in many Latin American countries. Early diagnosis is essential for effective treatment to eliminate

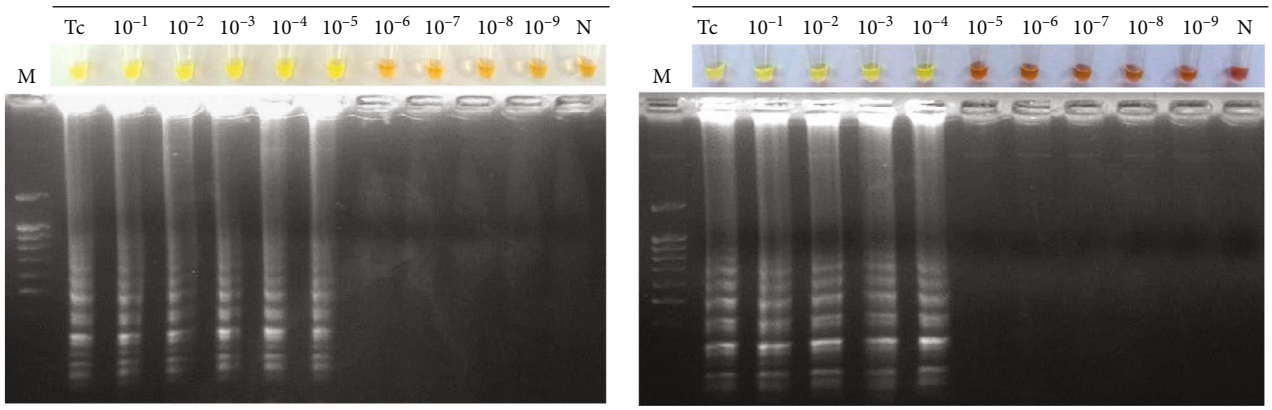

(a) CL Brener (b) Dm28

Figure 2: Assessment of Tc-LAMP analytical sensitivity for *Trypanosoma cruzi* using CL Brener and Dm28 strain gDNA serial dilutions. (a) Tc-LAMP sensitivity for the CL Brener strain. (b) Tc-LAMP sensitivity for the Dm28 strain. Lanes Tc: *T. cruzi* CL Brener and Dm28 strain gDNA (0.5 ng/μL); lanes 10^{-1}-10^{-9}: 10-fold serial dilutions; lanes M: molecular weight marker (100 bp Plus Blue DNA Ladder).

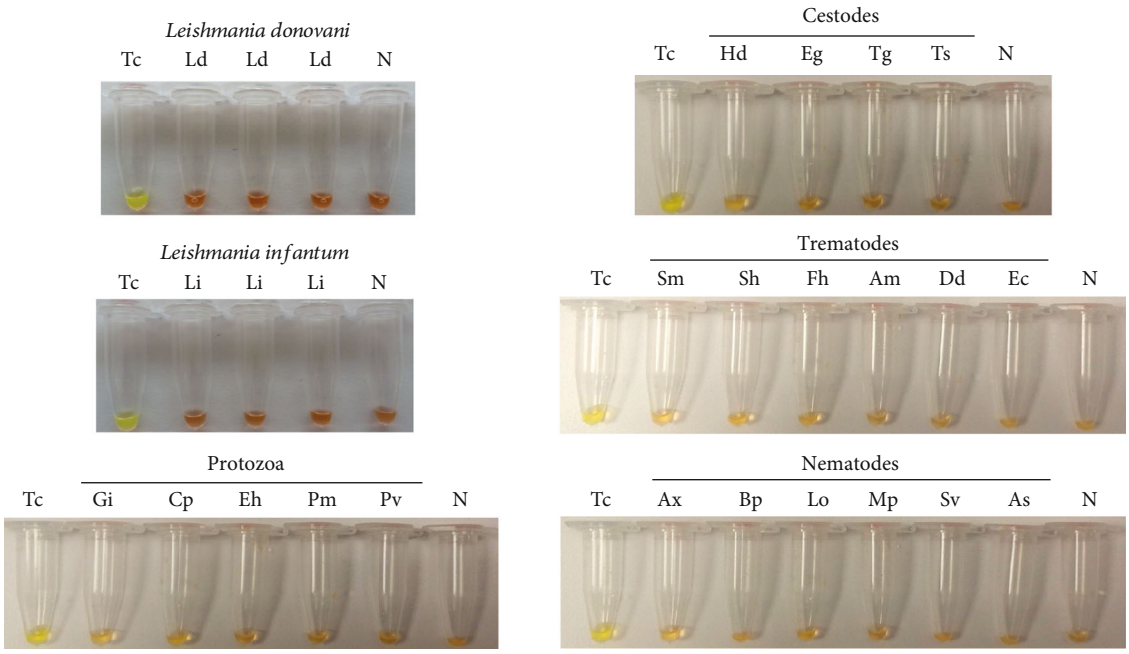

Figure 3: Tc-LAMP specificity: visual examination of LAMP products by adding SYBR Green I. Lanes Tc: *T. cruzi* CL Brener or Dm28 strain DNA (0.5 ng/μL); lanes N: negative controls (ultrapure water, no DNA). Trematode DNA in lanes Sm (*Schistosoma mansoni*), Sh (*S. haematobium*), Fh (*Fasciola hepatica*), Am (*Amphimerus* sp.), Dd (*Dicrocoelium dendriticum*), and Ec (*Echinostoma caproni*). Nematode DNA in lanes Ax (*Anisakis simplex*), Bp (*Brugia pahangi*), Lo (*Loa loa*), Mp (*Mansonella perstans*), Sv (*Strongyloides venezuelensis*), and As (*Ascaris suum*). Cestode DNA in lanes Hd (*Hymenolepis diminuta*), Eg (*Echinococcus granulosus*), Tg (*Taenia saginata*), and Ts (*T. solium*). Protozoan DNA in lanes Gi (*Giardia intestinalis*), Cp (*Cryptosporidium parvum*), Eh (*Entamoeba histolytica*), Pm (*Plasmodium malariae*), and Pv (*P. vivax*). Leishmania donovani DNA in lane Ld (*Leishmania donovani* in triplicate). Leishmania infantum DNA in lane Li (*Leishmania infantum* in triplicate).

the parasite. However, both direct parasitological and serological methods have problems regarding their sensitivity and specificity. Molecular methods represent an alternative to be used for amplifying *T. cruzi* DNA. This work has described a LAMP technology-based molecular method (Tc-LAMP) developed for detecting the parasite.

The available databases (i.e., TriTrypDB and GenBank) were used for selecting eight sequences from different *T. cruzi* genome regions for designing useful primers for the LAMP assay; these sequences had been previously used for detecting *T. cruzi* DNA and that of its variants by PCR [16, 26, 28]. A small 195 bp highly repeated (up to 9%) nuclear DNA sequence in the *T. cruzi* genome [24] was selected as the potential molecular target for amplification following in silico analysis. This sequence is identical for many strains and has 100% identity with the CL Brener and Tulahuen c12 strains. This sequence's drawback lies in its small size for primer design, since LAMP Designer software requires

a minimum 200-300 bp for proper operation. The genome sequence included in a greater 938 bp region was located in the *T. cruzi* genome to solve this problem. The selected sequence could thus be manually expanded to 231 bp, nearly the software's minimum size. The analysis gave a single set of 6 primers which included two loop primers. A repetitive nuclear DNA sequence amplifying a 231 bp fragment was selected from these in silico studies and used for developing the LAMP technique for *T. cruzi* DNA amplification.

The reaction conditions were established in line with the previous work by our group for detecting DNA from other parasites [33, 34]. CL Brener strain gDNA (a strain first used in sequencing the *T. cruzi* genome) [35] was amplified along with that from the Dm28 strain (a strain sequenced in 2014 and used in biochemical, immunological, gene expression, cell biology, and new drug development studies) [36]. Parasites involved in the domestic cycle belong to the CL Brener strain whilst circulating parasites in the sylvatic cycle belong to the Dm28 strain.

The Tc-LAMP detection limit was different for both strains tested: 5 fg for CL Brener and 50 fg for Dm28. Such differences regarding analytical sensitivity were probably due to variations among the DTUs distributed into six groups (TcI-TcVI) according to their molecular differences. There were also differences regarding the amount of their repetitive sequence content and genomic size, varying extensively among strains, even in the same DTU [37]. Thus, CL Brener strain genomic size (TcVI) was estimated to be 152.12 Mb, whilst Dm28 strain genomic size (TcI) was estimated to be 111.40 Mb. Satellite DNA was more abundant in the CL Brener strain (giving greater analytical sensitivity in our test) than in the Dm28 strain. The specificity studies involved a battery of available gDNA extracted from other parasites. The results were negative for the 16 helminth gDNA and the seven protozoan cDNA analyzed. It is worth highlighting the lack of gDNA detection in *Leishmania* species (*Leishmania donovani* and *Leishmania infantum*), although future studies would involve testing many more *Leishmania* species since coinfection with *T. cruzi* is a frequently occurring problem, especially in certain areas of the American continent. Moreover, trypanosomatid genomes share a high level of synteny [38, 39].

Only two LAMP assays were available for detecting *T. cruzi* gDNA when our LAMP assay was originally developed (both developed by the same research group) [40, 41]. A specific LAMP was developed for detecting *T. cruzi*, *T. congolense*, *T. evansi*, and *T. brucei gambiense* in one of the studies, using 5.8S rRNA gene internal transcribed spacer sequences (ITS2) for *T. brucei gambiense*, 18S rRNA gene ITS2 for *T. congolense* and *T. cruzi*, and the VSG RoTat1.2 surface glycoprotein for *T. evansi* [40]. The *T. cruzi* detection limit was 1 fg using Tulahuen strain DNA (TcVI human strain), such limit being greater than that detected in our assay. However, although specificity was evaluated in that study using gDNA from African trypanosomes and other protozoa, such as *Toxoplasma*, *Theileria*, and *Babesia*, specificity against *Leishmania* spp. species and *T. rangeli* mainly present on the American continent was not evaluated [42].

Significant advances in using LAMP for Chagas' disease diagnosis have currently been described [19]. However, more reagents and materials are needed for this which could thus increase the value of diagnosis for communities living in endemic areas, mainly in the third world.

5. Conclusion

Our study has described developing a specific LAMP method (Tc-LAMP) based on detecting a highly repeated and homologous satellite region among different strains for the sensitive and specific detection of *T. cruzi* DNA. The results led to proposing this marker/Tc-LAMP method as an accurate tool for Chagas' disease diagnosis, highlighting its advantages regarding speed, not needing specialized laboratory equipment or the need for highly trained personnel for running such tests.

Data Availability

The data used to support the findings of this study are available from the corresponding author upon request.

Conflicts of Interest

The authors declare that there is no conflict of interest regarding this publication.

Authors' Contributions

Diego Ordóñez and Pedro Fernández-Soto equally contributed as the first authors.

Acknowledgments

CL Brener and Dm28 DNA was kindly provided by Dr. Antonio Osuna (Universidad de Granada's Biochemistry and Molecular Parasitology Department, Granada, Spain). *Leishmania infantum* DNA was kindly provided by Dr. Pedro José Alcolea (Biological Research Center-CSIC, Madrid, Spain) and *L. donovani* DNA by Dr. Enrique Martínez (University Institute of Tropical Diseases, Tenerife, Canary Islands, Spain). We would also especially like to thank Jason Garry for translating and revising this manuscript. This work was funded by the Institute of Health Carlos III (ISCIII), Spain (http://www.isciii.es) (grants: RICET RD16/0027/0018 (AMA) and PI16/01784 (PFS)), cofunded by the European Union FEDER (Fondo Europeo de Desarrollo Regional) "Una manera de hacer Europa" programme, and also by the TCUE 2018–2020 Plan European Union and the Junta de Castilla y León. We would also like to acknowledge funding by the Universidad de Salamanca's Pre-PhD fellowship programme and cofinancing by the Banco Santander and Junta de Castilla y León Pre-PhD doctoral fellowship programme.

References

[1] A. Moncayo and A. C. Silveira, "Current epidemiological trends for Chagas disease in Latin America and future challenges in epidemiology, surveillance and health policy," *Memórias do Instituto Oswaldo Cruz*, vol. 104, Suppl 1, pp. 17–30, 2009.

[2] P. J. Hotez, E. Dumonteil, L. Woc-Colburn et al., "Chagas disease: "the new HIV/AIDS of the Americas"," *PLoS Neglected Tropical Diseases*, vol. 6, no. 5, 2012.

[3] K. M. Bonney, "Chagas disease in the 21st century: a public health success or an emerging threat?," *Parasite*, vol. 21, p. 11, 2014.

[4] J. Gascon, C. Bern, and M. J. Pinazo, "Chagas disease in Spain, the United States and other non-endemic countries," *Acta Tropica*, vol. 115, no. 1-2, pp. 22–27, 2010.

[5] M. Flores-Chávez, I. de Fuentes, T. Gárate, and C. Cañavate, "Laboratory diagnosis of imported Chagas' disease," *Enfermedades Infecciosas y Microbiología Clínica*, vol. 25, pp. 29–37, 2007.

[6] R. G. Strout, "A method for concentrating hemoflagellates," *The Journal of Parasitology*, vol. 48, no. 1, p. 100, 1962.

[7] C. Bern, S. Kjos, M. J. Yabsley, and S. P. Montgomery, "Trypanosoma cruzi and Chagas' disease in the United States," *Clinical Microbiology Reviews*, vol. 24, no. 4, pp. 655–681, 2011.

[8] WHO, *Control of Chagas disease: second report of the WHO expert committee*, World Health Organization, Geneva, 2002.

[9] M. Flores-Chávez, I. Cruz, M. Rodríguez et al., "Comparison of conventional and non-conventional serological tests for the diagnosis of imported Chagas disease in Spain," *Enfermedades Infecciosas y Microbiología Clínica*, vol. 28, no. 5, pp. 284–293, 2010.

[10] A. G. Schijman, "Molecular diagnosis of Trypanosoma cruzi," *Acta Tropica*, vol. 184, pp. 59–66, 2018.

[11] A. G. Schijman, M. Bisio, L. Orellana et al., "International study to evaluate PCR methods for detection of Trypanosoma cruzi DNA in blood samples from Chagas disease patients," *PLoS Neglected Tropical Diseases*, vol. 5, no. 1, 2011.

[12] M. L. Gomes, L. M. Galvao, A. M. Macedo, S. D. Pena, and E. Chiari, "Chagas' disease diagnosis: comparative analysis of parasitologic, molecular, and serologic methods," *The American Journal of Tropical Medicine and Hygiene*, vol. 60, no. 2, pp. 205–210, 1999.

[13] C. Barnabé, T. De Meeûs, F. Noireau et al., "_Trypanosoma cruzi_ discrete typing units (DTUs): Microsatellite loci and population genetics of DTUs TcV and TcI in Bolivia and Peru," *Infection, Genetics and Evolution*, vol. 11, no. 7, pp. 1752–1760, 2011.

[14] I. Molina, J. Gómez i Prat, F. Salvador et al., "Randomized trial of posaconazole and benznidazole for chronic Chagas' disease," *The New England Journal of Medicine*, vol. 370, no. 20, pp. 1899–1908, 2014.

[15] T. Duffy, M. Bisio, J. Altcheh et al., "Accurate real-time PCR strategy for monitoring bloodstream parasitic loads in Chagas disease patients," *PLoS Neglected Tropical Diseases*, vol. 3, no. 4, 2009.

[16] M. Piron, R. Fisa, N. Casamitjana et al., "Development of a real-time PCR assay for *Trypanosoma cruzi* detection in blood samples," *Acta Tropica*, vol. 103, no. 3, pp. 195–200, 2007.

[17] Y. Qvarnstrom, A. G. Schijman, V. Veron, C. Aznar, F. Steurer, and A. J. da Silva, "Sensitive and specific detection of Trypanosoma cruzi DNA in clinical specimens using a multi-target real-time PCR approach," *PLoS Neglected Tropical Diseases*, vol. 6, no. 7, 2012.

[18] H. M. Valadares, J. R. Pimenta, J. M. de Freitas et al., "Genetic profiling of Trypanosoma cruzi directly in infected tissues using nested PCR of polymorphic microsatellites," *International Journal for Parasitology*, vol. 38, no. 7, pp. 839–850, 2008.

[19] S. A. Besuschio, M. Llano Murcia, A. F. Benatar et al., "Analytical sensitivity and specificity of a loop-mediated isothermal amplification (LAMP) kit prototype for detection of Trypanosoma cruzi DNA in human blood samples," *PLoS Neglected Tropical Diseases*, vol. 11, no. 7, 2017.

[20] M. Parida, S. Sannarangaiah, P. K. Dash, P. V. Rao, and K. Morita, "Loop mediated isothermal amplification (LAMP): a new generation of innovative gene amplification technique; perspectives in clinical diagnosis of infectious diseases," *Reviews in Medical Virology*, vol. 18, no. 6, pp. 407–421, 2008.

[21] D. H. Paris, M. Imwong, A. M. Faiz et al., "Loop-mediated isothermal PCR (LAMP) for the diagnosis of falciparum malaria," *The American Journal of Tropical Medicine and Hygiene*, vol. 77, no. 5, pp. 972–976, 2007.

[22] Y. P. Wong, S. Othman, Y. L. Lau, S. Radu, and H. Y. Chee, "Loop-mediated isothermal amplification (LAMP): a versatile technique for detection of micro-organisms," *Journal of Applied Microbiology*, vol. 124, no. 3, pp. 626–643, 2018.

[23] T. Hall, "BioEdit: a user-friendly biological sequence alignment editor and analysis program for windows 95/98/NT," *Nucleic Acids Symposium Series*, vol. 41, pp. 95–98, 1999.

[24] A. Gonzalez, E. Prediger, M. E. Huecas, N. Nogueira, and P. M. Lizardi, "Minichromosomal repetitive DNA in Trypanosoma cruzi: its use in a high-sensitivity parasite detection assay," *Proceedings of the National Academy of Sciences of the United States of America*, vol. 81, no. 11, pp. 3356–3360, 1984.

[25] A. M. Silber, J. Bua, B. M. Porcel, E. L. Segura, and A. M. Ruiz, "Trypanosoma cruzi: specific detection of parasites by PCR in infected humans and vectors using a set of primers (BP1/BP2) targeted to a nuclear DNA sequence," *Experimental Parasitology*, vol. 85, no. 3, pp. 225–232, 1997.

[26] J. M. Requena, A. Jimenez-Ruiz, M. Soto, M. C. Lopez, and C. Alonso, "Characterization of a highly repeated interspersed DNA sequence of Trypanosoma cruzi: its potential use in diagnosis and strain classification," *Molecular and Biochemical Parasitology*, vol. 51, no. 2, pp. 271–280, 1992.

[27] P. Wincker, C. Britto, J. B. Pereira, M. A. Cardoso, W. Oelemann, and C. M. Morel, "Use of a simplified polymerase chain reaction procedure to detect Trypanosoma cruzi in blood samples from chronic chagasic patients in a rural endemic area," *The American Journal of Tropical Medicine and Hygiene*, vol. 51, no. 6, pp. 771–777, 1994.

[28] R. P. Souto and B. Zingales, "Sensitive detection and strain classification of Trypanosoma cruzi by amplification of a ribosomal RNA sequence," *Molecular and Biochemical Parasitology*, vol. 62, no. 1, pp. 45–52, 1993.

[29] E. M. Novak, M. P. de Mello, H. B. Gomes et al., "Repetitive sequences in the ribosomal intergenic spacer of Trypanosoma cruzi," *Molecular and Biochemical Parasitology*, vol. 60, no. 2, pp. 273–280, 1993.

[30] J. Araya, M. I. Cano, H. B. M. Gomes et al., "Characterization of an interspersed repetitive DNA element in the genome

ofTrypanosoma cruzi," *Parasitology*, vol. 115, no. 6, pp. 563–570, 1997.

[31] M. A. Chiurillo, I. Cano, J. F. Da Silveira, and J. L. Ramirez, "Organization of telomeric and sub-telomeric regions of chromosomes from the protozoan parasite Trypanosoma cruzi," *Molecular and Biochemical Parasitology*, vol. 100, no. 2, pp. 173–183, 1999.

[32] S. F. Altschul, W. Gish, W. Miller, E. W. Myers, and D. J. Lipman, "Basic local alignment search tool," *Journal of Molecular Biology*, vol. 215, no. 3, pp. 403–410, 1990.

[33] P. Fernández-Soto, J. G. Arahuetes, A. S. Hernández, J. L. Abán, B. V. Santiago, and A. Muro, "A loop-mediated isothermal amplification (LAMP) assay for early detection of Schistosoma mansoni in stool samples: a diagnostic approach in a murine model," *PLoS Neglected Tropical Diseases*, vol. 8, no. 9, 2014.

[34] J. Gandasegui, P. Fernández-Soto, C. Carranza-Rodríguez et al., "The rapid-heat LAMPellet method: a potential diagnostic method for human urogenital schistosomiasis," *PLoS Neglected Tropical Diseases*, vol. 9, no. 7, 2015.

[35] N. M. El-Sayed, P. J. Myler, D. C. Bartholomeu et al., "The genome sequence of Trypanosoma cruzi, etiologic agent of Chagas disease," *Science*, vol. 309, no. 5733, pp. 409–415, 2005.

[36] E. C. Grisard, S. M. R. Teixeira, L. G. P. de Almeida et al., "Trypanosoma cruzi clone Dm28c draft genome sequence," *Genome Announcements*, vol. 2, no. 1, 2014.

[37] R. T. Souza, F. M. Lima, R. M. Barros et al., "Genome size, karyotype polymorphism and chromosomal evolution in Trypanosoma cruzi," *PLoS One*, vol. 6, no. 8, 2011.

[38] E. Ghedin, F. Bringaud, J. Peterson et al., "Gene synteny and evolution of genome architecture in trypanosomatids," *Molecular and Biochemical Parasitology*, vol. 134, no. 2, pp. 183–191, 2004.

[39] L. L. Naves, M. V. da Silva, E. F. Fajardo et al., "DNA content analysis allows discrimination between Trypanosoma cruzi and Trypanosoma rangeli," *PLoS One*, vol. 12, no. 12, 2017.

[40] O. M. Thekisoe, N. Kuboki, A. Nambota et al., "Species-specific loop-mediated isothermal amplification (LAMP) for diagnosis of trypanosomosis," *Acta Tropica*, vol. 102, no. 3, pp. 182–189, 2007.

[41] O. M. Thekisoe, C. V. Rodriguez, F. Rivas et al., "Detection of Trypanosoma cruzi and T. rangeli infections from Rhodnius pallescens bugs by loop-mediated isothermal amplification (LAMP)," *The American Journal of Tropical Medicine and Hygiene*, vol. 82, no. 5, pp. 855–860, 2010.

[42] K. A. M. Ferreira, E. F. Fajardo, R. P. Baptista et al., "Species-specific markers for the differential diagnosis of Trypanosoma cruzi and Trypanosoma rangeli and polymorphisms detection in Trypanosoma rangeli," *Parasitology Research*, vol. 113, no. 6, pp. 2199–2207, 2014.

Hindawi
Disease Markers
Volume 2020, Article ID 1075942, 7 pages
https://doi.org/10.1155/2020/1075942

Research Article

The Accuracy of Single MicroRNAs in Peripheral Blood to Diagnose Ovarian Cancer: An Updated Meta-Analysis

Yubao Cui, Shanchao Hong, and Xuming Zhu

Department of Clinical Laboratory, Wuxi People's Hospital Affiliated to Nanjing Medical University, Wuxi, Jiangsu Province, China

Correspondence should be addressed to Xuming Zhu; 7091159@qq.com

Received 2 November 2019; Revised 9 December 2019; Accepted 23 December 2019; Published 14 January 2020

Academic Editor: Timo Sorsa

Background. Ovarian cancer is the 5th leading cause of death of women due to cancer in the United States. Although carbohydrate antigen 125 has a moderate diagnostic utility, the phenomenon of false-positive exists. As novel effective biomarkers, some single microRNAs (miRNAs) have diagnostic values for ovarian cancer, but the results lack consistency. In order to precisely and comprehensively assess the diagnostic value of single miRNAs for ovarian cancer, a meta-analysis is performed. *Methods*. Articles concerning the diagnostic value of single miRNAs for ovarian cancer were searched from databases. The pooled sensitivity (SEN), specificity (SPE), positive likelihood ratio (PLR), negative likelihood ratio (NLR), and diagnostic odds ratio (DOR) with the corresponding 95% confidence interval (CI) were calculated. Area under curve (AUC) of the summary receiver-operating characteristic (SROC) curve was also calculated. *Results*. In total, 22 studies including 8 kinds of single miRNAs were enrolled in this paper (6 studies for miR-200c, 3 studies for miR-200a and miR-200b, and 2 studies for miR-205, miR-145, miR-141, miR-429, and miR-125b). For miR-200c, the pooled SEN and SPE were, respectively, 0.768 (95% CI: 0.722-0.811) and 0.680 (95% CI: 0.624-0.732); the pooled PLR and NLR were, respectively, 2.897 (95% CI: 1.787-4.698) and 0.340 (95% CI: 0.276-0.417); the pooled DOR was 8.917 (95% CI: 4.521-17.587); and AUC of SROC curve was 0.815. For miR-200a, the pooled SEN and SPE were, respectively, 0.759 (95% CI: 0.670-0.833) and 0.717 (95% CI: 0.627-0.795); the pooled PLR and NLR were, respectively, 3.129 (95% CI: 0.997-9.816) and 0.301 (95% CI: 0.207-0.437); the pooled DOR was 11.323 (95% CI: 3.493-36.711); and AUC of SROC curve was 0.857. For miR-200b, the pooled SEN and SPE were, respectively, 0.853 (95% CI: 0.776-0.912) and 0.775 (95% CI: 0.690-0.846); the pooled PLR and NLR were, respectively, 4.327 (95% CI: 0.683-27.415) and 0.225 (95% CI: 0.081-0.625); the pooled DOR was 19.678 (95% CI: 2.812-137.72); and AUC of SROC curve was 0.90. For miR-205, miR-145, miR-141, miR-429, and miR-125b, each diagnostic value should be interpreted cautiously because only two studies were included. *Conclusions*. miR-200c, miR-200a, and miR-200b can be useful diagnostic biomarkers for ovarian cancer. More related studies are needed for miR-205, miR-145, miR-141, miR-429, and miR-125b.

1. Introduction

Ovarian cancer is the 5th leading cause of death of women due to cancer in the United States [1]. Ovarian cancer is often at an advanced stage by the time of diagnosis and has metastasized throughout the peritoneal cavity [2]. The overall 5-year survival rate of this fatal disease is only 45.6% [3]. A widely used biomarker to diagnose ovarian cancer is carbohydrate antigen 125 (CA125). With the sensitivity and specificity of, respectively, 0.78 and 0.84 [4], CA125 has a moderate diagnostic utility. However, elevated serum CA125 levels may be observed in other physiological or pathological conditions (menstruation, pregnancy, endometriosis, and inflammatory diseases of the peritoneum) [5], resulting in false-positive. Therefore, it is necessary to find novel effective biomarkers to diagnose ovarian cancer.

MicroRNAs (miRNAs), a family of small noncoding RNAs (19 ± 22 nucleotides), have shown great promise as biomarkers for cancer due to their stability and relative easiness to accurately measure [6]. Recently, some articles have reported that some single miRNAs have diagnostic values for ovarian cancer [7–17], but the results lack consistency. Take miR-429 as an example, Márton et al. demonstrated that the sensitivity and specificity to diagnose ovarian cancer

were, respectively, 0.857 and 0.683 [9], while Meng et al. found that the sensitivity and specificity were, respectively, 0.594 and 0.955 [14]. In order to precisely and comprehensively assess the diagnostic value of single miRNAs for ovarian cancer, this meta-analysis is performed.

2. Material and Methods

This meta-analysis was conducted according to the guidelines of the PRISMA statement (Table S1) [18].

2.1. Search Strategy. We systematically searched articles published prior to September 23, 2019 in the databases of PubMed, Embase, and Web of Knowledge. Search terms were as follows: ("microRNA" or "miRNA" or "miR") and ("ovarian cancer" or "ovarian carcinoma" or "ovarian neoplasm" or "ovarian cancers" or "ovarian carcinomas" or "ovarian neoplasms" or "cancer of ovary" or "carcinoma of ovary" or "neoplasm of ovary" or "cancers of ovary" or "carcinomas of ovary" or "neoplasms of ovary") and ("diagnosis" or "sensitivity" or "specificity" or "diagnosis" or "plasma" or "serum" or "blood" or "circulating"). After relevant articles were identified, we examined their cited references to select other relevant articles. Two reviewers independently searched the articles. Any disagreements between the two reviewers were resolved by a third author.

2.2. Selection Criteria. Inclusion criteria were as follows: (1) articles were designed to evaluate the accuracy of single miRNAs for diagnosing ovarian cancer; (2) 2×2 contingency tables could be directly extracted or calculated from the articles; (3) at least two studies concerning the same single miRNA; and (4) articles were written in English.

Exclusion criteria were as follows: (1) reviews, meta-analyses, letters, or expert opinions; (2) combined panels of different single miRNAs; and (3) overlapped publication article.

2.3. Data Extraction. The following data were extracted: first author, year of publication, country of participants, source of control group, sample size, single miRNAs as biomarker, miRNAs as control for normalization, relative expression in the case group compared to the control group, diagnostic sensitivity (SEN) and specificity (SPE) values, and the values of true positive (TP), false positive (FP), false negative (FN), and true negative (TN).

2.4. Quality Assessment. To assess the quality of each included study, we used the quality assessment of diagnostic accuracy studies-2 (QUADAS-2) tool [19]. QUADAS-2 comprises four key domains, including patient selection, index test, reference standard, and the timing of the index and reference tests (flow and timing). These four domains were used to evaluate the risk of bias, and the first three domains were applied to assess applicability concerns. Two reviewers independently assessed the quality. Any disagreements between the two reviewers were resolved by a third author.

2.5. Statistical Analysis. The pooled sensitivity (SEN), specificity (SPE), positive likelihood ratio (PLR), negative likelihood ratio (NLR), diagnostic odds ratio (DOR), and their corresponding 95% confidence interval (CI) were calculated. Area under curve (AUC) of the summary receiver-operating characteristic curve (SROC) was also calculated. A Cochrane-Q test of heterogeneity was performed using the inconsistency index. The value of $I^2 > 50\%$ and P value < 0.05 indicated the existence of significant heterogeneity among studies. If heterogeneity was detected, the random effects model was used; otherwise, the fixed effects model was used. Deeks' funnel plot asymmetry analysis was performed to identify publication bias. Sensitivity analysis was conducted to assess the stability of our analysis. Statistical analyses were undertaken using Stata software version 12.0 (College Station, TX, USA), Meta-DiSc XI for Windows (Cochrane Colloquium, Barcelona, Spain), and RevMan 5.3 (Cochrane Collaboration, Oxford, UK).

3. Results

3.1. Literature Search and Study Characteristics. A total of 862 articles were identified through database searching. After removing duplicates, the titles and abstracts for 538 records were screened for eligibility. Of these, 36 records were identified and full-text articles were retrieved. 25 manuscripts were then excluded through assessment of the full-text articles, and 11 remaining articles encompassing 22 studies were included in the meta-analysis (Figure 1).

These 22 studies included 2667 participants (1485 ovarian cancer patients and 1182 controls). Their characteristics and the numbers of TP, FP, FN, and TN are listed in Table 1. There were 8 kinds of single miRNAs enrolled in this paper (miR-200a, miR-200b, miR-200c, miR-205, miR-145, miR-141, miR-429, and miR-125b). The study number of miR-200c was six, the number of miR-200a and miR-200b were both two, and the number of miR-205, miR-145, miR-141, miR-429, and miR-125b were all two. Countries of participants included China, Korea, Hungary, India, Germany, and Australia. The specimen of all studies came from serum (including serum exosome) or plasma. Three studies regarded patients with benign disease as control groups, and the other 18 studies regarded healthy people as control groups. Except for one study, relative expressions of miRNAs in the case group were higher than those in the control group.

3.2. Methodological Quality Assessment. Quality assessment of included studies was conducted using the QUADAS-2 tool. For miR-200c (Figure 2), high risk and unclear situation existed in patient selection and index test. For miR-200a, miR-200b, miR-205, miR-145, miR-141, miR-429, and miR-125b (Figures S1–S7), the majority of included studies satisfied most domains of QUADAS-2. The high risk and unclear situation existed in the domains of patient selection and index test due to variances in the control group, specimen, and miRNAs as control for normalization.

3.3. Diagnostic Values. For miR-200c, the pooled SEN and SPE were, respectively, 0.768 (95% CI: 0.722-0.811) and 0.680 (95% CI: 0.624-0.732) (Figure 3). I^2 for SEN was 16.3% ($P = 0.308$), showing no significant heterogeneity

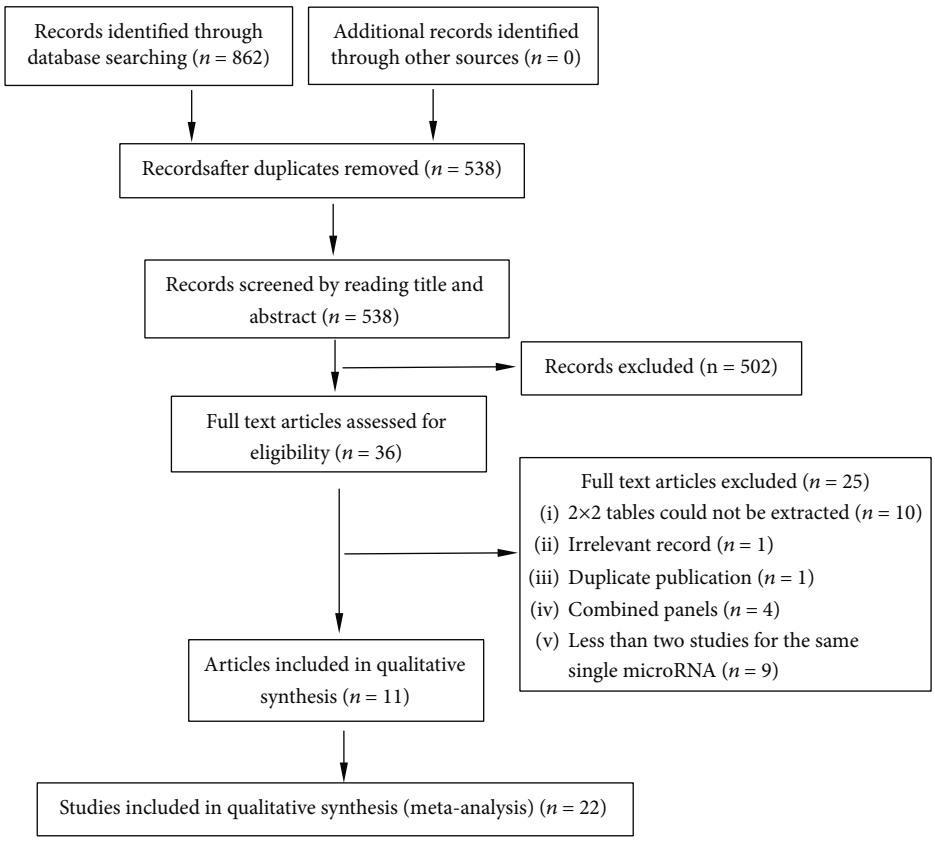

Figure 1: Flow diagram of study selection.

among studies. The pooled PLR and NLR were, respectively, 2.897 (95% CI: 1.787-4.698) and 0.340 (95% CI: 0.276-0.417) (Figure 3). The pooled DOR was 8.917 (95% CI: 4.521-17.587). AUC of SROC curve was 0.815.

For miR-200a (Table 2), the pooled SEN and SPE were, respectively, 0.759 (95% CI: 0.670-0.833) and 0.717 (95% CI: 0.627 - 0.795). I^2 for SEN was 66.1% ($P = 0.052$), showing significant heterogeneity among studies. The pooled PLR and NLR were, respectively, 3.129 (95% CI: 0.997-9.816) and 0.301 (95% CI: 0.207-0.437). The pooled DOR was 11.323 (95% CI: 3.493-36.711). AUC of SROC curve was 0.857.

For miR-200b (Table 2), the pooled SEN and SPE were, respectively, 0.853 (95% CI: 0.776-0.912) and 0.775 (95% CI: 0.690-0.846). I^2 for SEN was 78.1% ($P = 0.01$), showing significant heterogeneity among studies. The pooled PLR and NLR were, respectively, 4.327 (95% CI: 0.683-27.415) and 0.225 (95% CI: 0.081-0.625). The pooled DOR was 19.678 (95% CI: 2.812-137.72). AUC of SROC curve was 0.90.

Among miR-205, miR-145, miR-141, miR-429, and miR-125b, miR-145 had the highest diagnostic value (pooled SEN and SPE of, respectively, 0.958 and 0.933; pooled PLR and NLR of, respectively, 11.711 and 0.043; and pooled DOR of 278.62). For these 5 miRNAs, the AUC of SROC curve could not be obtained due to only two studies included (Table 2).

3.4. Publication Bias. As shown in Deeks' funnel plot (Figure 4), the plot of miR-200c had a symmetrical funnel shape, revealing that publication bias was not absent. Furthermore, the P value for Deeks' funnel plot asymmetry test was 0.24, indicating a lack of publication bias in this meta-analysis.

For miR-200a, miR-200b, miR-205, miR-145, miR-141, miR-429, and miR-125b, publication bias could not be assessed due to the small number of studies included.

3.5. Sensitivity Analysis. Sensitivity analysis was performed by eliminating studies one by one (Table S2). For miR-200c, the pooled SEN and corresponding heterogeneities were not dominant and a study by Márton et al. [9] may be the source of heterogeneities. For miR-200a, miR-200b, miR-205, miR-145, miR-141, miR-429, and miR-125b, sensitivity analysis could not be performed due to the small number of studies included.

4. Discussion

Mir-200c, a member of the miR-200 family, is an illustrious tumor suppressor and one of the highly studied miRNAs in terms of cancer development, proliferation, therapy resistance, and metastasis [20]. In our paper, the pooled SEN and SPE of miR-200c were, respectively, 0.768 and 0.680, presenting a similar diagnostic ability with CA125. The pooled PRL of 2.897 indicated that the probability to be ovarian cancer was 2.897-fold increased with a positive miRNA result. Conversely, the pooled NRL of 0.34 showed that the probability could decrease 66% when the miRNA result was negative. With the DOR value of 8.917 and an AUC of SROC

Table 1: Characteristics of included studies.

Author	Year	Country	Specimen	Control group	miRNA as biomarker	Case size	Control size	miRNA as control	Relative expression*	SEN	SPE	TP	FP	FN	TN
Wang et al. [7]	2019	China	Serum	HP	miR-200c	110	116	miR-103	High	0.809	0.517	89	56	21	60
Wang et al. [7]	2019	China	Serum	HP	miR-205	110	116	miR-103	High	0.764	0.526	84	55	26	61
Kim et al. [8]	2019	Korea	Serum exosome	PBOD	miR-200c	48	20	RNU48	High	0.729	0.9	35	2	13	18
Kim et al. [8]	2019	Korea	Serum exosome	PBOD	miR-145	48	20	RNU48	High	0.917	0.868	44	3	4	17
Márton et al. [9]	2019	Hungary	Plasma	HP	miR-200a	28	60	miR-103	High	0.857	0.783	24	13	4	47
Márton et al. [9]	2019	Hungary	Plasma	HP	miR-200b	28	60	miR-103	High	0.679	0.9	19	6	9	54
Márton et al. [9]	2019	Hungary	Plasma	HP	miR-200c	28	60	miR-103	High	0.714	0.867	20	8	8	52
Márton et al. [9]	2019	Hungary	Plasma	HP	miR-141	28	60	miR-103	High	0.857	0.9	24	6	4	54
Márton et al. [9]	2019	Hungary	Plasma	HP	miR-429	28	60	miR-103	High	0.857	0.683	24	19	4	41
Zuberi et al. [10]	2019	India	Serum	HP	miR-145	70	70	RNU6B	Low	0.991	0.957	69	3	1	67
Meng et al. [11]	2016	Germany	Serum	HP	miR-200a	60	32	miR-484	High	0.672	0.9	40	3	20	29
Meng et al. [11]	2016	Germany	Serum	HP	miR-200b	60	32	miR-484	High	0.931	0.9	56	3	4	29
Meng et al. [11]	2016	Germany	Serum	HP	miR-200c	60	32	miR-484	High	0.845	0.85	51	5	9	27
Zhu et al. [12]	2017	China	Serum	PBOD	miR-125b	135	54	miR-16	High	0.756	0.685	102	17	33	37
Zuberi et al. [13]	2016	India	Serum	HP	miR-125b	70	70	RNU6	High	0.623	0.771	44	16	26	54
Meng et al. [14]	2015	Germany	Serum	HP	miR-429	180	66	miR-484	High	0.594	0.955	107	3	73	63
Gao and Wu [15]	2015	China	Serum	HP	miR-141	93	50		High	0.69	0.72	64	14	29	36
Gao and Wu [15]	2015	China	Serum	HP	miR-200c	93	50		High	0.72	0.7	67	15	26	35
Zheng et al. [16]	2013	China	Plasma	HP	miR-205	134	70		High	0.301	0.942	40	4	94	66
Kan et al. [17]	2012	Australia	Serum	HP	miR-200a	28	28	miR-103	High	0.857	0.357	24	18	4	10
Kan et al. [17]	2012	Australia	Serum	HP	miR-200b	28	28	miR-103	High	0.857	0.357	24	18	4	10
Kan et al. [17]	2012	Australia	Serum	HP	miR-200c	28	28	miR-103	High	0.714	0.571	20	12	8	16

Abbreviation: HP—healthy people; PBOD—patients with benign ovarian disease; SEN—sensitivity; SPE—specificity; TP—true positive; FP—false positive; FN—false negative; TN—true negative. *Relative expression for microRNA as a biomarker of the case group compared to the control group.

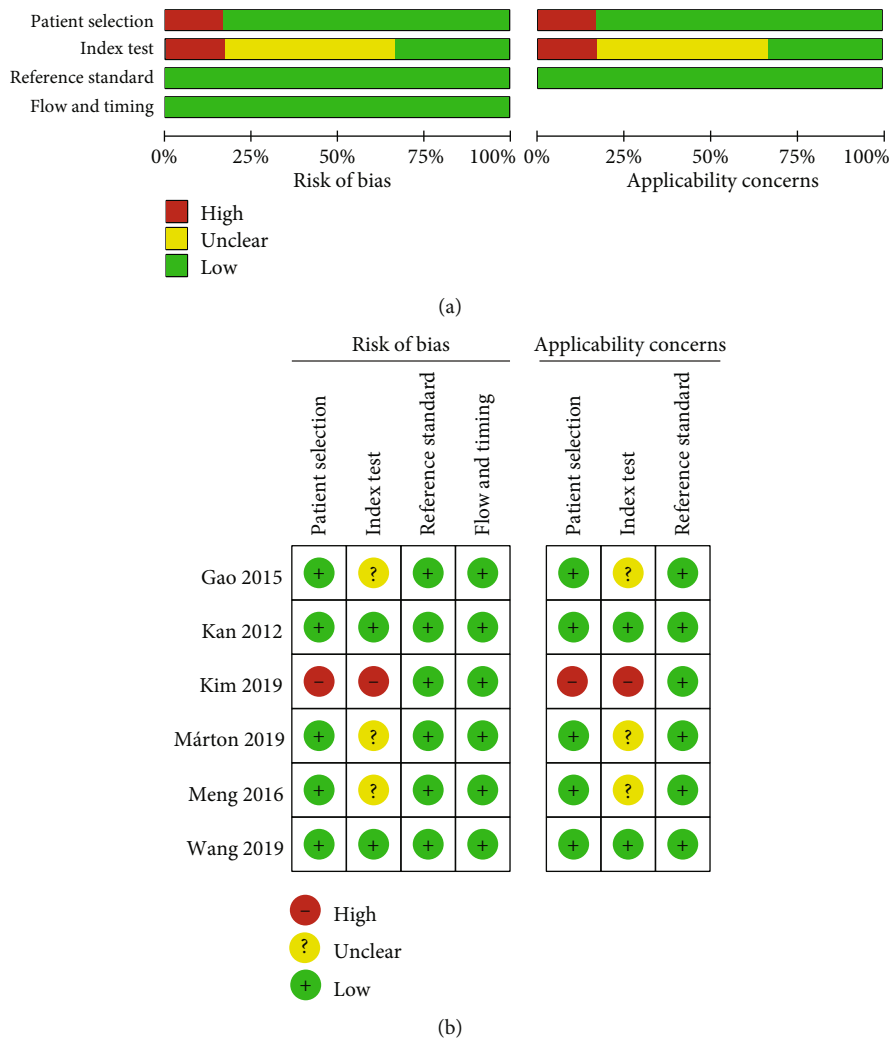

Figure 2: Quality assessment of miR-200c according to QUADAS-2 guidelines: (a) graph and (b) summary.

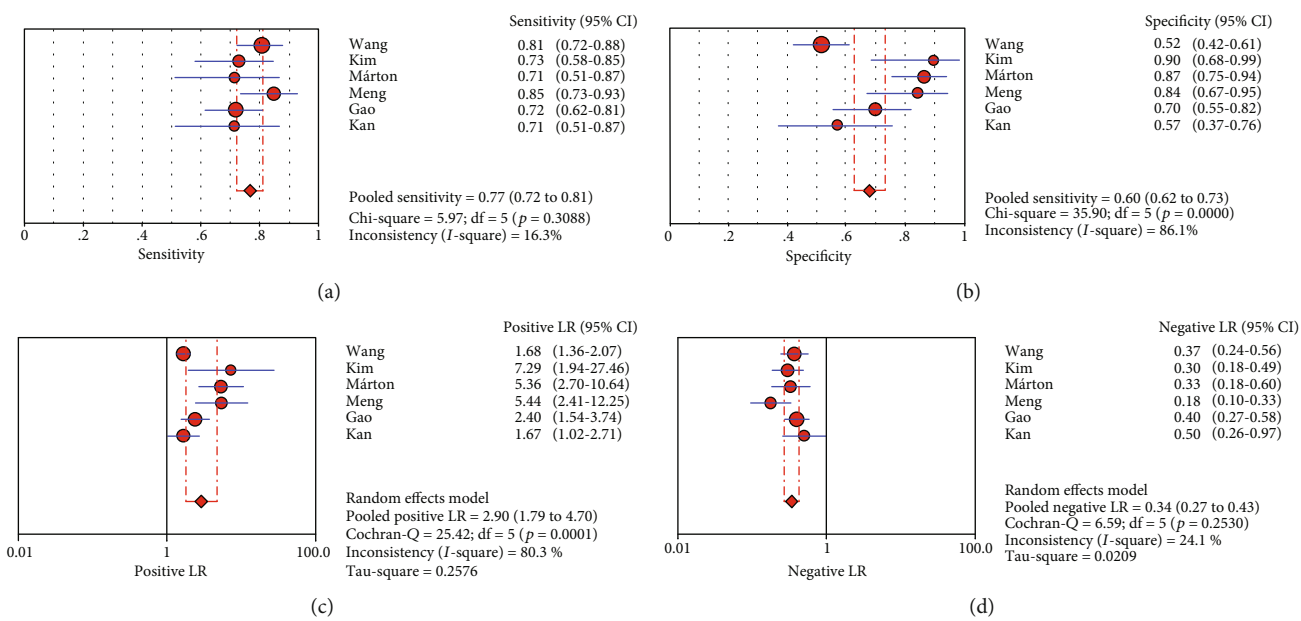

Figure 3: Forest plots of miR-200c: (a) sensitivity, (b) specificity, (c) positive likelihood ratio, and (d) negative likelihood ratio.

Table 2: Diagnostic values of miRNAs for ovarian cancer.

MicroRNA	*n*	SEN (95% CI)	SPE (95% CI)	PLR (95% CI)	NLR (95% CI)	DOR (95% CI)	AUC
miR-200a	3	0.759 (0.670-0.833)	0.717 (0.627-0.795)	3.129 (0.997-9.816)	0.301 (0.207-0.437)	11.323 (3.493-36.711)	0.857
miR-200b	3	0.853 (0.776-0.912)	0.775 (0.690-0.846)	4.327 (0.683-27.415)	0.225 (0.081-0.625)	19.678 (2.812-137.72)	0.90
miR-200c	6	0.768 (0.722-0.811)	0.680 (0.624-0.732)	2.897 (1.787-4.698)	0.340 (0.276-0.417)	8.917 (4.521-17.587)	0.815
miR-205	2	0.508 (0.444-0.573)	0.683 (0.611-0.749)	2.675 (0.740-9.672)	0.590 (0.310-1.122)	4.359 (2.716-6.996)	
miR-145	2	0.958 (0.904-0.986)	0.933 (0.861-0.975)	11.711 (3.108-44.130)	0.043 (0.004-0.461)	278.62 (11.704-6632.9)	
miR-141	2	0.727 (0.639-0.804)	0818 (0.733-0.885)	4.411 (1.298-14.988)	0.281 (0.093-0.856)	16.279 (1.797-147.47)	
miR-429	2	0.630 (0.560-0.696)	0.825 (0.748-0.887)	5.700 (0.618-52.568)	0.331 (0.148-0.736)	21.999 (9.595-50.438)	
miR-125b	2	0.712 (0.645-0.773)	0.734 (0.647-0.809)	2.539 (1.870-3.447)	0.420 (0.331-0.533)	6.219 (3.819-10.127)	

Abbreviation: SEN—sensitivity; SPE—specificity; PLR—positive likelihood ratio; NLR—negative likelihood ratio; DOR—diagnostic odds ratio; AUC—area under curve; CI—confidence interval.

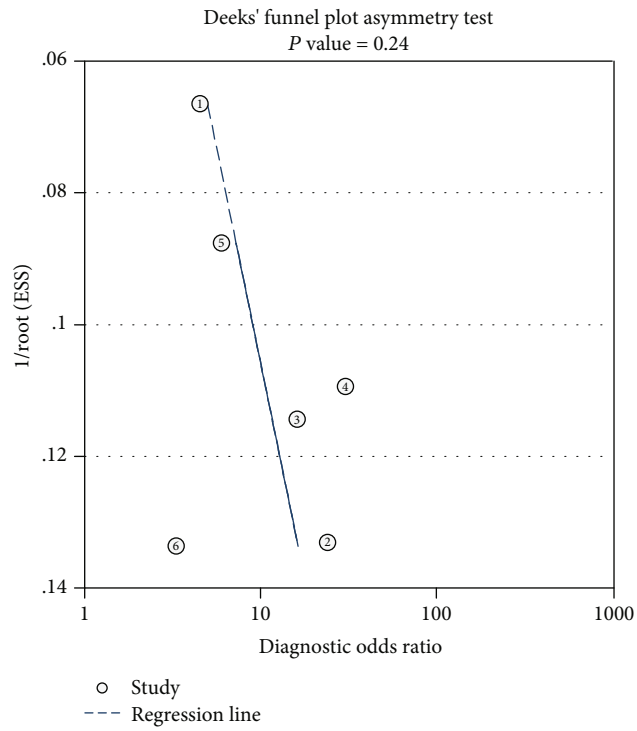

Figure 4: Deeks' funnel plot for miR-200c.

of 0.815, miR-200c could be a useful biomarker to diagnose ovarian cancer. Mir-200c was included in more studies, and the diagnostic values of Mir-200c were more convincing than other miRNAs in our paper.

miR-200a is also a member of the mir-200 family, one kind of long noncoding RNA that can promote invasion and metastasis of ovarian cancer through miR-200a [21]. Our paper enrolled 3 studies concerning miR-200a and showed that the diagnostic value of miR-200a was better than miR-200c.

As another member of the mir-200 family, miR-200b may improve the chemotherapeutic efficacy of ovarian cancer by targeting DNA methyl transferases [22]. Our paper enrolled 3 studies concerning miR-200b and showed that the diagnostic value of miR-200b was better than miR-200a and miR-200c.

Among miR-205, miR-145, miR-141, miR-429, and miR-125b, miR-145 had the highest diagnostic value. Because only 2 studies were included for these 5 miRNAs, the diagnostic values should be interpreted cautiously.

We noticed that three meta-analyses have also reported the diagnostic value of miRNAs for ovarian cancer [23–25]. We read them with great interest. For the meta-analysis by Wu et al. [23], it enrolled 11 studies concerning 5 single miRNAs (2 studies for miR-200a, 2 studies for miR-200b, 3 studies for miR-200c, 2 studies for miR-429, and 2 studies for miR-25) and combined them together to diagnose ovarian cancer. It is unreasonable to take all single miRNAs as a diagnostic biomarker for ovarian cancer because results of different single miRNAs cannot be combined in a meta-analysis. For the other two meta-analyses [24, 25], they also combined different single miRNAs to diagnose ovarian cancer. Compared to these previous meta-analyses, our paper only assessed the diagnostic value of the same single miRNA from different studies, which is more reasonable and practical.

There were several limitations in our meta-analysis. First, a high risk and an unclear situation existed in patient selection and an index test could lower methodological qualities. Second, significant heterogeneities existed among included studies. Third, our paper only enrolled studies concerning serum-based and plasma-based specimens but not other specimens such as tissue-based or urine-based specimens. Fourth, there was a small number of included studies for some single miRNAs. It is necessary to adopt a standardization of the control group and specimens and to conduct more related studies in the future.

Our meta-analysis showed that for ovarian cancer, miR-200c, miR-200a, and miR-200b can be useful diagnostic biomarkers. For miR-205, miR-145, miR-141, miR-429, and miR-125b, their value as diagnostic biomarkers should be interpreted cautiously.

Data Availability

The [DATA TYPE] data supporting this [SYSTEMATIC REVIEW or META-ANALYSIS] are from previously reported studies and datasets, which have been cited. The processed data are available [AT REPOSITORY NAME/IN THE SUPPLEMENTARY FILES/FROM THE CORRESPONDING AUTHOR UPON REQUEST].

Conflicts of Interest

The authors declare no conflict of interest.

Supplementary Materials

Table S1: PRISMA checklist. Table S2: sensitivity analysis for pooled sensitivities and corresponding heterogeneities. Figure S1: quality assessment of miR-200a according to QUADAS-2 guidelines. (A) Graph. (B) Summary. Figure S2: quality assessment of miR-200b according to QUADAS-2 guidelines. (A) Graph. (B) Summary. Figure S3: quality assessment of mir-205 according to QUADAS-2 guidelines. (A) Graph. (B) Summary. Figure S4: quality assessment of mir-145 according to QUADAS-2 guidelines. (A) Graph. (B) Summary. Figure S5: quality assessment of mir-141 according to QUADAS-2 guidelines. (A) Graph. (B) Summary. Figure S6: quality assessment of mir-429 according to QUADAS-2 guidelines. (A) Graph. (B) Summary. Figure S7: quality assessment of mir-125b according to QUADAS-2 guidelines. (A) Graph. (B) Summary. *(Supplementary Materials)*

References

[1] R. L. Siegel, K. D. Miller, and A. Jemal, "Cancer statistics, 2019," *CA: a Cancer Journal for Clinicians*, vol. 69, no. 1, pp. 7–34, 2019.

[2] L. Al-Alem and T. E. Curry, "Ovarian cancer: involvement of the matrix metalloproteinases," *Reproduction*, vol. 150, no. 2, pp. R55–R64, 2015.

[3] B. Oronsky, C. M. Ray, A. I. Spira, J. B. Trepel, C. A. Carter, and H. M. Cottrill, "A brief review of the management of platinum-resistant–platinum-refractory ovarian cancer," *Medical Oncology*, vol. 34, no. 6, p. 103, 2017.

[4] F. Li, R. Tie, K. Chang et al., "Does risk for ovarian malignancy algorithm excel human epididymis protein 4 and CA125 in predicting epithelial ovarian cancer: a meta-analysis," *BMC Cancer*, vol. 12, no. 1, p. 258, 2012.

[5] P. Buamah, "Benign conditions associated with raised serum CA-125 concentration," *Journal of Surgical Oncology*, vol. 75, no. 4, pp. 264-265, 2000.

[6] M. A. Cortez and G. A. Calin, "MicroRNA identification in plasma and serum: a new tool to diagnose and monitor diseases," *Expert Opinion on Biological Therapy*, vol. 9, no. 6, pp. 703–711, 2009.

[7] W. Wang, L. R. Wu, C. Li et al., "Five serum microRNAs for detection and predicting of ovarian cancer," *European Journal of Obstetrics & Gynecology and Reproductive Biology: X*, vol. 3, article 100017, 2019.

[8] S. Kim, M. C. Choi, J. Y. Jeong et al., "Serum exosomal miRNA-145 and miRNA-200c as promising biomarkers for preoperative diagnosis of ovarian carcinomas," *Journal of Cancer*, vol. 10, no. 9, pp. 1958–1967, 2019.

[9] É. Márton, J. Lukács, A. Penyige et al., "Circulating epithelial-mesenchymal transition-associated miRNAs are promising biomarkers in ovarian cancer," *Journal of Biotechnology*, vol. 297, pp. 58–65, 2019.

[10] M. Zuberi, R. Mir, I. Khan et al., "The promising signatures of circulating microRNA-145 in epithelial ovarian cancer patients," *MicroRNA*, vol. 9, no. 1, 2020.

[11] X. Meng, V. Müller, K. Milde-Langosch, F. Trillsch, K. Pantel, and H. Schwarzenbach, "Circulating cell-free miR-373, miR-200a, miR-200b and miR-200c in patients with epithelial ovarian cancer," *Advances in Experimental Medicine and Biology*, vol. 924, pp. 3–8, 2016.

[12] T. Zhu, W. Gao, X. Chen et al., "A pilot study of circulating microRNA-125b as a diagnostic and prognostic biomarker for epithelial ovarian cancer," *International Journal of Gynecological Cancer*, vol. 27, no. 1, pp. 3–10, 2017.

[13] M. Zuberi, I. Khan, R. Mir, G. Gandhi, P. C. Ray, and A. Saxena, "Utility of serum miR-125b as a diagnostic and prognostic indicator and its alliance with a panel of tumor suppressor genes in epithelial ovarian cancer," *PLoS One*, vol. 11, no. 4, article e0153902, 2016.

[14] X. Meng, S. A. Joosse, V. Müller et al., "Diagnostic and prognostic potential of serum miR-7, miR-16, miR-25, miR-93, miR-182, miR-376a and miR-429 in ovarian cancer patients," *British Journal of Cancer*, vol. 113, no. 9, pp. 1358–1366, 2015.

[15] Y. C. Gao and J. Wu, "MicroRNA-200c and microRNA-141 as potential diagnostic and prognostic biomarkers for ovarian cancer," *Tumour Biology*, vol. 36, no. 6, pp. 4843–4850, 2015.

[16] H. Zheng, L. Zhang, Y. Zhao et al., "Plasma miRNAs as diagnostic and prognostic biomarkers for ovarian cancer," *PLoS One*, vol. 8, no. 11, article e77853, 2013.

[17] C. W. Kan, M. A. Hahn, G. B. Gard et al., "Elevated levels of circulating microRNA-200 family members correlate with serous epithelial ovarian cancer," *BMC Cancer*, vol. 12, no. 1, p. 627, 2012.

[18] D. Moher, A. Liberati, J. Tetzlaff, D. G. Altman, and PRISMA Group, "Preferred reporting items for systematic reviews and meta-analyses: the PRISMA statement," *International Journal of Surgery*, vol. 8, no. 5, pp. 336–341, 2010.

[19] P. F. Whiting, A. W. S. Rutjes, M. E. Westwood et al., "QUADAS-2: a revised tool for the quality assessment of diagnostic accuracy studies," *Annals of Internal Medicine*, vol. 155, no. 8, pp. 529–536, 2011.

[20] M. Mutlu, U. Raza, Ö. Saatci, E. Eyüpoğlu, E. Yurdusev, and Ö. Şahin, "miR-200c: a versatile watchdog in cancer progression, EMT, and drug resistance," *Journal of Molecular Medicine*, vol. 94, no. 6, pp. 629–644, 2016.

[21] H. Gao, X. Li, G. Zhan et al., "Long noncoding RNA MAGI1-IT1 promoted invasion and metastasis of epithelial ovarian cancer via the miR-200a/ZEB axis," *Cell Cycle*, vol. 18, no. 12, pp. 1393–1406, 2019.

[22] J. Liu, X. Zhang, Y. Huang et al., "miR-200b and miR-200c co-contribute to the cisplatin sensitivity of ovarian cancer cells by targeting DNA methyltransferases," *Oncology Letters*, vol. 17, no. 2, pp. 1453–1460, 2019.

[23] L. Wu, W. Shang, H. Zhao et al., "*In Silico* Screening of Circulating MicroRNAs as Potential Biomarkers for the Diagnosis of Ovarian Cancer," *Disease Markers*, vol. 2019, Article ID 7541857, 12 pages, 2019.

[24] X. Wang, D. Kong, C. Wang et al., "Circulating microRNAs as novel potential diagnostic biomarkers for ovarian cancer: a systematic review and updated meta-analysis," *Journal of Ovarian Research*, vol. 12, no. 1, p. 24, 2019.

[25] H. Wang, T. Wang, W. Shi, Y. Liu, L. Chen, and Z. Li, "Comprehensive analysis on diagnostic value of circulating miRNAs for patients with ovarian cancer," *Oncotarget*, vol. 8, no. 39, pp. 66620–66628, 2017.

Hindawi
Disease Markers
Volume 2020, Article ID 4086929, 6 pages
https://doi.org/10.1155/2020/4086929

Research Article

scFv against HSP60 of *Strongyloides* sp. and Its Application in the Evaluation of Parasite Frequency in the Elderly

Camila Botelho Miguel,[1,2] **Marcelo Arantes Levenhagen**,[3] **Julia Maria Costa-Cruz**,[3] **Luiz Ricardo Goulart**,[3] **Patrícia Terra Alves**,[3] **Carlos Ueira-Vieira**,[3] **Patrícia Kellen Martins Oliveira Brito**,[4] **Angelica Oliveira Gomes**,[2] **Javier Emilio Lazo-Chica**,[2] **Carlo José Freire Oliveira**,[2] **and Wellington Francisco Rodrigues**[1]

[1]*Federal University of Triângulo Mineiro (UFTM), 38061-500 Uberaba, MG, Brazil*
[2]*University Center of Mineiros-Unifimes, 75., 830-000 Mineiros, GO, Brazil*
[3]*Federal University of Uberlândia, 38400-902, Uberlandia, MG, Brazil*
[4]*University of São Paulo, 14049900, Ribeirao Preto, SP, Brazil*

Correspondence should be addressed to Wellington Francisco Rodrigues; wellington.frodrigues@hotmail.com

Received 29 October 2019; Revised 20 December 2019; Accepted 24 December 2019; Published 11 January 2020

Guest Editor: Bruno Rivas-Santiago

The present study is aimed at evaluating serological method using scFv anti-*Strongyloides* sp. and reporting the frequencies of the results with conventional parasitological technique (faeces) in elderly individuals. Among 112 elderly individuals (≥60 years of age), 14.28% were positive for at least one enteroparasite, with one individual positive for *S. stercoralis*. Sera were evaluated for the presence of anti-*Strongyloides* sp. antibodies using total or detergent fraction extracts of *Strongyloides venezuelensis*, which presented positivity rates of 19.64% and 10.71%, respectively. An anti-HSP60 single-chain variable fragment from *Strongyloides* sp. was used to detect parasite antigens, with 5.36% (6 individuals) of ELISA-positive individuals returning a positive result. While the serological test indicates previous or recent infection and may be limited by antigen purification, the anti-HSP60 method reflects the presence of *Strongyloides* sp. immune complexes and exhibits greater sensitivity and specificity. Our results demonstrate the variable occurrence of enteroparasites in elderly individuals residing in long-term nursing homes and validate a novel epidemiological tool to describe infection cases by *Strongyloides* sp.

1. Introduction

Among the pathogenic helminths investigated, the one most often diagnosed is *Strongyloides stercoralis* (*S. stercoralis*), a nematode parasite that causes strongyloidiasis, a disease characterized by skin and digestive symptoms, in humans [1–5]. Parasitological surveys using more sensitive and rigorous techniques are needed to provide more reliable results and serve as the basis for future interventions involving sanitary and educational measures to improve health maintenance [2]. In this sense, research carried out for the refinement of techniques applied to the epidemiological survey to parasitic diseases, such as the strongyloidiasis, is necessary. It should be noted that infection by this parasite is becoming increasingly severe in vulnerable groups, such as immunosuppressed patients, children, and the elderly [5–7]. The major concern in these vulnerable groups is the low immune capacity to respond effectively to infectious processes. In the case of the elderly, this problem is increasing as this population experiences considerable growth and longer life expectancy; these changes will have profound impacts on public health in the coming decades.

One of the factors that is associated with quality of life and an increase in the number of elderly people worldwide is the high demand for long-term institutions known worldwide as retirement homes. In these environments, physical and social structures have particular characteristics that

may be associated with the emergence or control of infectious and/or parasitic diseases, including by *S. stercoralis*.

Studies to diagnose the incidence and/or prevalence of parasitic diseases at these institutions have been conducted over the years. For the diagnostic tests available and implemented so far, the results show that the prevalence of enteroparasites in the elderly is not associated with long-term institutions, sociodemographic characteristics, lifestyle, or health conditions [4, 5]. However, the frequencies of enteroparasites in the elderly appear to be underestimated because they may vary depending on the study and the country/region evaluated.

The choice and availability of techniques with greater specificity and good sensitivity for the screening of *S. stercoralis* are limiting factors for the precise diagnosis and epidemiological analysis of the disease, leading to underestimates of *S. stercoralis* infections [1, 8]. From among the existing techniques, the Baermann technique, involving the use of agar plate culture, contributed to an increase in the specificity of the detection of *Strongyloides* in the faeces, but it still exhibits a variable sensitivity due to the scarcity of larvae in many infections and the amount of faecal material collected and evaluated [1, 9]. Serological techniques represent promising alternatives in the search for greater diagnostic sensitivity. However, these techniques still present some limitations, such as crossreactions that lead to the antigenic recognition of other nematodes and compromise the diagnosis of these endoparasites [1, 9]. Therefore, there is an ongoing search for more efficient and safer methods of detection.

Recently, a study from our research group presented a serological method for the detection of immunocomplexes formed from the binding of a single-chain variable fragment (scFv) to a specific protein from *Strongyloides* sp., HSP60. This serological method of diagnosis demonstrated a sensitivity of 97.5% and specificity of 98.81% to *Strongyloides* sp. [10]. The anti-*Strongyloides* scFv was incorporated into this test after the use of phage display, a fast and reliable technique that allows for the selection of peptides, antibodies, or scFvs highly specific for a particular pathogen. Thus, the characteristics of this method enabled the discovery of a molecule with important diagnostic applicability due to its high specificity and ease of production [11]. In this study, we aimed to demonstrate the use of the newly developed technique for the detection of immunocomplexes of Strongyloides sp. We also used this serological and conventional method to evaluate the frequency of enteroparasites in elderly individuals living in long-term residences.

2. Material and Methods

2.1. Ethics. All procedures related to this research were approved by the research ethics committee of the Federal University of Triângulo Mineiro (number: 017430/2014) and are registered in Plataforma Brasil in accordance with resolution 466/2012 of the National Health Council.

2.2. Inclusion and Exclusion Criteria. For this study, 112 individuals of both sexes who were ≥60 years of age and who resided in long-term residences in the city of Uberaba, Minas Gerais, Brazil, were enrolled. Patients with unsatisfactory samples (failure to obtain at least three faecal samples and/or to obtain a serum sample) were excluded from the evaluation.

2.3. Biological Samples. Three faecal samples were collected on alternate days for a period of 7 days. Collection was carried out in labelled sterile plastic collectors, and a small portion (5 g) was used for larval research while the rest was stored in flasks containing 10% buffered formaldehyde. In addition, the peripheral blood was collected (dry tube) to obtain serum by centrifugation at $1831 \times g$ for 10 min. Sera were frozen at −80°C until use.

2.4. Detection of Enteroparasites in Faeces. Two methods were used to detect enteroparasites in the faeces: a spontaneous sedimentation test (Hoffman test) [12] and the Baermann-Moraes test [13]. The Hoffman method was used to detect larvae, helminth eggs, and protozoan cysts. For each individual, about 5 g of faeces was dissolved in 10 mL of water in a small vial, and then, the sample was filtered through four-part folded gauze using a sedimentation cup. These samples were incubated for 24 h. With the help of a pipette, the sample was removed from the apex of the chalice for evaluation. The material was stained with Lugol's solution and examined under a light microscope (40x). For the Baermann-Moraes method, water at 40°C was added to a glass funnel until the level reached 1/2 the height, at which point it was connected to a rubber tube and closed with forceps, so the sample was contained. Then, the gauze was placed with the faeces on a strainer in contact with the funnel and water, so that the faeces were submerged for a few minutes at rest. Later, the forceps were removed to collect the liquid. After transferring to a slide, the presence of larvae was evaluated under a light microscope (40x).

2.5. Detection of Anti-Strongyloides Antibodies. Anti-*Strongyloides* sp. antibodies in all samples were detected using a total or partial (fraction) extract of *Strongyloides venezuelensis* (fusiform larva, stage 3). The production of the total and partial extracts was performed according to the methods of Da Silva et al. [14], and immunoenzymatic assays were performed as described below. For the detection of antibodies, high-affinity polystyrene plates (BioAgency Laboratories, São Paulo, Brazil) were coated with 5 μg/mL of total salt extract (ES) or the detergent fraction (D) and incubated overnight at 4°C in 0.06 M bicarbonate buffer, pH 9.6. After incubation, the plates were washed three times for 5 min each with phosphate-buffered saline (PBS) plus 0.05% Tween 20 (PBS-T) and blocked with PBS-T plus 3% skim milk at 37°C for 45 min. Serum samples (diluted 1 : 80) were added and incubated for an additional 45 min at 37°C. After washing with PBS-T, peroxidase-conjugated anti-human IgG antibody (1 : 2000) was added and incubated for 45 min at 37°C. The reaction was revealed by the addition of enzyme substrate (0.03% H_2O_2) and chromogen (*o*-phenylenediamine (OPD)) in 0.1 M phosphate-citrate buffer (pH 5.0). The reaction was incubated for 15 min at 24°C and stopped by the addition of 2 N NH_2SO_4. Previously known positive and negative samples were used as controls of the analytical

run. Optical densities were determined at 492 nm in an enzyme-linked immunosorbent assay (ELISA) reader (Titertek Plus, Flow Laboratories, McLean, VA, USA).

2.6. Detection of Immunocomplexes in Human Sera Using scFv against Strongyloides sp. HSP60. For the detection of *Strongyloides* sp. immunocomplex in the sera of the elderly individuals included in the study, an enzymatic immunoabsorption assay was performed. To this end, high-affinity microtiter plates (Nunc MaxiSorp™, Thermo Fisher Scientific, Waltham, MA, USA) were incubated with 50 μL anti-HSP60 scFv (10 μg/mL) in bicarbonate buffer (0.06 M, pH 9.6) overnight at 4°C. Plates were blocked with 5% PBS/-bovine serum albumin (BSA) for 45 min at 37°C. Serum samples were diluted 1 : 50 in PBS-T and added to the wells, and the plates were incubated for 45 min at 37°C. Subsequently, peroxidase-conjugated human anti-human IgG diluted in PBS-T (1 : 10,000 dilution) was added to the wells, and the plates were incubated for 45 min at 37°C. Between the steps, three washes were performed with PBS-T. The reaction was revealed by the addition of OPD diluted in 0.1 M citrate-phosphate (pH 5.0) and 30% H_2O_2. Plates were incubated for 15 min at room temperature, and the reactions were quenched by the addition of 2 N H_2SO_4. Optical densities (OD) were determined at 492 nm on an ELISA reader (Titertek Plus, Flow Laboratories). Under these conditions, the TG-ROC curve obtained the best cut-off (0.7175), as already described in another study [10].

2.7. Research Quality Control. Internal quality control processes were incorporated into the study where there was a clear definition of objectives, procedures, criteria for tolerance limits, corrective actions, and recording of activities. Controls to evaluate the imprecision of the analyses were also monitored at the preanalytical, analytical, and postanalytical phases [15, 16].

2.8. Statistical Analysis. Statistical analysis was performed using Prism software (GraphPad Inc., San Diego, CA, USA) and Excel (Microsoft). The chi-square test was used to determine the statistical significance of the data, with differences with $p < 0.05$ (5%) considered significant.

3. Results

3.1. Detection of Enteroparasites in Faeces Using the Hoffman and Baermann-Moraes Methods. A total of 112 individuals with a mean age of 76 years (range 60–109) were analysed. For each individual, three faecal samples were obtained on alternate days over a period of 7 days. Peripheral blood samples were also collected to obtain serum (between faecal collection days). First, the presence of enteroparasites in the faeces of the elderly individuals was determined. Only 14.28% of the individuals (16 individuals) tested positive for at least one parasite in the faeces. Among the positive individuals, 81.25% (13 individuals) were positive for only one type of enteroparasite, and the other 18.75% (3 individuals) were positive for at least two species. The prevalence of enteroparasite species among the faecal samples of 16 positive individuals were as follows: *Entamoeba coli* (10 individuals), *Giardia lamblia* (2 individuals), *Endolimax nana* (2 individuals), *Blastocystis hominis* (1 individual), and *S. stercoralis* (1 individual). The frequencies of enteroparasite occurrence were also evaluated separately in the sexes, but no significant differences were observed in the samples evaluated.

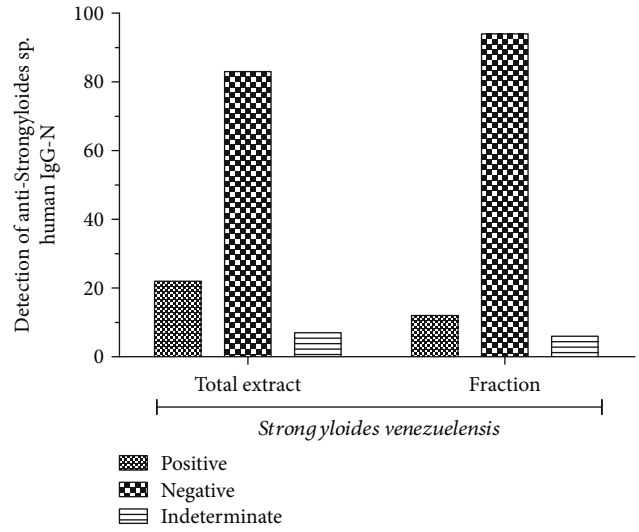

Figure 1: Positivity rates for anti-*Strongyloides* sp. antibodies among individuals residing in long-term institutions. After obtaining whole blood from elderly individuals living in long-term residences, samples were centrifuged to obtain the serum, and ELISA was performed. Plate sensitization was performed with the use of a total and/or partial extract of *Strongyloides venezuelensis*. Frequencies (positive, negative, and undetermined) were compared between the total and partial extract. No significant differences, chi-square test ($p > 0.05$).

Detection of anti-*Strongyloides* sp. IgG antibodies using total and partial extracts of *S. venezuelensis*.

In the above experiment, we detected *S. stercoralis*, an important enteroparasite related to morbidity and mortality in the elderly. However, because the parasitological test does not exhibit high sensitivity, we additionally tested whether we could detect the presence of anti-*Strongyloides* sp. IgG antibodies in the sera of the 112 individuals in this study. For detection, we tested the sera of the 112 patients against a total or partial extract of the parasite *S. venezuelensis*. Among the 112 individuals, 19.64% (22 individuals) were positive for anti-*Strongyloides* sp. IgG antibodies and 6.25% (7 individuals) of the samples were indeterminate using the total *S. venezuelensis* extract. When we used only the partial extract, 10.71% (12 individuals) of the samples were positive and 4.46% (5 individuals) were indeterminate. Importantly, although the use of the partial extract resulted in greater specificity, it was not significantly different from that of the total extract (Figure 1).

3.2. Detection of Immunocomplexes in Individuals Positive for Anti-Strongyloides sp. IgG Antibodies. The presence of IgG antibodies against *Strongyloides* sp. HSP60, per se, does not necessarily indicate clinical symptoms in the elderly, since an individual may have had contact with the parasite at any

Table 1: Serological and parasitological analysis of *Strongyloides* sp. in 112 individuals residing in long-term residences.

	Total extract	Serological Fraction	Immunocomplex	Parasitological Faeces
Positive (n)	22	12	6	1
Negative (n)	83	95	106	111
Indeterminate (n)	7	5	0	0
Positivity (%)	19.64	10.71	5.36	0.89

time over their lifetime. Recently, our group developed a serological method for the detection of immunocomplexes formed from the binding of an scFv to the *Strongyloides* sp. HSP60 protein. Therefore, we sought to describe epidemiological data, after specific immune response already established against *Strongyloides* sp. in the elderly. We evaluated the presence of immunocomplexes in the sera of the 22 individuals that were positive for IgG antibodies against *Strongyloides* sp. HSP60. Interestingly, 27.27% of these 22 elderly individuals tested exhibited the presence of immunocomplexes ($n = 6$). This represents 5.36% of the total population of 112 individuals enrolled in the study. The frequency of each result (positive, negative, and indeterminate) was compared among the serological tests (total extract, partial extract, and immunocomplex) and parasitological tests, which can be observed in Table 1. The detection of immunocomplexes for *Strongyloides* sp. by serological testing exhibited greater sensitivity and specificity.

4. Discussion

Enteroparasitoses are neglected diseases that affect millions of people worldwide, including the elderly, a population that has increased in number in recent decades [17]. Surveys of medically important enteroparasites show high rates of *S. stercoralis* infection among the populations that have been evaluated [4, 5, 18]. Among the various populations that have been studied, important findings have been observed in the elderly, especially those institutionalized in long-term residences [4, 18]. Despite these results, the World Health Organization has expressed concern over data involving the diagnosis of strongyloidiasis, and this may be due to the absence and/or imprecision of diagnostic tools [1]. In this study, we evaluated the most commonly used diagnostic methods, besides evaluating the application of a serological test for the detection of immunocomplexes previously developed by our research group. Our findings suggest that conventional tests (parasitological evaluation of faeces) may generate inaccurate and inferior data. However, the only test that would determine the incidence of *Strongyloides sp*. infection in the elderly in this study was the Hoffman test and the Baermann-Moraes test, which although they gave a low incidence, we cannot conclude that their sensitivity and specificity are less than the ELISA or the immune complex test, because they measure periods within the different parasite cycle stage.

Our results also enabled the evaluation of the frequency of enteroparasites in elderly individuals living in long-term residences, demonstrating that the newly developed test has an optimal level of safety independent of the evaluated population.

Our data showed that of the 112 individuals tested, the positivity rates for the conventional tests were very low for most of the endoparasites tested, including *S. stercoralis*. In contrast, the rate of detection of anti-*Strongyloides* sp. antibodies using the ELISA-based method and sensitization of the ELISA plates with total *S. venezuelensis* extract was higher; although the test is not able to demonstrate the early onset of infection, it is able to indicate the humoral adaptive immune response installed in previously infected individuals. The higher positivity rate associated with total rather than partial *S. venezuelensis* extract may reflect crossreactions to other antigens, which has been previously discussed in other studies [1, 10, 19–21].

Importantly, 27.27% ($n = 6$) of individuals positive for anti-*S. stercoralis* IgG antibodies were also positive for the presence of immunocomplexes. If we compare this with the use of the conventional faecal test, only one individual was positive for *S. stercoralis*, and this same individual was among those positive for the presence of immunocomplex. Thus, we believe that these techniques complement each other, as the parasite in question has a biological cycle that includes diverse forms due to its developmental and larval stages and may be linked to haematological and allergic manifestation [22].

Frequent efforts of the scientific community have been made to improve the diagnostic accuracy of tests for different enteroparasites of medical interest, including *S. stercoralis* [10, 23, 24]. To understand the need for these new diagnostic or epidemiological study tools, a recent comparative study with 98 samples concluded that there were discrepancies between molecular tests (real-time PCR) and microscopic methods for the diagnosis of 20 enteroparasites [25]. As previously mentioned, the method for the detection of immunocomplexes using the anti-*Strongyloides* sp. scFv ELISA assay showed excellent specificity (98.81%) and sensitivity (97.5%) [10], which is highly relevant if we take into account the diagnostic capacity of this tool, after humoral adaptive immune response, specifically for this disease.

This test in addition to its diagnostic contributions serves studies like this one provide epidemiological data that contribute to the improvement of health services, enabling the selection of appropriate forms of intervention for the control of these parasitoses [2].

Recent evaluations contribute to demonstrate the need to increase diagnostic sensitivity in the strongyloidiasis. One of

the alternatives evaluated was the use of molecular biology techniques such as the real-time polymerase chain reaction (PCR), where it was shown to be more sensitive than the conventional parasitological test [26]; on the other hand, a sensitivity of 63% of qPCR for the diagnosis of *S. stercoralis* in faeces and 17% in urine has been demonstrated, indicating that the sensitivity is varied and there is a need for more implementations for the validation of the technique [27]. We thus believe that the detection of serum immunocomplexes can contribute to the diagnosis and for epidemiological surveys, quickly and inexpensively, in association with other techniques, including the detection of parasites in faeces.

The results of this survey indicated a 14% positivity rate among the evaluated individuals for at least one endoparasite, including rates of *Entamoeba coli*, *G. lamblia*, *Endolimax nana*, *B. hominis*, and *S. stercoralis* of 65%, 15%, 10%, 5%, and 5%, respectively. These results differ somewhat from previously published results. For example, in a study of 183 subjects conducted in the southwestern region of Saudi Arabia, the rate of positivity for enteroparasites was 70.5% and the highest prevalence was found in individuals under the age of 30 [28]. In this study, the researchers observed a high frequency of amoebas associated with amebiasis (*Entamoeba histolytica* and *Entamoeba dispar*). In contrast, in our survey, the highest incidence was for the commensal protozoan *Entamoeba coli*. Commensal bacteria and protozoa are commonly found to be associated with enteroparasites in epidemiological studies [2]. Another study reported frequencies of *Entamoeba coli* of 47.5% among individuals in long-term institutions and 60.9% among geriatric outpatients [2]. The same researchers reported a frequency of enteroparasites of 12.9% among institutionalized elderly. Thus, although frequencies appear to vary, parasitic infections along with bacterial infections remain a serious public health problem.

Data on the distribution of intestinal parasitic infections in the metropolitan area of Rio de Janeiro, Brazil, also indicate a significant number of enteroparasitoses, including in the elderly [18]. In one study, the authors found an association between the socioeconomic status of the population and the incidence of infections, demonstrating that the infection rate may track socially vulnerable areas [18]. In the same study, the authors observed a high rate of *S. stercoralis* among the described helminths. Similarly, our evaluation pointed to *S. stercoralis* as an important helminth, corroborating the data from Naves and Costa-Cruz [4] and emphasizing the need to increase the diagnostic capacity and new epidemiologic reports of these enteroparasites.

5. Conclusions

In conclusion, this study provided an analysis of the occurrence and variability of enteroparasites among individuals residing in long-term residences in a city in the southeastern region of Brazil. In addition, the efficiency of an innovative technique determines the frequency of *Strongyloides* sp. in the elderly and the importance of implementing multiple different techniques in order to increase the sensitivity and specificity of diagnosis. Thus, our results will contribute to the appropriate clinical management and maintenance of elderly health.

Data Availability

The data used to support the findings of this study are included within the article.

Conflicts of Interest

The authors declare that they have no conflicts of interest.

Acknowledgments

The authors gratefully acknowledge the Pro-Rectory of Research and Graduate Studies and the Postgraduate Programs of Federal University of Triângulo Mineiro and Federal University of Uberlandia. This study was supported by the Foundation for Research Support of the State of Minas Gerais (FAPEMIG), Coordination for the Improvement of Higher Education Personnel (CAPES), and National Council for Scientific and Technological Development (CNPq). WFR received postdoctoral fellowships from the National Postdoctoral Program of the Coordination for the Improvement of Higher Education Personnel (Social Demand/PNPD/CAPES).

References

[1] Z. Bisoffi, D. Buonfrate, A. Montresor et al., "Strongyloides stercoralis: a plea for action," *PLoS Neglected Tropical Diseases*, vol. 7, no. 5, p. e2214, 2013.

[2] L. S. Ely, P. Engroff, G. T. Lopes, M. Werlang, I. Gomes, and G. A. De Carli, "Prevalência de enteroparasitos em idosos," *Revista Brasileira de Geriatria e Gerontologia*, vol. 14, no. 4, pp. 637–646, 2011.

[3] L. Gétaz, R. Castro, P. Zamora et al., "Epidemiology of Strongyloides stercoralis infection in Bolivian patients at high risk of complications," *PLoS Neglected Tropical Diseases*, vol. 13, no. 1, article e0007028, 2019.

[4] M. M. Naves and J. M. Costa-Cruz, "High prevalence of Strongyloides stercoralis infection among the elderly in Brazil," *Revista do Instituto de Medicina Tropical de São Paulo*, vol. 55, no. 5, pp. 309–313, 2013.

[5] P. H. S. Santos, R. C. S. Barros, K. V. G. Gomes, A. A. Nery, and C. A. Casotti, "Prevalence of intestinal parasitosis and associated factors among the elderly," *Revista Brasileira de Geriatria e Gerontologia*, vol. 20, no. 2, pp. 244–253, 2017.

[6] R. Berahmat, A. Spotin, E. Ahmadpour et al., "Human cryptosporidiosis in Iran: a systematic review and meta-analysis," *Parasitology Research*, vol. 116, no. 4, pp. 1111–1128, 2017.

[7] C. N. Nkenfou, S. M. Tchameni, C. N. Nkenfou et al., "Intestinal parasitic infections in human immunodeficiency virus-infected and noninfected persons in a high human immunodeficiency virus prevalence region of Cameroon," *The American Journal of Tropical Medicine and Hygiene*, vol. 97, no. 3, pp. 777–781, 2017.

[8] J. D. Machicado, L. A. Marcos, R. Tello, M. Canales, A. Terashima, and E. Gotuzzo, "Diagnosis of soil-transmitted helminthiasis in an Amazonic community of Peru using multiple diagnostic techniques," *Transactions of the Royal Society*

of Tropical Medicine and Hygiene, vol. 106, no. 6, pp. 333–339, 2012.

[9] A. P. Sudré, H. W. Macedo, R. H. S. Peralta, and J. M. Peralta, "Diagnóstico da estrongiloidíase humana: importância e técnicas," *Revista de Patologia Tropical*, vol. 35, no. 3, pp. 174–184, 2006.

[10] M. A. Levenhagen, F. A. Santos, P. T. Fujimura, A. P. Carneiro, J. M. Costa-Cruz, and L. R. Goulart, "Erratum: Corrigendum: Structural and functional characterization of a novel scFv anti-HSP60 of _Strongyloides_ sp.," *Science Reports*, vol. 5, no. 1, p. 12181, 2015.

[11] C. F. Barbas, "Recent advances in phage display," *Current Opinion in Biotechnology*, vol. 4, no. 5, pp. 526–530, 1993.

[12] W. A. Hoffman, J. A. Pons, and S. L. Janer, "The concentration methods in Schistosomiasis mansoni," *Journal of Public Health*, vol. 9, pp. 281–298, 1934.

[13] G. Baermann, "Eine einfache methode zur auffindung von Ankylostomun-(Nematoden)-larven In erdproben," in *Mededelingen uit het Geneeskundig Laboratorium te Weltevreden*, G. Baermann, Ed., pp. 41–47, Javasche Boekhandel & Drukkerij, Batavia, 1917.

[14] H. da Silva, C. J. de Carvalho, M. A. Levenhagen, and J. M. Costa-Cruz, "The detergent fraction is effective in the detection of IgG anti-Strongyloides stercoralis in serum samples from immunocompromised individuals," *Parasitology International*, vol. 63, no. 6, pp. 790–793, 2014.

[15] R. J. Henry and M. Segalove, "The running of standards in clinical chemistry and the use of the control chart," *Journal of Clinical Pathology*, vol. 5, no. 4, pp. 305–311, 1952.

[16] W. F. Rodrigues, C. B. Miguel, M. H. Napimoga, C. J. Oliveira, and J. E. Lazo-Chica, "Establishing standards for studying renal function in mice through measurements of body size-adjusted creatinine and urea levels," *BioMed Research International*, vol. 2014, Article ID 872827, 8 pages, 2014.

[17] T. M. Dall, P. D. Gallo, R. Chakrabarti, T. West, A. P. Semilla, and M. V. Storm, "An Aging Population And Growing Disease Burden Will Require ALarge And Specialized Health Care Workforce By 2025," *Health Affairs*, vol. 32, no. 11, pp. 2013–2020, 2013.

[18] C. P. Faria, G. M. Zanini, G. S. Dias et al., "Geospatial distribution of intestinal parasitic infections in Rio de Janeiro (Brazil) and its association with social determinants," *PLoS Neglected Tropical Diseases*, vol. 11, no. 3, article e0005445, 2017.

[19] Z. Bisoffi, D. Buonfrate, M. Sequi et al., "Diagnostic accuracy of five serologic tests for Strongyloides stercoralis infection," *PLoS Neglected Tropical Diseases*, vol. 8, no. 1, article e2640, 2014.

[20] S. A. Repetto, P. Ruybal, M. E. Solana et al., "Comparison between PCR and larvae visualization methods for diagnosis of _Strongyloides stercoralis_ out of endemic area: A proposed algorithm," *Acta Tropica*, vol. 157, pp. 169–177, 2016.

[21] A. Requena-Méndez, P. Chiodini, Z. Bisoffi, D. Buonfrate, E. Gotuzzo, and J. Muñoz, "The laboratory diagnosis and follow up of strongyloidiasis: a systematic review," *PLoS Neglected Tropical Diseases*, vol. 7, no. 1, article e2002, 2013.

[22] J. F. Magnaval, G. Laurent, N. Gaudré, J. Fillaux, and A. Berry, "A diagnostic protocol designed for determining allergic causes in patients with blood eosinophilia," *Military Medical Research*, vol. 4, p. 15, 2017.

[23] M. C. Espírito-Santo, M. V. Alvarado-Mora, P. L. Pinto et al., "Comparative study of the accuracy of different techniques for the laboratory diagnosis of Schistosomiasis mansoni in areas of low endemicity in Barra Mansa city, Rio de Janeiro state, Brazil," *BioMed Research International*, vol. 2015, Article ID 135689, 16 pages, 2015.

[24] F. S. Yanet, N. F. Fidel Angel, N. Guillermo, and S. P. Sergio, "Comparison of parasitological techniques for the diagnosis of intestinal parasitic infections in patients with presumptive malabsorption," *Journal of Parasitic Diseases*, vol. 41, no. 3, pp. 718–722, 2017.

[25] D. Sow, P. Parola, K. Sylla et al., "Performance of real-time polymerase chain reaction assays for the detection of 20 gastrointestinal parasites in clinical samples from Senegal," *The American Journal of Tropical Medicine and Hygiene*, vol. 97, no. 1, pp. 173–182, 2017.

[26] E. Dacal, J. M. Saugar, T. Soler et al., "Parasitological versus molecular diagnosis of strongyloidiasis in serial stool samples: how many?," *Journal of Helminthology*, vol. 92, no. 1, pp. 12–16, 2018.

[27] F. Formenti, G. La Marca, F. Perandin et al., "A diagnostic study comparing conventional and real-time PCR for _Strongyloides stercoralis_ on urine and on faecal samples," *Acta Tropica*, vol. 190, pp. 284–287, 2019.

[28] S. A. Al-Harthi and M. B. Jamjoom, "Enteroparasitic occurrence in stools from residents in southwestern region of Saudi Arabia before and during Umrah season," *Saudi Medical Journal*, vol. 28, no. 3, pp. 386–389, 2007.

Hindawi
Disease Markers
Volume 2019, Article ID 4956016, 15 pages
https://doi.org/10.1155/2019/4956016

Research Article

Diet Alters Serum Metabolomic Profiling in the Mouse Model of Chronic Chagas Cardiomyopathy

Kezia Lizardo,[1] Janeesh Plakkal Ayyappan,[1] Usha Ganapathi,[1] Walderez O. Dutra,[2] Yunping Qiu,[3] Louis M. Weiss,[3,4] and Jyothi F. Nagajyothi[1]

[1]*Department of Microbiology, Biochemistry and Molecular Genetics, Public Health Research Institute, New Jersey Medical School, Newark, USA*
[2]*Laboratory of Cell-Cell Interactions, Instituto de Ciências Biológicas, Departamento de Morfologia, Belo Horizonte, Brazil*
[3]*Department of Medicine, Albert Einstein College of Medicine, New York, USA*
[4]*Department of Pathology, Albert Einstein College of Medicine, New York, USA*

Correspondence should be addressed to Jyothi F. Nagajyothi; jfn31@njms.rutgers.edu

Received 10 July 2019; Accepted 21 August 2019; Published 20 December 2019

Guest Editor: Marcos Vinícius Silva

Chagas disease is caused by *Trypanosoma cruzi* which is endemic in Latin America. *T. cruzi* infection results in a latent infection with approximately a third of latently infected patients developing chronic Chagas cardiomyopathy (CCM). CCM is a common cause of cardiomyopathy in endemic regions and has a poor prognosis compared to other cardiomyopathies. The factors responsible for the transition from the asymptomatic indeterminate latent stage of infection to CCM are poorly understood. Our previous studies demonstrated that lipid metabolism and diet are important determinants of disease progression. In the present study, we analyzed various serum metabolomic biomarkers such as acylcarnitines, amino acids, biogenic amines, glycerophospholipids, and sphingolipids in murine models of CCM, where the mice specifically develop either left or right ventricular cardiomyopathy based on the diets fed during the indeterminate stage in a murine model of Chagas disease. Our data provide new insights into the metabolic changes that may predispose patients to CCM and biomarkers that may help predict the risk of developing cardiomyopathy from *T. cruzi* infection. *Author Summary*. Chronic Chagas cardiomyopathy (CCM) is a parasitic disease prevalent in Latin America. Currently, no effective drugs or vaccines are available to prevent or cure CCM. The factors involved in the disease severity and progression are poorly understood to design new therapeutic interventions. In order to rapidly identify Chagas patients with a higher risk to develop CCM, a new set of biomarkers specific to Chagas disease is needed. We performed serum metabolomic analyses in chronic *T. cruzi*-infected mice fed on different diets and identified cardiac ventricular-specific metabolite biomarkers that could define CCM severity. In this paper, we present the results of serum metabolomic analyses and discuss its correlations to the diet-induced metabolic regulations in the pathogenesis of CCM in a murine model of Chagas disease.

1. Introduction

Chagas disease, caused by the protozoan parasite *Trypanosoma cruzi*, is endemic to Latin America, where approximately 8-10 million people are infected [1]. Following the acute phase of infection, most infected individuals enter into a prolonged asymptomatic form of disease termed the "chronic indeterminate phase," which can persist for life without developing Chagas-related symptoms [2]; however, approximately 30% of "chronic indeterminate phase" individuals will develop debilitating and sometimes life-threatening Chagas-related symptoms including chronic Chagas cardiomyopathy (CCM) [3]. It is estimated that the number of annual deaths due to CCM is around 50,000. Of these, 60% are related to sudden cardiac death (SCD), 25% to heart failure, and 15% to stroke [4]. Chagas disease is a major cause of heart disease and cardiovascular-related deaths in Latin America.

Chronic Chagas cardiomyopathy is characterized by its various degrees of severity, and Chagas patients have a

poorer prognosis than non-Chagas cardiac patients [5]. There are no vaccines or effective drugs to prevent or treat chronic Chagas cardiomyopathy. Furthermore, the lack of prognosis and progression markers for chronic Chagas disease is a barrier for testing new drugs to prevent the progression of cardiomyopathy. Several inflammatory and protein molecules such as NT-proBNP and Hs-cTnT have been identified as diagnostic biomarkers in distinguishing the severity of CCM [6, 7], but these markers are not specific to this cardiomyopathy [8]. There has been a lack of biomarker identification for Chagas disease severity-specific biomarkers that could predict the risk of developing cardiac dysfunction/cardiomyopathy during the asymptomatic indeterminate phase. Identification and development of such biomarkers would help to develop strategies to prevent the transition from indeterminate to symptomatic stage.

Our research has identified that *T. cruzi* infection results in cardiac lipidopathy [9]. *T. cruzi* binds to cholesterol-rich lipoproteins and invades host cells through LDL receptors and other scavenger receptors, resulting in intracellular lipid accumulation [10], and in CCM, there are significantly increased lipid levels in the myocardium [9]. Increased intracellular lipids impair lipid metabolism in the myocardium exacerbating mitochondrial oxidative and ER stress and exhaust mitochondrial oxidative capacity, which contributes to the development of CCM [11]. CCM, which develops after several years of infection, is essentially an immunometabolic disease.

Various mouse models of Chagas disease have been used to investigate cardiac pathology during acute and chronic stages of infection [12, 13]. Previously, we demonstrated that diet plays a major role in determining cardiac pathology in *T. cruzi*-infected CD1 mice [14, 15]. In particular, a high-fat diet (HFD) significantly modulates cardiac pathology and improves survival during acute infection as compared to mice fed on a regular diet (RD) that is carbohydrate-rich [14, 15]. HFD and RD contain the same protein calories and differ in fat and carbohydrate-derived calories. When the *T. cruzi*-infected mice were fed on either a HFD or a RD during the indeterminate stage, i.e., starting after the end of acute infection to late chronic stage (from 35 DPI to 150 DPI), they developed diet-specific ventricular enlargements during chronic infection [16]. These studies in a murine model of chronic Chagas disease established an interesting hypothesis that a long-term HFD treatment causes right ventricular dilation and wall thinning, and a long-term RD treatment results in left ventricular dilation [16]. This suggests that specific diets can alter the metabolic status in the host, which in turn regulates cardiac pathogenesis specific to either left ventricle (LV) or right ventricle (RV). Therefore, the abundance of specific serum metabolites in *T. cruzi*-infected mice fed on different diets during the indeterminate and early chronic phases may be indicative of disease progression specific to LV and RV.

In Chagas disease patients, dysfunction and dilation only of the LV have historically been studied; however, recent studies have demonstrated that RV dysfunction and dilation are predominantly seen in Chagas disease patients with heart failure [1, 17]. Enlargement of the liver and other signs of systemic and pulmonary congestion are also commonly observed in severe CCM patients who die after the onset of heart failure [18].

Alterations in the global metabolomic profiling during the acute stage of *T. cruzi* infection in a murine model have been demonstrated [19]. However, the metabolomic profiles differ between acute and chronic stages of Chagas disease, and the progression to CCM is associated with the chronic phase of infection. Herein, we report the first analysis of the serum metabolic profile in an experimental model of chronic Chagas disease and identify potential metabolite biomarkers that are associated with the progression from the indeterminate to the symptomatic stage of disease. We also demonstrate the effect of various diets on glucose tolerance and hepatic lipid metabolism at 150 days postinfection (DPI).

2. Materials and Methods

2.1. Mouse Infection and Sample Collection. A global metabolomic analysis of mice was used to assess the effect of diets on the pathogenesis of chronic Chagas cardiomyopathy and host metabolism. *T. cruzi* infection and maintenance of infected mice have been previously described [14, 16]. In brief, male 6-8 weeks CD1 mice (purchased from Jackson Laboratory) were infected intraperitoneally (i.p.) at 6 to 8 weeks of age with 5×10^3 trypomastigotes of the Brazil strain and fed on rodent chow diet (PicoLab Mouse Diet 20 #5058 containing 23.19% calories of protein, 21.63% fat, and 55.17% carbohydrates). After 35 days postinfection (after acute infection, 35 DPI), mice were randomly divided into two groups ($n = 20$ per group) and fed on either a high-fat diet (HFD; 60% fat calories (20% calories of protein and 20% calories of carbohydrates) D12492 Research Diets, Inc., New Brunswick, NJ) or a low-fat control diet (RD; 10% calories of fat). Although RD diet was designed to be used as a control diet, it is also considered a carbohydrate-rich diet (RD; 70% carbohydrate calories (20% calories of protein and 10% calories of fat)) when compared to the "standard" rodent diet PicoLab #5058. [14, 16]. Uninfected mice were fed on either HFD ($n = 20$) or RD ($n = 20$) and used as respective controls in all the experiments. Mice were euthanized and livers were harvested after a cardiac MRI imaging analysis for biochemical analysis at 150 DPI [16]. Serum samples were obtained from 75 μl of blood collected from the orbital venous sinus (using isoflurane anesthesia) 150 DPI. The experiment was repeated to confirm all results.

2.2. Ethics Statement. All animal experimental protocols were approved by the Institutional Animal Care and Use Committee (IACUC) of the Albert Einstein College of Medicine (No. 20130202) and the Rutgers Biomedical and Health Sciences (No. 15107), which adhere to the National Research Council guidelines (Guide for the Care and Use of Laboratory Animals: Eighth Edition, Washington, DC: The National Academies Press, 2011).

2.3. Fasting Blood Glucose. Tail blood was drawn seven hours after food was removed. Glucose was measured on whole

blood with AlphaTRAK 2 blood glucose test strips and monitoring system (Abbott) [15].

2.4. Oral Glucose Tolerance Test (OGTT). After a 6-hour fast, the mice (5 per group) were weighed and their base line glucose was measured using an AlphaTRAK® Blood Glucose Monitoring System. Mice were gavaged orally with a glucose solution of 2 mg glucose/g body weight, and blood glucose was measured after 15, 30, 60, and 120 minutes [15].

2.5. Sample Processing and Metabolomic Analysis. Serum samples were measured using the AbsoluteIDQ p180 targeted metabolomic kit (Biocrates Life Sciences AG, Innsbruck, Austria), and a UPLC-MS/MS (Xevo TQ, Waters, Pittsburgh, PA, USA) following the manufacturer's instruction. Serum samples were prepared according to the manufacturer's instructions adding several stable isotope-labelled standards to the samples prior to the derivatization and extraction steps. Using LC/MS, up to 184 metabolites from 5 different compound classes, namely, acylcarnitines, amino acids, biogenic amines, glycerophospholipids, and sphingolipids can be quantified [20]. Sample order was randomized, and pooled quality control (QC) samples (minimum 3) were plated at different positions on the 96-well plate and injected multiple times for covariance variation (CV) calculation for data quality control. Data were normalized between batches using the results of quality control level 2 repeats across the plate and between plates using Biocrates METIDQ software. Metabolites with <20% CVs were treated as accurate quantification, and CVs between 20 and 30% were treated as relatively accurate quantification. Metabolites with CVs > 30% were excluded.

Heat maps were used to depict the relatively altered and unbalanced metabolic signature among different groups of mice (infected RD-fed, uninfected HFD-fed, and infected HFD-fed mice) compared to uninfected RD mice. Heat maps were generated using the Excel software based on the abundance of the differentially expressed metabolite data with the increased metabolite levels colored in red and decreased metabolite levels colored in green compared to the level of specific metabolite in uninfected RD mice (colored in pale yellow). To identify diet-specific alterations in the left and right ventricle pathology, we compared the uninfected and the infected groups fed on the respective diets and a percentage change was calculated.

2.6. Immunoblot Analysis. Protein analysis was performed as previously described [14, 16] using the following antibodies: fatty acid synthase (FAS) Rabbit Polyclonal antibody (1 : 1000 dilution, ab22759) from Abcam Inc. (Cambridge, MA); phospho-ATP-citrate lyase (pACL) (Ser455) Rabbit Polyclonal Antibody (1 : 1000 dilution, #4331), Cell Signaling Technology; AceCS1 (D19C6) Rabbit monoclonal Ab (1 : 1000 dilution #36585), Cell Signaling Technology; Phospho-Acetyl-CoA Carboxylase (pACC) (Ser79) Rabbit Polyclonal Antibody (1 : 1000 dilution #3661), Cell Signaling Technology; anti-CPT1A, mouse monoclonal antibody (CPT1) 1 : 1000 dilution (8F6AE9) (ab128568), Abcam Inc.; Anti-Lipin 1 Rabbit Polyclonal antibody (Lipin 1) 1 : 1000 dilution (ab70138) Abcam Inc.; and Peroxisome Proliferator Activated Receptor Alpha Rabbit Polyclonal antibody (PPARα) 1 : 1000 dilution (PA1-822A), ThermoFisher. Horseradish peroxidase- (HRP-) conjugated goat anti-mouse immunoglobulin (1 : 2000 dilution, Thermo Scientific Catalog #32230) or horseradish peroxidase- (HRP-) conjugated goat anti-rabbit immunoglobulin (1 : 2000 dilution, Thermo Scientific Catalog #31463) was used to detect specific protein bands (explained in the figure legends) using a chemiluminescence system [14]. GDI (Rabbit Polyclonal 1 : 10000 dilutions, Thermo Scientific QG223848) and a secondary antibody horseradish peroxidase-conjugated goat anti-rabbit (1 : 2000 dilution, Thermo Scientific Catalog #31463) were used to normalize protein loading [16].

2.7. Cholesterol Measurement. Cholesterol levels were quantified in the hearts and livers of mice at 150 DPI using a colorimetric assay kit, and samples were prepared and assayed following the manufacturer's protocol (total cholesterol colorimetric assay kit, Cell Biolabs Inc., CA).

2.8. Statistical Analysis. Statistically significant differences were tested using Student's t-test, and the corrected p values (q-value) < 0.05 were deemed as statistically significant. The identified metabolites influenced by *T. cruzi* infection and/or diet compared to uninfected RD mice are presented according to p values.

3. Results

3.1. Experimental T. cruzi Infection. Infection of CD1 mice with *T. cruzi* (Brazil strain) causes cardiomyopathy during the chronic stages of infection [16]. Feeding HFD during the indeterminate stage of infection led to the development of RV dilation and accelerated the development of cardiac pathology [16] (Table 1(a)). Feeding a carbohydrate-rich RD during the indeterminate stage of infection led to the development of LV dilation (Table 1(a)) [16]. While feeding different diets during the indeterminate stage of infection showed no significant difference on the survival rate of mice, we did observe significant differences in the metabolic status of animals on different diets including differences in body weight, liver weight, glucose levels, and glucose clearance at 150 DPI (Figure 1). Therefore, to understand further the effect of diet on plasma metabolites and its link to cardiomyopathy with either LV or RV dysfunction in *T. cruzi*-infected mice, we analyzed plasma metabolomic profiles of infected mice on different diets.

3.2. Body Weight, Glucose, and Glucose Clearance. A comparative body weight measurement analysis showed a significant decrease in the weights of infected mice compared to uninfected mice fed the same diets (either RD or HFD), as detailed below. In uninfected control groups, though the body weights of RD mice were lower compared to HFD-fed mice, there was no statistically significant difference in these groups. The body weights of infected HFD-fed mice were significantly ($p \leq 0.01$) greater than those of infected RD-fed mice (Figure 1(a)). We also measured the weights of the hearts and livers (Figures 1(b) and 1(c)). The weights

Table 1: Effect of different diets on (a) ventricular (RV and LV) dilations and (b) accumulation of cholesterol (in the liver and heart mg/g wet weight) in *T. cruzi*-infected CD1 mice chronic stage at 150 DPI. (RVID: right ventricle internal diameter, LVID: left ventricle internal diameter measured at diastole). $^{**}p \leq 0.01$ or $^{***}p \leq 0.001$ compared to uninfected RD mice. $^{\#}p \leq 0.05$, $^{\#\#}p \leq 0.01$ or $^{\#\#\#}p \leq 0.001$ compared to infected RD mice. $^{\wedge\wedge}p \leq 0.01$ compared to uninfected HFD mice.

(a)

	Composition (%kcal)		LVID (mm)	RVID (mm)
Carb-rich diet (RD) (research diet #D12450J)	Carbohydrate -70 Fat -10 Protein -20	Uninfected Infected	3.5 ± 0.08 4.5±0.2***	2.1 ± 0.05 1.98 ± 0.1
High fat diet (HFD) (research diet #D12492)	Carbohydrate -20 Fat -60 Protein -20	Uninfected Infected	3.5 ± 0.08 4.5±0.2***	1.97 ± 0.09 2.9±0.12$^{***\#\#\wedge\wedge}$

(b)

		RD	HFD
Heart	Uninfected	2.64 ± 0.26	3.843±0.39**
	Infected	3.158±0.18**	3.77±0.32$^{**/\#}$
Liver	Uninfected	3.867 ± 0.81	7.547±0.52***
	Infected	3.68 ± 0.62	6.587±0.49$^{***\#\#\#}$

of the hearts of infected mice (RD and HFD fed) were greater than in uninfected mice fed the same respective diets (Figure 1(b)). The weights of the livers of HFD mice were significantly greater compared to RD-fed mice, irrespective of infection (Figure 1(c)). Mice showed significant differences in cholesterol levels in the hearts between uninfected and infected groups and between HFD-fed mice and RD-fed mice (Table 1(b)). The livers of HFD-fed mice (both infected and uninfected) showed significantly greater cholesterol levels than the RD-fed mice (Table 1(b)). The weights of the hearts and livers may correlate with the cardiac and hepatic levels of cholesterol, respectively, in these experimental groups (Figures 1(b) and 1(c) and Table 1(b)).

Blood glucose, after an 8-hour fast, was measured at 150 DPI (Figure 1(d)). HFD mice showed significantly higher eight-hour fasting blood glucose levels compared with RD mice in both uninfected ($p \leq 0.005$) and infected groups ($p \leq 0.01$). There was no significant difference in the basal glucose levels between the infected and the uninfected groups of RD-fed mice. However, the levels of glucose were significantly lower ($p \leq 0.05$) in the infected HFD mice compared to uninfected HFD-fed mice. At 150 DPI, oral glucose tolerance was determined after an 8-hour fast (Figure 1(e)). We observed decreased glucose tolerance in the infected mice compared to the respective diet-fed uninfected mice. To our surprise, even though the basal levels of glucose were higher in uninfected HFD mice, HFD mice displayed enhanced glucose tolerance when compared to RD mice (Figure 1(d)).

3.3. Effect of Diet on Hepatic Lipid Metabolism during Chronic Chagas Disease. The livers of HFD-fed mice demonstrated higher levels of cholesterol compared to RD-fed mice suggesting an impaired lipid accumulation in HFD-fed mice (Table 1(b)). Therefore, we analyzed lipid metabolism biomarkers in the livers of RD- and HFD-fed uninfected and infected mice, and this suggested disrupted lipid metabolism in the livers of infected mice (Figure 2). Protein levels of fatty acid synthase (FAS), phosphorylated ATP-citrate lyase (pACL), acetyl CoA-synthase (AceCS1), and phosphorylated acetyl co A carboxylase (p-ACC) were determined in liver lysates of infected and uninfected mice. The levels of pACL, AceCS1, and p-ACC were not significantly altered in infected RD mice compared to uninfected RD mice; however, the protein levels of FAS, pACL, and p-ACC were significantly decreased in HFD-fed mice (both uninfected and infected groups) compared to uninfected RD mice. Immunoblot analyses of carnitine palmitoyltransferase I (CPT1), a mitochondrial enzyme that catalyzes the biosynthesis of acyl carnitines by transferring the acyl group of a long-chain fatty acyl-CoA from coenzyme A to l-carnitine [21], demonstrated significantly decreased levels of CPT1 during infection and HFD further affecting the levels (Figure 2(f)). Lipin 1, a critical regulator of intermediary fat metabolism, acts as a lipid phosphatase to dephosphorylate phosphatidic acid to form diacylglycerol—a key step in glycerolipid metabolism and triglyceride synthesis [22] was also significantly decreased in infected HFD mice compared to other groups (Figure 2(g)). Infection significantly increased hepatic PPARα levels compared to uninfected RD mice, and infected HFD mice showed significantly greater levels of PPARα compared to infected RD mice (Figures 2(a) and 2(h)). Although the biosynthesis of hepatic lipids was impaired during chronic *T. cruzi* infection, the levels of fatty acid oxidation increased in the livers as demonstrated by the PPARα level.

3.4. Amino Acid Metabolism. A comparative amino acid profiling of serum samples demonstrated significant alterations in their levels between uninfected and infected, and between

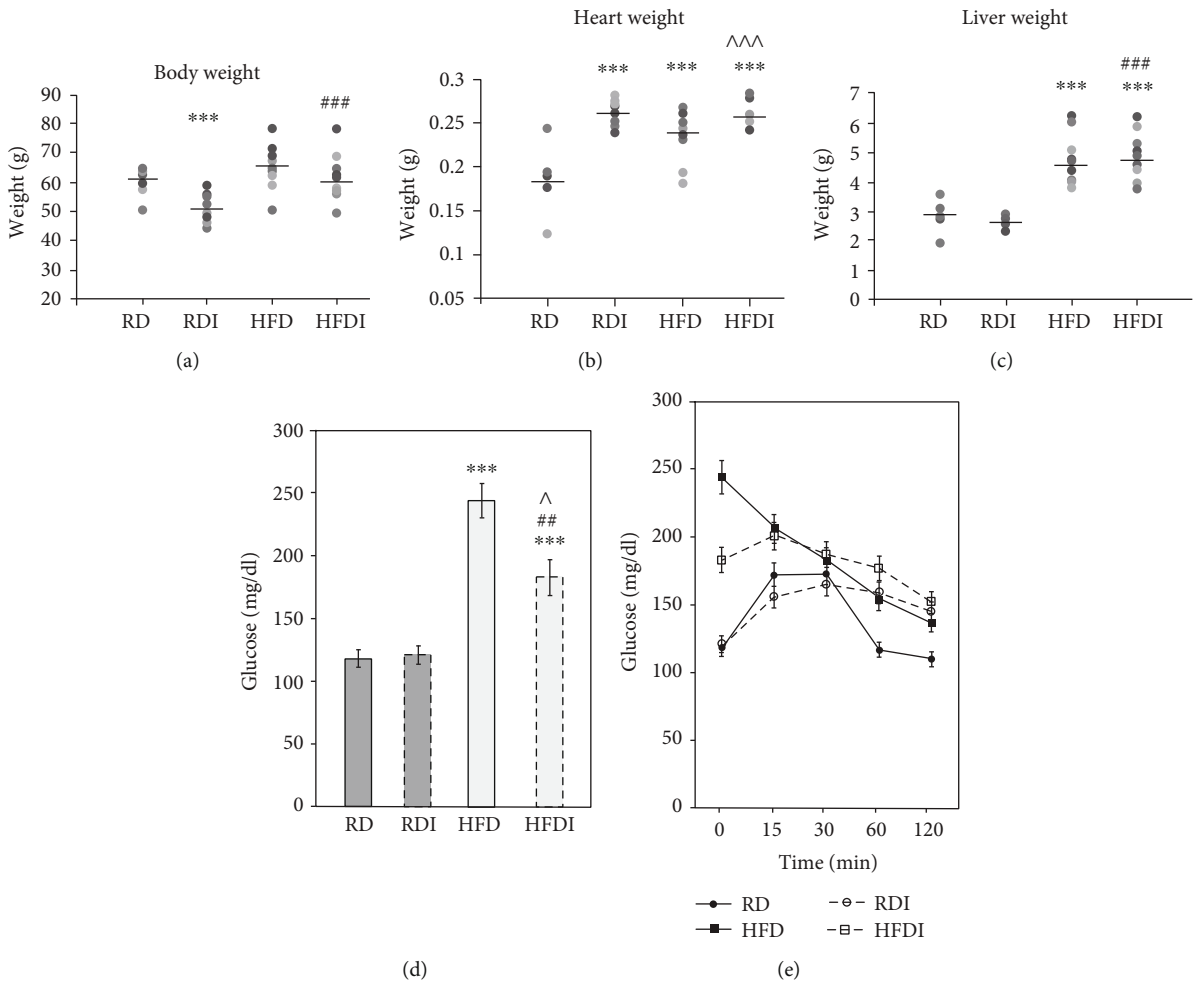

Figure 1: *T. cruzi* infection altered body weights and glucose levels in chronic mice fed on different diets. (a) *T. cruzi*-infected HFD mice displayed greater body weight compared to infected RD-fed mice at 150 DPI. (b) *T. cruzi* infection increased the weights of the hearts compared to uninfected mice irrespective of the diets fed at 150 DPI. (c) The weights of the livers of HFD-fed mice (both uninfected and infected) were significantly increased compared to RD-fed (both uninfected and infected) mice. *T. cruzi* infection showed no significant effect on the weights of the livers. (d) Serum glucose measurements demonstrated that chronic *T. cruzi* infection has no significant effect on the levels of fasting glucose in RD-fed mice. However, the levels of fasting glucose significantly increased in infected HFD mice compared to infected RD-fed mice. (e) Infected HFD mice showed a better clearance of glucose during OGTT analysis compared to infected RD mice even though the basal levels of glucose were significantly greater in infected HFD mice compared to infected RD mice. The error bars represent standard error of the mean. $^{*}p \leq 0.05$, $^{**}p \leq 0.01$, or $^{***}p \leq 0.001$ compared to uninfected RD mice. $^{\#}p \leq 0.05$, $^{\#\#}p \leq 0.01$, or $^{\#\#\#}p \leq 0.001$ compared to infected RD mice. $^{\wedge}p \leq 0.05$, $^{\wedge\wedge}p \leq 0.01$, or $^{\wedge\wedge\wedge}p \leq 0.001$ compared to uninfected HFD mice. A bar represents the mean value in (a–c).

RD and HFD groups (Figure 3(a)). The levels of essential amino acids, such as isoleucine, leucine, phenylalanine, tryptophan, and valine, were decreased in both RD- and HFD-fed infected mice compared to uninfected mice fed the same respective diets (Figure 3(b)). Interestingly, the levels of lysine and threonine were significantly increased in infected HFD-fed mice compared to uninfected HFD-fed mice and infected RD-fed mice (Figure 3(b)). Both lysine and threonine are essential immune modulators [23]. Nonessential amino acid profiling also differed between infected and uninfected, and between RD and HFD diets (Figure 3(a)). Amino acids, such as alanine, aspartic acid, and tyrosine, significantly decreased in RD-fed groups and significantly increased HFD-fed groups during infection compared to their respective diet-fed uninfected groups (Figure 3(b)). The levels of asparagine and glycine significantly increased in infected RD mice compared to uninfected RD mice (Figure 3(b)). However, the levels of glycine in infected HFD mice were significantly decreased compared to uninfected HFD mice. Glutamine levels were significantly reduced during infection irrespective of diet (Figure 3(b)). We observed no significant change in the levels of glutamic acid in RD-fed mice (between uninfected and infected), but a significant decrease in infected HFD mice compared to uninfected mice. Interestingly, the serum amino acid profiling of uninfected HFD mice was significantly differed compared to uninfected RD mice (Supplemental Fig. 1a).

3.5. Biogenic Amine Profiling. Among the 15 bioamines analyzed, the serum levels of many bioamines measured were

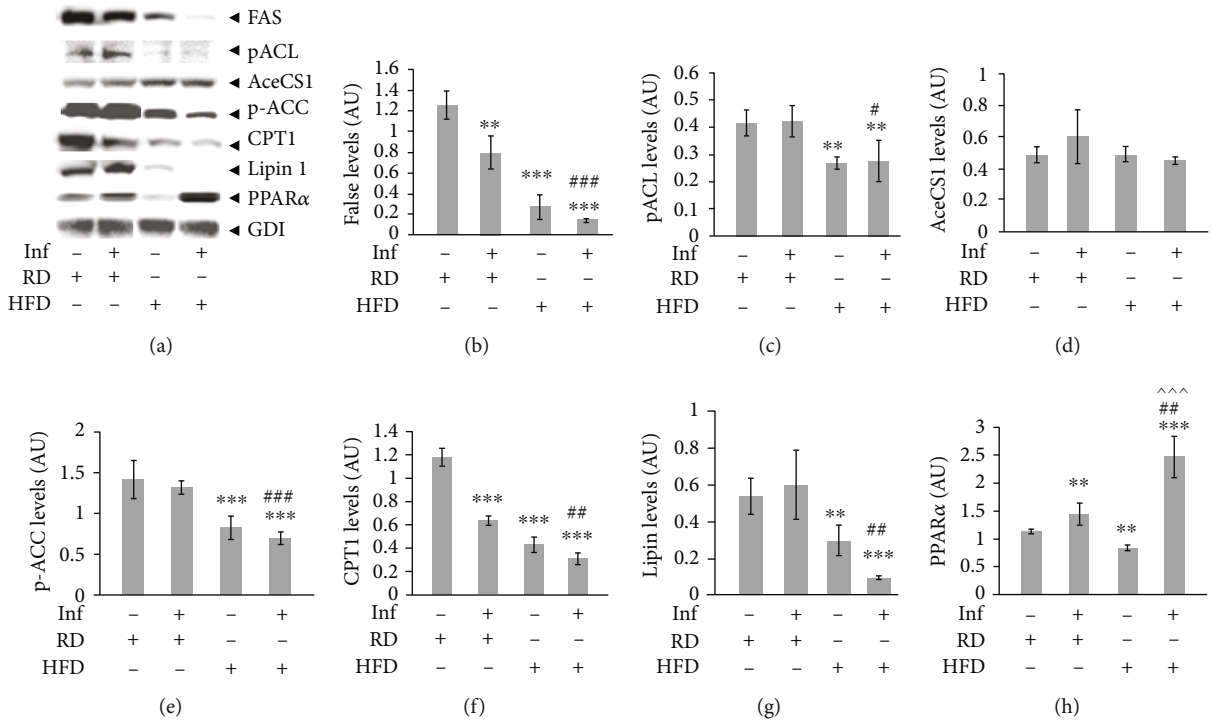

Figure 2: Immunoblot analysis of the livers demonstrated disrupted lipid metabolism in *T. cruzi*-infected mice and HFD further enhanced interruption of hepatic lipid metabolism during chronic Chagas disease. (a) *T. cruzi*-infected HFD-fed mice showed significantly reduced hepatic lipid metabolism compared to infected RD-fed mice as demonstrated by immunoblot analysis probed for various lipid metabolism markers such as fatty acid synthase (FAS), phosphorylated ATP-citrate lyase (pACL), phosphorylated acetyl co A carboxylase (p-ACC), carnitine palmitoyltransferase I (CPT1), and Lipin 1. Infected mice showed significantly increased hepatic levels of PPARα, a regulator of fatty acid oxidation compared to uninfected mice, and HFD further enhanced the levels of PPARα in the livers of infected mice. (b–h) Fold changes in the protein levels of FAS, pACL, acetyl CoA-synthase (AceCS1), pACC, CPT1, Lipin 1, and PPARα were normalized to GDI expression and represented as the bar graphs (b–h, respectively). The error bars represent the standard error of the mean. $^{*}p \leq 0.05$, $^{**}p \leq 0.01$, or $^{***}p \leq 0.001$ compared to uninfected RD mice. $^{\#}p \leq 0.05$, $^{\#\#}p \leq 0.01$, or $^{\#\#\#}p \leq 0.001$ compared to infected RD mice. $^{\wedge}p \leq 0.05$, $^{\wedge\wedge}p \leq 0.01$, or $^{\wedge\wedge\wedge}p \leq 0.001$ compared to uninfected HFD mice.

significantly differed between infected RD and infected HFD compared to uninfected RD mice (Figure 4). The levels of some of the bioamines measured were significantly higher in the serum of uninfected HFD mice compared to uninfected RD mice (Supplemental Fig. 1b) such as alpha-AAA, methionine sulfoxide (Met-SO), and serotonin. The levels of Met-SO, kynurenine, and alpha-AAA were significantly higher in the infected groups (both in HFD and RD) compared to the respective diet-fed uninfected groups (Figure 4(b)). Methionine sulfoxide is an indicator of oxidative stress. Increased kynurenine and alpha-AAA are associated with increased immune functions and metabolic dysfunctions, respectively [24]. The serum levels of serotonin significantly increased and the levels of creatinine and dopamine significantly decreased in infected RD mice compared to uninfected RD mice (Figure 4(b)), whereas the levels of sarcosine and putrescine significantly increased and serotonin significantly decreased in infected HFD mice compared to uninfected HFD mice (Figure 4(b)). However, the levels of serotonin significantly increased in infected HFD mice compared to uninfected RD mice (Figure 4(a)). It has been shown that the serum levels of serotonin increases in the patients with Takotsubo cardiomyopathy [25].

3.6. Lipid Metabolite Profiling. We have previously demonstrated that cardiac lipid metabolism plays a major role in the pathogenesis of cardiomyopathy in *T. cruzi*-infected mice [14, 16]. It has been shown that diets with different fat content alter cellular lipid metabolism [26]. We have demonstrated significantly reduced cardiac lipid metabolism in chronically infected HFD mice compared to infected RD mice which displayed significant RV and LV dilations, respectively. Therefore, we quantitated the levels of various lipid metabolites such as acylcarnitines, sphingolipids, and glycerol-phospholipids to analyze the effect of diet compositions in the pathogenesis of cardiomyopathy and identify potential lipid biomarkers of this disease specific to RV and LV dilations.

3.6.1. Acylcarnitines. Most of the measured acylcarnitines were significantly altered between uninfected and infected groups and between different diet groups (Figure 5, Supplemental Fig. 2a). The serum levels of C2, C3, C14, and C18 were significantly altered between uninfected RD and uninfected HFD groups (Supplemental Fig. 2a). The serum levels of carnitine (C0) significantly reduced during infection compared to uninfected groups fed the same respective diets.

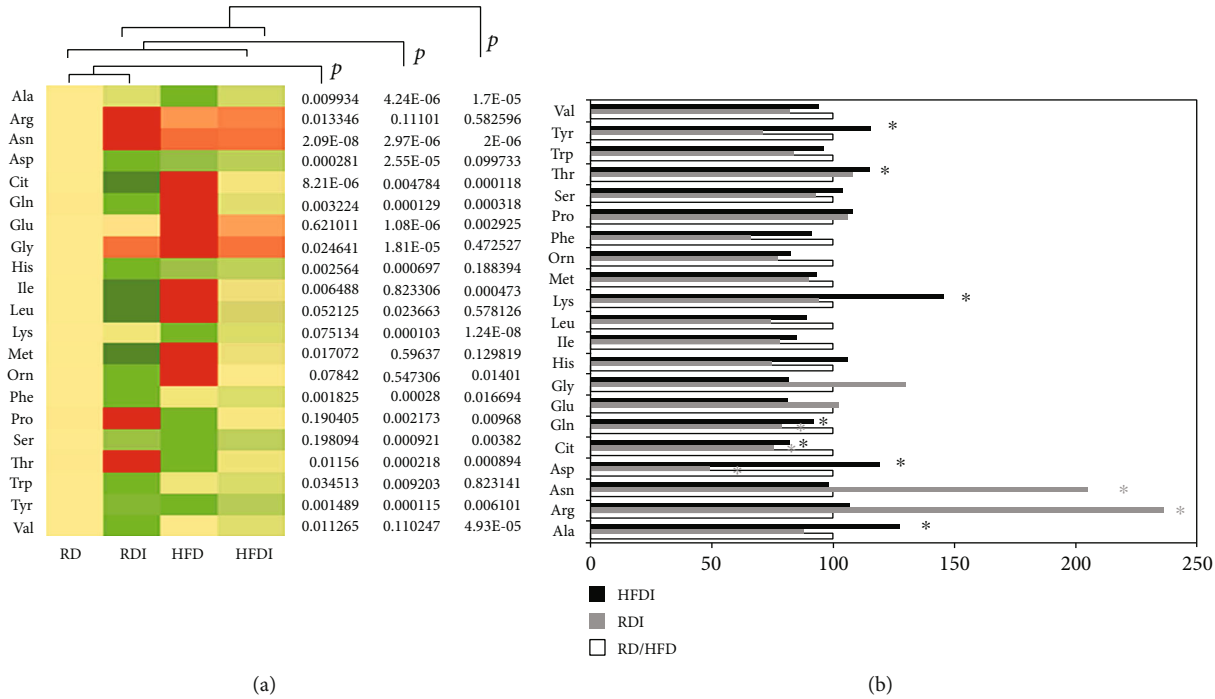

Figure 3: Comparison of amino acid profiling between *T. cruzi*-infected and uninfected mice fed on different diets at 150 DPI. (a) Heat map representing the serum levels of various amino acids during chronic infection in mice fed on either a RD or a HFD compared to uninfected RD mice at 150 DPI. Each row represents data for a specific metabolite, and each column represents the RD-fed uninfected (RD), RD-fed infected (RDI), HFD-fed uninfected (HFD), or HFD-fed infected (HFDI) mouse group. Different colors correspond to the different intensity level of metabolites (red > the control RD group and green < the control RD group). Statistically significant differences were tested using Student's *t*-test, and the corrected *p* values (*q*-value) are presented next to the heat map. Red, yellow, and green rectangles indicate high, moderate, and low expressions, respectively. (b) The percentage changes in the levels of amino acid metabolites in infected mice compared to the respective diet-fed (RD and HFD) uninfected mice represented by a bar graph (*significant change).

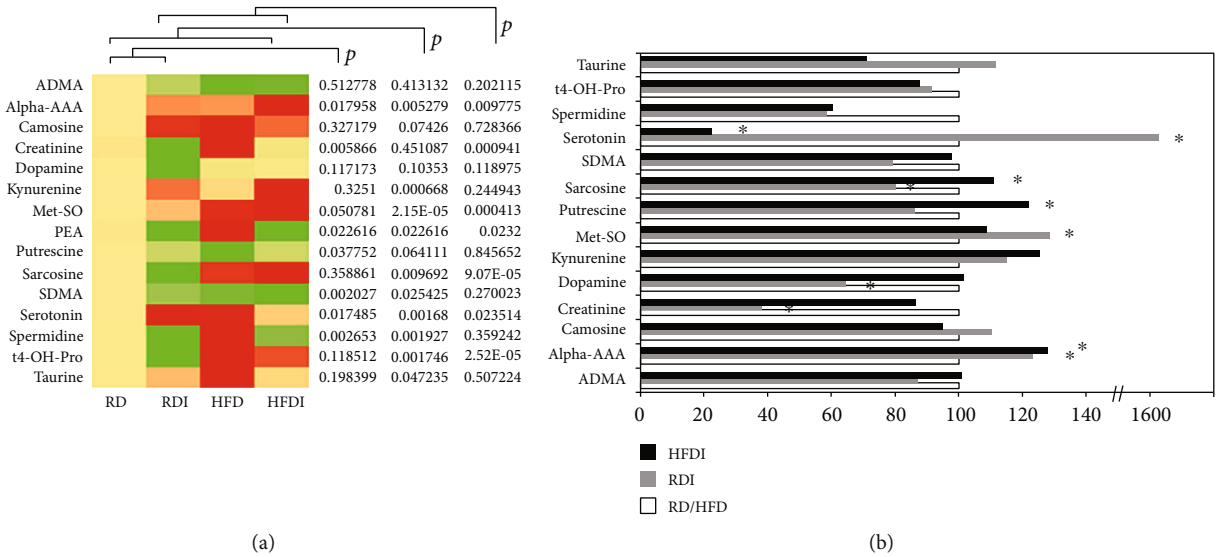

Figure 4: Comparison of biogenic amines profiling between *T. cruzi*-infected and uninfected mice fed on different diets at 150 DPI. (a) Heat map representing the serum levels of various biogenic amines during chronic infection in mice fed on either a RD or a HFD compared to uninfected RD mice at 150 DPI. Each row represents data for a specific metabolite, and each column represents the RD-fed uninfected (RD), RD-fed infected (RDI), HFD-fed uninfected (HFD), or HFD-fed infected (HFDI) mouse group. Different colors correspond to the different intensity level of metabolites (red > the control RD group and green < the control RD group). Statistically significant differences were tested using Student's *t*-test, and the corrected *p* values (*q*-value) are presented next to the heat map. Red, yellow, and green rectangles indicate high, moderate, and low expressions, respectively. (b) The percentage changes in the levels of biogenic amines in infected mice compared to the respective diet-fed (RD and HFD) uninfected mice represented by a bar graph (*significant change).

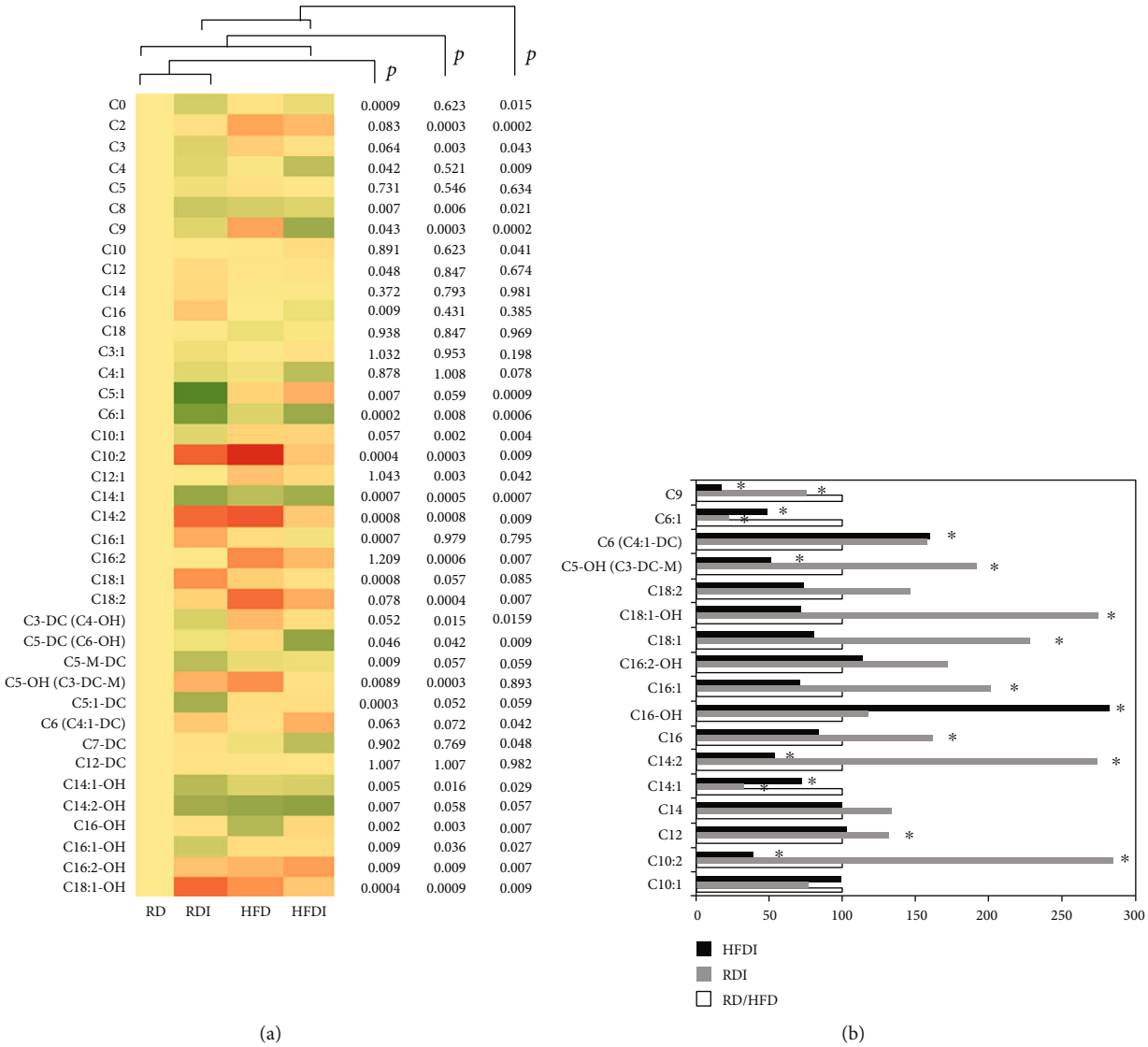

Figure 5: Comparison of acylcarnitine profiling between *T. cruzi*-infected and uninfected mice fed on different diets at 150 DPI. (a) Heat map representing the serum levels of various acylcarnitines during chronic infection in mice fed on either a RD or a HFD compared to uninfected RD mice at 150 DPI. Each row represents data for a specific metabolite, and each column represents the RD-fed uninfected (RD), RD-fed infected (RDI), HFD-fed uninfected (HFD), or HFD-fed infected (HFDI) mouse group. Different colors correspond to the different intensity level of metabolites (red > the control RD group and green < the control RD group). Statistically significant differences were tested using Student's t-test, and the corrected p values (q-value) are presented next to the heat map. Red, yellow, and green rectangles indicate high, moderate, and low expressions, respectively. (b) The percentage changes in the levels of acylcarnitines in infected mice compared to the respective diet-fed (RD and HFD) uninfected mice represented by a bar graph (*significant change).

Among the analyzed carnitines, the levels of C0, C14:1, C14:1-OH, C14:2-OH, C4, C4:1, C5-DC (C6-OH), C5-M-DC, C6:1, C8, and C9 were significantly lowered in the infected mice (RD and HFD mice) compared to uninfected RD mice (Figure 5(a)). However, the levels of some of the carnitines, such as C10:2, C12, C14, C14:2, C16, C16:1, C18:1, C18:1-OH, and C5-OH (C3-DC-M), were significantly increased in infected RD mice compared to infected HFD mice and uninfected RD controls (Figure 5(a)). The serum levels of C10, C10:1, C12:1, C16-OH, C16:1-OH, C16:2, C16:2-OH, C18:2, C2, C3, C3-DC (C4-OH), C3:1, C5:1, C5:1-DC, and C6 (C4:1-DC) significantly increased in infected HFD mice compared to infected RD mice and uninfected RD controls (Figure 5(a)).

The serum levels of C9, C6:1, and C14:1 were significantly reduced, and the levels of C6 (C4:1-DC) significantly increased in infected RD and infected HFD mice compared to the respective diet-fed uninfected groups (Figure 5(b)) and thus may represent specific biomarkers of CCM. The levels of C5-OH (C3-DC-M), C18:1-OH, C18:1, C16:1, C16, C14, and C12 were significantly higher in infected RD mice compared uninfected RD mice as well as HFD (both uninfected and infected) mice, which may represent as specific biomarkers of LV enlargement in CCM pathogenesis

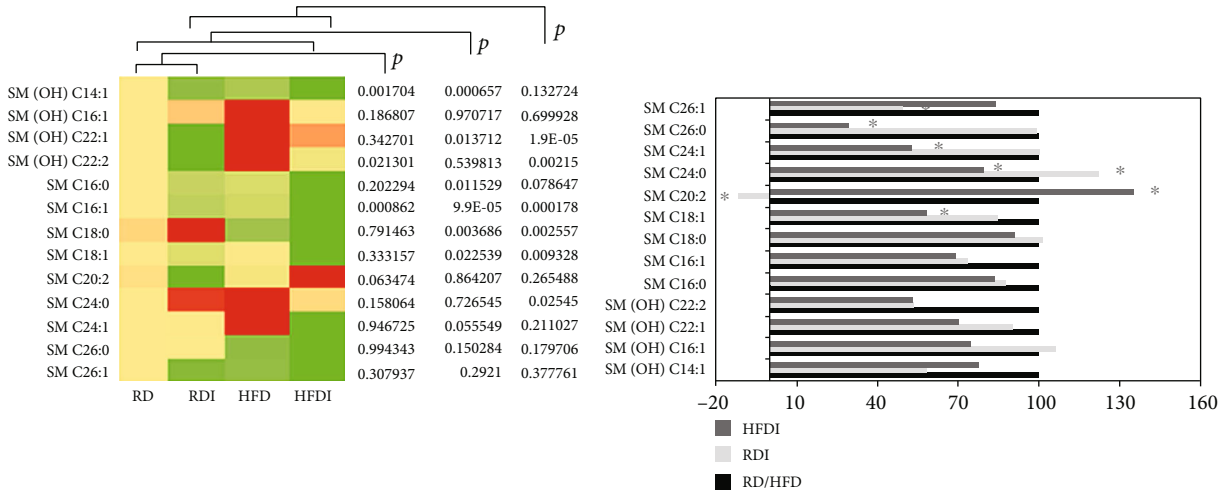

Figure 6: Comparison of sphingolipid profiling between *T. cruzi*-infected and uninfected mice fed on different diets at 150 DPI. (a) Heat map representing the serum levels of various sphingolipids during chronic infection in mice fed on either a RD or a HFD compared to uninfected RD mice at 135 DPI. Each row represents data for a specific metabolite, and each column represents the RD-fed uninfected (RD), RD-fed infected (RDI), HFD-fed uninfected (HFD), or HFD-fed infected (HFDI) mouse group. Different colors correspond to the different intensity level of metabolites (red > the control RD group and green < the control RD group). Statistically significant differences were tested using Student's t-test, and the corrected p values (q-value) are presented next to the heat map. Red, yellow, and green rectangles indicate high, moderate, and low expressions, respectively. (b) The percentage changes in the levels of sphingolipid metabolites in infected mice compared to the respective diet-fed (RD and HFD) uninfected mice represented by a bar graph (*significant change).

(Figures 5(a) and 5(b) and supplemental Fig. 2a). And increased serum levels of C16: OH may represent as a biomarker of RV dilation in CCM pathogenesis.

3.6.2. Sphingolipids. We quantified 14 sphingolipids, including both hydroxylated ($n = 5$) and nonhydroxylated ($n = 9$) ceramide phosphocholines (sphingomyelins) (Figure 6(a)). HFD significantly increased the serum levels of SM (OH) C22:1, C22:2, C24:0, and C24:1 compared to RD (Supplemental Fig. 2b) in uninfected mice. In general, the serum levels of other sphingomyelins were reduced in HFD-fed (+/- infection) mice compared to RD controls, except the levels of SM C24:0 and SM C24:1, which significantly increased in HFD-fed controls (Figure 6(a)).

The levels of many sphingolipids such as SM C18:1, C16:1, and C16, and SM (OH) C22:2, C22:1, and C14:1 significantly decreased during infection in mice compared to their respective diet-fed control groups (Figure 6(b)). In addition, SM C 20:2 significantly decreased in infected RD mice and significantly increased in infected HFD mice compared to other groups (Figure 6(b)). These data suggest that the serum levels of SM C 20:2 can be a potential biomarker of CCM pathogenesis.

3.6.3. Glycerophospholipids. A total of 87 glycerophospholipids ($n = 14$ lysophosphatidylcholines; $n = 73$ phosphocholines) were quantified in the collected serum samples (Figure 7). Of 14 quantified lysophosphatidylcholines, 8 metabolites (57%) such as lysoPC as' C14:0, C16:0, C16:1, C18:0, C18:1, C18:2, C20:3, and C20:4 were significantly decreased in uninfected HFD-fed mice (Supplemental Fig 2c) compared to uninfected RD mice. *T. cruzi* infection significantly reduced the levels of a lysoPC C17:0 in both RD- and HFD-fed mice compared to their respective diet-fed uninfected groups (Figure 7(b)). The levels of lysoPCs C26:0 and C26:1 significantly increased in infected RD groups compared to uninfected RD groups. Although the levels of many lysoPCs significantly decreased in HFD-fed groups compared to RD-fed groups (Figure 7(a), Supplemental Fig. 2c), the levels of lysoPCs C18:1, C18:2, C20:3, and C28:1 significantly decreased in infected HFD groups compared to uninfected HFD groups (Figure 7(b)), which could be potential markers of RV dilation in *T. cruzi*-infected mice (Figure 7(b)).

HFD significantly decreased the levels of diacyl and acyl-alkyl phosphatidylcholines (Supplemental Fig 3 and b, respectively) compared to RD fed in uninfected groups. 26 of the 34 quantified diacyl phosphatidylcholines (PC-aa) were significantly reduced in HFD groups compared to RD groups (Figure 8(a) and Supplemental Fig. 3a). Between the uninfected and the infected groups, 16 PC-aa's significantly decreased in infected groups compared to uninfected controls, and HFD further reduced the levels of these PC-aa's (Figure 8(a)). The levels of PC-aa C36:3, PC-aa-C38, and PC-aa-C38:3 were significantly decreased in infected RD and HFD mice compared to uninfected (both RD and HFD) mice (Figures 8(a) and 8(c)). We observed a similar trend in the levels of acyl-alkyl phosphatidylcholines (PC-ae), most of which were reduced in infected groups and even further reduced in HFD-infected mice (Figure 8(b) and Supplemental Fig. 3b). The levels of PC-ae-C36:2, PC-ae-C38:3, PC-ae-C38:4, PC-ae-C40:4, PC-ae-C40:6, and PC-ae-C42 were significantly reduced in infected mice compared to uninfected RD mice (Figure 8(b)). However, the levels of

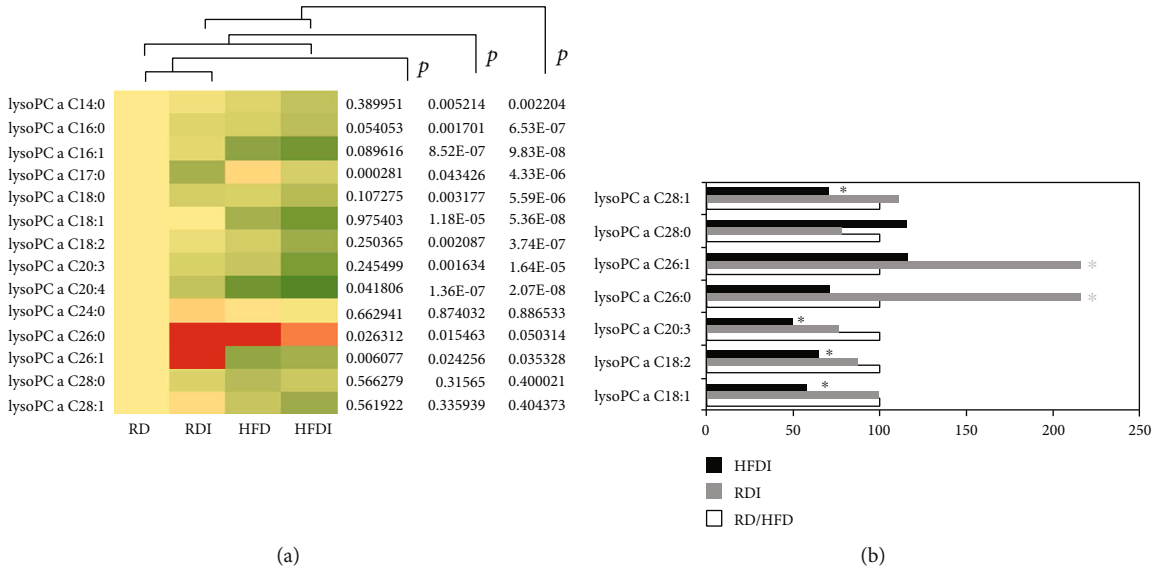

Figure 7: Comparison of 14 lysophosphatidylcholines profiling between *T. cruzi*-infected and uninfected mice fed on different diets at 150 DPI. (a) Heat map representing the serum levels of various lysophosphatidylcholines during chronic infection in mice fed on either a RD or a HFD compared to uninfected RD mice at 150 DPI. Each row represents data for a specific metabolite, and each column represents the RD-fed uninfected (RD), RD-fed infected (RDI), HFD-fed uninfected (HFD), or HFD-fed infected (HFDI) mouse group. Different colors correspond to the different intensity level of metabolites (red > the control RD group and green < the control RD group). Statistically significant differences were tested using Student's *t*-test, and the corrected *p* values (*q*-value) are presented next to the heat map. Red, yellow, and green rectangles indicate high, moderate, and low expressions, respectively. (b) The percentage changes in the levels of LPC metabolites in infected mice compared to the respective diet-fed (RD and HFD) uninfected mice represented by a bar graph (*significant change).

PC-ae C30:1 was significantly higher in the infected groups (both in RD and HFD fed) compared to uninfected RD mice (Figure 8(b)). The levels of PC-ae-C38:2 significantly reduced compared to all the other groups and thus may represent as a biomarker of LV-specific dilation in CCM.

4. Discussion

CCM is the most important clinical manifestation of Chagas disease, resulting in the mortality and morbidity in the endemic regions of Latin America. The factors responsible for the transition between asymptomatic to symptomatic CCM forms are not completely understood, and thus, the prognosis of chronic Chagas disease is difficult. Moreover, Chagas patients display various severity cardiac forms during the chronic stages [27], and the severity-specific markers are not greatly explored that could have served as a set of biomarkers in the prognosis of CCM pathogenesis. Using murine models of Chagas disease, we previously demonstrated that feeding a high calorie fat or carbohydrate diets may differentially influence the cardiac pathology and outcome of chronic Chagas disease [16]. *T. cruzi*-infected mice fed RD developed LV dilation and mice fed HFD developed RV dilation at 160 DPI [16]. Histological analysis demonstrated increased lipid droplets and enlarged capillaries in the RVs of infected HFD mice compared to infected RD mice [16]. We demonstrated that cholesterol efflux mechanisms, lipid oxidation, and mitochondrial dysfunction were all affected by HFD during chronic stages of infection, resulting in aggravated cardiac lipotoxicity, vascular and cardiac accumulation of lipid droplets, and vascular dilation [16]. In the later stages of chronic infection, HFD-fed infected mice showed lower levels of proinflammatory markers (TNFα and IFNγ) in the hearts compared to RD-fed infected mice although the levels of inflammatory cells were higher in infected HFD mice [16]. However, the levels of proinflammatory cytokines were significantly increased in infected RD mice compared to uninfected RD-fed mice suggesting that inflammation may play a major role in LV enlargement. Diets regulate the immunometabolic status of the host, which influences the severity of the disease, and thus, the serum metabolic profiling differs between different pathological conditions. Changes in host metabolomic profiling were demonstrated during acute stages of infection in a murine model of *T. cruzi* infection [19]; however, those observations cannot be extrapolated to evaluate the metabolic changes during the chronic stage of infection (occurring after several weeks in the murine model and after years/decades of infection in human disease), and the disease pathways are different between the acute and the chronic stage of infection. The current study analyzed the serum metabolomic profile of *T. cruzi*-infected mice fed on different diets that specifically developed RV and LV dilations. These metabolomic data demonstrate significant differences in the serum levels of amino acids, biogenic amines, and lipid metabolites between chronic *T. cruzi*-infected and uninfected mice, which further differed between mice fed fat-rich (HFD) and carbohydrate-rich (RD) diets. HFD and RD also differentially regulated hepatic and systemic lipid and glucose metabolism, which could influence cardiac morphology, physiology, and

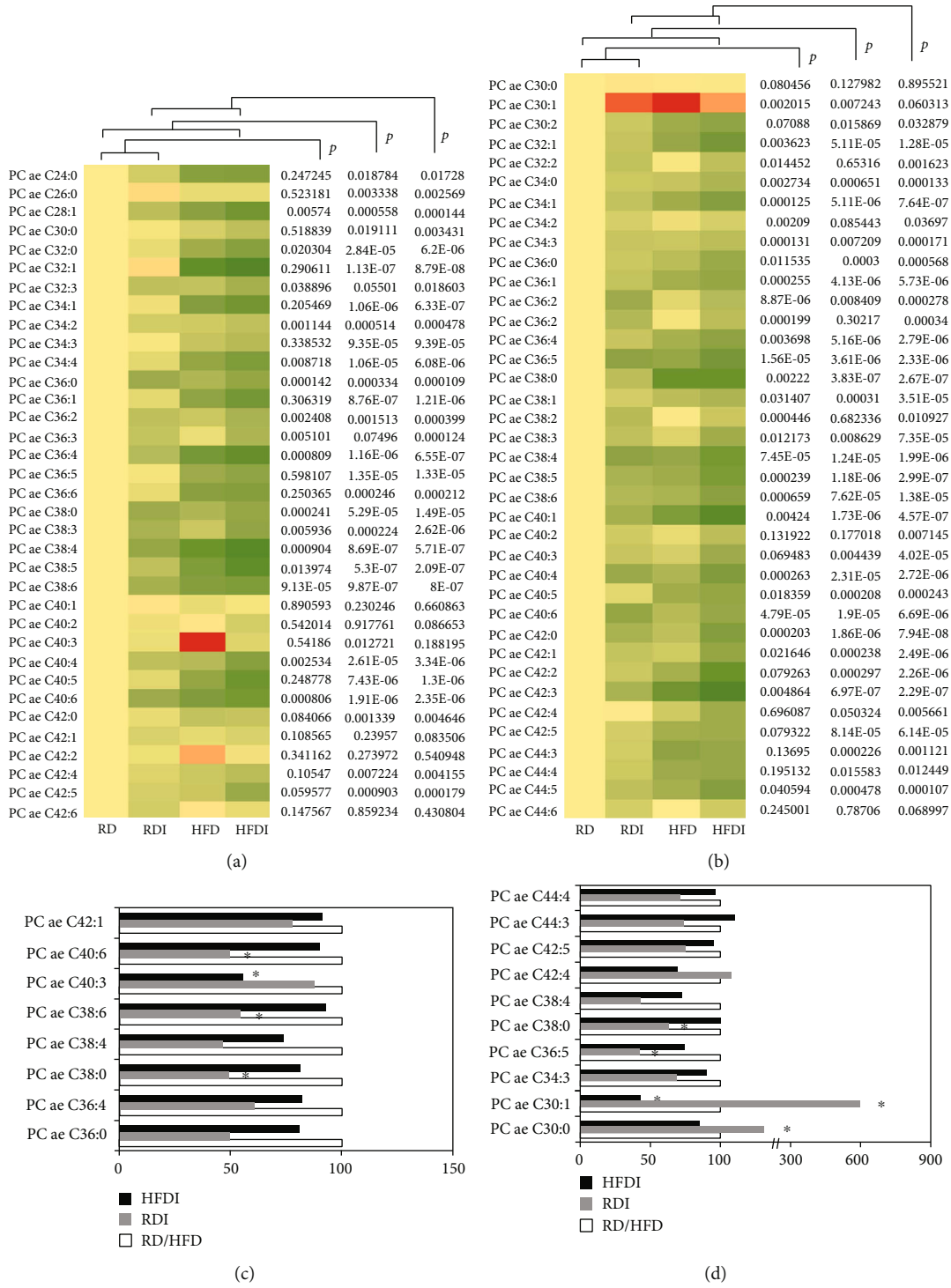

Figure 8: Comparison of phosphocholine (73) profiling between *T. cruzi*-infected and uninfected mice fed on different diets at 150 DPI. (a, b) Heat map representing the serum levels of various glycerol-phospholipids that included (a) diacyl PC and (b) acyl-alkyl PC during chronic infection in mice fed on either a RD or a HFD compared to uninfected RD mice at 150 DPI. Each row represents data for a specific metabolite, and each column represents the RD-fed uninfected (RD), RD-fed infected (RDI), HFD-fed uninfected (HFD), or HFD-fed infected (HFDI) mouse group. Different colors correspond to the different intensity level of metabolites (red > the control RD group and green < the control RD group). Statistically significant differences were tested using Student's *t*-test, and the corrected *p* values (*q*-value) are presented next to the heat map. Red, yellow, and green rectangles indicate high, moderate, and low expressions, respectively. (c, d) The percentage changes in the levels of phosphocholine metabolites that included (c) diacyl PC and (d) acyl-alkyl PC in infected mice compared to the respective diet-fed (RD and HFD) uninfected mice represented by a bar graph (*significant change).

pathology during chronic *T. cruzi* infection. These metabolomic studies provide new insights into metabolic changes that could significantly influence cardiomyopathy during chronic Chagas disease and may define new biomarkers to identify Chagas patients at risk of cardiomyopathy.

Infected mice fed on HFD showed significantly greater body weight gain compared to infected RD mice, while no significant difference was observed between the HFD-fed and the RD-fed uninfected mice consistent with a gain in body weight with age with both diets. It is likely that the amount of carbohydrates (70% kcal) in the RD might have allowed uninfected RD-fed mice to gain a similar amount of weight as uninfected HFD-fed mice. In infected animals, however, HFD-fed mice had increased body weights that may be a consequence of enlarged livers (Figure 1; no significant change was observed with other organs, data not provided). HFD may further aggravate hepatic dysfunction during chronic *T. cruzi* infection and is reflected in the difference in serum metabolomic profiles between infected mice on HFD or RD. The basal glucose levels were significantly higher in HFD-fed groups compared to RD-fed groups (both infected and uninfected), suggesting that there is a difference in metabolic requirements between HFD- and RD-fed mice. HFD fed may prefer to utilize mainly lipids (fatty acids) as their energy source compared to glucose since excessive fat is available in their diet, especially in the infected HFD mice as indicated by significantly increased PPARα levels (Figure 2). However, infected mice (both RD and HFD mice) had a decreased glucose tolerance compared to uninfected mice, which agrees with our previous report that *T. cruzi* infection causes pancreatitis and deregulated insulin signaling that persists into the stage of chronic infection [14].

Increased uptake of dietary lipids in HFD groups (both uninfected and infected) might have caused reduction in lipid biosynthesis metabolism as demonstrated by significantly decreased levels of lipid metabolism biomarkers compared to RD-fed mice (Figure 2). Fatty acid anabolism was significantly decreased, as shown by reduced protein levels of fatty acid synthase (FAS), which is involved in the biosynthesis of long-chain fatty acids from acetyl CoA and malonyl CoA (Figures 2(a) and 2(b)) [28]. However, the initial steps of fatty acid biosynthesis were not significantly altered during infection, as demonstrated by the protein levels of phosphorylated ATP-citrate lyase (pACL), acetyl CoA-synthase (AceCS1), and phosphorylated acetyl co A carboxylase (p-ACC) in the livers of RD-fed mice compared to uninfected RD-fed mice (Figures 2(a), 2(c), 2(d), and 2(e)). pACL catalyzes the synthesis of acetyl CoA and oxaloacetate [29]; the levels of which are unaltered in the livers during infection in RD-fed mice (Figures 2(a) and 2(c)). The formation of acetyl CoA and oxaloacetate in the cytoplasm is the key step for the biosynthesis of fatty acids, cholesterol, and acetylcholine [26]. In fact, the levels of AceCS1, an enzyme that synthesizes acetyl CoA in the cytoplasm, a precursor for fatty acid and lipid biosynthesis, slightly increased (not significantly) in the infected RD mice compared to uninfected RD mice [30]. However, the levels of pACL and p-ACC significantly decreased in HFD (uninfected and infected) mice compared to RD (uninfected and infected) mice (Figures 2(a), 2(c), and (e)). A significant decrease in the levels of pACL suggests that acetyl CoA synthesis is impaired or reduced in the livers of HFD-fed mice, which could impact lipid biosynthesis. Interestingly, the levels of PPARα were significantly increased in infected groups suggesting a high demand for fatty acids during chronic *T. cruzi* infection. Increased fatty acid oxidation in the livers could cause lipotoxicity and impair liver functions (carbohydrate, protein, and fat metabolism) resulting in distinct serum metabolomic profiles.

The levels of amino acids significantly differed between infected and uninfected, and between RD- and HFD-fed groups. The levels of many essential and nonessential amino acids were significantly reduced in infected mice compared to uninfected groups. It is well known that amino acids play a major role in regulating the immune system, nutritional status, and energy homeostasis [23, 31]. Leucine, isoleucine, and valine are the branched chain aa's that influences immune responses which were significantly decreased in infected mice. Glutamine, which regulates B cell differentiation to plasma cells and proliferation of T cells, is significantly reduced in infected mice compared to uninfected groups (Figure 3) [32]. Reduced glutamine levels and metabolism impacts the levels of its end product citrulline in infected mice, especially in infected RD mice which is significantly decreased compared to infected HFD mice (Figure 3). Increased glycine levels in HFD mice (uninfected) are associated with regional body fat and altered energy homeostasis compared to uninfected RD-fed mice [33]. However, the levels of glycine were significantly increased in infected RD mice and significantly decreased in infected HFD mice compared to the respective uninfected groups (Figure 3); this suggests that the composition of a diet could significantly alter hepatic amino acid metabolism and energy homeostasis during chronic *T. cruzi* infection. Based on our data, we hypothesize that significantly decreased serum levels of citrulline and glutamine are associated with CCM pathogenesis and increased arginine and asparagine levels are associated with LV dysfunction and dilation (Table 2).

To facilitate the required energy supply, the human body oxidizes significant amounts of lipids besides glucose [9]. We demonstrated significantly increased PPARα, a regulatory of fatty acid oxidation in the livers of infected mice especially in infected HFD mice (Figure 2). L-carnitine transports activated long-chain fatty acids from the cytosol into the mitochondrion, a step crucial for fatty acid oxidation [21]. Defects in fatty acid oxidation result in increased plasma acyl carnitine levels, which are well supported by the acyl carnitine profiles of patients with a fatty acid oxidation defect [34]. Incomplete fatty acid oxidation may cause increased plasma acyl carnitine levels [35]. Our data showing significantly increased levels of serum carnitines especially long- and medium-chain acyl carnitines can be attributed to low fatty acid oxidation rates due to decreased levels of hepatic CPT1 (even with increased PPARα levels) during chronic infection compared to uninfected RD groups (Figure 2(a)). The branched chain amino acid-derived C3, C4, and C5 carnitines were significantly lower in infected RD mice compared to uninfected RD mice and infected HFD mice (except C4 carnitine). In general, the serum levels of long-

Table 2: A list of predicted metabolic biomarkers involved in the pathogenesis of CCM and RV and LV dilations in the murine models of chronic Chagas disease (arrows indicate decrease or increase).

Amino acids	CCM	RV	LV
	Citrulline↓ Glutamine↓		Arginine↑ Asparagine↑
Amino derivative			
	Alpha-AAA↑ PEA↓ Spermidine↓	Sarcosine↑	Sarcosine↓
Carnitines			
	C9↓ C6:1↓ C14:1↓ C6 (C4:1-DC)↑	C16:OH↑ C16↓ C5-OH (C3-DC-M)↓	C12↑ C16↑ C16:1↑ C18:1↑ C18:1OH↑ C5-OH (C3-DC-M)↑
Sphingolipids			
	SM(OH)C14:1↓ SM C16:1↓	SM C20:2↑	SM C20:2↓
lysoPC			
		lysoPC a C18:1↓ lysoPC a C18:2↓ lysoPC a C20:3↓ lysoPC a C28:1↓	lysoPC a C26:0↑ lysoPC a C26:1↑
PC-aa/ae			
	PC-aa-C36:3↓ PC-aa-C38↓ PC-aa-C38:3↓ PC-ae-C36:2↓ PC-ae-C38:3↓ PC-ae-C38:4↓ PC-ae-C40:4↓ PC-ae-C40:6↓ PC-ae-C42↓		PC-ae-C38:2↓

and medium-chain acyl carnitines were significantly greater in uninfected HFD mice compared to uninfected RD mice (supplemental Fig. 2). Compared to their respective diet-fed uninfected groups, infected groups displayed a significantly different pattern of serum acyl carnitine profile between infected RD and HFD mice. In support of these data, we found decreased levels of C9, C6:1, and C14:1 and increased levels of C6 (C4:1-DC) as the impaired carnitine metabolism markers in CCM pathogenesis (Table 2). Based on these data, we propose that increased levels of C16:OH and decreased serum levels of C16 and C5-OH (C3-DC-M) and increased levels of C12, C16, C16:1, C18:1, C18:1OH, and C5-OH (C3-DC-M) may be the distinct markers of RV and LV dilations, respectively, in CCM (Table 2).

LPC is an important signaling molecule with diverse biological functions, which is involved in regulating cellular proliferation, tumor cell invasion, and inflammation [36]. In particular, LPC is a chemotactic factor that stimulates immune cells and regulates the balance between pro- and anti-inflammatory cytokines [37]. As chronic Chagas cardiomyopathy is associated with proinflammatory signals [27, 38], one might expect LPCs to be increased in association with cardiac pathology. However, our results demonstrated that decreased levels of serum LPCs are associated with the pathogenesis of cardiomyopathy during chronic infection. The levels of lysoPCs C18:1, C18:2, C20:3, and C28:1, significantly decreased in infected HFD groups compared to all other groups (Figure 7(b)), which could be potential markers of RV dilation *in T. cruzi*-infected mice (Figure 7(b)) (Table 2). Infected mice showed significantly decreased levels of LPCs and other glycerophospholipids (diacyl-PC and acyl-alkyl-PC) compared to uninfected RD-fed mice. Feeding a HFD during *T. cruzi* chronic infection further decreased the levels of glycerophospholipids compared to infected RD mice and increased susceptibility to develop cardiomyopathy. Our previous data demonstrated that HFD decreased inflammatory signaling in the hearts of chronically infected mice, which may be attributed to the low levels of LPCs.

We have previously reported on the accumulation of lipids in different organs, including the liver and the heart, in murine Chagas disease [9, 39]. We also showed significantly decreased hepatic neutral lipids, increased hepatic cholesterol levels, and decreased fatty acid synthesis and mitochondrial oxidation in a murine model of acute *T. cruzi* infection [39]. In the present study, our results suggest that even during the chronic stages of infection, hepatic fatty acid and cholesterol metabolism remain significantly altered, especially in the mice fed on a HFD (Figure 3). These alterations could affect cardiac lipid metabolism. In support of this hypothesis, we have found that cardiac lipid metabolism was significantly reduced in infected HFD mice that developed RV dilation compared to infected RD mice during the chronic stage of infection [16].

5. Conclusion

CCM is an important disease in the endemic regions of Latin America. The majority of *T. cruzi*-infected patients are asymptomatic until they present with severe and typically irreversible cardiac complications. Though multiple biomarkers have been identified in Chagas patients, they are not specific to disease severity nor are they predictors of progression in asymptomatic patients. The identification of new metabolic biomarkers would greatly facilitate studies on disease progression and prevention and allow the identification of the subgroup of patients at a higher risk to develop ventricular-specific dilation and heart failure. Our data demonstrates many metabolic alterations in the experimental chronic Chagas disease model, which can be attributed to diet composition. Importantly, HFD induced much greater variations in serum metabolite levels compared to RD during chronic infection, which may impair liver functions by increased loads of lipids, which may in turn affect cardiac

functions. These data help link the risk of developing cardiomyopathy to the levels of these serum metabolites (Table 2). Serum metabolite analysis in patients with indeterminate Chagas disease may, therefore, help identify those at risk for developing cardiomyopathy, providing a much needed early tool to prevent the progression of cardiomyopathy and may be useful in gauging cardiac dysfunction. Investigations of serum metabolomic profiles in various stages of human Chagas disease hence warrants further analyses.

Data Availability

The metabolomic data used to support the findings of this study are included within the article.

Conflicts of Interest

None of the authors have conflict of interest.

Authors' Contributions

KL performed Western blotting analyses and metabolomic data analyses; UG performed metabolomic data analyses. JPA contributed to data analysis. YQ analyzed the metabolomic data and edited the manuscript. WD and LMW reviewed and edited the manuscript. JFN acquired the samples, analyzed all the data, edited the figures, and wrote the manuscript.

Acknowledgments

We thank Erika Shor at the Public Health Research Institute for the critical reading of the manuscript. We thank Dr. Jeffery Pessin of the Albert Einstein College of Medicine for their moral support in our studies. This study was supported by grants from the National Heart, Lung, and Blood Institute (National Institutes of Health HL-122866) to Jyothi Nagajyothi. We also acknowledge the Stable Isotope and Metabolomics Core Facility of the Diabetes Research and Training Center (DRTC) of the Albert Einstein College of Medicine (supported by the NIH/NCI grant P60DK020541).

Supplementary Materials

The representative bar graphs showing the difference in the serum levels of (1) amino acids and amines and (2 and 3) lipid metabolites between uninfected mice fed HFD and RD. *(Supplementary Materials)*

References

[1] G. Mora, "Chagas cardiomyopathy," *E-Journal of Cardiology Practice*, vol. 14, p. 31, 2016.

[2] Z. A. Andrade, S. G. Andrade, M. Sadigursky, R. J. Wenthold, S. L. Hilbert, and V. J. Ferrans, "The indeterminate phase of Chagas' disease: ultrastructural characterization of cardiac changes in the canine model," *The American Journal of Tropical Medicine and Hygiene*, vol. 57, no. 3, pp. 328–336, 1997.

[3] S. G. Muñoz-Saravia, A. Haberland, G. Wallukat, and I. Schimke, "Chronic Chagas heart disease: a disease on its way to becoming a worldwide health problem: epidemiology, etiopathology, treatment, pathogenesis and laboratory medicine," *Heart Failure Reviews*, vol. 17, no. 1, pp. 45–64, 2012.

[4] J. D. Stanaway and G. Roth, "The burden of Chagas disease: estimates and challenges," *Global Heart*, vol. 10, no. 3, pp. 139–144, 2015.

[5] Z. M. Cucunuba, O. Okuwoga, M. G. Basáñez, and P. Nouvellet, "Increased mortality attributed to Chagas disease: a systematic review and meta-analysis," *Parasites & Vectors*, vol. 9, no. 1, p. 42, 2016.

[6] M. J. Pinazo, M. C. Thomas, J. Bustamante, I. C. Almeida, M. C. Lopez, and J. Gascon, "Biomarkers of therapeutic responses in chronic Chagas disease: state of the art and future perspectives," *Memórias do Instituto Oswaldo Cruz*, vol. 110, no. 3, pp. 422–432, 2015.

[7] N. Iqbal, B. Wentworth, R. Choudhary et al., "Cardiac biomarkers: new tools for heart failure management," *Cardiovascular diagnosis and therapy*, vol. 2, no. 2, pp. 147–164, 2012.

[8] E. E. Okamoto, J. E. Sherbuk, E. H. Clark et al., "Biomarkers in *Trypanosoma cruzi*-infected and uninfected individuals with varying severity of cardiomyopathy in Santa Cruz, Bolivia," *PLoS Neglected Tropical Diseases*, vol. 8, no. 10, article e3227, 2014.

[9] C. Johndrow, R. Nelson, H. Tanowitz, L. M. Weiss, and F. Nagajyothi, "*Trypanosoma cruzi* infection results in an increase in intracellular cholesterol," *Microbes and Infection*, vol. 16, no. 4, pp. 337–344, 2014.

[10] F. Nagajyothi, L. M. Weiss, D. L. Silver et al., "*Trypanosoma cruzi* utilizes the host low density lipoprotein receptor in invasion," *PLoS Neglected Tropical Diseases*, vol. 5, no. 2, article e953, 2011.

[11] J. P. Ayyappan, K. Lizardo, S. Wang, E. Yurkow, and J. F. Nagajyothi, "Inhibition of ER stress by 2-aminopurine treatment modulates cardiomyopathy in a murine chronic Chagas disease model," *Biomolecules & Therapeutics*, vol. 27, no. 4, pp. 386–394, 2019.

[12] L. A. Jelicks and H. B. Tanowitz, "Advances in imaging of animal models of Chagas disease," *Advances in Parasitology*, vol. 75, pp. 193–208, 2011.

[13] L. Ny, H. Huang, B. Holmqvist et al., "A magnetic resonance imaging study of intestinal dilation in *Trypanosoma cruzi*–infected mice deficient in nitric oxide synthase," *The American Journal of Tropical Medicine and Hygiene*, vol. 79, no. 5, article 18981519, pp. 760–767, 2008.

[14] F. Nagajyothi, L. M. Weiss, D. Zhao et al., "High fat diet modulates *Trypanosoma cruzi* infection associated myocarditis," *PLoS Neglected Tropical Diseases*, vol. 8, no. 10, article e3118, 2014.

[15] W. Brima, D. J. Eden, S. F. Mehdi et al., "The brighter (and evolutionarily older) face of the metabolic syndrome: evidence from *Trypanosoma cruzi* infection in CD-1 mice," *Diabetes/-Metabolism Research and Reviews*, vol. 31, no. 4, article 25613819, pp. 346–359, 2015.

[16] K. Lizardo, J. P. Ayyappan, M. H. Cui, R. Balasubramanya, L. A. Jelicks, and J. F. Nagajyothi, "High fat diet aggravates cardiomyopathy in murine chronic Chagas disease," *Microbes and Infection*, vol. 21, no. 1, pp. 63–71, 2018.

[17] M. M. D. Romano, H. T. Moreira, A. Schmidt, B. C. Maciel, and J. A. Marin-Neto, "Imaging diagnosis of right ventricle involvement in Chagas cardiomyopathy," *BioMed Research International*, vol. 2017, Article ID 3820191, 14 pages, 2017.

[18] M. C. P. Nunes, A. Beaton, H. Acquatella et al., "Chagas cardiomyopathy: an update of current clinical knowledge and management: a scientific statement from the American Heart Association," *Circulation*, vol. 138, no. 12, pp. e169–e209, 2018.

[19] N. Girones, S. Carbajosa, N. A. Guerrero, C. Poveda, C. Chillon-Marinas, and M. Fresno, "Global metabolomic profiling of acute myocarditis caused by *Trypanosoma cruzi infection*," *PLoS Neglected Tropical Diseases*, vol. 8, no. 11, article e3337, 2014.

[20] G. Paglia, F. M. Del Greco, B. B. Sigurdsson, J. Rainer, C. Volani, and A. A. Hicks, "Influence of collection tubes during quantitative targeted metabolomics studies in human blood samples," *Clinica Chimica Acta*, vol. 486, pp. 320–328, 2018.

[21] N. Longo, M. Frigeni, and M. Pasquali, "Carnitine transport and fatty acid oxidation," *Biochimica et Biophysica Acta (BBA)-Molecular Cell Research*, vol. 1863, pp. 2422–2435, 2016.

[22] T. Y. Li, L. Song, Y. Sun et al., "Tip60-mediated lipin 1 acetylation and ER translocation determine triacylglycerol synthesis rate," *Nature Communications*, vol. 9, no. 1, article 1916, 2018.

[23] N. Paßlack, M. G. Doherr, and J. Zentek, "Effects of free amino acids on cytokine secretion and proliferative activity of feline T cells in an in vitro study using the cell line MYA-1," *Cytotechnology*, vol. 68, no. 5, pp. 1949–1961, 2016.

[24] D. M. Libert, A. S. Nowacki, and M. R. Natowicz, "Metabolomic analysis of obesity, metabolic syndrome, and type 2 diabetes: amino acid and acylcarnitine levels change along a spectrum of metabolic wellness," *PeerJ*, vol. 6, article e5410, 2018.

[25] K. J. Selke, G. Dhar, and J. M. Cohn, "Takotsubo cardiomyopathy associated with titration of duloxetine," *Texas Heart Institute Journal*, vol. 38, no. 5, pp. 573–576, 2011.

[26] F. Pietrocola, L. Galluzzi, J. M. Bravo-San Pedro, F. Madeo, and G. Kroemer, "Acetyl coenzyme A: a central metabolite and second messenger," *Cell Metabolism*, vol. 21, no. 6, pp. 805–821, 2015.

[27] E. Cunha-Neto and C. Chevillard, "Chagas disease cardiomyopathy: immunopathology and genetics," *Mediators of Inflammation*, vol. 2014, Article ID 683230, 11 pages, 2014.

[28] J. A. Menendez, A. Vazquez-Martin, F. J. Ortega, and J. M. Fernandez-Real, "Fatty acid synthase: association with insulin resistance, type 2 diabetes and cancer," *Clinical Chemistry*, vol. 55, no. 3, pp. 425–438, 2009.

[29] S. N. Pentyala and W. B. Benjamin, "Effect of oxaloacetate and phosphorylation on ATP-citrate lyase activity," *Biochemistry*, vol. 34, no. 35, pp. 10961–10969, 1995.

[30] P. S. Ariyannur, J. R. Moffett, C. N. Madhavarao et al., "Nuclear-cytoplasmic localization of acetyl coenzyme a synthetase-1 in the rat brain," *The Journal of Comparative Neurology*, vol. 518, no. 15, pp. 2952–2977, 2010.

[31] R. Mazzoli and E. Pessione, "The neuro-endocrinological role of microbial glutamate and GABA signaling," *Frontiers in Microbiology*, vol. 7, article 1934, 2016.

[32] E. P. Neis, C. H. Dejong, and S. S. Rensen, "The role of microbial amino acid metabolism in host metabolism," *Nutrients*, vol. 7, no. 4, pp. 2930–2946, 2015.

[33] M. S. Lustgarten, L. L. Price, E. M. Phillips, and R. A. Fielding, "Serum glycine is associated with regional body fat and insulin resistance in functionally-limited older adults," *PLoS One*, vol. 8, no. 12, article e84034, 2013.

[34] M. Wajner and A. U. Amaral, "Mitochondrial dysfunction in fatty acid oxidation disorders: insights from human and animal studies," *Bioscience Reports*, vol. 36, no. 1, article e00281, 2015.

[35] S. H. Adams, C. L. Hoppel, K. H. Lok et al., "Plasma acylcarnitine profiles suggest incomplete long-chain fatty acid β-oxidation and altered tricarboxylic acid cycle activity in type 2 diabetic African-American women," *The Journal of Nutrition*, vol. 139, no. 6, pp. 1073–1081, 2009.

[36] F. Mansilla, K. A. da Costa, S. Wang et al., "Lysophosphatidylcholine acyltransferase 1 (LPCAT1) overexpression in human colorectal cancer," *Journal of Molecular Medicine*, vol. 87, no. 1, pp. 85–97, 2009.

[37] Y. Smani, J. Domínguez-Herrera, J. Ibáñez-Martínez, and J. Pachón, "Therapeutic efficacy of lysophosphatidylcholine in severe infections caused by Acinetobacter baumannii," *Antimicrobial Agents and Chemotherapy*, vol. 59, no. 7, pp. 3920–3924, 2015.

[38] F. S. Machado, W. O. Dutra, L. Esper, K. J. Gollob, M. M. Teixeira, and S. M. Factor, "Current understanding of immunity to Trypanosoma cruzi infection and pathogenesis of Chagas disease," *Seminars in Immunopathology*, vol. 34, no. 6, pp. 753–770, 2012.

[39] K. Lizardo, V. Almonte, C. Law, J. P. Ayyappan, M. H. Cui, and J. F. Nagajyothi, "Diet regulates liver autophagy differentially in murine acute *Trypanosoma cruzi* infection," *Parasitology Research*, vol. 116, no. 2, pp. 711–723, 2017.

Hindawi
Disease Markers
Volume 2019, Article ID 3632906, 10 pages
https://doi.org/10.1155/2019/3632906

Review Article

Cardiac Chagas Disease: MMPs, TIMPs, Galectins, and TGF-β as Tissue Remodelling Players

Arthur Wilson Florencio da Costa,[1] Jose Rodrigues do Carmo Neto,[1] Yarlla Loyane Lira Braga,[1] Beatriz Aquino Silva,[2] Amanda Borges Lamounier,[2] Bárbara Oliveira Silva,[2] Marlene Antônia dos Reis,[3] Flávia Aparecida de Oliveira,[1] Mara Rúbia Nunes Celes,[1] and Juliana Reis Machado[1,3]

[1]*Institute of Tropical Pathology and Public Health, Federal University of Goiás, 74605-450 Goiânia, GO, Brazil*
[2]*Faculty of Medicine, Federal University of Goiás, 74605-050 Goiânia, GO, Brazil*
[3]*Department of General Pathology, Federal University of Triângulo Mineiro, 38025-180 Uberaba, MG, Brazil*

Correspondence should be addressed to Juliana Reis Machado; juliana.patologiageral@gmail.com

Received 16 August 2019; Accepted 1 November 2019; Published 25 November 2019

Guest Editor: Bruno Rivas-Santiago

A century after the discovery of Chagas disease, studies are still needed to establish the complex pathophysiology of this disease. However, it is known that several proteins and molecules are related to the establishment of this disease, its evolution, and the appearance of its different clinical forms. Metalloproteinases and their tissue inhibitors, galectins, and TGF-β are involved in the process of infection and consequently the development of myocarditis, tissue remodeling, and fibrosis upon infection with *Trypanosoma cruzi*. Thus, considering that the heart is one of the main target organs in Chagas disease, knowledge regarding the mechanisms of action of these molecules is essential to understand how they interact and trigger local and systemic reactions and, consequently, determine whether they contribute to the development of Chagas' heart disease. In this sense, it is believed that the inflammatory microenvironment caused by the infection alters the expression of these proteins favoring progression of the host-parasite cycle and thereby stimulating cardiac tissue remodeling mechanisms and fibrosis. The aim of this review was to gather information on metalloproteinases and their tissue inhibitors, galectins, and TGF-β and discuss how these molecules and their different interrelationships contribute to the development of Chagas' heart disease.

1. Introduction

Chagas disease is caused by infection of the flagellated protozoan *Trypanosoma cruzi* (*T. cruzi*), a parasite native to Latin America, which is an endemic region of the disease. Currently, about 6 to 7 million people worldwide are infected by this parasite, and in Brazil, this number reaches 1 million. Additionally, approximately 20 million individuals live in areas which are at a risk for this disease [1].

This disease is usually manifested asymptomatically and may evolve with different clinical manifestations characterizing its different forms, which are as follows: cardiac, digestive, and cardiodigestive. After infection, the individual goes through an acute phase, in which nonspecific symptoms are usually presented [2]. The disease progresses for 20 years or more, wherein the symptoms become chronic and more severe, and, when left untreated, leads to death of the individual [3, 4].

Cardiac involvement results in the development of heart disease, which is generally the most severe form of Chagas disease affecting about 20-30% of infected individuals [5]. Chagasic cardiomyopathy is a complex process resulting in the destruction of cardiac cells, cellular hypertrophy, alteration of electrical signals, dilatation of the cardiac chambers, proliferation of cardiac fibroblasts, and tissue matrix remodeling [2, 3, 6]. According to the World Health Organization

(WHO), there are about 50,000 deaths per year associated with chagasic cardiomyopathy and related to sudden cardiac death (60%), heart failure (25%), and strokes (15%) [7–10].

In the acute phase of infection, cardiomyopathy is characterized by an intense infiltration of inflammatory, mono, and polymorphonuclear cells, which release inflammatory cytokines and chemokines favoring continuous cell recruitment. In the chronic phase, the profile of infiltrated cells is predominantly mononuclear [11] and cardiac damage is mainly associated with inflammation caused by parasitism in the cardiomyocytes, tissue aggression resulting from the immune response [12], and high intensity of tissue remodeling, which is a product of collagen fiber deposition [13].

Additionally, these phenomena of parasitism, immune response, and tissue matrix remodeling are directly dependent on the interaction of numerous proteins, the expressions of which have been altered due to infection. Matrix metalloproteinases (MMPs) [14, 15], specific tissue metalloproteinase inhibitors (TIMPs) [16, 17], galectins (Gals) [17–20], and the transforming growth factor-beta (TGF-β) [21] are examples of molecules that have been studied in the context of Chagas disease in both experimental and human models.

MMPs are molecules directly involved with cardiac remodeling because they occur constitutively and are responsible for the degradation of extracellular matrix components [22], and TIMPs, at appropriate levels, are responsible for regulating the activity of the MMPs in the tissues. Infection with *T. cruzi* results in a proinflammatory environment causing an increased expression of MMPs 2 and 9. In this context, the high expression of MMPs inhibitors, TIMP-1 and TIMP-2, has been associated with the severity of the fibrotic process in experimental chagasic cardiomyopathy. In the process of cardiac tissue remodeling, galectins can activate collagen-producing cells as well, stimulating the production of proinflammatory cytokines such as TGF-β. This growth factor, in turn, acts on the tissue repair process and cardiac matrix remodeling.

Supposedly, this complex network of interactions involving these molecules depends directly on the inflammatory microenvironment and protozoan biological characteristics associated with the Chagas disease. This review proposes a complete understanding of the correlation of these proteins, as significant molecules in the cardiac tissue that help in understanding the pathophysiology of Chagas' heart disease at the expense of tissue remodeling.

2. The Role of Matrix Metalloproteinases in the Pathophysiology of Chagas Disease

MMPs are regulatory proteins involved in important physiological processes such as embryogenesis, angiogenesis, and tissue remodeling and may be inappropriately activated in various pathological processes, such as Chagas' heart disease, resulting in cell dysfunction and consequent tissue destruction [22].

MMPs form a group of enzymes (endopeptidases) comprising collagenases, gelatinases, stromelysins, matrilysins, membrane-like MMPs (MT-MMPs), and other MMPs responsible for degradation of the extracellular matrix (EM) and basement membrane components [23, 24]. Under physiological conditions in the myocardium, these enzymes may be inactive and inhibited by a group of proteins known as TIMPs. It has been demonstrated that these enzymes are expressed in different parasitic diseases, including Chagas disease. In this context, changes in the interactions between these molecules appear to be correlated with the changes in the myocardial tissue matrix observed in Chagas disease, and studies suggest that this imbalance affects both the geometry and overall cardiac function [23, 24].

According to Geurts et al. [25], the production of MMPs may also occur directly by the parasite, and the process of fibrogenesis is favored by uncontrolled levels and activity of MMPs and, consequently, results in the development of cardiomyopathy suggesting that MMPs may be an interesting therapeutic target. Among the MMPs, the following deserve special mention with respect to Chagas disease: MMP-2, as it is the most abundant and naturally expressed molecule in all cells, including cardiomyocytes, and plays important roles in homeostasis and the constant remodeling of matrix, and MMP-9, which is a cytokine-induced proteinase produced by different cell types [26]. The transcription and activation of these MMPs occur due to an increased expression of several cytokines such IL-6, IL-8, and TGF-β, which are induced in the inflammatory state. This phenomenon is observed in the acute phase of Chagas disease at the expense of strong seropositivity for *T. cruzi* [27].

Interestingly, it has already been shown by Pérez et al. [28] and Savino [29] that infectious agents, such as *T. cruzi*, in the endocrine system may contribute to the recruitment of inflammatory cells and the release of proinflammatory cytokines that contribute to the production extracellular matrix stimulating and maintaining more inflammatory processes.

Bautista-López et al. [22] demonstrated by densitometry analysis using blood plasma samples that a significant increase in the levels of MMP-2 and MMP-9 occurs in patients infected with *T. cruzi*. They also demonstrated a significant increase in the MPP activity when compared to the electrocardiogram of patients with cardiomyopathy and the control groups. They found that abnormal cardiac relaxation can be positively correlated with high levels of MMP-2 in patients with cardiac dilation occurring due to cardiomyopathy and then suggested that the MMPs 2 and 9 may act as potential biomarkers that can be used to identify not only the advent of cardiomyopathy but also its occurrence and progression in individuals infected with *T. cruzi*.

The hearts of wild-type mice, in which MMP-2 was overexpressed, were evaluated by Bergman et al. [30], who observed that significant cardiac damage such as cardiac dilation and thinning of the ventricular walls was associated with the high levels of expression of this molecule. Still, in this sense, other authors have reinforced the idea that MMPs 2 and 9 are involved in the pathogenesis of Chagas disease as they are able to degrade the components of the cellular matrix components in the heart, which contributes, at least in part, to cardiac tissue remodeling [27].

This cardiac remodeling is dependent on the type of MMPs produced. Hence, the action of MMP-9 on the myocardium may be by exacerbating the remodeling and contributing to the evolution of the heart shape development of the disease while, on the other hand, increasing the levels of MMP-2. Interestingly, this microenvironment results in a more discreet cardiac remodeling, contributing in some way such that the host remains in the undetermined phase of the disease. In this sense, Gutierrez et al. [31] have demonstrated that a significant regression of the cardiac inflammatory process and improved survival rates were observed in animals treated with the MMP-2 and MMP-9 inhibitors. The authors have further reinforced the role of MMPs in chagasic myocarditis induced by *T. cruzi* as well as suggesting a possible therapeutic target for heart disease caused by Chagas disease, which, however, needs further study.

It is undeniable that MMPs 2 and 9 are not only involved in stimulating tissue damage but also contribute to the exacerbation of the inflammatory response by activating various cytokines and chemokines and by costimulating tissue repair by depositing EM proteins [15]. It is clear these MMPs play a significant role in the pathogenesis of Chagas' heart disease, sometimes by stimulating the inflammatory process and cardiac remodeling and otherwise by curiously regulating these processes negatively. The findings of this review support the real need for further studies evaluating the role of MMPs as well as their inhibitors (TIMPs) in Chagas disease.

3. Tissue Inhibitors of MMPs in Chagas' Heart Disease

TIMPs, as regulators of MMPs, comprise a group of four molecules that bind with high affinity to the active MMPs and ultimately result in their proteolytic inactivation. These molecules are therefore known as the key regulators of MMPs [32]. This interaction between the TIMPs and MMPs occurs specifically and is of particular interest in the context of Chagas disease. TIMPs 2, 3, and 4 and TIMPs 1 and 3 inhibit MMP-2 and MMP-9, respectively [33].

According to Brew and Nagase [16] an imbalance in the production of these active enzymes and/or their inhibition may result in the development of diseases associated with extracellular matrix rearrangement, exacerbation of the inflammatory process, growth, and cell migration, which are phenomena frequently observed in Chagas disease. These authors have also demonstrated that the biological effects of TIMPs, such as the influence on cell differentiation and migration, synaptic plasticity, and antiangiogenic and antiproapoptotic activities, can be MMP-independent.

Among the different biological activities of TIMPs, type 1 is an important molecule involved in the regulation of cardiac remodeling, as demonstrated by Roten et al. [34], who evaluated that important changes associated with impaired cardiac function took place in the left ventricles of mice that did not express this enzyme. TIMP-1 acts by promoting fibroblast growth by activating the mitogen-activated protein kinase (MAP) leading to increased levels of Ras-GTP, which in turn results in increased levels of collagen favoring the occurrence of fibrosis [16].

However, it has been observed that the overexpression of TIMP-1 after gene therapy does not appear to be an effective tool in preventing cardiac remodeling. Gutierrez et al. [31] reported that, in *T. cruzi* infection, the expression of TIMP-1 was associated with an increased induction of collagen synthesis, thus favoring cardiac fibrosis. The overexpression of these TIMPs may even contribute to the pathogenesis of the chronic phase of the disease, in which an exacerbated fibrotic response of the cardiac form is observed.

On the other hand, some authors evaluating the knockout of TIMP-3 mice in different organs had observed an increase in the lung airspace and occurrence of apoptotic cell death during mammary gland involution [35]. According to these authors, both phenomena could have resulted from defects in the inhibition of MMPs, which reinforces the importance of the biological role of TIMPs, which can contribute to matrix degradation by preventing the inactivation of MMPs. This imbalance of TIMPs and MMPs involved in the process of matrix degradation was also observed in the heart, which resulted in cardiomyopathy [36]. Interestingly, Geurts et al. [24] have shown that uncontrolled activities of MMPs as well as the overregulation of MTPs may favor fibrogenesis and, consequently, may result in the development of cardiomyopathy.

In an experimental study by Gutierrez et al. [31], mice with induced Chagas' heart disease showed increased levels of both TIMP-1 and TIMP-3 but a direct relationship with the TIMP-2 levels was not observed. This corroborates the findings of Bergman et al. [30], who demonstrated that the overexpression of MMP-2 is associated with lower cardiac tissue remodeling and is able to reduce the progression of Chagas' heart disease.

Therefore, although Gutierrez et al. [31] revealed that the TIMPs had acted against the counterregulation of MMPs, this response may be considered to be insufficient in preventing myocardial damage. TIMPs can also modulate other critical signaling pathways independent of MMP inhibition, thus suggesting that an understanding of the mechanisms of action of these enzymes should be explored for a better understanding of the pathogenesis of Chagas disease [37] as well as its potential biomarkers.

There is no doubt about the importance of the role of TIMPs in the regulation of the MMPs involved in the process of tissue matrix remodeling, both physiologically and pathologically, and their involvement can be detected during cardiac remodeling in Chagas' heart disease.

4. The Dualistic Action of Galectins in Chagasic Cardiomyopathy

Galectins are glycan-binding proteins similar to the MMPs and are widely expressed in various cell types. They are mainly present in the cytoplasm but may also be found in the nucleus, cell surface, and extracellular environment [38, 39]. Fifteen members of the galectin family have been described in vertebrates [40], two of which have been

identified as EC-specific proteins, which are as follows: galectins 1 (Gal-1) and 3 (Gal-3).

These proteins have a range of effects associated with the inflammatory processes [20] and are related and expressed under the conditions of fibrogenesis and myocardial failure [17]. Their functions remain uncertain, and studies have contradictively demonstrated their positive and negative effects on the pathophysiology of Chagas disease [18, 41].

High levels of Gal-1 [42] have been reported in the hearts of patients with Chagas' heart disease although cells such as the B lymphocytes [43] produce high levels of Gal-1 when infected with *T. cruzi*. This lectin is believed to be released into the extracellular medium only after cell lysis of the myocardiocytes mediated by the trypomastigote forms [18].

Poncini et al. [41] demonstrated a negative role of Gal-1 in Chagas disease after infection and during immune response modulation, which contributed to the process of cellular infection. The authors demonstrated that dendritic cells (DCs), which play a crucial role in initiating the immune response, interact with galectins during the acute phase of infection and promote tolerance of the immune system to the parasite. This occurs by stimulating the differentiation of tolerogenic dendritic cells and regulatory T cells, which favors the evolution of the disease. According to the same authors, DCs play a different role, in which they prevent the induction of an inflammatory response. They promote T cell anergy and stimulate regulatory T cells, which suppresses the inflammatory response and, consequently, tissue damage.

Benatar et al. [18] demonstrated that, in a HL-1 myocardiocyte lineage, the presence of galectin decreases *T. cruzi* cell infection, as well as phosphatidylserine exposure, which is important for the induction of apoptosis. These authors demonstrated that if the extent of parasitemia in Lgals1$^{-/-}$ animals infected with the Tulahuén strain was higher, the survival rates were lower compared to those of the wild animals.

Additionally, a gene study has suggested that infection with *T. cruzi* increases the expression of the LGASL3 gene responsible for coding another galectin, Gal-3 [42]. Gal-3 plays a key role in the adhesion of the trypomastigote forms to the host cells during the initial process of infection. In this process, Gal-3 binds to parasite-specific mucins and interacts with laminins [43] increasing their adhesion to the EC components [43, 44], favoring the accumulation of tissue parasites and causing cardiomyocyte infection [44].

Pineda et al. [19] demonstrated that the affinity with which this lectin binds to the intracellular amastigotes is greater than that with the trypomastigote form, in which binding to the galactosides occurs on the surface of the parasite. Using immunofluorescence, it was observed that the amastigote forms are coated with a pool of cytosol galectins. Based on these observations, the authors have suggested that Gal-3 increases the extent of *T. cruzi* cell infection. This would occur as the released cell amastigotes would increase and alter the pool of galectins favoring the adhesion and invasion of new cells more rapidly. The authors also suggest that other mechanisms such as the rearrangement of the structures of the galectin receptor would allow the amastigotes to survive in the extracellular environment. Alternatively, the labeling of extracellular amastigotes in order to enable the macrophages to detect and phagocyte the protozoan would also contribute to the infection.

Contrarily, under physiological conditions, Gal-3 is involved in the binding of CD with T cells after activation of the L-selectins. In vivo and in vitro studies have shown that *T. cruzi* infection increases the concentration of Gal-3 in the acute phase as well as in their CD binding sites. Additionally, the migration capacity of CD is found to be impaired. Because these cells promote antigen presentation, it may characterize a negative immunomodulation mechanism promoted by *T. cruzi* [42].

In addition to CD, the expression of this lectin is also higher in the B lymphocytes upon infection, and this increase promotes a negative effect on the activity of interleukin 4. This results in a lack of stimulation and inhibition of plasma cell differentiation, subsequent decrease in the antibody production, and parasite clearance favoring the evolution of the disease [45].

Some studies have shown that in the evolution of Chagas' heart disease, which results in intense cardiac remodeling, Gal-3 also participates in the process of collagen production. Gal-3 induces the proliferation of cardiac fibroblasts converting them to myofibroblasts and thereby stimulating TGF-β synthesis [17, 39, 46]. By mediating TGF-β production, Gal-3 could be involved in the activation of a profibrotic pathway known as TGF-β1/α-SMA/Col-1, as demonstrated by Henderson et al. [46] in a model of atrial fibrosis. This pathway results in the production of TGF-β1, procollagen, and α-SMA, which are important components involved in the differentiation of fibroblasts into myofibroblasts [47], which may be important sources of Gal-3 in pathological conditions such as the Chagas disease [39, 48].

The expression of myocardial lectin in mice infected with *T. cruzi* is high [42, 45]. In addition to cardiac fibrosis, other studies have shown that Gal-3 is also involved in the development of fibrosis in other organs [46–49]. This suggests that the expression of Gal-3 would then be directly related to cardiac remodeling.

Contrarily, when infected with the Colombian strain and treated with N-Lac, a Gal-3 blocker, mild fibrosis and myocardial inflammatory cell migration were observed in the mice [50]. In this sense, Ferrer et al. [51] observed that experimental infection with *T. cruzi* results in an increased expression of profibrotic genes, which include the following: Col-1, α-SMA, and Gal-3 in regions of fibrosis and inflammation in the myocardium. Pineda et al. [19] have reinforced these findings by revealing that a reduction in the inflammatory infiltrate and mild myocardial fibrosis was observed in the Lgals1$^{-/-}$ mice. The same observations were noted when using G-CSF, a Gal-3 modulator [52].

Thus, finding alternatives that interfere with the expression of Gal-3 in patients with the indeterminate form of Chagas disease, who are naturally at an imminent risk of developing Chagas' heart disease, seems promising [52]. According to Pineda et al. [19], a deficient Gal-3 phenotype is compatible with an anti-inflammatory profile at the expense of promoting deregulation in the Toll-like receptor

expression. These authors have demonstrated that, during *T. cruzi* infection, these effects observed in the deficient Gal-3 phenotype would increase blood parasitism but not cardiac parasitism in the antigen-presenting cells and further reduce cytokine production, inflammation, and myocardial fibrosis.

Therefore, Gal-3 is involved in the pathophysiology of the cardiac form of Chagas disease. Thus, studies on these lectins in chagasic cardiomyopathy models may result in the identification of new therapeutic targets leading to better prognosis.

5. TGF-β, a Marker of the Progression of Chagas' Heart Disease

TGF-β is a cytokine belonging to the group of the "TGF-β superfamily" and has three isoforms, TGF-β1, 2, and 3. This cytokine participates in immune response modulation and inflammation and is involved in cellular growth mechanisms, differentiation, and cell death [53]. Additionally, it plays an important role in collagen synthesis and is considered as one of the main profibrotic factors stimulating the phenotypic transition from the fibroblast to its effector fibrotic form, the myofibroblast [54].

Under normal conditions, this cytokine stimulates collagen production and inhibits MMP activity through the synthesis of protease inhibitors [55, 56]. During cardiac injury, it in turn promotes tissue remodeling and repair [56]. Some studies have shown that TGF-β plasma and cardiac elevated levels are associated with some type of cardiac dysfunction [57–60] such as Chagas' heart disease [55]. A 10- to 20-fold increase in serum TGF-β1 levels has been observed in CD patients compared to uninfected healthy subjects. Elevated serum levels of this cytokine have been associated with more severe forms of heart disease in chronic patients [55, 61].

TGF-β is produced in the individuals in the acute and chronic stages of the Chagas disease. Thus, it participates in different processes influencing progression of the disease. For example, it has been shown that cell invasion by the Silvio and Tulahuén strains is dependent on TGF-β signaling, since infection was extremely inefficient in MvlLu cells with TβRI and TβRII receptor defects [62]. Using the strain Y, Waghabi and colleagues [63] demonstrated that in vitro treatment of cardiomyocytes with anti-TGF-β antibody slowed the process of cell invasion. Other authors suggest that this dependence was due in part to the SMAD pathway [64], since the binding of TGF-β to its receptors stimulates phosphorylation of intracellular proteins such as Smad2/3 [65].

TGF-β appears to favor infection as it is released from cells in its inactive form due to binding with the latency-associated protein (LAP) [66, 67]. In order to enable binding of this cytokine to its receptor, it is necessary to break the interaction of LAP with TGF-β, which is catalyzed by numerous agents including integrins [66], thrombospondin [68], and proteases (plasmin, MMP-2, and MMP-9) [68, 69], which would activate the latent TGF-β.

This latent or inactive form of TGF-β can be activated by both the amastigote and trypomastigote forms of the strains Y and Dm28, which favor the parasite cycle and facilitate host cell infection [63]. Similar mechanisms have also been observed in infections by other protozoa such as *Leishmania* [70, 71] and *Plasmodium* [72].

This activation may also be directly related to the exacerbated production of EC components [73], as demonstrated in a cardiac biopsy analysis of patients with Chagas disease. In these cases, an increase in the fibrosis associated with high levels of TGF-β was observed by perivascular fibronectin and strong tissue phosphorylated SMAD-2 nuclear labeling [55].

Nevertheless, the activation of latent TGF-β dependent on *T. cruzi* is still a poorly studied mechanism and is believed to occur mainly via the action of cruzipain, a peptidase expressed at all stages of the parasitic infection [73]. Waghabi et al. [63] suggested that TGF-β is captured and accumulated within the parasite mainly in the amastigote phase, suggesting that this cytokine plays an important role during the multiplication and differentiation period. The authors have suggested that this accumulation occurs through the "flagellar pocket," which is capable of encompassing the TGF-β-rich vesicles from the host endoplasmic reticulum during the infection process.

Some authors believe that after the period of infection and during the development of the inflammatory process and immune response, this cytokine increases the replication of *T. cruzi* at the expense of inhibiting the microbicidal effects on macrophages induced by IFN-γ [74–76]. This would contribute to the evolution of the disease and cardiac dysfunction. In an in situ evaluation of the heart of patients with chronic Chagas disease, no significant relationship was found between the TGF-β expression and cardiac dysfunction [77]. However, the role of TGF-β as a profibrotic factor has been reported in other pathological processes: diabetic nephropathy in in vitro models and experimental models [78, 79], chronic intestinal inflammation [80], and rheumatoid arthritis [81, 82].

In this case, a series of molecules are being developed in an attempt to intervene in the TGF-β pathway, which are as follows: oligonucleotides, aiming at blocking the synthesis of TGF-β1 and TGF-β2 ligands; monoclonal antibodies capable of neutralizing the different TGF-β isoforms; synthetic peptides containing TGF-β receptor domains capable of sequestering free TGF-β from the extracellular medium; and small chemical compounds that block signal transduction of the TGF-β pathway [73].

These pharmacological inhibitors of TGF-β receptors such as SB-431542 (type I) and GW-788388 (type I and type II) have been tested in a murine experimental model for Chagas' heart disease. In an experimental evaluation of the acute phase with the strain Y, the mice were treated intraperitoneally with SB-431542 three days after infection. After treatment, a reduction in the levels of parasitemia, mortality rates, inflammatory infiltrate, parasitic load, and electrical conduction in the heart of the infected and treated animals [83] was observed. A decrease in the number of intracellular amastigotes and the release of trypomastigotes were observed upon in vitro evaluation of SB-431542-treated cardiomyocytes infected with the strain Y and Dm28c, which reinforces

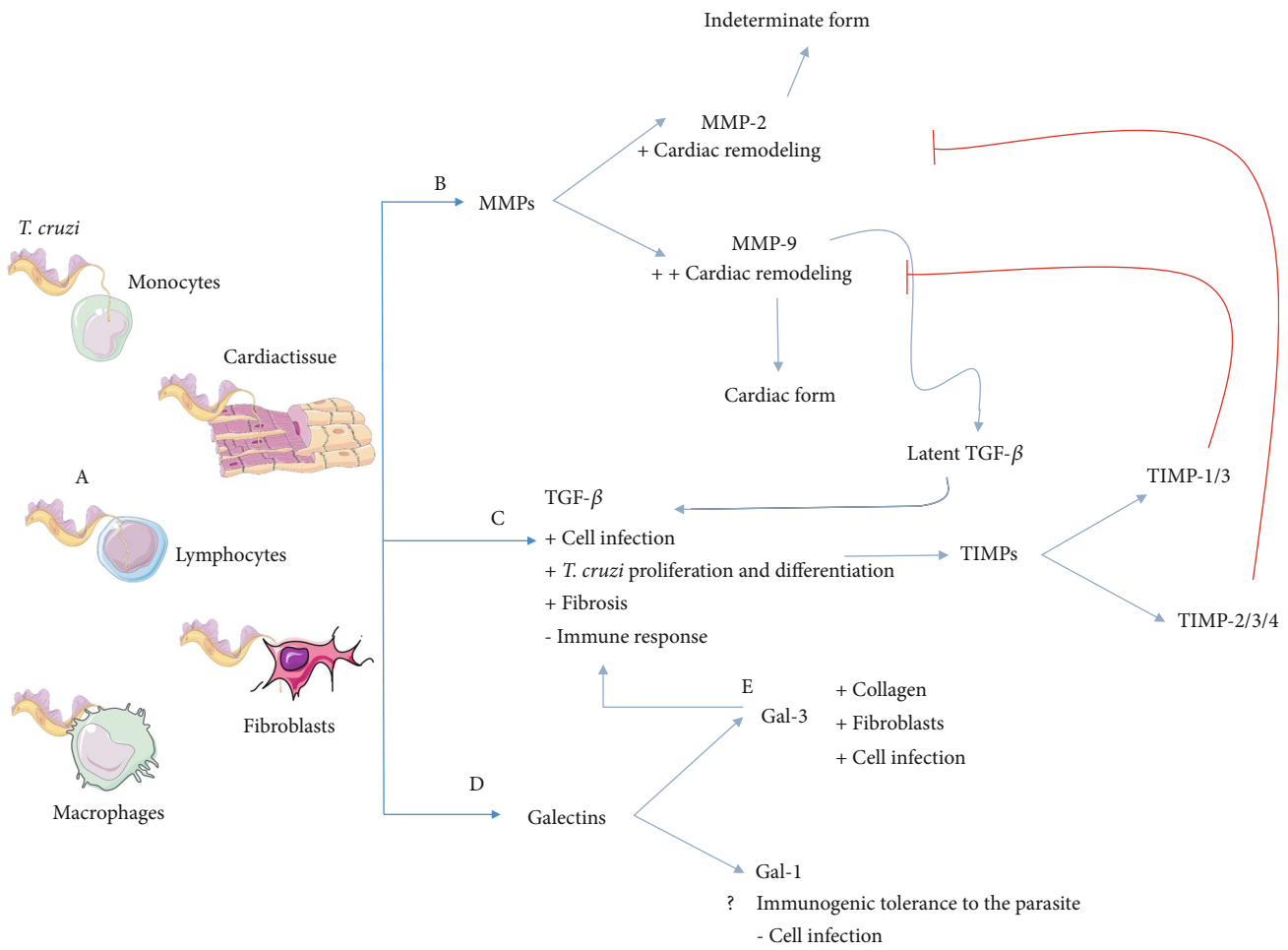

Figure 1: (A) Scheme representing the interrelation and regulation between metalloproteinases (MMPs), tissue inhibitors of metalloproteinases (TIMPs), galectins, and TGF-β in *Trypanosoma cruzi* infection. (B) MMPs act primarily on cardiac remodeling and activate latent TGF-β. (C) This cytokine supports the parasite intracellular cycle and stimulates fibrosis and cardiac damage. May also increase TIMP levels, favoring inhibition of MMPs. (D) While galectin-1 function is still controversial, this protein may be related to decreased protozoal infection and proinflammatory immune response. (E) Galectin-3 also stimulates cardiac remodeling and favors the parasite cycle via its own mechanism and also by stimulating TGF-β production. This figure is a derivative of "Servier Medical Art" by Servier, used under CCBy 3.0.

the role of this cytokine in the process of cellular infection and differentiation [76].

In an analysis performed on SB-431542 and *T. cruzi*, it was observed that inhibition of the TGF-β pathway resulted in a decrease in parasitic load and fibronectin expression in a three-dimensional model of cell culture "cardiac spheroids" that reproduced an infection similar to that observed in vivo after Y strain infection. As collagen production depends on the balance between its production and degradation, mainly mediated by MMPs and TIMPS activity, a decrease in MMP-2 and MMP-9 activity was observed in infected cells. Thus, after treatment, a significant increase in MMP-2 activity was observed, as well as a reduction in TIMP-1 activity in infected cells [84].

Mice with chronic Chagas' heart disease infected by the Colombian strain were treated orally with GW788388, an inhibitor of TGF-β type I and II receptor kinases. Although the treatment showed no effects on parasite load on the myocardium, the treatment was able to reverse cardiac fibrosis, showing lower levels of type 1 collagen and fibronectin when compared to untreated infected mice. The treatment was also able to improve cardiac function, and this may be associated with the high levels of MMP-9 and the low levels of TIMP-1, TIMP-2, and TIMP-4. In addition, the same authors demonstrated that treatment with GW788388 induced a lower influx of $CD3^+$ cells into the heart of infected mice [85].

Thus, TGF-β, which was evaluated using different experimental models, presents itself as an important cytokine involved in the progression of Chagas' heart disease. When interacting with the trypomastigote and amastigote forms, this cytokine favors myocardiocyte infection and intracellular multiplication of the parasite. Thus, use of inhibitors of the TGF-β activation pathway may affect the parasite cycle and result in lower levels of parasitemia and cell infection. Thus, these therapies seem promising in reducing cardiac fibrosis and a better prognosis on the evolution of myocarditis.

6. Conclusions

The inflammatory microenvironment generated by the Chagas disease results in an imbalance in the production, secretion, and activities of MMPs, TIMPs, galectins, and TGF-β. The interaction of these molecules (Figure 1), in different ways, directly or indirectly favors both, the infection and cardiac remodeling processes, consequently causing fibrosis that results in Chagas' heart disease.

Conflicts of Interest

The authors declare that they have no conflict of interests.

Authors' Contributions

Arthur Wilson Florencio da Costa and Jose Rodrigues do Carmo Neto equally contributed to this review.

Acknowledgments

We thank the funding and research agencies such as CNPq (Conselho Nacional de Desenvolvimento Científico e Tecnológico) and CAPES (Coordenação de Aperfeiçoamento de Pessoal de Nível Superior), as well the Universidade Federal de Goiás and Universidade Federal do Triângulo Mineiro.

References

[1] J. C. P. Dias, A. N. Ramos, E. D. Gontijo et al., "II Consenso Brasileiro em Doença de Chagas, 2015," *Epidemiologia e Serviços de Saúde*, vol. 25, no. 21, pp. 1–10, 2016.

[2] A. Rassi Jr., A. Rassi, and J. A. Marin-Neto, "Chagas disease," *The Lancet*, vol. 375, no. 9723, pp. 1388–1402, 2010.

[3] R. C. Pedrosa, J. R. Cancado, and W. Decache, "Estudo longitudinal do eletrocardiograma na doença de Chagas desde a fase aguda," *Revista da Sociedade Brasileira de Medicina Tropical*, vol. 26, no. 3, pp. 163–174, 1993.

[4] J. S. Cruz, F. S. Machado, C. Ropert, and D. Roman-Campos, "Molecular mechanisms of cardiac electromechanical remodeling during Chagas disease: role of TNF and TGF-β," *Trends in Cardiovascular Medicine*, vol. 27, no. 2, pp. 81–91, 2017.

[5] K. C. F. Lidani, L. Bavia, A. R. Ambrosio, and I. J. de Messias-Reason, "The complement system: a prey of *Trypanosoma cruzi*," *Frontiers in Microbiology*, vol. 8, pp. 1–14, 2017.

[6] J. A. Marin-Neto, E. Cunha-Neto, B. C. Maciel, and M. V. Simões, "Pathogenesis of chronic Chagas heart disease," *Circulation*, vol. 115, no. 9, pp. 1109–1123, 2007.

[7] R. B. Bestetti and A. Cardinalli-Neto, "Sudden cardiac death in Chagas' heart disease in the contemporary era," *International Journal of Cardiology*, vol. 131, no. 1, pp. 9–17, 2008.

[8] A. Rassi Jr., A. Rassi, and S. G. Rassi, "Predictors of mortality in chronic Chagas Disease," *Circulation*, vol. 115, no. 9, pp. 1101–1108, 2007.

[9] A. Rassi Jr., A. Rassi, W. C. Little et al., "Development and validation of a risk score for predicting death in Chagas' heart disease," *The New England Journal of Medicine*, vol. 355, no. 8, pp. 799–808, 2006.

[10] R. F. Rosa, A. S. Neto, and R. A. Franken, "Chagas' disease and the use of implantable cardioverter-defibrillators in Brazil," *The American Journal of Geriatric Cardiology*, vol. 15, no. 6, pp. 372–376, 2006.

[11] R. L. Tarleton, "Chagas disease: a solvable problem, ignored," *Trends in Molecular Medicine*, vol. 22, no. 10, pp. 835–838, 2016.

[12] T. C. Simões, L. F. Borges, A. C. Parreira de Assis, M. V. Silva, J. dos Santos, and K. C. Meira, "Chagas disease mortality in Brazil: a Bayesian analysis of age-period-cohort effects and forecasts for two decades," *PLoS Neglected Tropical Diseases*, vol. 12, no. 9, p. e0006798, 2018.

[13] M. Lopez, H. B. Tanowitz, and N. J. Garg, "Pathogenesis of chronic Chagas disease: macrophages, mitochondria, and oxidative stress," *Current Clinical Microbiology Reports*, vol. 5, no. 1, pp. 45–54, 2018.

[14] M. Garcia-Saldivia, G. Lopez-Mendez, L. Berrueta, S. Salmen, J. H. Donis, and D. F. Davila, "Metalloproteinases 2 and 9 in different stages of chronic Chagas disease," *International Journal Of Cardiology*, vol. 179, pp. 79–81, 2015.

[15] N. I. Medeiros, J. A. S. Gomes, and R. Correa-Oliveira, "Synergic and antagonistic relationship between MMP-2 and MMP-9 with fibrosis and inflammation in Chagas' cardiomyopathy," *Parasite Immunology*, vol. 39, no. 8, p. e12446, 2017.

[16] K. BREW and H. NAGASE, "The tissue inhibitors of metalloproteinases (TIMPs): an ancient family with structural and functional diversity," *Biochimica et Biophysica Acta (BBA) - Molecular Cell Research*, vol. 1803, no. 1, pp. 55–71, 2010.

[17] U. C. Sharma, S. Pokharel, T. J. van Brakel et al., "Galectin-3 marks activated macrophages in failure-prone hypertrophied hearts and contributes to cardiac dysfunction," *Circulation*, vol. 110, no. 19, pp. 3121–3128, 2004.

[18] A. F. Benatar, G. A. García, J. Bua et al., "Galectin-1 prevents infection and damage induced by *Trypanosoma cruzi* on cardiac cells," *PLOS Neglected Tropical Diseases*, vol. 9, no. 10, p. e0004148, 2015.

[19] M. A. Pineda, H. Cuervo, M. Fresno, M. Soto, and P. Bonay, "Lack of galectin-3 prevents cardiac fibrosis and effective immune responses in a murine model ofTrypanosoma cruziInfection," *Journal Of Infectious Diseases*, vol. 212, no. 7, pp. 1160–1171, 2015.

[20] M. A. Pineda, L. Corvo, M. Soto, M. Fresno, and P. Bonay, "Interactions of human galectins with *Trypanosoma cruzi*: binding profile correlate with genetic clustering of lineages," *Glycobiology*, vol. 25, no. 2, pp. 197–210, 2015.

[21] P. M. Ferrão, L. M. Nisimura, O. C. Moreira et al., "Inhibition of TGF-β pathway reverts extracellular matrix remodeling in *T. cruzi*-infected cardiac spheroids," *Experimental Cell Research*, vol. 362, no. 2, pp. 260–267, 2018.

[22] N. L. Bautista-López, C. A. Morillo, P. López-Jaramillo et al., "Matrix metalloproteinases 2 and 9 as diagnostic markers in the progression to Chagas cardiomyopathy," *American Heart Journal*, vol. 165, no. 4, pp. 558–566, 2013.

[23] S. Klotz, R. F. Foronjy, M. L. Dickstein et al., "Mechanical unloading during left ventricular assist device support increases left ventricular collagen cross-linking and myocardial stiffness," *Circulation*, vol. 112, no. 3, pp. 364–374, 2005.

[24] R.-K. Li, G. Li, D. A. G. Mickle et al., "Overexpression of transforming growth factor-β1 and insulin-like growth factor-I in patients with idiopathic hypertrophic cardiomyopathy," *Circulation*, vol. 96, no. 3, pp. 874–881, 1997.

[25] N. Geurts, G. Opdenakker, and P. E. van den Steen, "Matrix metalloproteinases as therapeutic targets in protozoan

parasitic infections," *Pharmacology & Therapeutics*, vol. 133, no. 3, pp. 257–279, 2012.

[26] M. A. M. Ali, X. Fan, and R. Schulz, "Cardiac sarcomeric proteins: novel intracellular targets of matrix metalloproteinase-2 in heart disease," *Trends in Cardiovascular Medicine*, vol. 21, no. 4, pp. 112–118, 2011.

[27] R. C. G. Fares, J. d. A. S. Gomes, L. R. Garzoni et al., "Matrix metalloproteinases 2 and 9 are differentially expressed in patients with indeterminate and cardiac clinical forms of Chagas disease," *Infection and Immunity*, vol. 81, no. 10, pp. 3600–3608, 2013.

[28] A. R. Pérez, O. Bottasso, and W. Savino, "The impact of infectious diseases upon neuroendocrine circuits," *Neuroimmunomodulation*, vol. 16, no. 2, pp. 96–105, 2009.

[29] W. Savino, "Endocrine immunology of Chagas disease," *Frontiers of Hormone Research*, vol. 48, pp. 160–175, 2017.

[30] M. R. Bergman, J. R. Teerlink, R. Mahimkar et al., "Cardiac matrix metalloproteinase-2 expression independently induces marked ventricular remodeling and systolic dysfunction," *American Journal of Physiology-Heart and Circulatory Physiology*, vol. 292, no. 4, pp. H1847–H1860, 2007.

[31] F. R. S. Gutierrez, M. M. Lalu, F. S. Mariano et al., "Increased activities of cardiac matrix metalloproteinases matrix metalloproteinase (MMP)-2 and MMP-9 are associated with mortality during the acute phase of experimental *Trypanosoma cruzi* infection," *The Journal of Infectious Diseases*, vol. 197, no. 10, pp. 1468–1476, 2008.

[32] M. Corbel, E. Boichot, and V. Lagente, "Role of gelatinases MMP-2 and MMP-9 in tissue remodeling following acute lung injury," *Brazilian Journal of Medical and Biological Research*, vol. 33, no. 7, pp. 749–754, 2000.

[33] H. Nagase and G. Murphy, "Tailoring TIMPs for selective metalloproteinase inhibition," in *The Cancer Degradome*, D. Edwards, G. Hoyer-Hansen, F. Blasi, and B. F. Sloane, Eds., pp. 787–810, Springer New York, New York, 2008.

[34] L. Roten, S. Nemoto, J. Simsic et al., "Effects of gene deletion of the tissue inhibitor of the matrix metalloproteinase-type 1 (TIMP-1) on left ventricular geometry and function in mice," *Journal of Molecular and Cellular Cardiology*, vol. 32, no. 1, pp. 109–120, 2000.

[35] J. E. Fata, K. J. Leco, E. B. Voura et al., "Accelerated apoptosis in the Timp-3-deficient mammary gland," *The Journal of Clinical Investigation*, vol. 108, no. 6, pp. 831–841, 2001.

[36] P. W. M. Fedak, D. S. Smookler, Z. Kassiri et al., "TIMP-3 deficiency leads to dilated cardiomyopathy," *Circulation*, vol. 110, no. 16, pp. 2401–2409, 2004.

[37] J. Sun, "Matrix metalloproteinases and tissue inhibitor of metalloproteinases are essential for the inflammatory response in cancer cells," *Journal of Signal Transduction*, vol. 2010, Article ID 985132, 7 pages, 2010.

[38] W. C. Meijers, A. R. van der Velde, D. A. Pascual-Figal, and R. A. de Boer, "Galectin-3 and post-myocardial infarction cardiac remodeling," *European Journal Of Pharmacology*, vol. 763, no. Part A, pp. 115–121, 2015.

[39] X. Zhong, X. Qian, G. Chen, and X. Song, "The role of galectin-3 in heart failure and cardiovascular disease," *Clinical And Experimental Pharmacology And Physiology*, vol. 46, no. 3, pp. 197–203, 2019.

[40] L. C. Reignault, E. S. Barrias, L. C. S. Medeiros, W. de Souza, and T. M. U. de Carvalho, "Structures containing galectin-3 are recruited to the parasitophorous vacuole containing *Trypanosoma cruzi* in mouse peritoneal macrophages," *Parasitology Research*, vol. 113, no. 6, pp. 2323–2333, 2014.

[41] C. V. Poncini, J. M. Ilarregui, E. I. Batalla et al., "*Trypanosoma cruzi* infection imparts a regulatory program in dendritic cells and T cells via galectin-1–dependent mechanisms," *The Journal Of Immunology*, vol. 195, no. 7, pp. 3311–3324, 2015.

[42] B. Vray, "Up-regulation of galectin-3 and its ligands by *Trypanosoma cruzi* infection with modulation of adhesion and migration of murine dendritic cells," *Glycobiology*, vol. 14, no. 7, pp. 647–657, 2004.

[43] T. N. Moody, J. Ochieng, and F. Villalta, "Novel mechanism thatTrypanosoma cruziuses to adhere to the extracellular matrix mediated by human galectin-3," *FEBS Letters*, vol. 470, no. 3, pp. 305–308, 2000.

[44] P. N. Nde, M. F. Lima, C. A. Johnson, S. Pratap, and F. Villalta, "Regulation and use of the extracellular matrix by Trypanosoma cruzi during early infection," *Frontiers in Immunology*, vol. 3, 2012.

[45] E. V. Acosta-Rodríguez, C. L. Montes, C. C. Motrán et al., "Galectin-3 mediates IL-4-induced survival and differentiation of B cells: functional cross-talk and implications duringTrypanosoma cruziInfection," *The Journal Of Immunology*, vol. 172, no. 1, pp. 493–502, 2003.

[46] N. C. Henderson, A. C. Mackinnon, S. L. Farnworth et al., "Galectin-3 regulates myofibroblast activation and hepatic fibrosis," *Proceedings of the National Academy of Sciences*, vol. 103, no. 13, pp. 5060–5065, 2006.

[47] N. C. Henderson, A. C. Mackinnon, S. L. Farnworth et al., "Galectin-3 expression and secretion links macrophages to the promotion of renal fibrosis," *The American Journal Of Pathology*, vol. 172, no. 2, pp. 288–298, 2008.

[48] S. L. Farnworth, N. C. Henderson, A. C. MacKinnon et al., "Galectin-3 reduces the severity of pneumococcal pneumonia by augmenting neutrophil function," *The American Journal Of Pathology*, vol. 172, no. 2, pp. 395–405, 2008.

[49] L. Calvier, M. Miana, P. Reboul et al., "Galectin-3 mediates aldosterone-induced vascular fibrosis," *Arteriosclerosis, Thrombosis, And Vascular Biology*, vol. 33, no. 1, pp. 67–75, 2013.

[50] B. S. de Freitas Souza, D. N. Silva, R. H. Carvalho et al., "Association of cardiac galectin-3 expression, myocarditis, and fibrosis in chronic Chagas disease cardiomyopathy," *The American Journal Of Pathology*, vol. 187, no. 5, pp. 1134–1146, 2017.

[51] M. F. Ferrer, C. A. Pascuale, R. M. Gomez, and M. S. Leguizamón, "DTU I isolates of *Trypanosoma cruzi* induce upregulation of galectin-3 in murine myocarditis and fibrosis," *Parasitology*, vol. 141, no. 6, pp. 849–858, 2014.

[52] J. F. Vasconcelos, B. S. F. Souza, T. F. S. Lins et al., "Administration of granulocyte colony-stimulating factor induces immunomodulation, recruitment of T regulatory cells, reduction of myocarditis and decrease of parasite load in a mouse model of chronic Chagas disease cardiomyopathy," *The Faseb Journal*, vol. 27, no. 12, pp. 4691–4702, 2013.

[53] D. Chin, G. M. Boyle, P. G. Parsons, and W. B. Coman, "What is transforming growth factor-beta (TGF-β)?," *British Journal of Plastic Surgery*, vol. 57, no. 3, pp. 215–221, 2004.

[54] A. Biernacka, M. Dobaczewski, and N. G. Frangogiannis, "HHS public access," *Growth Factors*, vol. 29, no. 5, pp. 196–202, 2015.

[55] T. C. Araújo-Jorge, M. C. Waghabi, A. M. Hasslocher-Moreno et al., "Implication of transforming growth factor–β1 in Chagas disease myocardiopathy," *The Journal of Infectious Diseases*, vol. 186, no. 12, pp. 1823–1828, 2002.

[56] M. Dobaczewski, W. Chen, and N. G. Frangogiannis, "Transforming growth factor (TGF)-β signaling in cardiac remodeling," *Journal of Molecular and Cellular Cardiology*, vol. 51, no. 4, pp. 600–606, 2011.

[57] Y. Y. Li, Y. Feng, C. F. McTiernan et al., "Downregulation of matrix metalloproteinases and reduction in collagen damage in the failing human heart after support with left ventricular assist devices," *Circulation*, vol. 104, no. 10, pp. 1147–1152, 2001.

[58] M. Pauschinger, D. Knopf, S. Petschauer et al., "Dilated cardiomyopathy is associated with significant changes in collagen type I/III ratio," *Circulation*, vol. 99, no. 21, pp. 2750–2756, 1999.

[59] L. E. Felkin, E. Lara-Pezzi, R. George, M. H. Yacoub, E. J. Birks, and P. J. R. Barton, "Expression of extracellular matrix genes during myocardial recovery from heart failure after left ventricular assist device support," *Journal of Heart and Lung Transplantation*, vol. 28, no. 2, pp. 117–122, 2009.

[60] M. C. Waghabi, C. M. L. M. Coutinho, M. N. C. Soeiro et al., "Increased *Trypanosoma cruzi* invasion and heart fibrosis associated with high transforming growth Factor Levels in mice deficient in 2-Macroglobulin," *Infection and Immunity*, vol. 70, no. 9, pp. 5115–5123, 2002.

[61] A. R. Pérez, S. D. Silva-Barbosa, L. R. Berbert et al., "Immunoneuroendocrine alterations in patients with progressive forms of chronic Chagas disease," *Journal of Neuroimmunology*, vol. 235, no. 1-2, pp. 84–90, 2011.

[62] M. Ming, M. E. Ewen, and M. E. A. PEREIRA, "Trypanosome invasion of mammalian cells requires activation of the TGFβ signaling pathway," *Cell*, vol. 82, no. 2, pp. 287–296, 1995.

[63] M. C. Waghabi, M. Keramidas, S. Bailly et al., "Uptake of Host Cell Transforming Growth Factor-β by *Trypanosoma cruzi* Amastigotes in Cardiomyocytes : Potential Role in Parasite Cycle Completion," *American Journal of Pathology*, vol. 167, no. 4, pp. 993–1003, 2005.

[64] B. S. Hall and M. A. Pereira, "Dual role for transforming growth factor beta -Dependent signaling in *Trypanosoma cruzi* infection of mammalian cells," *Infection and Immunity*, vol. 68, no. 4, pp. 2077–2081, 2000.

[65] J. O. A. N. Massagué, "A very private TGF-β receptor embrace," *Molecular Cell*, vol. 29, no. 2, pp. 149-150, 2008.

[66] J. S. Munger, X. Huang, H. Kawakatsu et al., "A Mechanism for Regulating Pulmonary Inflammation and Fibrosis: The Integrin αvβ6 Binds and Activates Latent TGF β1," *Cell*, vol. 96, no. 3, pp. 319–328, 1999.

[67] S. Schultz-Cherry and J. E. Murphy-Ullrich, "Thrombospondin causes activation of latent transforming growth factor-beta secreted by endothelial cells by a novel mechanism," *The Journal of Cell Biology*, vol. 122, no. 4, pp. 923–932, 1993.

[68] Y. Sato and D. B. Rifkin, "Inhibition of endothelial cell movement by pericytes and smooth muscle cells: activation of a latent transforming growth factor-beta 1-like molecule by plasmin during co-culture," *The Journal of Cell Biology*, vol. 109, no. 1, pp. 309–315, 1989.

[69] Q. Yu and I. Stamenkovic, "Cell surface-localized matrix metalloproteinase-9 proteolytically activates TGF-beta and promotes tumor invasion and angiogenesis," *Genes & Development*, vol. 14, no. 2, pp. 163–176, 2000.

[70] A. Somanna, V. Mundodi, and L. Gedamu, "Functional analysis of cathepsin B-like cysteine proteases from Leishmania donovani complex. Evidence for the activation of latent transforming growth factor beta," *The Journal of Biological Chemistry*, vol. 277, no. 28, pp. 25305–25312, 2002.

[71] K. R. Gantt, S. Schultz-Cherry, N. Rodriguez et al., "Activation of TGF-beta by *Leishmania chagasi*: importance for parasite survival in macrophages," *Journal of Immunology*, vol. 170, no. 5, pp. 2613–2620, 2003.

[72] F. M. Omer, J. B. de Souza, P. H. Corran, A. A. Sultan, and E. M. Riley, "Activation of transforming growth factor β by malaria parasite-derived metalloproteinases and a thrombospondin-like molecule," *The Journal of Experimental Medicine*, vol. 198, no. 12, pp. 1817–1827, 2003.

[73] P. M. Ferrão, C. M. d'Avila-Levy, T. C. Araujo-Jorge et al., "Cruzipain activates latent TGF-β from host cells during *T. cruzi* invasion," *PLoS One*, vol. 10, no. 5, p. e0124832, 2015.

[74] T. C. Araújo-Jorge, M. C. Waghabi, C. S. Maria de Nazaré, M. Keramidas, S. Bailly, and J. J. Feige, "Pivotal role for TGF-β in infectious heart disease: The case of *Trypanosoma cruzi* infection and consequent Chagasic myocardiopathy," *Cytokine and Growth Factor Reviews*, vol. 19, no. 5–6, pp. 405–413, 2008.

[75] J. S. Silva, D. R. Twardzik, and S. G. Reed, "Regulation of *Trypanosoma cruzi* infections in vitro and in vivo by transforming growth factor beta (TGF-beta)," *The Journal of experimental medicine*, vol. 174, no. 3, pp. 539–545, 1991.

[76] D. . L. Martin, M. Postan, P. Lucas, R. Gress, and R. . L. Tarleton, "TGF-β regulates pathology but not tissue CD8+ T cell dysfunction during *experimentalTrypanosoma cruzi* infection," *European Journal of Immunology*, vol. 37, no. 10, pp. 2764–2771, 2007.

[77] D. B. R. Rodrigues, M. A. dos Reis, A. Romano et al., "*In Situ* Expression of regulatory cytokines by heart inflammatory cells in chagas' disease patients with heart failure," *Clinical and Developmental Immunology*, vol. 2012, Article ID 361730, 7 pages, 2012.

[78] K. Yoshioka, T. Takemura, K. Murakami et al., "Transforming growth factor-beta protein and mRNA in glomeruli in normal and diseased human kidneys," *Laboratory Investigation*, vol. 68, no. 2, pp. 154–163, 1993.

[79] F. N. Ziyadeh, K. Sharma, M. Ericksen, and G. Wolf, "Stimulation of collagen gene expression and protein synthesis in murine mesangial cells by high glucose is mediated by autocrine activation of transforming growth *factor-beta*," *Journal of Clinical Investigation*, vol. 93, no. 2, pp. 536–542, 1994.

[80] C. Kay, O. E. Lorthioir, N. J. Parr et al., "Solid-phase reaction monitoring - chemical derivatization and off-bead analysis," *Biotechnology and Bioengineering*, vol. 71, no. 2, pp. 110–118, 2000.

[81] S. M. Wahl, J. B. Allen, G. L. Costa, H. L. Wong, and J. R. Dasch, "Reversal of acute and chronic synovial inflammation by anti-transforming growth factor beta," *The Journal of Experimental Medicine*, vol. 177, no. 1, pp. 225–230, 1993.

[82] H. Cheon, S. -J. Yu, D. H. Yoo, I. J. Chae, G. G. Song, and J. Sohn, "Increased expression of pro-inflammatory cytokines and metalloproteinase-1 by TGF-β1 in synovial fibroblasts from rheumatoid arthritis and normal individuals," *Clinical and Experimental Immunology*, vol. 127, no. 3, pp. 547–552, 2002.

[83] M. C. Waghabi, E. M. de Souza, G. M. de Oliveira et al., "Pharmacological Inhibition of Transforming Growth Factor β Signaling Decreases Infection and Prevents Heart Damage in Acute Chagas' Disease," *Antimicrobial Agents and Chemotherapy*, vol. 53, no. 11, pp. 4694–4701, 2009.

[84] M. C. Waghabi, M. Keramidas, C. M. Calvet et al., "SB-431542, a transforming growth Factor Inhibitor, Impairs *Trypanosoma cruzi* infection in cardiomyocytes and parasite cycle completion," *Antimicrobial Agents and Chemotherapy*, vol. 51, no. 8, pp. 2905–2910, 2007.

[85] R. R. Ferreira, R. da Silva Abreu, G. Vilar-Pereira et al., "TGF-β inhibitor therapy decreases fibrosis and stimulates cardiac improvement in a pre-clinical study of chronic Chagas' heart disease," *PLOS Neglected Tropical Diseases*, vol. 13, no. 7, p. e0007602, 2019.